THE PETROGENESIS OF HIGH GRADE CONTACT METAMORPHIC MINERAL ASSEMBLAGES IN CALC-SILICATE XENOLITHS, EASTERN BUSHVELD COMPLEX, SOUTH AFRICA

by

Thomas Wallmach

Submitted in partial fulfilment of the requirements
for the degree of
Doctor of Science
in the Faculty of Science,
University of Pretoria.

Pretoria, 1988

CONTENTS

Page

Page

Page

Abstract

One of the most spectacular but least studied thermal metamorphic aureoles is undoubtedly that surrounding the intrusive rocks of the Bushveld Complex. Apart from displaying a vast range of metamorphic assemblages in pelitic rocks of the Pretoria Group, xenoliths of calc-silicates within the intrusive rocks of the complex host some unique assemblages unknown from other localities. The degree of thermal metamorphism belongs to the highest ever recorded.

A petrogenetic grid is proposed, which covers the highest degrees of metamorphism occurring in the system $CaO-MgO-SiO_2-CO_2$. This petrogenetic grid involves 65 stable and metastable mineral reactions and serves to predict the fate of siliceous dolomites under extreme contact metamorphic conditions. With increasing temperature akermanite, monticellite, merwinite and periclase formed from mainly irreversible decarbonation reactions in which calcite was an important reactant. From diagnostic mineral parageneses overburden load pressures of 1.1 - 2.2 kbar for the emplacement of the critical zone magma and 0.6 - 1.6 kbar for the marginal zone magma can be inferred. Forsterite exsolutions in monticellite with an unusual optical positive sign and dehydroxylated Ba-phlogopite indicate magma temperatures higher than 1200°C, while the lack of melting of the present high-temperature mineral assemblages gives an upper temperature limit of 1400°C.

The minerals and mineral assemblages found in the marginal and critical zone xenoliths were hardly affected by hydration during retrograde metamorphism. The upper zone xenoliths consist mainly of vesuvianite-, grandite- and melilite-bearing mineral assemblages, which became stable during relatively late stages of retrograde metamorphism. In the upper zone xenoliths most of the minerals present belong to the system $CaO-MgO-SiO_2-Al_2O_3-H_2O-CO_2$. There are strong indications that they formed from minerals similar to those found in the high temperature mineral assemblages of the marginal zone xenoliths. The average Al_2O_3 content in the melilites originally present in the upper zone xenoliths was higher than in the marginal zone xenoliths. This, together with an influx of a H_2O-rich fluid phase

during retrograde metamorphism led to the formation of the vesuvianite- and grandite-bearing mineral assemblages. Microprobe analyses of different coloured Mg-Fe-vesuvianites, garnets of different composition, prehnite and xanthophyllite show unusual variations in their chemical composition.

Samevatting

Een van die mees indrukwekkende maar min bestudeerde termale metamorfe oureool is ongetwyfeld die een wat die intrusiewe gesteentes van die Bosveldkompleks omring. Afgesien van die wye reeks van metamorfe mineraalassosiasies in die pelitiese gesteentes van die Pretoria Groep, bevat die xenoliete van kalksilikate in die intrusiewe gesteentes van die kompleks onder andere ook unieke assosiasies wat nog nie voorheen in die literatuur gedokumenteer is nie. Die grade van termale metamorfose behoort tot die hoogste ooit beskryf.

'n Petrogenetiese ruit, wat meer as 65 stabiele en metastabiele mineraalreaksies in die sisteem $CaO-MgO-SiO_2-CO_2$ insluit, is ontwikkel ten einde die gedrag van silikadraende dolomiete onder toestande van uiterste kontakmetamorfose te voorspel.

In xenoliete van die randsone en kritieke sone het met toenemende temperature akermaniet, montiselliet, merwiniet en periklaas van hoofsaaklik onomkeerbare dekarbonasiereaksies ontstaan, waarin kalsiet 'n belangrike reagent was. Van diagnostiese mineraalparageneses is belastingsdrukke van 1.1 tot 2.2 kbar vir inplasing van die kritieke sone magma en 0.6 tot 1.6 kbar vir die randsone magma afgelei. Forsterietontmengings in montiselliet met 'n ongewone optiese positiewe teken en dehidroksileerde Ba-flogopiet dui op magmatemperature hoër as 1200°C, terwyl afwesigheid van smelting van die teenwoordige hoogtemperatuur mineraalassosiasies 'n boonste temperatuurlimiet van 1400°C aandui. Die minerale en mineraalassosiasies in die randsone en kritieke sone is feitlik gladnie deur hidrasie tydens retrogressiewe metamorfose geaffekteer nie.

Die xenoliete in die bosone bestaan meestal uit vesuvianiet-, grandiet- en melilietdraende mineraalassosiasies, wat gedurende relatief laat stadiums van retrogressiewe metamorfose stabiel geword het. Die meeste minerale in die bosone xenoliete behoort tot die sisteem $CaO-MgO-SiO_2-Al_2O_3-H_2O-CO_2$. Daar is sterk aanduidings dat hierdie minerale ontstaan het uit minerale soortgelyk as die in die hoogtemperatuur mineraalassosiasies van die xenoliete in die randsone.

Die gemiddelde Al_2O_3 inhoud in die meliliete oorspronklik teenwoordig in die bosone xenoliete was hoër as in die randsone xenoliete. Hierdie, tesame met die toevoeging van 'n H_2O-ryk fluiede fase tydens retrogressiewe metamorfose het tot die totstandkoming van die vesuvianiet- en grandietdraende mineraalassosiasies gelei. Mikrosonde analises van verskillend gekleurde Mg-Fe vesuvianiete, verskeie granate, prehniet en xanthofilliet toon ongewone variasies in hulle chemiese samestelling.

A Introduction

The Bushveld Complex, with an areal extent of 66 000 km^2 and a thickness of about 6 to 9 km (von Gruenewaldt, 1977; Hattingh, 1980), is the largest layered intrusion in the world, hosting some of the largest known ore deposits. A vast number of publications covers the mechanisms that led to the formation of the different rock types and their associated mineral deposits, of which a comprehensive account is given a.o. in a special issue of 'Economic Geology (v.80, 1985)' devoted to the Bushveld Complex. Compared to this, little work has been done on the intrusion depths or the magma temperatures of the different magmas which gave rise to the Rustenburg Layered Suite of the Bushveld Complex. Overload pressures were usually estimated or inferred from the calculated and assumed thickness of Bushveld- and roof rocks. There is still considerable controversy regarding their origin and their thickness at the time of the emplacement of the layered mafic and ultramafic rocks (e.g.: Coetzee, 1970; Rhodes, 1974; French and Twist, 1983; Twist and Harmer, 1987).

1 Aims and Purposes of the Present Study

The present work attempts to shed some light on the temperatures and pressures during emplacement of some of the Bushveld magmas.

In order to determine these pressure- and temperature constraints, geothermometers and geobarometers with the following properties had to be found:

1) They have to provide a means of deducing the depth or overload pressure and the temperature at which the mafic magmas of the Complex were emplaced; and
2) they have to preserve this information over more than 2 b.y., i.e. the age of the Bushveld Complex (Hamilton, 1977; Harmer and Sharpe, 1985).

Some of the calc-silicate xenoliths, found in different stratigraphic levels of the Rustenburg Layered Suite of the Bushveld Complex proved to meet these requirements. As the investigated xenoliths are

relatively small (a few 1 000 m^3) they were most probably in thermal equilibrium with the surrounding magma. Within these xenoliths chemical reactions, involving minerals and gases in a supercritical state, were promoted by the heat of the surrounding magma and led to the formation of unique and exotic mineral assemblages. At about the time of peak metamorphism these mineral assemblages were 'frozen in' and provide an excellent record of some of the physical conditions, like pressures and temperatures, at which the emplacement of the Bushveld Complex took place.

It stands to reason that the maximum pressures, now reflected in the critical mineral assemblages in the metamorphic aureole of the Bushveld Complex, increased as the pile of igneous rocks increased as a result of the successive emplacement of magma into the chamber. While the compiled pressure and temperature data reflect the conditions of peak metamorphism, that is the maximum temperatures and maximum pressures, no data are available which reflects the depth of emplacement of the individual Bushveld magmas at the time of their respective intrusion. The present investigation aims to show that calc-silicate xenoliths in the Bushveld Complex have the potential to be used as geothermometers and geobarometers which can provide constraints on the physical conditions under which the different Bushveld magmas intruded.

Some of the xenoliths are located in the proximity of chromitite layers in the critical zone and the magnetite layers in the upper zone so that the metamorphic assemblages also provide some constraints on the physical conditions that led to the formation of these deposits.

Observed mineral assemblages comprising vesuvianite and garnet, which formed during retrograde metamorphism, reflect metamorphic conditions and processes that prevailed after peak metamorphism. These are discussed in the light of recently published experimental data.

2 Previous P-T Estimations on Metamorphic Rocks Associated with the Northern and Eastern Bushveld Complex

Figure 1 presents a compilation of pressure and temperature data derived from critical mineral parageneses and index minerals in the metamorphic aureole of the eastern Bushveld Complex (modified after Hulbert and Sharpe, 1981a). The P-T data for the areas around Burgersfort, Havercroft and Faugh Ballagh have been calculated by Hulbert and Sharpe (1981a,b). For the pressure estimates they applied the metamorphic reactions:

$$3CaAl_2Si_2O_8 = Ca_3Al_2Si_3O_{12} + 2Al_2SiO_5 + SiO_2$$
plagioclase garnet sillimanite

(Ghent, 1976; Schmid and Wood, 1976) and

$$3Fe_2Al_4Si_5O_{18} = 2Fe_3Al_2Si_3O_{12} + 4Al_2SiO_5 + 5SiO_2$$
cordierite garnet sillimanite

(Wood and Fraser, 1976).

Calculations using these reactions yielded pressure values of 5 and 5.3 kbar. Hulbert and Sharpe (1981a) state that a summation of 6 km felsites, 9 km of mafic and ultramafic rocks and 1 km floor-rocks, together with a contribution of some directed stress (ca. 0.5 kbar), could account for these pressures. The same authors regard their pressure estimates to be in good agreement with those inferred from the occurrence of kyanite reported by Hall (1911). The maximum temperature estimate by Hulbert and Sharpe (1981a) of about 720°C was determined on biotite-garnet pairs according to the method of Ferry and Spear (1978), and from the $Mg/(Mg+Fe^{2+})$ ratios of coexisting cordierite and biotite.

Human (1975), who investigated almandine-bearing metamorphic rocks on the farm Havercroft in the eastern Transvaal, inferred temperatures similar to those obtained by Hulbert and Sharpe (1981a) for the same area, but lower pressures (1 - 2 kbar). He states that almanidine, even though it is a high-pressure mineral, can be stable at low pressures as well, depending on the rock composition. These considerations are based on the observed reaction:

sillimanite + magnetite + quartz = almandine.

This reaction will take place at 600°C±10°C and P_f=2 kbar under conditions of declining oxygen fugacity (Miyashiro, 1973). Human (1975)

suggested that only a part of the Bushveld Complex was directly overlying the area under discussion, in order to account for the relatively low observed pressures.

Sharpe and Förtsch (1981) used the garnet-clinopyroxene assemblage at Houtenbek to estimate the temperature of a garnetite formation. The estimates are based on the equation:

$$3CaMgSi_2O_6 + Fe_3Al_2Si_3O_{12} = 3CaFeSi_2O_6 + Mg_3Al_2Si_3O_{12}$$

clinopyroxene almandine clinopyroxene pyrope

Sharpe and Förtsch (1981) applied the method of Råheim and Green (1974) and Wells (1979) and calculated a temperature of 560°C on the assumption that the overload pressure was 3.5 kbar.

Pressure- and temperature data from xenoliths on the farms Maandagshoek and Thorncliffe, were published by Cameron (1976). From these localities the minerals corundum, sillimanite, mullite and sapphirine were previously described by Hall and Nel (1926) and Willemse and Viljoen (1970). By applying the experimental results of Seifert (1974) and estimating a pressure of 4.5 kbar, Cameron (1976) postulated a temperature of 1200±50°C. At lower pressure estimates the temperature increases slightly and for a pressure of 1 kbar the calculated temperature is 1250±50°C. The aforementioned temperature estimates are based on the coexistence of mullite and sillimanite and the reaction:

cordierite + corundum = sapphirine + mullite (Seifert, 1974).

Nell (1985) described two stages of metamorphism in the metamorphic aureole in the northern limb of the Bushveld Complex, near Potgietersrus. He calculated a pressure of 1.5 kbar and a maximum temperature of 750°C due to the intrusion of the lower zone magma, from the assemblage cordierite-olivine-orthopyroxene±spinel±quartz. The second stage metamorphism occurred during the intrusion of the upper critical-, main- and upper zones. He used different geothermobarometers for the assemblages garnet-cordierite-orthopyroxene-biotite, clinopyroxene-plagioclase-quartz, and cordierite-spinel±sillimanite±corundum±orthopyroxene±olivine to calculate a maximum temperature of 900°C and pressures of 4 - 5 kbar. Nell (1985) stated that this pressure is about 2 kbar higher than the lithostatic pressure probably due to a directed stress contribution.

Calc-silicate xenoliths consisting of diopside hornfels and of monticellite-diopside-forsterite hornfels were described by Mostert (1982) from the Platreef in the northern limb of the Bushveld Complex. These xenoliths consist of diopside hornfels and of monticellite-diopside-forsterite hornfelses. The assumed pressures of 3 - 4 kbar and calculated equilibrium temperatures of 957°C and 967°C, respectively, are based on the experimental data of Walter (1963a) and from volumetrically measured forsterite exsolutions in monticellite (Warner and Luth, 1973).

The pressure and temperature estimates outlined above appear to be somewhat contradictory - especially those calculated by Hulbert and Sharpe (1981a) and by Human (1975) for the locality at Havercroft. Hulbert and Sharp (1981a) and Nell (1985) emphasize that where the whole Bushveld Complex was emplaced over the metamorphosed sediments the maximum pressure may have been 4 - 5.3 kbar. Where only parts of the Bushveld Complex had intruded at the time of peak metamorphic conditions, as in parts of the northern limb of the Bushveld Complex (Nell, 1985), this pressure was lower. There the critical mineral assemblage which is developed in the Pretoria Group sediments beneath the lower zone, indicates a pressure of 1.5 kbar. The maximum temperatures reached during metamorphism depend on the distance between the sediments and the igneous rocks. Temperatures inferred from the mineral assemblages within the xenoliths on the farms Maandagshoek and Thorncliffe, which are situated in the critical zone, are the highest ($T \geq 1200°C$) so far recorded from the Bushveld Complex.

3 Previous Work on Calc-silicate Xenoliths in the Northern and Eastern Bushveld Complex

Although several authors have described calc-silicate xenoliths in the Bushveld Complex (Willemse and Bensch, 1964; Page, 1970; Joubert, 1979; Mostert, 1982), the most comprehensive petrological study of some of the minerals and mineral parageneses occurring in xenoliths within the marginal and the upper zone of the Bushveld Complex (localities A and B in Fig. 1) is that by Willemse and Bensch (1964). From xenoliths in the marginal zone they described an intergrowth of

wollastonite and monticellite, and the mineral assemblage clinopyroxene-monticellite-olivine-akermanite. Olivine and akermanite were found to be separated from each other by a reaction seam consisting of monticellite and clinopyroxene. Two retrograde reactions were proposed to explain these textures and parageneses:

1) akermanite = monticellite + wollastonite; and

2) akermanite + forsterite = diopside + monticellite.

From the experimental work of Walter (1963a) Willemse and Bensch (1964) concluded that temperatures higher than 900°C must have prevailed in the xenoliths. The same authors found very fine olivine exsolutions in monticellite. They also reported kalsilite from a xenolith in the marginal zone and gave a chemical analysis of a mineral mixture in which kalsilite participates. Kalsilite is extremely rare and is mostly found as a mineral in ultrabasic volcanic rocks. The only occurrence of metamorphic kalsilite has been reported from a calc-silicate xenolith from Brome Mountain, Quebec, Canada (Philpotts et al., 1967) where kalsilite is associated with melilite, diopside and spinel. In the present thesis, an average analysis of several microprobe analyses of pure kalsilite is presented that provides further evidence for the existence of kalsilite in metamorphic rocks.

Upper zone xenoliths investigated by Willemse and Bensch (1964) from the upper zone of the complex are one consisting mainly of vesuvianitefels on the farm Avontuur (locality B, Fig. 1) and another one consisting mainly of olivinefels on the farm Magnet Heights.

Willemse and Bensch (1964) noted a distinct difference in the mineralogy between xenoliths in the marginal zone norite and those in the upper zone magnetite gabbro, with akermanite and monticellite only developed in the marginal zone xenoliths but not in the upper zone xenoliths where vesuvianite and garnet are abundant. These authors assumed that a rather dry environment favoured the occurrence of akermanite and monticellite while a higher content of volatiles and aluminium led to the formation of vesuvianite and garnet.

Mostert's (1982) description on metasedimentary inclusions, consisting of diopside hornfels and monticellite-diopside-forsterite

hornfelses, in the Platreef of the northern limb of the Bushveld Complex, has already been mentioned in the previous chapter.

Joubert (1976), who investigated three calc-silicate xenoliths in the upper zone of the eastern Bushveld Complex, found them to consist mainly of akermanite-monticellite-clinopyroxene-vesuvianitefels. He assumed two phases of contact-metamorphism, viz. a first phase during which no metasomatic reactions took place, and a second phase during which titanium, aluminium and iron were introduced. From calculations involving the thickness of overlying upper zone lithologies and roof-rocks, mainly of the Rooiberg felsites and associated pyroclastic rocks, he concluded that the overload pressure at the time of emplacement of the upper zone magma was about 1800 bar, at a metamorphic temperature of at least 800°C.

Some of the mineralogical and petrological features found in the Bushveld xenoliths are similar to those described for the Cascade Slide xenolith in the Adirondacks (Valley and Essene, 1980) and monticellite-bearing Adirondack marbles (Tracy, 1978).

The two compositional triangles indicated in Figure 2 represent the major mineral phases of the two calc-silicate xenolith groups encountered in the Bushveld. Figure 2a shows the minerals and mineral assemblages present in the marginal zone xenoliths. The minerals connected by dashed lines coexist only in retrograde mineral assemblages displaying symplectic textures (assemblages 3 and 4 in Fig. 2a). The minerals connected by dotted lines do not coexist. Assemblages 1 and 2 appear in polygonal textures and indicate peak metamorphic conditions. Figure 2b represents the minerals and mineral assemblages that are present in the critical zone xenoliths.

B CALC-SILICATE XENOLITHS IN THE MARGINAL AND CRITICAL ZONE OF THE EASTERN BUSHVELD COMPLEX

1 Locality and General Description of the Marginal and Critical Zone Xenoliths

On the farm Hendriksplaats and Doornbosch two different groups of calc-silicates can be distinguished. The xenoliths on the farm Hendriksplaats are situated in a gabbronorite of the marginal zone (locality A in Fig. 1). Their exact location on the 1:50,000 map of South Africa (sheet 2430 CA Steelpoort) is 30°11'15" E and 24°38'00" S. Simplified maps of this area indicating the position of the xenoliths are presented in Figures 3 and 4a to 4c (xenoliths A1 to A6). These xenoliths were priviously mapped and described in detail by Willemse and Bensch (1964). The xenoliths or xenolithic fragments are relatively small and are either oval or wedge-shaped. They consist mainly of banded akermanite-monticellite rocks with varying amounts of spinel (Plate 1a and 1b). A thin pyroxenite seam often marks the contact between the xenolith and the gabbronorites (Plate 1c and 1d). As the mineralogical features of those xenoliths are very similar, the mineral assemblages and the mineral reactions, which led to their formation, are treated together.

On the farm Doornbosch the second group of xenoliths, that consist mainly of monticellite-brucite rocks, is situated in a feldspathic pyroxenite in the lower critical zone (locality C in Fig. 1). Samples from those xenoliths were taken from underground from the Winterveld Chromite Mine. Their exact location on the 1:50,000 map of South Africa (sheet 2430 CA Steelpoort) is: 30°11'20" E and 24°40'40" S. No mapping of the critical zone xenoliths has been undertaken.

2. Mineralogy of the Marginal Zone Xenoliths

The major minerals occurring in the marginal zone xenoliths are akermanite-rich $Ca_2MgSi_2O_7$ melilite (Ak), monticellite $CaMgSiO_4$ (Mo), fassaite and diopside $CaMgSi_2O_6$ (Di), forsterite Mg_2SiO_4 (Fo) and

calcite $CaCO_3$ (Cc). Accessory minerals in this group of xenoliths are spinel $(Mg,Fe^{2+})(Al,Fe^{3+})_2O_4$ (Sp), kalsilite $K[AlSiO_4]$, larnite Ca_2SiO_4, Ba-rich phlogopite $K_2(Mg,Fe)_6[Si_6Al_2O_{20}](OH,F)_4$, vesuvianite $Ca_{10}(Mg,Fe)_2Al_4[Si_2O_7]_2[SiO_4]_5(OH)_4$, wollastonite $CaSiO_3$ (Wo) and apatite $Ca_5[PO_4]_3(OH,F,Cl)$. In some places spinel is a major mineral and indicates relatively Al-rich portions in the xenoliths.

Willemse and Bensch (1964) gave a very thorough description of the minerals and their parageneses in the marginal zone xenoliths which shall only be repeated where necessary for the understanding of the discussion in the following chapters.

Some new mineralogical features were observed, which shall be briefly summarized.

2.1 Forsterite Exsolutions in Monticellite

Some of the observed monticellites from the locality A (Fig. 1) contain fine exsolution lamellae of forsterite parallel to (010) (Plate 1e and Analysis I3 in Table 1 and 1a). This was already microscopically observed by Willemse and Bensch (1964) from another locality (Wintersveld). These forsterite exsolutions were also described in the Cascade Slide xenolith (Adirondack Mountains) by Tracy (1978) and Valley and Essene (1980). They are quite rare in terrestrial rocks and appear more commonly in chondritic meteorites. Furthermore, this monticellite has an optically positive sign which is most unusual and is probably due to the high temperature of formation and distortion or restructuring of the crystal structure by solid solution and subsequent exsolution of forsterite in monticellite. The refractive indices for this high temperature monticellite are: n_x=1.640, n_y=1.644 and n_z=1.649 and indicate a temperature of formation of at least 1200°C (Adams and Bishop, 1985). Microprobe analyses showed that forsterite and monticellite are very close to end-member compositions.

2.2 Exsolutions in Akermanite

Akermanite also contains very fine exsolution lamellae (Plate 1f and 1g) that are too fine for quantitative microprobe analyses, but qualitative microprobe analyses strongly suggest that these exsolutions consist of diopside. Nurse and Midgley (1953) observed exsolutions of an undetermined mineral in synthesized akermanite, which they referred to as "peg structure". Yoder (1973) described this "peg structure" in melilite from a melilite basalt. This texture has not been described previously from thermally metamorphosed limestones

2.3 Occurrence of Ba-rich Phlogopite, Dehydroxylated Kinoshitalite and Kalsilite

Phlogopite is a common mineral in metamorphosed, impure magnesian limestones and dolomites. The chemical composition of the phlogopites that generally occur within the xenoliths is unusual. The grains are found as inclusions in polygonal akermanite (Plate 1h) and monticellite or in symplectic intergrowth in the mineral assemblage akermanite-diopside-monticellite-forsterite (Plate 2a). Ba-rich phlogopite was also observed in a very fine grained assemblage together with kalsilite, forsterite, diopside and wollastonite (Plate 2b), whereas in the same sample a coarser grained assemblage of kalsilite, forsterite and diopside was observed (Plate 2c). Microprobe analyses of these minerals are given in Table 1 and 1a (J21). The inclusions in akermanite and monticellite have remarkably high Ba contents (up to 14.60 wt.%) and can be referred to as kinoshitalite (Ba:K>1:2) (Yoshii and Maeda, 1975), which has also been reported from the Noda-Tamagawa mine in Japan (Yoshii and Maeda, 1975) and from the Alaska Range (Solie and Su, 1987). Some of the Ba-rich phlogopite grains found in the xenoliths are zoned and have outer parts which are totally dehydroxylated (analyses J6a (core) and J6b (rim) in Table 1a). The Ba content increases towards the rim of the mineral, concomitant with a decrease of the water-, alumina- and potassium content. No dehydroxylated Ba-rich phlogopite has, to the best of the author's knowledge, yet been documented in the literature. Trioctahedral micas have generally a very high thermal stability and the OH^- groups are strongly

bound in these micas (Olesch and Seifert, 1976). Yoder and Eugster (1955) showed that phlogopite decomposes at high temperatures (Fig. 5) to form orthorhombic kalsilite, leucite, forsterite and H_2O (vapour). Only one small occurrence at the outermost part of a xenolith could be found where Ba-rich phlogopite (Ba content <9 wt.%), kalsilite, forsterite, clinopyroxene and wollastonite form a mineral assemblage. Figure 5 shows three reactions that are pertinent to explain this mineral assemblage. The two prograde reactions describe the formation and the decomposition of phlogopite. The lower temperature reaction, from which the formation of phlogopite in impure magnesian limestones was assumed (e.g. Deer et al. 1975), was calculated by means of the thermodynamic data given in Table 2. The presence of clinopyroxene instead of leucite in the observed assemblage could be explained by the retrograde reaction

2wollastonite + leucite + forsterite = 2diopside + kalsilite,

the calculated position of which is also shown in Figure 5.

The occurrence of isolated Ba-rich mica inclusions in akermanite and monticellite indicates an increase of the stability field at higher temperatures due to the Ba content. In contrast, common phlogopite decomposes at lower temperatures than those necessary for dehydroxylation. The amount of the extension of the Ba-rich phlogopite stability field towards higher temperatures requires experimental work and data which are not yet available.

2.4 Larnite

Larnite occurs exclusively as rare, small, rounded inclusions in akermanite and seems to have formed before the akermanite during prograde metamorphism. A microprobe analysis (J8, Table 1a) shows it to be very pure and nearly stoichiometric Ca_2SiO_4.

2.5 Vesuvianite

Vesuvianite was found only in one sample where it occurs together with spinel in an about 2 cm wide band in akermanitefels. It has a

white or honey-yellow colour, forms fibrous aggregates and sheaves, but is rarely also seen to have a granular form. Its pseudomorphic replacement of melilite (Al_2O_3=8.77 wt.%) is obvious from Plates 2d and 2e. The interference colours of this vesuvianite are very low, usually anomalous blue or brown in the case of granular grains. Microprobe analyses of akermanite and vesuvianite of this assemblage are given in Table 1a (I15). Akermanite shows different degrees of alteration and it is evident that vesuvianite is an alteration product of this Al-bearing akermanite (melilite). Reactions that led to the replacement of melilite are discussed in Chapter D 1. A pseudomorphic replacement of melilite by fibrous idocrase in a zoned calc-silicate skarn situated in the Christmas Mountains, Texas, was described by Joesten (1974). There, the replacement of the Al-rich melilites occurred along veins. In the marginal zone xenoliths this replacement starts in the centre of the zoned melilites, because the Al-richer core favours the formation of vesuvianite (Chapter D 1).

3 Mineralogy of the Critical Zone Xenoliths

The dominant minerals in the critical zone xenoliths are monticellite $CaMgSiO_4$, periclase MgO (Pe) mostly altered to brucite $Mg(OH)_2$, merwinite $Ca_3MgSi_2O_8$ (Me) and gehlenite-rich melilite $Ca_2Al_2SiO_7$ (Ge). Spinel $(Mg,Fe^{2+})(Al,Fe^{3+})_2O_4$ (Sp) is the only accessory mineral.

3.1 Brucite and Periclase

Brucite occurs only with periclase, monticellite and spinel. Where brucite is the dominant mineral it forms together with monticellite the so called predazzites or brucite-marbles. Ferrobrucite $(Mg,Fe)(OH)_2$ replaces brucite along fissures and small cracks (Plate 2f). Periclase is always enclosed and obviously replaced by fibrous brucite. Remnants of forsterite and calcite are present in most of the observed brucites.

3.2 Monticellite

Monticellite occurs together with all the minerals present in the critical zone xenoliths. The exsolution lamellae of forsterite present in the critical zone monticellites are usually much wider than those observed in the marginal zone monticellites (Plate 2g). The optical sign of the monticellites with exsolutions is positive, while the monticellites without exsolutions have the usual optical negative sign. In and along the exsolution lamellae small spinel grains seem to be concentrated (Plate 2h) and appear to have exsolved together with the forsterite. This is only possible if a certain amount of aluminium can be dissolved in monticellite at high temperatures. As yet, this has not been proven.

3.4 Melilite

Melilites $Ca_2MgSi_2O_7$-$Ca_2Al_2SiO_7$ are less abundant than brucite and monticellite. The melilites in the critical zone as well as in the marginal zone xenoliths are strongly zoned in that the Al_2O_3 content increases towards the centre (Plate 3b and Table 1, Analyses Wila=rim and Wilb=centre). The average Al content in the critical zone melilites is higher than of those in the marginal zone melilites, which makes them more susceptible to alteration (Plate 3a). The influence of the composition of melilites on their alteration is extensively discussed in Chapter D 1.

3.5 Merwinite

Merwinite $Ca_3MgSi_2O_8$ occurs in two modes. The first consists of subidioblastic or rounded grains together with monticellite and melilite (Plate 3a and 3b). Merwinite displays the two systems of polysynthetic twinning lamellae intersecting at an angle of 43^o (Plate 3c), with c the twinning axis and {110} the twinning plane. This results in the so called "fishbone" pattern (Trüger, 1969) that is visible in some merwinite blasts (Plate 3b). The second type of merwinite forms polygonal grains which contain "lamellae" consisting, where fresh,

also of merwinite (Plate 3c). These "lamellae" can be distinguished from the host mineral by slightly higher refractive indices and different birefringence colours. Their arrangement reflects the pseudotrigonal crystal symmetry of the monoclinic merwinite (Moore amd Araki, 1972). These "lamellae" seem to alter faster than the host mineral and some are totally altered. Their width varies considerably, so that in some cases the "lamellae" seem to be the host mineral. These "lamellae" are no ordinary twin lamellae. They could be a high temperature modification, which preferentially replaces the low temperature modification along certain crystallographical directions. This remains speculative until more crystallographical work on these "lamellae" is carried out. Representative microprobe analyses of unexsolved merwinite (Wi), together with host-merwinite (Wia) that shows 'lamellae' (Wib) are given in Table 1. The host-merwinite comes closest to the stoichiometric composition $Ca_3MgSi_2O_8$, whereas the "lamellae" seem to be slightly depleted in Ca and enriched in Si.

Neither olivine nor clinopyroxene have been observed together with merwinite, and this association has not, to the best of the author's knowledge, been reported from any other natural occurrence. This indicates that this paragenesis is metastable.

3.6 Spinel

Spinel $(Mg,Fe^{2+})(Al,Fe^{3+})_2O_4$ is not very abundant in the critical zone xenoliths but appears to be a major mineral in some places especially in association with monticellite and brucite. It never occurs together with merwinite. The size of the spinel grains varies (Plate 3d). It occurs in the form of stringers, chain-like, and intergranular as isolated grains or as fine grained inclusions in almost all minerals present, except merwinite. An analytical comparison of the spinels from the marginal zone xenoliths (J6, J8 and I3 in Table 1a) with those of the critical zone xenoliths (Wi7 and Wia in Table 1a) shows that the latter are richer in iron (almost only Fe^{3+}), while the spinels of the marginal zone xenoliths contain both Fe^{2+} and Fe^{3+}. The chemical differences are reflected by a colour difference in that the iron-poor spinels have a green colour while the

iron-rich spinels have a yellowish-brown colour in transmitted light.

4 Mineral Parageneses and Inferred Bulk Composition

The crucial mineral parageneses in the marginal zone xenoliths are (Fig. 2a) the following:

1: calcite-akermanite-monticellite (±spinel)
2: calcite-forsterite-monticellite (±spinel)
3: akermanite-diopside-monticellite (±spinel)
4: diopside-forsterite-monticellite (±spinel).

The mineral assemblage monticellite-wollastonite (±spinel), resulting from the previously mentioned retrograde reaction of akermanite, is not shown in Figure 2a. The mineral assemblages 3 and 4 connected by the dashed lines in Figure 2a coexist only under retrograde metamorphic conditions and display symplectic textures. In contrast, mineral assemblages 1 and 2 appear in polygonal-granoblastic textures and indicate peak metamorphic conditions.

Figure 2b shows mineral assemblages that occur in the critical zone xenoliths. They are:

5: calcite-periclase-monticellite (±spinel)
6: merwinite-akermanite-monticellite (±spinel)
7: forsterite-periclase-monticellite (±spinel).

Although spinel may sometimes constitute part of the assemblages, it is not regarded to form part of the respective parageneses (Chapter B 5.5) and is consequently shown in parentheses.

Some of the above-mentioned parageneses are known from other occurrences in metamorphic rocks, e.g. parageneses 1 and 6 from the gabbro-lime contact zone of Camas Mòr, Muck, Inverness-shire (Tilley, 1948), 2 and 4 from monticellite-marble at Cascade Mountain, Adirondack Mountain (Tracy et al., 1978). The parageneses 3 and monticellite-wollastonite were found in the Cascade Slide xenolith, Adirondacks (Valley and Essene, 1980). Parageneses 5 and 7 have not been described before from a natural occurrence.

In Table 3 mineral assemblages together with textural features are compiled. Microprobe analyses of the important minerals occurring in these assemblages are given in Table 1 and 1a. Rocks from marginal zone xenoliths are designated with "J" and "I", whereas those from the critical zone xenoliths are designated "Wi".

Modal analyses of the marginal zone xenoliths indicate that the original rocks were siliceous dolomites with their bulk compositions plotting somewhere near the centre of the compositional triangles shown in Figures 2a. Most of the reactions traced in the xenoliths are shown in Figures 6, 7 and 8, of which the only common compositional field is represented by the shaded area in Figure 2a. The construction of the P-T-X_{CO2} diagrams shown in Figures 6, 7 and 8 is discussed in Chapter 5.

The mineral parageneses of the critical zone xenoliths provide less constraints on the possible bulk composition. It is assumed that they also originated from a siliceous dolomite, but they contain less silica than the marginal zone xenoliths. The appearance of periclase in the critical zone xenoliths is probably not only due to metamorphic conditions but also to a higher MgO content.

In order to obtain the stability fields of the mineral parageneses present in the marginal and critical zone xenoliths, it is necessary to compute all possible reaction curves, with pressure, temperature and the fluid phase composition as variables.

5 The Construction of P-T Diagrams and a Petrogenetic Grid in the System CaO-MgO-SiO_2-CO_2

5.1 Introduction

This chapter is mainly based on Zen's (1966) discussion on the construction of P-T diagrams for multicomponent systems after the method of Schreinemakers (1915-25).

The Gibbs phase rule (F=n+2-p) provides the degrees of freedom (F)

of a reaction involving a number (n) of independent components that are necessary to define the compositions of all phases in the system. A system is termed invariant, univariant, divariant and so forth when F=0,1,2 and so forth. By convention an invariant, univariant and divariant equilibrium is designated by the phase or phases that do not participate in the respective equilibrium assemblage.

In the simplest case one deals with n+2 phases in a system of n components and n+2 reaction curves. Along each univariant reaction curve n+1 phases are in equilibrium. Within a divariant field between the univariant reaction curves, n phases are supposed to be stable, while at each invariant point n+2 phases are in equilibrium.

Zen (1966), Roseboom and Zen (1982) and Guo (1984) discussed some basic assumptions for equilibria consisting of n+k (k>2) phases. They state that the total number of possible in-, uni- and divariant assemblages in a given multisystem must obey the combinatorial rule. This states that the maximum number of invariant points (=invariant assemblages) in an n+k (k>2) phase multisystem will be:

$$^{n+k}C_{n+2}=(n+k)!/(n+2)!(k-2)!,$$

where C is the maximum number of possible invariant assemblages. In a nondegenerate system each invariant point is intersected by n+k univariant reaction curves.

According to Zen (1966) a system is called degenerate if

a) two or more phases, participating at a given invariant point, have the same composition, or
b) if three or more phases are compositionally colinear (for n=3,4,5,...); four or more phases are compositionally coplanar (for n=4,5,6,...), and so forth.

The compositional triangle in Figure 2a can be taken as an example of a compositional colinearity of phases in a ternary (n=3) system. Calcite, akermanite, diopside are colinear, so are akermanite, monticellite and wollastonite.

Compositional coplanarity can be explained with the aid of CO_2 in this system. Carbon dioxide is a dependent phase and component as it occurs only in association with calcite. If CO_2 were an independent

phase and component (n=4; p=7), all phases but calcite could be regarded as compositionally coplanar. If compositional colinearity and/or coplanarity exists, less than (n+k) univariant reaction curves will emit from each invariant point. P-T diagrams that are degenerate in this sense will be discussed later in this chapter.

Applying the combinatorial rule to the ternary system shown in Figure 2a including merwinite as an additional phase results in 21 invariant points and invariant assemblages, each involving (n+2) phases (Reaction 1 to 20 in Table 4). Each invariant point is part of a subsystem. The compositional triangles and a listing of all reactions belonging to all the 21 subsystems is presented in Table 5a and are diagrammatically presented in Figure 9. The phases in brackets behind the subsystem number or reactions do not participate in the respective subsystems or reactions and are conventionally used to label them. Merwinite is included in these considerations because even though not present in the marginal zone xenoliths, the absence of merwinite gives important P-T constraints (Chapter 5.2).

Each ternary subsystem (n=3) involves 5 (=n+2) phases. If the phases show a nondegenerate relation, 5 univariant reaction curves should intersect the invariant point, in which all 5 phases are in equilibrium. Furthermore, 5 univariant assemblages consisting of 4 (=n+1) phases and 10 divariant assemblages consisting of 3 (=n) phases should exist about the invariant point. With the exception of subsystem 11 all subsystems are degenerate in Figure 9 as they display in each case at least one compositionally colinear relation of three phases.

5.2 Discussion and Application to the Minerals and Mineral Assemblages in the investigated Xenoliths

The upper and lower pressure and temperature limits of the peak metamorphic conditions in the marginal zone xenoliths can be calculated by means of the compositional triangle in Figure 2a which presents the phases dominating in the marginal zone xenoliths. There are 6 (+merwinite=7) solid phases consisting of 3 independent components.

For geometrical analyses it is sufficient to deal only with 3 components (CaO-MgO-SiO_2), because CO_2 is limited to reactions in which calcite is involved, and therefore is not an independent component. An extension of this system by the components Al_2O_3 and H_2O is considered in Chapters B 5.3 and B 8.4, respectively. As FeO appears only in minor amounts, it has been omitted in the following considerations. Tracy et al. (1978) concluded that small amounts of iron would not lower the temperature significantly.

The position of the univariant curves about the invariant points can be calculated by means of the computer program discussed in Appendix II and the thermodynamic data compiled in Table 2. The relative position of the stable and metastable parts of the univariant curves about the invariant points can be ascertained with a geometrical analysis based on Schreinemakers rule (Zen, 1966; Roseboom and Zen, 1982; Guo, 1984). Furthermore, Schreinemakers analysis gives an indication as to the relative position of the univariant curves, which should agree with the calculated results. Subsystem 1 and 5 (Fig. 10) shall serve as examples.

According to the definition of Zen (1966), subsystem 1 is degenerate. In subsystem 1 (Fig. 10) there exists a compositional colinearity of diopside, akermanite, merwinite and also of forsterite, monticellite and merwinite. From the reactions involving monticellite, diopside, akermanite and forsterite it is obvious that diopside and akermanite as well as forsterite and monticellite always appear on opposite sides of the reactions. This implies that the stable parts of [Fo] and [Mo], both describing the reaction 3Mo + Di = 2Ak + Fo, as well as [Di] and [Ak], designating the reaction Me + Fo = 3Mo, appear on different sides of the reaction curve ([Me] in subsystem 1, Fig. 10). In the case of subsystem 1, the stable parts of the reaction curves designated by [Mo] and [Di] coincide with the metastable extensions of reaction curves [Fo] and [Ak], which have their stable extension on the other side of the invariant point, and vice versa. Each of these reactions involve less than (n+1) phases, which makes them degenerate with respect to subsystem 1. Reaction [Me] is not degenerate and consists of a stable and metastable part on different sides of the invariant point. On one side of reaction [Me] monticel-

lite and diopside is stable, while on the other side akermanite and forsterite are stable besides each other. This fixes the relative position of univariant curve [Me], because the stable parts of curve [Mo] and [Di] have to be on one side of curve [Me], while the stable parts of curve [Ak] and [Fo] have to be on the other side. Because the phases in brackets do not participate in the respective reaction, due to absence or metastability, the direction of [Me] with respect to the temperature is given. Diopside has to appear on the low temperature side of reaction [Me], because the "diopside absent" reaction [Di] indicates that diopside is not supposed to be stable at higher temperatures in subsystem 1. Reaction [Mo] as well as [Di] lie on the high-temperature side of [Me] which determines diopside and monticellite to occur together only on the low-temperature side of [Me]. The direction of a reaction obtained with this method must agree with the calculations of the Gibbs free energy of the reaction at different P-T conditions. As [Me] indicates the stable part of the "merwinite absent" reaction, no merwinite may occur in the divariant fields bordered by the stable parts of [Me]-[Fo] and [Me]-[Di]. This determines the stable and metastable parts of [Me].

In subsystem 5 (Fig. 10) the combined curves [Me][Di] and [Wo][Mo] have their respective stable parts on the same side of the invariant point and become metastable by crossing it (dashed line). This can be inferred from the fact that merwinite, diopside and wollastonite, monticellite, respectively, lie on the same side of reaction [Ak]. Zen (1966) referred to this general rule as the "coincidence rule".

The chemography in the sectors (divariant fields) about the invariant point 1 is shown by means of compositional triangles indicating the critical mineral parageneses for each sector. For instance, akermanite-forsterite-monticellite is a critical mineral assemblage which can only be stable in the sector that is bordered by the stable part of reaction [Me] and [Di]. That means that all phases, except those that designate the bordering reaction curves, are stable within the divariant field. While the critical mineral parageneses is stable only in one specific divariant fields, other mineral parageneses that are possible in this divariant field, but which are not critical, can also be stable in other sectors. The noncritical parageneses can also

be inferred from the chemographic representations within the divariant fields, and include minerals which are not explicitely named at each subtriangle. For instance, akermanite-diopside-forsterite and akermanite-merwinite-monticellite are not only possible noncritical mineral parageneses in sector [Me]-[Di], but are alo noncritical parageneses in sectors [Di]-[Mo] and [Me]-[Fo], respectively.

The first 21 subsystems are derived from the compositional triangle in Figure 2a including merwinite as additional phase. If periclase is included as an additional phase, the number of subsystems (invariant points) increases to 56. Because periclase and wollastonite are not stable together (Chapter B 5.5), this number can be reduced to 36 (Subsystems 1 to 36 in Table 5a).

5.3 The Influence of a Fluid Phase on the P-T Position of a Decarbonation Reaction

Until now, only solid-solid reactions have been taken into consideration. Subsystem 2 in Figure 8 is an example in which a fluid phase in the form of a H_2O-CO_2 mixture is involved. Monticellite is a so called absolute indifferent (Zen 1966) phase and does not participate in any of the reactions of subsystem 2. Nonetheless, as monticellite is present in the chemography of this subsystem (upper right corner in Figure 8), it is part of all mineral parageneses within the divariant fields. The position of decarbonation reactions and the respective invariant points in a P-T field is a function of the fluid phase composition (X_{CO2}). The position of the decarbonation reactions and the invariant points at different carbondioxide molefractions X_{CO2}=0.1, 0.3 and 1.0 are indicated in most of the subsystems that involve decarbonation reactions.

The direction of a decarbonation reaction and also most of other devolatization reactions can usually be predicted by using the following criteria:

1) A reaction that produces CO_2 leads usually to an entropy increase and therefore is favored by increasing temperature.
2) The products of a decarbonation reaction have usually a greater

molar volume (due to a great molar volume of gases) and therefore are favoured by low pressures.

5.4 Construction of a Petrogenetic Grid

In order to obtain a petrogenetic grid (Fig. 11) that comprises the components CaO-MgO-SiO_2-CO_2, the solid phases akermanite, calcite, diopside, forsterite, merwinite, monticellite, periclase and a fluid phase consisting of a CO_2-H_2O mixture, it is necessary to plot all subsystems (1 to 36) on top of one another. Usually, a reaction is part of different subsystems and connects different invariant points with one another. In all subsystems these reaction curves are stable or metastable over different P-T ranges. In the case where two stable parts of univariant reaction curves are plotted on top of each other, the resulting curve remains stable. If only a single metastable part of a univariant curve covers a stable univariant curve it will result in the metastability of the specific reaction over the specific range. Any invariant point that finds its position on a metastable part of such a curve becomes automatically metastable.

5.5 Inferred Metastability of Parageneses Involving Periclase and Wollastonite

Figure 12 illustrates the chemographic relations of 20 invariant points (subsystem 73 to 92), in which wollastonite and periclase are represented together. Eight reactions (reaction 33-40 in Table 4) involve wollastonite and periclase simultaneously. In each of the 8 P-T diagrams (subsystems), outlined in Figure 7 and 8, at least one of these reactions participate.

From thermodynamic calculations it can be concluded that only 5 invariant points exist at a realistic P-T range (subsystems 78, 79, 80, 87, 91). Three invariant points plot at "negative" pressures or temperatures (subsystems 74, 85, 86) and prevents them from being stable. After comparing all 8 subsystems (Fig. 13a and 13b), there exists no reaction involving wollastonite and periclase that is stable

in all 8 subsystems, over a realistic P-T range (P <100 kbar, T <2000°C). Because one line of evidence for metastability is sufficient to declare a specific curve as metastable in the overall system, a treatment of the remaining 12 subsystems is not necessary. Therefore, the addition of subsystems involving periclase and wollastonite to the proposed petrogenetic grid leads only to an increase of 20 metastable invariant points (73-92 in Table 5c) and eight univariant reactions (33-40 in Table 4) that are metastable over a realistic P-T range.

5.6 Al_2O_3 as an Additional Component

Spinel is fairly abundant in some places and occurs in the form of stringers, intergranular and as inclusions in most of the phases present (e.g. Plate 3d). For this reason it seems necessary to add Al_2O_3 as a further component to the system $CaO-MgO-SiO_2-CO_2$. This increases the number of invariant points (subsystems 43-72 in Table 5 and Appendix III) and the number of theoretically possible reactions (41-65 in Table 4). The methods described in Chapter B 5.4 were applied to distinguish between stable and metastable reactions and invariant points. From this it follows that only three invariant points shown in subsystems 58, 61 and 62 are stable at possible P-T conditions. The reaction

spinel + 2monticellite = gehlenite + periclase + forsterite

(reaction 58 in Table 4) in subsystems 61 and 62 limits the stability of monticellite-spinel-bearing assemblages to high temperatures. As gehlenite is usually not of end-member composition, this limiting reaction occurs usually at lower temperatures than indicated in Figure 14a and 14b, while the invariant point occurs at lower pressures. From this it is evident that there is no spinel forming reaction during prograde metamorphism in the presence of CO_2 and at reasonable pressures (P >0.5 kbar). During retrograde metamorphism the "CO_2-absent" reaction

gehlenite + periclase + forsterite = spinel + 2monticellite

becomes stable, but no mineral paragenesis was observed that indicates that this retrograde reaction took place.

From the previous considerations it must be concluded that the

spinels formed at much earlier stages of metamorphism, probably from clay minerals without being involved in any of the high temperature reactions. Therefore, the component Al_2O_3, as well as spinel and gehlenite have been omitted from the petrogenetic grid (Fig. 11), because there is no indication that any of the stable reactions involving gehlenite and spinel occurred within the rocks under consideration. It can be mentioned that, in the system considered, the only stable reaction producing spinel at pressures between 0.5 and 7.5 kbar is

gehlenite + periclase + forsterite = spinel + 2monticellite.

This leads to the conclusion that the Al_2O_3 component present in melilites does not stem from spinels but from akermanite-producing reactions involving Al_2O_3-bearing clinopyroxenes which formed at a much lower temperatures (Chapter B 8.1).

6 Thermodynamic Data for Akermanite, Monticellite and Merwinite. A Comparison of Experimental Results with Calculations

In this chapter thermodynamic data for the minerals akermanite, monticellite and merwinite will be considered. The calculations of reaction equilibria involving these minerals will be compared with experimental brackets for various solid-solid and solid-fluid reactions (Table 6 and Fig. 15a and 15b) in order to show the reliability of the thermodynamic data used and to prove their internal consistency.

With the exception of the enthalpy of formation data for akermanite, monticellite and merwinite, the isothermal compressibility coefficients and the thermal expansion coefficients, all thermodynamic data were taken from Helgeson et al. (1978). These authors mentioned that their tabulated enthalpy data for akermanite, monticellite and merwinite, which are based on acid calometry by Neuvonen (1952a,b), are not always consistent with experimental results. Furthermore, Helgeson et al. (1978) state that neither Walter (1963a,b) nor Yoder (1968) determined the extent of solid solution in akermanite, monti-

cellite and merwinite which could have affected their experimental results. Figure 15a shows the experimentally bracketed equilibrium reactions of Yoder (1968, 1973) which involve akermanite, monticellite and merwinite. The recalculation of these experimentally determined equilibrium reactions using the data tabulated in Helgeson et al. (1978) and the computer program discussed in Appendix II, results in the dotted reaction curves in Figure 15a. The results of these calculations are identical with those of Helgeson et al. (1978) for the same reactions. For the reactions

2wollastonite + 2monticellite = diopside + merwinite,

diopside + merwinite = 2akermanite, and

wollastonite + monticellite = akermanite

the recalculated reaction equilibria are very close to the experimental brackets. For the reactions

3monticellite + diopside = 2akermanite + forsterite, and

3monticellite = merwinite + forsterite,

though, the recalculations result in temperatures which are about 400°C too high. Helgeson et al. (1978) state that, although either the experiments or the used thermodynamic data could be in error, a less negative enthalpy of formation of 3580 cal/mol for akermanite (ΔH^{o}_{298}=-923357 cal/mol) and monticellite (ΔH^{o}_{298}=-537220 cal/mol) and 7160 cal/mol for merwinite (ΔH^{o}_{298}=-1084296 cal/mol) could yield better agreement with the experimental results. Even though these new data are still not in very good agreement with all experimental results, the general assumption that the enthalpies are less negative was confirmed by the experimental work of Brousse et al. (1984) who measured enthalpies of formation, close to those assumed by Helgeson et al. (1978), by alkali borate solution calorimetry. Their measured enthalpies of formation of akermanite, monticellite and merwinite at 298°K which are less negative by 3160 cal/mol (ΔH^{o}_{298}=-923777 cal/mol), 3270 cal/mol (ΔH^{o}_{298}=-537530 cal/mol), and 7250 cal/mol (ΔH^{o}_{298}=-1084206 cal/mol), respectively, than those tabulated by Helgeson et al. (1978). Applying these enthalpies of formation together with all other thermodynamic data from the tabulation presented by Helgeson et al. (1978), yields an excellent agreement with the experimentally bracketed reactions

wollastonite + monticellite = akermanite,

calcite + diopside = akermanite + CO_2,

$$2\text{calcite} + \text{diopside} + \text{forsterite} = 3\text{monticellite} + 2CO_2, \text{ and}$$

$$\text{calcite} + \text{forsterite} + \text{akermanite} = 3\text{monticellite} + CO_2$$

(Fig. 15a and 15b). The experimentally bracketed positions of the reactions involving merwinite (Yoder, 1968) and the experimental results on mineral reactions involving solid solutions of akermanite, monticellite and forsterite (Yoder, 1973) do not match the calculated reaction curves (Fig. 15a). If an enthalpy of formation of ΔH^{o}_{298}= -1085060 cal/mol, which lies between the values of -1084206 cal/mol proposed by Brousse et al. (1984) and -1091456 cal/mol tabulated by Helgeson et al. (1978), is assumed, a much better agreement with the experimentally bracketed reaction equilibria involving merwinite is obtained. The difference of 854 cal/mol (=0.08%) from the enthalpy of formation of merwinite ascertained by Brousse et al. (1984) is in their given range of error, which amounts to about $\pm$0.9%, but depresses significantly the pressures at which the equilibria reactions are calculated to occur according to these authors (Fig. 15a). However, the recalculations of reactions involving phases of end-member composition still do not match Yoder's (1973) experimental results involving solid solutions of akermanite, monticellite and forsterite (Fig. 15a). Brousse et al.'s (1984) enthalpies of formation for akermanite and monticellite, the corrected enthalpy of formation value for merwinite together with the internally consistent dataset tabulated by Helgeson et al. (1978) was used for all mineral equilibria recalculations. The deviation from the experimental results are probably due to solid solution effects between monticellite and forsterite discussed later in this chapter.

More recent data concerning the heat capacities of monticellite and akermanite were introduced by Sharp et al. (1986) and Hemingway et al. (1986), respectively. Sharp et al. (1986) introduced the heat capacity term for monticellite $Cp(cal/mol^{o}K)$=

$$55.3069-2.03906\times10^{-4}T-0.29814\times10^{6}T^{-2}-388.007\times T^{-0.5}-0.319\times10^{-6}T^{2}$$

together with an entropy of S^{o}_{298}=25.8365$\pm$0.04 cal/mol^{o}K. Hemingway et al. (1986) ascertained from experiments the heat capacity, the enthalpy of formation, and the entropy for akermanite to be: $Cp(cal/mol^{o}K)$=

$$18.677+39.6114\times10^{-3}T-16.22969\times10^{5}T^{-2}+684.6654\times T^{-0.5}-7.99168\times10^{-6}T^{2},$$

ΔH^{o}_{298}=-923637.67$\pm$956 cal/mol, and S^{o}_{298}=50.7887$\pm$0.09 cal/mol^{o}K, respectively. Calculations based on the data of Sharp et al. (1986) and

Hemingway et al. (1986) provide the best match with the experimental results on minerals close to end-member composition, if the enthalpy of formation of akermanite and monticellite is assumed to be ΔH^{o}_{298}=923090 cal/mol and ΔH^{o}_{298}=537900 cal/mol, respectively. Both values are in the range of the experimental error given by Brousse et al. (1984) and Hemingway et al. (1986). The results of recalculations based on the corrected enthalpy of formation values are also given in Figure 15a. They are identical with the recalculations based on the data proposed by Helgeson et al. (1978) and Brousse et al. (1984), except for the slight correction for merwinite. Furthermore, they also agree very well with the experimental brackets for the reactions

3monticellite + diopside = 2akermanite + forsterite,

calcite + diopside = akermanite + CO_2,

2calcite + diopside + forsterite = 3monticellite + $2CO_2$, and

calcite + forsterite + akermanite = 3monticellite + CO_2

(Fig. 15b) which have been experimentally investigated by Walter (1963a).

The reactions

calcite + forsterite = monticellite + periclase + CO_2

(reaction e in Fig. 15b), and

calcite + akermanite = merwinite + CO_2

(reaction d in Fig. 15b) were calculated to occur at higher temperatures than those determined experimentally by Walter (1963b) and Shmulovich (1969), respectively. The experimental results of Walter (1963a and b) were doubted by Helgeson et al. (1978) as they described them to plot on top of each other and therefore contravene the phase rule. This is actually true only for reaction a, b and c in Figure 15b, because reaction e plots at slightly lower temperatures (Walter, 1963b). On the basis of natural occurrences and thermodynamic calculations, Turner (1968) states that reaction e in Figure 15b must lie at higher temperatures (ca. 220°C at 700 bar) than those proposed by Walter (1963b), which was also borne out by Sharpe (1986) and the calculations carried out in the present thesis. The reasons for the difference between the caculated and the experimentally investigated positions are not clear. One reason could be the addition of a small amount of water which increased the rate of reaction under experimental conditions considerably (Walter, 1963b).

The experimentally investigated (Shmulovich, 1969) and the recalculated position (Sharp et al., 1986; present thesis) of the reaction

$$\text{calcite} + \text{akermanite} = \text{merwinite} + CO_2$$

(reaction d in Fig. 15b) show a difference of ca. 40°C (at 700 bar). The reason for this difference has to remain unexplained.

Sharp et al. (1986) used a dataset based on sources different from those which served for Helgeson et al.'s (1978) tabulation. While most data are similar or comparable, Sharp et al. (1986) described a problem in fitting merwinite involving reaction curves to the experiments and assumed that the entropy data for merwinite, which was measured by Weller and Kelley (1963), are incorrect. This problem can be overcome by applying the data for merwinite discussed above and listed in Table 6. The discrepancy noted by Sharp et al. (1986) is evidently due to the different molar volume data used by these authors and by Helgeson (1978) (2.35 cm^3 and 2.50 cm^3, respectively).

The positions of the decarbonation reactions caculated with the data presented by Sharp et al. (1986) are, with one exception, identical with those calculated by means of the dataset presented in Table 6. This exception involves the reaction

$$\text{calcite} + \text{forsterite} = \text{monticellite} + \text{periclase} + CO_2$$

(reaction e in Fig. 15b), which should lie according to Sharp et al. (1986) on the lower temperature side of the reaction

$$\text{calcite} + \text{akermanite} = \text{merwinite} + CO_2$$

(reaction d in Fig. 15b), and therefore contradicts the calculations presented in this thesis. As periclase is the only mineral which is not involved in any of the other reactions found to be identical with the calculations presented of Sharp et al. (1986), it appears very probable that the thermodynamic data for periclase or a calculation error causes this discrepancy. Recalculations of the position of this reaction by using the thermodynamic data of periclase tabulated by Robie and Waldbaum (1978) and Helgeson et al. (1978) clearly places reaction e on the high temperature side of reaction d. The tabulated data of the Gibbs free energy of formation, entropy and molar volume is very similar or identical to that used by Sharp et al. (1986) and need to be very different to cause a significant change in the position of the decarbonation (solid-fluid) reactions.

It has to be emphasized that a relatively small change in the enthalpy of formation values often has a great influence on the position of the solid-solid reaction lines. Taking the reactions

2wollastonite + 2monticellite = diopside + merwinite, and

diopside + merwinite = 2akermanite

(Fig. 15a) for example shows that an error in the enthalpy of formation of akermanite of $\pm$956 cal/mol ($=\pm$0.1%), as indicated by Hemingway et al. (1986), results in an uncertainty of the positions of the reactions of more than $\pm$400°C. The slope of a solid-solid reaction line, on the other hand, is mainly determined by the entropy, heat capacity and molar volume data of the participating minerals, and slight errors in their determination have less pronounced effects on the position of the mentioned reaction lines.

From the previous paragraphs it becomes obvious that the available thermodynamic data are not always consistent. The introduction of each new set of data has to be tested as to its consistency with other existing thermodynamic data as well as experimental results involving the respective phase. As long as inconsistencies of thermodynamic data exist it is generally accepted that the data may be adjusted within certain limits to fit independent experimental results. The thermodynamic data of akermanite, monticellite and merwinite presented in Table 2 required the least adaption of experimentally investigated data to match the experimentally investigated equilibrium reactions considered in Figure 15a and 15b, as none of the changes exceeds the experimental errors.

Sharp et al. (1986) discussed the discrepancies of their recalculated positions of the end-member reactions 3monticellite = merwinite + forsterite, and 3monticellite + diopside = 2akermanite + forsterite and the same reactions involving solid solutions of akermanite, monticellite and forsterite (Yoder, 1973), which are shown in Figure 15a. They ascribed these discrepancies to solid solutions, mainly involving monticellite and forsterite as experimentally investigated by Adams and Bishop (1985), which have the effect of shifting the recalculated reaction lines towards the experimentally determined positions (Sharp et al. 1986). Nevertheless, there are strong indications of a phase transition of monticellite at temperatures $\geq$1200°C (Chapter B 2.1) and

a concomitant change of the thermodynamic properties, including entropy and heat capacity, can be expected. This, together with the existence of solid solution between forsterite and monticellite, could also result in a shift of the recalculated equilibrium position of the reaction 3monticellite = merwinite + forsterite. At about 1200°C and 10 kbar the experimental brackets coincide with the recalculated position of the reaction, but at higher and lower temperatures the discrepancy increases in that the reaction involving the end-members at ±1400°C is calculated to take place at about 3 kbar compared with about 8.5 kbar.

A further comparison of experimentally determined reaction equilibria with calculated positions of reaction curves at temperatures lower than the above-mentioned ones is presented in Chapter C 3.6.1.

7 Composition and Mixing Behaviour of the Fluid Phase

7.1 Composition of the Fluid Phase

The composition of the fluid phase taking part in metamorphic reactions has a major influence on the pressure and temperature conditions under which equilibrium reactions occur. The dilution of a pure fluid phase that evolves from a mineral reaction shifts the reaction temperatures usually towards lower temperatures. In metamorphic decarbonation reactions H_2O is the most common diluent and is often assumed to be present in order to facilitate high temperature decarbonation reactions. Tracy (1978) and Valley and Essene (1980) postulate a very low X_{CO2} mole fraction in the fluid phase to produce mineral parageneses comprising akermanite, monticellite and wollastonite in the Cascade Slide Xenolith in the Adirondacks and in the Adirondack marbles. Nearby metapelites were assumed to be the source of the diluting H_2O.

Mineral reactions and invariant points at different values of X_{CO2} (0.1, 0.3, 1.0) are shown in most of the present P-T-X_{CO2} diagrams (Fig. 6 to 8 and Appendix III). During the formation of the specific high temperature mineral assemblages found in the Bushveld xenoliths a

fluid phase composition with X_{CO2} near to unity can be assumed. This is based on the following considerations:

1) The decomposition and dehydration of water-bearing sedimentary minerals begin usually at much lower temperatures than those reached within the xenoliths. In general, low-temperature fluids are water dominanated but the content of CO_2 increases with grade if carbonate rocks are present (Fyfe et al. 1978). With the exception of minor amounts of partly dehydroxylated Ba-rich phlogopite, no water-bearing minerals were found. Winkler (1979) stated that no noticeable dilution of a CO_2-rich phase takes place even when water is liberated in the surrounding noncarbonate rocks during metamorphism. He also mentioned that there is no extensive mixing of fluids produced in various layers of sediments so that the X_{CO2} tends to remain high in carbonate rocks.

2) Influx of water into the xenolith during decarbonation is improbable because the decarbonation reactions would ensure that the partial pressure of the fluid phase within the xenolith was equal to the total pressure, while the partial pressure of the fluid phase within the surrounding magma was much lower.

3) Relatively fast heating and concomitant degasing during decarbonation not only results in a calculated loss of volume of ca. 40%, but also prohibits magmatic fluids from pervading the xenoliths.

4) Fluid inclusions in high grade rocks mostly contain high concentrations of CO_2 or are almost pure CO_2 (Roedder, 1984).

7.2 Mixing Behaviour of the Fluid Phase

For the thermodynamic calculations of reaction equilibria involving a fluid phase consisting of H_2O and CO_2 it is necessary to calculate their fugacities at different pressures and temperatures. A knowledge of these fugacities allows the calculation or prediction of P-T-X_{CO2} conditions of mineral reactions involving a fluid phase consisting of H_2O and CO_2, which are the most abundant components in metamorphic fluids. The behaviour of H_2O-CO_2 mixtures at elevated temperatures is still under discussion. There exists a miscibility gap between H_2O and CO_2 at temperatures lower than the critical temperature of water (T $<373^oC$)(e.g. Fyfe et al. 1978). At higher temperatures this miscibility gap disappears, but H_2O and CO_2 still do not mix ideally due to

intermolecular interaction forces.

There are various models explaining the behaviour of the fluid phase. Kerrick and Jacobs (1981) applied a non-ideal mixing model for H_2O and CO_2 at temperatures less than 800°C (P>1 kbar), whereas de Santis (1974) and Flowers (1979) preferred a non-ideal mixing model for H_2O and CO_2 even at highly elevated temperatures. They considered a positive deviation from ideality at temperatures lower than 650°C and a negative deviation from ideality at higher temperatures. The latter is due to the complex-forming reaction of water and carbon dioxide ($H_2O + CO_2 = H_2CO_3$). Chou and Williams (1977, 1979) derived negative departures from ideal mixing in H_2O-CO_2 mixtures at 600 and 700°C and pressures to 8 kbar. The temperatures of high-grade reactions involving a CO_2-H_2O mixture are therefore lower than those estimated from an ideal mixing model, especially at highly elevated temperatures. De Santis et al. (1974) and Flowers (1979) assumed that the negative deviation from ideality is still not sufficient to explain the discrepancy between many calculated and experimentally investigated positions of high-temperature decarbonation reactions. This is borne out by the experiments carried out by Zharikov et al. (1977). These experiments involved calcite, forsterite, diopside, akermanite, monticellite, merwinite and periclase at temperatures higher than 700°C and a pressure of 1 kbar. Zharikov et al. (1977) compared their results with other experimental results (Walter, 1963; Shmulovich, 1969) and calculations based on those experiments and ascertained reaction temperatures for low carbon dioxide mole fractions which are even lower than those calculated after de Santis et al. (1974) and Flowers (1979).

It can be assumed that the negative deviation from ideality is due to further complex-forming reactions in which a mineral phase participates. The most likely participant in high temperature reactions involving calc-silicates is calcite (e.g.: $CaCO_3 + CO_2 + H_2O = CaH_2[CO_3]_2$). The excess energy of reaction for H_2O and CO_2, respectively, is most probably due to complex-forming reactions involving calcite at temperatures higher than 700°C. In a first approach, the following term is used to evaluate this molar excess free energy:

$$G^{ex}(cal) \cong [(51.0 - 0.053 * T) * X^2] / 0.004184,$$

where T is the temperature in K, the mole fraction X refers to H_2O in decarbonation reaction and to CO_2 in a dehydration reaction. This term is derived from fitting the experimentally determined positions of high-temperature decarbonation reactions (Zharikov et al. 1977) and produces an even more negative deviation from ideality at high temperatures than described by the modified Redlich-Kwong equation (Flowers, 1979). Figures 16a to 16d represent graphical comparisons of the experimental results of Zharikov et al. (1977) and the different mixing models, where $CaH_2[CO_3]_2$ designates calculated reaction equilibria involving the introduced excess enrgy term. For reaction a), b) and e) of Table 6 represented in Figure 16a to 16c, respectively, an excellent agreement with the experimental results is obtained. Even though the calculated equilibrium temperatures are somewhat too low for reaction curve d) (Fig. 16d), the applicability of this factor is furthermore supported by the very good results, that were obtained in Chapter C 3.6.1, where this factor was applied to decarbonation reactions that involve calcite and CO_2 at temperatures higher than 700°C. As no experimental results on complex-forming reactions between fluids and minerals at temperatures higher than 700°C and pressures in the kbar range are available, this empirical "make fit"-factor was used for all reactions occurring at temperatures higher than 700°C that involve calcite and CO_2. The factor was applied for the calculation of equilibrium curves in Figures 6, 7, 8, 23, 24 and in the phase diagrams presented in the Appendix.

Experimental results and data on complex-forming reactions between calcite, H_2O and CO_2 at supercritical conditions are available only for temperatures lower than 620°C and for low X_{CO2} (<0.15) (Sharp and Kennedy, 1965; Fein and Walther, 1987). These experiments show that the solubility of calcite in H_2O-CO_2 solutions increases with increasing pressure but decreases with increasing temperatures. Sharp and Kennedy (1965) suggest that calcite can be dissolved in the form of calcium bicarbonate $Ca(HCO_3)_2$. Fein and Walther (1987) assumed that Ca^{2+} is the dominant calcium species in solution and that $CO_{2(aq)}$ and HCO_3^- are the important carbonate species. The same authors could show that there is a positive departure from ideality below ~500°C relative to pure CO_2, where the positive departure from ideality is even greater than the departure predicted by Flowers (1979). At 1 kbar and

above 540°C there is a progressive and systematic negative departure from ideality, which Fein and Walther (1987) assumed to be due to an artifact of uncertainties in measurements of calcium in solution. This departure even exceeds the negative departure from ideality calculated after Flowers (1979) for high temperatures and could account for the shift of reactions involving calcite, H_2O and CO_2 towards lower temperatures, as shown in Figures 16a - d.

It can be concluded that there is strong evidence for a non-ideal behaviour of H_2O-CO_2 solutions in equilibrium with calcite at temperatures higher than 700°C. As H_2O and CO_2 are the most common constituents of fluids in the earth's crust, and calcite is a common mineral not only in carbonates but in all kind of sediments, it is of major importance to consider the chemical interaction mechanisms of those phases. There is strong evidence that for thermodynamic calculations of reactions involving calcite and H_2O-CO_2 fluids an excess free energy has to be taken into account which results from intermolecular interaction forces and probably the formation of CaO-H_2O-CO_2 complexes.

8 P-T Conditions of the Formation of the Mineral Assemblages in the Marginal Zone Xenoliths

8.1 Akermanite

Figure 6 graphically illustrates the reactions that occurred within the marginal zone xenoliths during prograde and subsequent retrograde metamorphism. The starting minerals calcite, diopside and forsterite form at earlier stages of metamorphism (Bowen, 1940). On moving from lower to higher temperatures (maintaining pressures at more than 0.4kbar) the first reaction line crossed is [CO_2]. Because there are no monticellite-forming reactions at low temperatures and high X_{CO2} the reaction [Cc,CO_2]:

diopside + 3monticellite = 2akermanite + forsterite

does not take place. The first reaction that occurs is [Mo]:

calcite + diopside = akermanite + CO_2.

In some places, depending on the bulk composition, akermanite and cal-

cite are the only phases present. Akermanite encloses calcite (Plate 3e) or clinopyroxene (Plate 3f), which strongly indicates that this reaction line has been crossed. The melilites are zoned with the Al_2O_3 contents decreasing towards the outer parts of the grains. Analyses of melilite in samples J6 and J6a in Table 1 give an average core and rim composition, respectively. An increase of the Al component in akermanite shifts the akermanite producing reaction towards lower temperatures. Therefore, the compositional changes towards the grain boundaries indicate an increase in temperature for the melilite-producing reaction., the equilibrium constant for solids for this reaction is:

$$K_D = a_{(Ak)} / a_{(Cc)}\, a_{(Di)} = 1.01$$

The activities have been calculated from the analyses given in Table 1 (akermanite J8(2): $a_{(Ak)}=0.75$; clinopyroxene J8: $a_{(Di)}=0.74$; $a_{(Cc)}$ equals unity) assuming ideal mixing, which is a simplification for monticellite and for clinopyroxene but relatively realistic for melilite- (Charlu et al. 1981) and olivine crystalline solutions at high temperatures (Saxena 1973):

$$a_{(Ak)} = (X_{Ca})^2 (X_{Mg})$$
$$a_{(Mo)} = (X_{Ca}) (X_{Mg})$$
$$a_{(Di)} = (X_{Ca}) (X_{Mg})$$
$$a_{(Fo)} = (X_{Mg})^2$$

Even though $a_{(Di)}$ and $a_{(Ak)}$ deviate considerably from unity, which is mainly due to their Al_2O_3 contents, the equilibrium constant is close to unity, as the activities of the solid solutions equalize each other in the reaction. As $K_D \sim 1$, the calculated reaction curves from end-member compositions of the minerals involved can be used, and the reaction curve does not need to be shifted to account for solid solution effects. The activity for akermanite has been calculated from the rim composition, because the outermost parts of the akermanite grains have been formed under the highest degrees of metamorphism.

8.2 Monticellite

The next stable reaction line to be crossed is [Di]:

calcite + forsterite + akermanite = 3monticellite + CO_2.

The mineral parageneses calcite-akermanite-monticellite (Plate 3g) and calcite-forsterite-monticellite (Plate 3h) are derived from this

reaction.

8.2.1 'High-temperature' Monticellite

This monticellite contains exsolution lamellae of forsterite (Plate 1e). There is an unusual change of the optical sign of this 'high-temperature' monticellite which seems to depend on the amount of exsolved forsterite it contains. Monticellite void of exsolutions has the usual negative optical sign, while the optical sign of the monticellite shown in Plate 1e is clearly positive. This is probably due to the high temperature of formation and subsequent distortion of the crystal structure by the solid solution of forsterite in monticellite. The degree of distortion is obviously dependent on the amount of forsterite in solid solution in the monticellite. The refractive indices for optically positive high-temperature and optically negative low-temperature monticellite, respectively, are:

n_x =	1.640	1.659
n_y =	1.644	1.652
n_z =	1.649	1.650
Δ	+ 0.009	- 0.009

The positive optical sign of the high-temperature monticellite indicates a formation temperature of at least 1200°C (Adams and Bishop, 1985). Microprobe analyses showed that forsterite and monticellite have compositions very close to their respective end-members (analyses Wi1, Wi7, and I3 for monticellite and forsterite in Table 1 and 1a). Calcite, which is involved in this reaction, has also end-member composition. The equilibrium constant for the solid phases is:

$$K_D = a_{(Mo)}^3 \; / \; a_{(Ak)} \; a_{(Fo)} \; a_{(Cc)} \sim 1.33.$$

The deviation from K_D=1 is due to some Al_2O_3 present in akermanite, which has an activity of $a_{(Ak)}$=0.75 (J8(2) in Table 1). This shifts reaction curve [Di] in Figure 6 towards slightly higher temperatures.

8.2.2 'Low-temperature' Monticellites

Besides the locally limited reaction

akermanite = monticellite + wollastonite,

the only retrograde reaction within the Al_2O_3-free system that can be seen abundantly is the solid-solid reaction [Cc,CO_2] in Figure 6:

2akermanite + forsterite = 3monticellite + diopside.

This reaction forms a second generation of monticellite. While prograde decarbonation reactions gave rise to more polygonal textures, this retrograde solid-solid reaction resulted in a symplectic intergrowth of akermanite-diopside-monticellite or diopside-forsterite-monticellite (Plate 4a), depending on the original bulk composition. The resulting "low temperature" monticellite has the usual negative optical sign. The activity of this monticellite is also lower and does not exceed $a_{(Mo)}=0.90$. The calculated activities of the minerals within this symplectic intergrowth are: $a_{(Mo)}=0.90$; $a_{(Ak)}=0.75$; $a_{(Di)}=0.74$; $a_{(Fo)}=0.92$. These activities refer to the microprobe analyses of monticellite (J8), melilite (J8(2)), fassaitic clinopyroxene (J8) and forsterite (J8). The equilibrium constant for solid phases is:

$$K_D = a_{(Mo)}^3 \, a_{(Di)} \; / \; a_{(Ak)}^2 \, a_{(Fo)} \sim 1.04$$

As the equilibrium constant is very close to unity, the reaction line in Figure 6 has not to be shifted to account for solid solution effects.

8.3 The Lack of Melting as a Constraint for the Marginal Zone Magma Temperature

The marginal zone xenoliths show no textural evidence that melting occurred during highest degrees of metamorphism. The non-occurrence of melting can be used to put further constraints on the temperatures reached during peak metamorphic conditions.

The onset of melting of akermanite in the presence of H_2O, CO_2 and in a dry system, was investigated by Kushiro (1964) and Yoder (1973). Yoder's position of this solidus curve ($P = P_{CO2}$) is shown in curve a in the respective P-T-X_{CO2} diagrams for subsystems 1 to 21 (Appendix III). At a CO_2-pressure of 1 kbar the onset of melting occurs at about 1410°C, but decreases gradually at higher pressures. Kushiro (1964) states that in a dry system this temperature is about 1430°C and hardly pressure dependent (Curve b in Figure 10). The maximum

temperature was most probably lower, as is borne out by melting experiments in the "dry" system $CaO-MgO-Al_2O_3-SiO_2$ (Osborn et al. 1969). According to this system, the solidus temperatures of the phase assemblages that are similar to those found in the marginal zone xenoliths are:

1) 1285-1400°C : $Fo_{74-80}+Ak_{63-70}+Sp$
2) 1380°C : $Fo_{75}+Ak_{63}+Sp$
3) 1380-1400°C : $Ak_{63}+Mo_{75-100}+Sp$
4) 1375-1437°C : $Fo_{74-75}+Ak_{63-100}$
5) 1250-1357°C : $Di+Fo_{75-83}+Ak_{70-100}$

With exception of assemblage 4, the melting temperatures are all below 1400°C.

8.4 Further P-T Evaluation for the Marginal Zone Magma Intrusion

Although the bulk composition was favourable, no merwinite formed within the marginal zone xenoliths. Figure 7 shows a subsystem that includes merwinite. The hatched area indicates the P-T conditions at the peak of metamorphism in the marginal zone xenoliths, if end-member compositions of the mineral phases are assumed.

As the akermanite analysed contains a certain amount of aluminium, the akermanite-involving reaction curves in Figure 7 become shifted towards higher temperatures. The peak metamorphic conditions calculated from reactions involving akermanite with an activity of $a_{(Ak)}=0.75$ (e.g. Analysis J8 in Table 1) is given in the form of a dotted field in Figure 7. At estimated magma temperatures between 1200 and 1300°C (Sharpe and Irvine, 1983), the inferred overburden pressure was between 1.1 and 2.4 kbar during the emplacement of the marginal zone magma.

At temperatures higher than 1390°C and pressures higher than 3.1 kbar, that is on the high P-T side of the invariant point in Figure 7, merwinite would form (reaction [Mo]) and the monticellite-forming reaction [Me] becomes metastable. From this, together with the fact that no merwinite was observed in the marginal zone xenoliths and high-temperature monticellite, akermanite and calcite are abundant, it

can be concluded that the magma temperature was definitely below 1390°C and the pressure did not exceed 3.1 kbar.

The represented high-temperature decarbonation reactions (Fig. 7) can be used for geobarometry as they are very "shallow" in a P-T diagram at relatively low temperatures. Up to a temperature of 1300°C, an uncertainty of the positions of the reaction curves of ±50°C results in a pressure uncertainty of less than about ±0.5 kbar (ca. ±1.5 km). This uncertainty increases only slightly with increasing temperatures but decreses drastically with decreasing temperatures. Comparison of the calculated data with the available experimental data (Chapter B 6) always indicates deviations lower than the assumed ±50°C and consequently a pressure uncertainty of less than ±0.5 kbar. These considerations are also valid for the estimations of the maximum pressure and temperature conditions within the critical zone xenoliths (Chapter B 9.3).

9 The P-T Conditions of the Formation of Mineral Assemblages in the Critical Zone Xenoliths

9.1 Merwinite- and Periclase Producing Reactions

The critical zone xenoliths are characterized by the presence of merwinite and periclase, which occur in the same rock but never together in the same mineral paragenesis. The merwinite producing reaction [Mo]:

$$\text{calcite} + \text{akermanite} = \text{merwinite} + CO_2$$

is illustrated in Figure 7. From this and the previously mentioned reactions (Chapter 8) one obtains the mineral parageneses merwinite-akermanite (gehlenite)-monticellite (Plate 3a and 3b).

Figure 17 shows reaction curves in a stable subsystem that serves to explain the coexistence of monticellite and periclase (Plate 2f). The monticellite and periclase forming reaction curve [Me] was crossed during prograde metamorphism, although periclase reacted to brucite ($MgO + H_2O = Mg(OH_2)$) during retrograde metamorphism. Evidence for this is found in remnants of forsterite or calcite, which were reac-

tants in reaction [Me], in brucite. The temperatures were too low to cross reaction curve [Fo], which explains the absence of mineral assemblages including both merwinite and periclase.

For the recalculation of reaction [Me] it was assumed that the equilibrium constant is unity, because the phases participating in this reaction have end-member compositions (Analyses Wi7 in Table 1 and 1a).

Some of the observed monticellites, which occur together with brucite, display forsterite exsolutions (Plates 2g and 2h) and are, as already mentioned previously, optically positive (Chapter B 8.2.1). It differs from the marginal zone "high-temperature" monticellite in that its axial angle appears to be greater, and in that its forsterite exsolutions are bigger and more abundant (Chapter B 8.2.1; Plate 1e) which seems to have an influence on the axial angle. As in the marginal zone, the occurrence of the "high-temperature" monticellite indicates temperatures greater than 1200°C. The greater abundance and size of the forsterite exsolutions, compared with those observed in the marginal zone xenoliths, suggests a larger amount of forsterite originally in solid solution, possibly as a result of higher metamorphic temperatures.

9.2 The Lack of Melting as a Constraint for the Critical Zone Magma Temperature

The already mentioned melting experiments (Chapter B 8.3) in the system $CaO-MgO-Al_2O_3-SiO_2$ by Osborn et al. (1969), are also pertinent in providing some constraints on the temperature of the magma that led to the formation of the feldspathic pyroxenite of the upper critical zone. The experimentally determined solidus temperatures of mineral assemblages that are similar to those found in the critical zone xenoliths are:

1) 1380-1390°C : Ak_{37-63}+Me+Sp
2) 1400°C : Me+Mo+Pe+SP
3) 1400°C : Mo_{74-100}+Pe+Sp
4) 1400°C : Fo_{74}+Mo_{74}+Pe+Sp

5) 1380-1436°C : Ak_{63-100}+Me+Mo

With exception of assemblage 5 the melting temperature is at or below 1400°C. Seeing that no melting of the xenolith assemblages did take place the temperature of 1380°C was not attained. Consequently the maximum critical zone magma temperature must have been below 1380°C.

9.3 Further P-T Evaluation for the Critical Zone Magma

The pressure during crystallization of the critical zone magma at the estimated magma temperature of between 1200 and 1300°C (Sharpe and Irvine, 1983) must have been between 0.6 and 1.6 kbar (hatched field in Fig. 17). At temperatures higher than 1400°C and pressures higher than 2.3 kbar the monticellite- and periclase-forming reaction [Fo] becomes metastable and the monticellite-periclase assemblage would not form (Fig. 17). Again, even without having the given constraints on the magma temperature, it is possible to conclude that the critical zone magma temperature was below 1400°C and the pressure did not exceed 2.4 kbar.

The reliability of the calculated pressures and temperatures are discussed in Chapter B 8.4, and uncertainties are most probably less than $\pm$50°C and $\pm$0.5 kbar, respectively.

10 Conclusions

The following criteria can be used to define the pressures and temperatures that were reached within the marginal and critical zone calc-silicate xenoliths:

1. The occurrence of forsterite exsolutions within a newly described high temperature modification of monticellite with a positive optic sign suggests a temperature of formation in excess of 1200°C.
2. The presence of dehydroxylated Ba-rich phlogopite which is stable at temperatures above 1050°C at pressures of more than 1 kbar.
3. The polygonal textured mineral paragenensis of calcite-akerma-

nite-monticellite in the marginal zone xenoliths formed at temperatures below 1390°C and at pressures below 3.1 kbar.

4. The absence of melting in the marginal and critical zone xenoliths indicates that temperatures of 1400°C were not attained.
5. The polygonal textured mineral paragenesis of forsterite-periclase-monticellite in the critical zone xenoliths formed at temperatures below 1390°C and pressures below 2.3 kbar.

Experimental work (Sharpe and Irvine, 1983) has shown that the Bushveld magma temperature was between 1200 and 1300°C. On this basis the overload pressure at the time of emplacement of the marginal zone was between 1.1 and 2.4 kbar (dotted field in Fig. 7), while the overload pressure of the critical zone magma was between 0.6 and 1.6 kbar (hatched field in Fig. 17). Because merwinite and periclase are absent in the marginal zone xenoliths, it can be concluded that the gabbronoritic magma of the marginal zone had a lower temperature than the magma from which the feldspathic pyroxenites of the critical zone crystallized. This conclusion is also supported by the observation that the forsterite exsolutions in monticellite are much more abundant and also bigger in the critical zone xenoliths than in the marginal zone xenoliths. Assuming a temperature of 1200°C for the marginal zone magma and 1300°C for the critical zone magma, the pressure estimates overlap in the range 1.1 to 1.6 kbar.

A graphical summary of decarbonation reactions that provide P-T constraints on the formation of critical mineral assemblages in the marginal and critical zone xenoliths is given in Figure 18.

11 Metasomatic Interaction Seam around Marginal Zone Xenoliths

An impersistent metasomatic reaction rim (Plate 1c, 1d and 4b), which consists mainly of a green clinopyroxene, surrounds the marginal zone xenoliths. This seam of clinopyroxene is generally only a few centimetres wide, but because of the green colour and the greater susceptibility to weathering it differs markedly from the adjacent two pyroxene gabbro and the akermanite-monticellite-forsterite-clinopyroxene-fels. Where pure akermanite-fels abuts the igneous rocks this

clinopyroxene seam is not developed (Plate 4c).

The formation of the metasomatic seam was evidently caused by the difference in composition between the marginal zone magma and the calc-silicate xenoliths. These compositional differences can be expressed in terms of differences between the chemical potentials of the components that form the adjacent rocks (e.g. Powell, 1978). Each of these rocks can be regarded as two adjacent subsystems, and differences in the chemical potential resulted in the transport or movement of atoms or molecules across the boundary in order to equalize the chemical potential gradient. This can happen a) by transport of atoms or molecules (infiltration), or b) by diffusion along grain boundaries or through grains. Generally a combination of both occurs, although infiltration plays a more dominant role at relatively low temperatures.

The two subsystems under consideration consist of a) a magma that crystallized to yield two pyroxene gabbro, and b) the calc-silicate xenoliths consisting of an akermanite-monticellite-forsterite-fels; the most common high temperature mineral assemblage. Representative microprobe analyses of the minerals composing the gabbronorite and the metasomatic seam are given in Table 7. Analyses J1 refer to bytownite, orthopyroxene and clinopyroxene (Plate 4d) of the two pyroxene gabbro. Analyses J2 are of clinopyroxene and anorthite (Plate 4e) in the metasomatic clinopyroxene seam. Analyses J3 are from the metasomatic seam where it contains apart from clinopyroxene also some forsterite (Plate 4f). These minerals, together with the average composition of the minerals forming the assemblage akermanite-monticellite-forsterite are plotted in 2 compositional triangles (Fig. 19a and 19b). Triangle A and B are projections from Al_2O_3 into the plane SiO_2-CaO-(Mg,Fe)O, and from SiO_2 into the plane Al_2O_3-CaO-(Mg,Fe)O, respectively. A modal analysis of the gabbronorite (upper hatched areas in Figures 19a and 19b) yields the approximate phase proportions of 2 plagioclase : 1 clinopyroxene : 1 orthopyroxene, whereas modal analyses of the mineralogically very heterogeneous calc-silicates gives bulk compositions that plot in the lower hatched areas in Figures 19a and 19b. The arrows between the "Gabbronorite" and the "Xenolith" schematically represent the chemical potential gradient between those two kinds of

rocks.

Two double arrows were chosen for each triangle to illustrate the origin of the metasomatic mineral assemblages present, viz. clinopyroxene-anorthite and clinopyroxene-forsterite. The arrows between "Ak" and "Gabbronorite" cross the tielines byt-cpx(1) and an-cpx(2) (byt: Plagioclase J1, an: Plagioclase J2, cpx(1) and cpx(2): Clinopyroxene J1 and J2 in Table 7) while the other arrows cross the tieline forsterite-cpx(3) (forsterite: Ol. J3, cpx(3): Clinopyroxene J3 in Table 7). In the latter case the tielines are crossed relatively close to the points representing clinopyroxenes, especially cpx(3), which results in a very well developed clinopyroxene seam. Besides clinopyroxene only one other phase can be stable depending on the tieline that has been crossed during the equilibration of the chemical potential gradients.

A representative analysis (J8 in Table 1) of a xenolithic clinopyroxene (cpx (4) in Fig. 19A and 19B) was also plotted in the compositional triangles to show its close relationship to the metasomatic clinopyroxene (cpx (3)). There exists also a close compositional relationship between the gabbronoritic clinopyroxene (cpx(1)) and the metasomatic clinopyroxene (cpx(2)).

The chances of encountering a metasomatic clinopyroxene rim are least if a gabbronorite abuts an akermanite-fels. In this case the arrows between "Ak" and "Gabbronorite" cross the anorthite-clinopyroxene tieline only at some distance from cpx(2) and do not cross the tielines involving cpx(3).

C CALC-SILICATE XENOLITHS IN THE UPPER ZONE OF THE EASTERN BUSHVELD COMPLEX

1 Introduction

Two calc-silicate xenoliths situated in the upper zone of the eastern Bushveld Complex, north of Magnet Heights (Arrow B in Figure 1) and near Roossenekal (Arrow D in Figure 1) were reinvestigated and are respectively referred to as xenoliths B and D below. Although Willemse and Bensch (1964) carried out a thorough petrological study of xenolith B and Joubert (1979) investigated xenolith D, these xenoliths were reinvestigated because of recent published experimental results concerning some of the encountered minerals and mineral assemblages together with the availability of an electron microprobe to analyse the minerals.

2 Xenolith B

2.1 Position and General Description of Xenolith B

Xenolith B is situated on the farm Avontuur in a magnetite gabbro of subzone A of the upper zone of the Bushveld Complex. Its exact location on the 1:50 000 map of South Africa (sheet 2429 DB Sekwati) is: 30°00'00" E and 24°40'10" S. The relatively resistent calc-silicates appear as a low hill rising to a maximum of 10 metres over a turf-covered plain (Plate 4g). A map of this xenolith showing the distribution of the main minerals is presented in Figure 20.

The major minerals occurring in xenolith B are red vesuvianite, greenish-yellow vesuvianite, garnets, clinopyroxenes, wollastonite and magnetite. Accessory minerals are titanite, apatite, plagioclase and chlorite. Vesuvianite-, garnet- and wollastonite-bearing assemblages have been described by Willemse and Bensch (1964) and shall only be repeated where necessary for the understanding of the discussions below. Mineral assemblages and microprobe analyses of some of the minerals described are compiled in Tables 8, and 9.

2.2 Vesuvianite

2.2.1 Vesuvianite as Main Constituent in the Mineral Assemblages Present

Vesuvianite is the dominant mineral in xenolith B. Both a red and a greenish-yellow variety are developed. The red vesuvianite is very coarse-grained in places and crystal fragments with intensely striated crystal faces can measure more than 10 cm across. The greenish-yellow vesuvianite has a smaller grain size and appears to be altered on crystal surfaces. Both varieties have very low birefringence and display anomalous blue or brown interference colours in thin section. In some thin sections they are even optically isotropic. Microprobe analyses of a vesuvianite grain (0.5 mm diameter), which displayed blue interference colours in the centre, and which is optically isotropic at the rim, shows only very subtle differences (analyses Av32 and Av33 respectively in Table 9). This change of the interference colours could be attributed either to small differences between the non-volatiles, or to an increase of volatile components towards the rim of the grain. The latter seems to be more probable and is assumed by Deer et al. (1982). The vesuvianite crystals are often intensly intergrown with garnet. Both the red and greenish-yellow vesuvianites occur in the same mineral assemblages, which are:

a) vesuvianite-garnet
b) vesuvianite-garnet-diopside±calcite
c) vesuvianite-wollastonite±apatite

2.2.2 General Chemistry of the Vesuvianites

The composition and crystal structure of (Mg-) vesuvianite has been discussed by several authors in the past (e.g. Christophe-Michel-Levy, 1960; Christie, 1961; Walter, 1966; Ito and Arem, 1970 and 1971; Olesch, 1978; Hochela et al., 1982; Hoisch, 1985), and still cannot be regarded as finalized.

The general formula for vesuvianite is given by Coda et al. (1970) as $2[Ca_{19}(Mg,Fe,Al,Ti,Mn)_5Al_8(O,OH)_{10}(SiO_4)_{10}(Si_2O_7)_4$, and by Ruck-

lidge et al. (1975) as $2[Ca_{19}Fe(Fe,Ti,Mn,Mg,Al)_8Al_4Si_{18}O_{70}(OH,F)_8]$. Both formulae can be simplified to become $X_{19}Y_{13}Z_{18}(O,OH,F)_{78}$, where X=Ca Y=(Al,$Fe^{3+}$,$Fe^{2+}$,Mg,Ti,Zn,Mn), Z=Si. The formulae of vesuvianites of xenoliths A, B and D have been calculated from microprobe analyses given in Table 1, 9 and 11, respectively, and are listed in Table 10. These formulae are normalized to 50 cations and, with the exception of analysis Ma2a, Fe is assumed to be Fe^{3+}. The latter assumption is based on the work of Manning and Tricker (1975), who state that in low-Ti vesuvianites more than 90 % of the total iron occurs as Fe^{3+}, but in crystals with more than 1 wt.% TiO_2 most of the iron is present as Fe^{2+}.

It can be seen from Table 10 that some of the formulae deviate markedly from the ideal values for X and Y. Ito and Arem (1971) have taken these deviations into account and proposed the following general formula for vesuvianite:

$$Ca_{18}(Ca_{2-x}Mg_x)Mg_2(Mg_{2-y}Al_y)Al_8(Al_ySi_{2-y})Si_{16}O_{68}(OH)_8,$$

where $0.0 \leq x < 1.5$ and $0.0 < y < 1.5$. With exception of analysis Av8, this general formula is applicable for the analyses given in Table 10. Analysis Av8 stems from a vesuvianite that is probably partly altered to hydrogarnet.

2.2.3 Chemical Differences between Red Vesuvianite and Greenish-yellow Vesuvianite from Xenolith B

From Table 10 it is obvious that the main difference between the red and the greenish-yellow vesuvianite is in the different X- and Y values. For the red vesuvianites X>19 and Y<13 while for the greenish-yellow vesuvianites X<19 and Y>13. The red vesuvianites have higher Ca-, Fe- and Al contents, but the greenish-yellow vesuvianites are richer in Si and Mg. The composition of the reddish vesuvianites from xenolith D resembles the red vesuvianites of xenolith B more closely than the greenish-yellow variety.

2.3 Garnets and their Chemical Variations

The chemical composition of the garnets in xenolith B varies markedly. Microprobe analyses of different garnets (Table 9) show that they are grandites and that, with the exception of one analysis (Av6), in which the grossular component predominates, the garnets are mainly andraditic. They are black or reddish-brown in hand specimen depending on the Ti- and Fe^{3+} content. Even in thin sections the Ti-andradite idioblasts display intensive reddish-brown colours. Whenever the grossular component dominates, they have greenish colours in hand specimen but are colourless in thin section. In handspecimen the andraditic Fe^{3+}-rich garnets can easily be confused with red vesuvianite, with which they are either intimately intergrown or form granoblastic assemblages (Plate 4h and 5a).

2.4 The Mineral Assemblages of Xenolith B

2.4.1 The Mineral Assemblage Vesuvianite-Garnet±Chlorite ±Magnetite

Vesuvianite very often occurs together with garnet, which seems to replace the vesuvianite. The mineral assemblage vesuvianite-garnet-magnetite, shown in Plate 4h, is developed at the contact of vesuvianite-garnetfels and a small lenticular magnetite body in the eastern part of the xenolith (Fig. 20). Chlorite often occurs as an accessory mineral together with vesuvianite and garnet. Microprobe analyses of these minerals are given in Table 9 (Av18 and Av19). The Fe_2O_3 content of magnetite was calculated with the aid of the computer program ALLOX (Merkle, 1985, unpublished), which assumes stoichiometric composition. Willemse and Bensch (1964) regarded this magnetite as a metamorphosed sedimentary iron ore, because the low Ti content attests against an origin from the upper zone magma.

The andraditic garnets contain an appreciable amount of Ti, with the highest values of 11.89 wt.% recorded in garnet Av4. This Ti-andradite can be referred to as melanite (Huggins et al., 1977). The formula of this melanite has been calculated by taking the following

considerations into account: a) Titanium was assigned to the octahedral position where it replaces Fe^{3+}, because the relative preference for the tetrahedral site is in the order Al≥Fe≥Ti (Huggins et al., 1977), and b) according to Finger's (1972) correction procedure for microprobe analyses all Fe can be assumed to be Fe^{3+}. On the basis of 24 O the formula for melanite Av4 is:

$$(Ca_{6.11}Mg_{0.12}Mn_{0.01})(Ti_{1.51}Fe3+_{1.25})(Al_{0.80}Fe^{3+}_{0.49}Si_{4.71})$$

Microprobe analyses of the black garnets in vesuvianitefels, reported by Willemse and Bensch (1964), proved to be melanite which owed its dark colour to a rather high Ti content.

2.4.2 The Mineral Assemblage Vesuvianite-Garnet-Diopside±Calcite

Two different textures of the mineral assemblage vesuvianite-garnet-diopside were observed. In the one, diopside appears to be fibrous and intergranular between vesuvianite and melanite (Plate 5a, analyses Av4 in Table 9), whereas in the other textural variety diopside appears granular and relatively coarse-grained together with a symplectic intergrowth of vesuvianite and garnet (Plate 5c, analyses Av5 in Table 9). Calcite is an accessory mineral in this mineral assemblage.

2.4.3 The Mineral Assemblage Vesuvianite-Wollastonite±Apatite

Wollastonite forms a graphic intergrowth with vesuvianite (Plate 5d). Apatite is an accessory mineral but nevertheless of special interest, because of the rather high SiO_2 content of 2.30 wt.%. While SiO_2 usually appears only as trace constituent in apatites, silicate apatites can occur in calcareous rocks which have undergone high-temperature, low-pressure contact metamorphism (Speer and Ribbe, 1982). Analyses of the minerals of this assemblage are given in Table 9 (Av3).

2.4.4 The Mineral Assemblage Wollastonite-Clinopyroxene-Garnet

The mineral assemblage wollastonite-clinopyroxene-garnet (analyses Av6 in Table 9) has a granoblastic texture (Plate 5e). In contrast to clinopyroxenes that occur together with vesuvianite, and which consist of unaltered diopside, these clinopyroxenes are slightly altered and of salitic composition.

2.4.5 The Mineral Assemblage Wollastonite-Titanite-Calcite-Clinopyroxene

The mineral assemblage wollastonite-titanite-calcite-clinopyroxene (Plate 5f, Table 8 (Av2)) was found in a wollastonitefels that occupies a fairly large area in the southwestern part of xenolith B. Poikiloblastic wollastonite and clinopyroxene contain inclusions of idioblastic titanite and probably formed after the titanite. While titanite appears also intergranular, calcite occurs only as a relict mineral in wollastonite (Plate 5g). The observed minerals belong to the system $CaO-MgO-SiO_2-TiO_2-CO_2$, in which the clinopyroxene could have formed according to either of the following two reactions (Winkler, 1977):

dolomite + 2quartz = diopside + $2CO_2$ at high X_{CO2}, or at low X_{CO2}:

tremolite + 3calcite + 2quartz = 5diopside + $3CO_2$ + H_2O.

As calcite occurs only together with wollastonite and titanite, but is never in direct contact with clinopyroxene, the mineral paragenesis wollastonite-titanite-calcite (Plate 5g) can be treated separately. The calcite and titanite inclusions in wollastonite can be explained with the aid of the system $CaO-SiO_2-TiO_2-CO_2$ (Fig. 21). The reaction curves in this figure are presented at different X_{CO2} (0.15 and 1.00) to illustrate the dependence of water as diluent on the reaction temperatures. Rutile was assumed to have provided the Ti component that was necessary for the formation of titanite (Reaction [Wo]). By using another TiO_2 modification such as anatase, reaction [Wo] occurs only at slightly higher temperatures (Schuiling and Vink, 1967). Experimental work and thermodynamic calculations yielded different results with respect to the $P-T-X_{CO2}$ position of reaction [Wo]

(Schuiling and Vink, 1967; Hunt and Kerrick, 1977) and places reaction [Wo] at the same or slightly higher temperatures compared with those presented in Figure 21 but always on the low temperature side of reaction [Ru].

Calcite and quartz were present originally to form wollastonite at higher temperatures (Reaction [Ru]). It is obvious from the chemographic representation in the upper left corner of Figure 21 that by crossing reactions [Wo] and [Ru] the observed mineral parageneses wollastonite-titanite-calcite originates.

The clinopyroxene forming reactions have been omitted from Figure 21 but the present observations and calculations place them between reactions [Wo] and [Ru].

3 Xenolith D

Xenolith D (Fig. 22) is situated on the farm Luipershoek in a magnetite gabbro which forms part of subzone B of the upper zone of the eastern Bushveld Complex. Its exact position on the 1:50 000 map of South Africa (sheet 2529 BB Roossenekal) is 29°52'20" E and 25°08'20" S. Similar to xenolith B, xenolith D forms a little hill, because the relatively hard calc-silicates are more resistant to weathering than the magnetite gabbros (Plate 5h).

3.1 Mineralogy and Mineral Assemblages of Xenolith D

A brief description of the minerals and mineral assemblages occurring in this xenolith is given by Joubert (1976) in an unpublished MSc thesis. An extension and partial reevaluation of this work was necessary to show the relation of this xenolith to the previously described xenoliths A, B and C. Furthermore, microprobe analyses of most of the present minerals provide some interesting new information on the crystal chemistry of some minerals and the mineral assemblages in which they appear.

Akermanite is the predominant mineral in xenolith C. The other major minerals are: wollastonite, monticellite, vesuvianite, garnet, clinopyroxene, and calcite. Acessory minerals are spinel, muscovite, perovskite, prehnite, xantophyllite, K-feldspar, chlorite and magnetite. The mineral assemblages in which these minerals occur are listed in Table 8. Microprobe analyses of most of these minerals are given in Table 11 and 11a. Vesuvianite is much less abundant than in xenolith B and occurs in only two of the six observed assemblages.

3.2 The Mineral Assemblage Vesuvianite-Grossular-Diopside-Calcite±Chlorite

The textural features of the assemblage vesuvianite-grossular-diopside-calcite±chlorite (Plates 6a, 6b and 6c) are the same as those of the similar assemblage encountered in xenolith B (Chapter C 2.7).

Two different generations of diopside seem to coexist in this assemblage, viz. a fibrous diopside and a granular coarse-grained variety. Microprobe analyses of the silicates in this assemblage are given in Table 11 and 11a (Ma2b).

Chlorite is an accessory mineral in this assemblage, but is noteworthy because of its very high MgO and SiO_2 content of 33.16 and 33.26 wt.%, respectively, and its very low Al_2O_3 and total FeO content (15.97 and 0.69 wt.%, respectively). The chlorite is of the penninite variety according to the nomenclature of Hey (1954).

3.3 The Mineral Assemblage Vesuvianite-Grossular-Monticellite-Xanthophyllite±Calcite±Spinel

In the assemblage vesuvianite-grossular-monticellite-xanthophyllite± calcite±spinel (Plates 6d, 6e and 6f; analyses Ma22 in Table 11 and 11a) vesuvianite and garnet seem to replace monticellite along grain margins and fractures (Plate 6g). While vesuvianite, grossular and xanthophyllite are of retrograde origin (Chapter D 1), monticellite formed during prograde metamorphism. The most probable reaction that led to the formation of monticellite is calcite + forsterite + akermanite = 3monticellite + CO_2 and indicates temperatures >850°C (P>1 kbar and X_{CO2}>0.3, Figure 6, Reaction [Di]). At an X_{CO2}=1.0 this temperature would even exceed 1040°C (Figure 6).

Xanthophyllite shows an unusual compositional variation. It is related to phlogopite by the substitution of Ca for K and has the same formula as clintonite, both of which are monoclinic with an optically negative sign. The difference between clintonite and xanthophyllite lies probably in polymorphism of the layer stacking; clintonite having a two-layer and xanthophyllite a one layer cell (Deer et al. 1975). As xanthophyllite is more frequently described in the literature, especially together with vesuvianite (Ito and Arem, 1971), the observed and analysed mineral is most probably xanthophyllite. Deer et al. (1975), who consider the ideal formula for xanthophyllite to be $Ca_2(Mg,Fe)_{4.6}Al_{1.4}[Si_{2.5}Al_{5.5}O_{20}][OH]_4$, state that the totals of the X and Y sites vary little from their ideal values, 2 and 6, and believe

that only very limited substitution of K and Na for Ca is possible. Two formulae, both normalized to 16 cations, were calculated for each of the two representative microprobe analyses (analyses Ma22b and Ma22c in Table 11a), viz. one with total Fe as FeO and the other one with total Fe as Fe_2O_3. Their calculated 16 cation normalized formulae (for Fe^{2+} and Fe^{3+}) are:

Ma22a: $(Ca_{1.91}Na_{0.02})(Mg_{4.35}Fe^{2+}_{0.21}Ti_{0.01}Al_{1.50})(Al_{5.46}Si_{2.54})$
X=1.93 Y=6.07 Z=8.00

Ma22a: $(Ca_{1.91}Na_{0.02})(Mg_{4.34}Fe^{3+}_{0.24}Ti_{0.01}Al_{1.48})(Al_{5.47}Si_{2.53})$
X=1.93 Y=6.07 Z=8.00

Ma22b: $(Ca_{2.06}Na_{0.00})(Mg_{4.05}Fe^{2+}_{0.23}Cr_{0.03}Al_{1.63})(Al_{5.90}Si_{2.10})$
X=2.06 Y=5.94 Z=8.00

Ma22b: $(Ca_{2.06}Na_{0.00})(Mg_{4.04}Fe^{3+}_{0.26}Cr_{0.03}Al_{1.61})(Al_{5.91}Si_{2.09})$
X=2.06 Y=5.94 Z=8.00

These formulae indicate that there exists a remarkable variation in composition.

3.4 The Mineral Assemblage Akermanite-Monticellite-Wollastonite

Melilite (akermanite)-monticellite-wollastonite is the most abundant mineral assemblage in xenolith D (analyses Ma16 in Table 11 and 11a). It is obvious from the microphotograph shown in Plates 6h and 7a that akermanite is replaced by a fine grained and sometimes even submicroscopic mineral mixture of monticellite and wollastonite. The reaction akermanite = monticellite + wollastonite was already mentioned in Chapter A 1.1 and occurs during retrograde metamorphism at about 700°C (Harker and Tuttle, 1956). The most probable reaction that accounts for the formation of akermanite is the reaction calcite + diopside = akermanite + CO_2. At a pressure of 1 kbar and a relatively low X_{CO2} (=0.3) the equilibrium temperature for this reaction is 850°C and increases to 1000°C if X_{CO2}=1.0 (reaction [Mo] in Figure 6,

and Reaction [Me,Mo] in Figure 8).

In hand specimen the akermanite-monticellite-wollastonite-fels has a light grey colour where akermanite predominates, but it is white where monticellite and wollastonite are the major phases (Plate 7b).

3.5 The Mineral Assemblage Clinopyroxene-Calcite-Perovskite-Magnetite-Spinel

The assemblage clinopyroxene-calcite-perovskite-magnetite-spinel (Plate 7c) is present only in a very small occurrence in the northern part of xenolith D and forms part of the pyroxenefels indicated in Figure 22. The rock is predominantly black and has white specks consisting of calcite. Granoblastic clinopyroxene is the dominant mineral in this assemblage which includes the symplectic intergrown calcite, perovskite and magnetite. Spinel is always attached to, or included in magnetite which seems to replace the spinel. Microprobe analyses of the silicates are given in Table 11 and 11a (Ma9).

Noteworthy is the relatively high Ti content of almost 4 wt.% in the clinopyroxene. These Ti-augites have a very small 2V and in some cases even appear to be optically uniaxial. This effect was mentioned by Dixon and Kennedy (1933) and Deer et al. (1961) who state that Ti has the effect of lowering the 2V. The Ti-augites of this specific assemblage are not zoned which is also rather uncommon.

The symplectic intergrowth of calcite, perovskite and magnetite could be due to one of the three following reactions:

a) calcite + TiO_2 = perovskite + CO_2 (with magnetite already present)

b) calcite + ilmenite + 0.5 O_2 = perovskite + magnetite + CO_2

c) calcite + $(2Fe_2O_3 + 2FeO + TiO_2)_{solution}$ = perovskite + magnetite + CO_2

Reaction a) is the least complex reaction that leads to the formation of perovskite. Titanium could have been introduced metasomatically or may have been present in a Ti-bearing phase. In reaction b) it is assumed that Ti is present in ilmenite (Tröger,

1969). This reaction, which leads to the formation of magnetite, requires oxidizing conditions. Reaction c) is based on the assumption that Fe^{2+}, Fe^{3+} and Ti are of metasomatic or pneumatolytic origin and that these elements reacted with calcite to form perovskite and magnetite. The replacement of spinel by magnetite indicates strongly that Fe was introduced during pneumatolytical metamorphism which favours reaction c) but does not exclude reaction a) and b).

3.6 The Mineral Assemblage Clinopyroxene-Garnet-Prehnite-Muscovite

This assemblage contains some stable and metastable mineral sub-assemblages that can provide constraints on the temperatures reached during peak metamorphic conditions. These assemblages also give some insight into the composition of the fluid phase involved during retrograde metamorphism.

Plates 7d and 7e show nodules of sub-idioblastic hydrogrossular that is partly altered to a very fine-grained intergrowth of prehnite, muscovite and calcite. It occurs in and between zoned granoblastic ferrosalite grains (Mal0 in Table 11 and 11a) which displays equilibrium angles at triple points. According to representative centre- and rim composition of this ferrosalite (analyses Mal0a (centre) and Mal0b (rim) in Table 11) the Si content increases towards the rim concomitant with a decrease in Ti, Al, Fe, Mg and Ca.

From the minerals present it can be concluded that the original rock was probably a marl consisting of Al-bearing clay minerals, quartz, dolomite and calcite.

Three mineral assemblages can be distinguished (Plate 7d and 7e):

1) ferrosalite-hydrogrossular
2) ferrosalite-hydrogrossular-prehnite-muscovite±calcite
3) ferrosalite-prehnite-muscovite±calcite

These assemblages represent different alteration states of grossular. The ferrosalite does not seem to be affected by any alteration.

3.6.1 The Stability of Grossular and Prehnite

A T-X_{CO2} phase diagram, which is given in Figure 23, illustrates probable reactions that resulted in the observed mineral assemblages introduced in the previous paragraph. Figure 23 deals with idealized end-member compositions of the minerals involved in these reactions, and therefore the positions of the reaction curves deviate slightly from the real positions. This does not affect the following considerations as most of the observed minerals are close to end-member composition.

Three invariant points (A, B and C) are shown, of which only the positions of invariant point A and B were experimentally investigated (Boettcher, 1969; Gordon and Greenwood, 1971; Hoschek, 1974; Huckenholz et al. 1974; Zharikov et al. 1977). The position of the other invariant point was calculated by means of the thermodynamic data compiled in Table 2 and the Fortran computer program GG5 (Appendix II).

The minerals involved belong to the system CaO-MgO-SiO_2-Al_2O_3-CO_2-H_2O. The iron- and titianium content in some of the observed minerals can be largely attributed to metasomatism and shall be neglected in the following discussion. The position of invariant points A, B and C and the reactions curves shown in Figure 23 were calculated for a pressure of 1 kbar and, where available, compared with experimental brackets. The following reactions, numbered in accordance with these in Figure 23, have been experimentally investigated:

1) 2grossular = gehlenite + anorthite + 3wollastonite — Boettcher (1970) and Huckenholz et al. (1975)
2) 2calcite + anorthite = gehlenite + wollastonite + $2CO_2$ — Hoschek (1974)
3) calcite + grossular = gehlenite + 2wollastonite + CO_2 — Hoschek (1974)
4) grossular + quartz = 2wollastonite + anorthite — Huckenholz et al. (1975)
6) calcite + anorthite + wollastonite = grosssular + CO_2 — Hoschek (1974) and Zharikov et al. (1977)
7) calcite + quartz = wollastonite + CO_2 — Greenwood (1967)
9) 3calcite + 2anorthite = gehlenite + grossular + $3CO_2$ — Hoschek (1974)

For the calculations of the mineral reactions shown in Figure 23, a

fluid pressure of one 1 kbar was chosen. This is based on the fact that the intrusions of the upper zone magmas occurred at a somewhat lower depth and a higher stratigraphic level than the critical zone magmas for which a pressure of 1.1 - 1.6 kbar has been calculated in Chapter A 8.9.

By applying the excess free energy term "w", which is discussed in Chapter B 7.2 for reaction temperatures higher than 600°C, most of the recalculated reaction curves lie within the experimental brackets (solid lines in Fig. 23). The application of an ideal mixing model, or the excess free energy term applied in the modified Redlich and Kwong equation (MRK), results in reaction temperatures that are too high (dotted lines in Fig. 23). At temperatures lower than 600°C, the MRK-equation gives better results. As already discussed in Chapter B 7.2, this could be due to complex-forming reactions involving calcite, CO_2 and H_2O. Only the calculated position of reaction 2 occurs at higher temperatures than the experimentally bracketed position. The reason for this discrepancy is not readily apparent but according to Helgeson et al. (1978), who discussed this and other grossular-involving reactions, it appears to be due to inconsistencies in the experimental data reported by Hoschek (1974).

3.6.2 Constraints on the Maximum Temperatures reached during Metamorphism

Grossular is stable only under those conditions defined in Figure 23. At temperatures higher than 850°C at $X_{CO2}<0.5$ and 1 kbar pressure, grossular reacts to gehlenite, anorthite and wollastonite (reaction 1). At lower temperatures and lower X_{CO2} the stability boundary of grossular is mainly defined by reaction 6. During peak metamorphic conditions the stability field of grossular was definitely exceeded, because the temperature must have been the magma temperature and therefore higher than 900°C. If melting had occurred, clinopyroxene (ferrosalite) could be expected in the nodule-like mineral aggregates, resulting from a crystallization of an eutectic melt involving clinopyroxene and the minerals which are stable on the high-temperature side of reaction 1 and 2 in Figure 23, viz. gehlenite, anorthite and

wollastonite. The following discussion depicts the implications of these considerations on the maximum temperature reached during peak metamorphism.

The decomposition products of grossular, i.e. wollastonite, gehlenite and anorthite, begin to melt at about 1260°C at 1 kbar, if neither liquid nor vapor is involved in the reaction (Huckenholz et al. 1970). If vapor is involved, the melting temperature decreases to 1150°C at 1 kbar in the presence of excess H_2O (Huckenholz et al. 1970). In the present calc-silicates, CO_2 seems to have been more dominant than H_2O. Unfortunately, no experimental results involving CO_2 in the described system are available to show to what extent the presence of CO_2 depresses the melting temperature in comparison with a vapor-free system. Nonetheless, experiments in the system $CaO-CO_2-H_2O$ (Wyllie and Tuttle, 1960) and some general considerations on CO_2 solubility in magmas (Burnham, 1979) as well as experiments in the system akermanite-H_2O and akermanite-CO_2 discussed by Yoder (1973), indicate a much less pronounced depression of the melting temperature by CO_2 than by H_2O. Provided that most of the devolatization reactions had already occurred at relatively low temperatures, the resultant low vapor pressure would not depress the melting temperature significantly.

The ferrosalites which are associated with the observed mineral assemblages (Plate 7d and 7e), should have had some influence on the beginning of melting. Experiments carried out by Huckenholz et al. (1974) give pertinent information on a) the melting behaviour of a mineral assemblage that is related to the observed assemblages, and b) the minimum temperature that was reached during peak metamorphism.

The experimentally investigated mineral assemblage pseudowollastonite-gehlenite$_{ss}$-anorthite-fassaite$_{ss}$, that evolves from garnet$_{ss}$ (and$_{45}$gross$_{55}$ to and$_{15}$gross$_{85}$), begins to melt at a constant temperature of 1202$\pm$3°C at 1 bar (Huckenholz et al. 1974). This indicates that the melting temperature in the mineral assemblage pseudowollastonite-gehlenite$_{ss}$-anorthite-fassaite$_{ss}$ does not depend on the Al_2O_3- and Fe_2O_3 content in the solid solutions. The melting temperature is also presumed to remain rather stable if the diopside component in

fassaite$_{ss}$ or the gehlenite component in gehlenite$_{ss}$ increases. At a higher pressure, e.g. 1 kbar, the beginning of melting occurs probably at a similar or slightly higher temperature.

The experiments carried out by Huckenholz et al. (1974) involve granditic garnets and fassaitic pyroxenes, an intimate intergrowth of which was described by Willemse and Bensch (1964) in another upper zone calc-silicate xenolith near Magnet Heights. Huckenholz et al. (1974) explain this specific mineral assemblage by means of the reaction: fassaite$_{ss}$ + wollastonite = garnet$_{ss}$ which takes place at 935$\pm$20^{o}C and increases between 70 to 80^{o}C per kbar. This reaction therefore suggests an upper zone magma temperature of at least 1000^{o}C at pressures equal or greater than 1 kbar.

The P-T conditions in the xenolith described in this chapter must have been similar to those inferred above from the reaction investigated by Huckenholz et al. (1974) although the reactions that led to the formation of the ferrosalite-hydrogrossular assemblage were different, due to a different original bulk composition. Seeing that the decomposition of pure grossular does not produce any clinopyroxene, the formation of the present mineral assemblage ferrosalite-hydrogrossular requires at least one additional reaction involving a Mg-bearing phase. No mineralogical evidence is preserved that helps to formulate such a reaction. It is therefore concluded that the MgO content in the clinopyroxene stems from a MgO-bearing mineral, most probably dolomite.

3.6.3 The Formation of Prehnite during Retrograde Metamorphism

During retrograde metamorphism the composition of the fluid phase was governed by a comparatively H_2O-rich postmagmatic fluid. Grossular became stable again at temperatures <850^{o}C and X_{CO2}<0.5 (Reaction 1). The present hydrogrossular-prehnite assemblage provides a strong indication that at lower temperatures reaction curve 6 and subsequently reaction curve 8 (Coombs et al., 1959) were crossed. This, together with the formation of hydrogrossular from grossular at temperatures lower than 500^{o}C (Roy and Roy, 1957), led to the mineral assemblage

hydrogrossular-prehnite-anorthite-calcite. None of the stable reaction curves intersecting at invariant point B were crossed, because no quartz that would have evolved from these reactions is present. Hydrothermal sericitization of anorthite (3anorthite + K_2O + $2H_2O$ = 2sericite + 3CaO) formed the mineral assemblage ferrosalite-prehnite-sericite$\pm$calcite.

3.6.4 Conclusions

Even though the proposed model, which serves to explain the observed mineral assemblages without applying major ion exchange mechanisms due to metasomatism, is rather speculative, the following conclusions may be drawn:

1) The observed prehnite appeared during retrograde metamorphism as prehnite decomposes at temperatures much lower than those reached during peak metamorphic conditions (Coombs et al., 1959).
2) Prehnite occurs as a final decomposition product of grossular.
3) The stability field of grossularite was exceeded during retrograde metamorphism.
4) The lack of any indications of melting indicates a maximum metamorphic temperature that was definitely below 1260°C and probably below 1200°C.
5) From the experimental data of Huckenholz et al. (1974) it can be concluded that the peak metamorphic temperatures were higher than 1000°C.

3.7 Indications for Chemical Variations in the Formula of Prehnite

Chemical analyses of prehnites compiled by Deer et al. (1961, 1975) do not show any marked variation in composition. These authors state that the amount of alkalis, manganese and magnesium are usually low ($\leq$0.32, $\leq$0.06 and $\leq$0.25 wt.%, respectively) and the only appreciable substitution is that of iron for aluminium.

Three representative microprobe analyses (Mala, Malb and Mal0) are given in Table 11a. Analysis Mal0 refers to a prehnite that occurs in the previously described mineral assemblage ferrosalite-hydrogrossular-prehnite-muscovite±calcite, while Mala and Malb represent prehnite analyses from an altered gabbro or magnetitegabbro adjacent to the calc-silicate xenolith. Analysis Mal0 is very close to the "ideal" composition $Ca_4Al_2[Al_2Si_6O_{20}](OH)_4$.

From the prehnite analyses in Deer et al. (1961, 1975) and from the description by Tröger (1969), it is obvious that the ratio Fe^{3+}/Fe^{2+} is usually much greater than 1. As the ratio could not be determined by microprobe techniques, the total iron present was assumed to be Fe^{3+}. Three formulae for prehnite have been calculated from the analyses given in Table 11a, all three normalized to 14 cations:

Mala: $(Ca_{3.38}Mg_{0.34}Na_{0.06})(Fe^{3+}_{0.27}Al_{1.95})(Al_{1.97}Si_{6.03})$

Malb: $(Ca_{2.95}Mg_{0.64}Na_{0.09})(Fe^{3+}_{0.57}Ti_{0.01}Al_{1.74})(Al_{2.11}Si_{5.89})$

Mal0: $(Ca_{3.93}K_{0.01}Na_{0.03})(Fe^{3+}_{0.02}Al_{2.01})(Al_{2.04}Si_{5.96})$

A normalized recalculation on the basis of $(OH)_4$ is almost identical to the above formulae:

Mala: $(Ca_{3.36}Mg_{0.34}Na_{0.06})(Fe^{3+}_{0.27}Al_{1.91})(Al_{2.00}Si_{6.00})(OH)_4$

Malb: $(Ca_{2.94}Mg_{0.63}Na_{0.06})(Fe^{3+}_{0.57}Ti_{0.01}Al_{1.72})(Al_{2.12}Si_{5.88})(OH)_4$

Mal0: $(Ca_{3.93}K_{0.01}Na_{0.03})(Fe^{3+}_{0.02}Al_{2.02})(Al_{2.03}Si_{5.97})(OH)_4$

The prehnites display an unusually high magnesium- and iron content concomitant with an a unusually low calcium content, where the oxides of those elements seem to replace each other. The replacement mechanisms appear to be complex as only the sum of octahedral $Al^{3+} + Fe^{3+} + Mg^{2+} + Ca^{2+}$ is constant, while the octahedral trivalent and divalent ions, respectively, do not replace one another stoichiometrically. Further investigations on this problem are necessary.

3.8 The Mineral Assemblage Wollastonite-K-Feldspar-Muscovite-Apatite±Calcite

The mineral assemblage wollastonite-K-feldspar-muscovite-apatite±calcite, which was found in sample Mal3, is significant in that it provides some constraints on the fluid phase composition during prograde and retrograde metamorphism.

A photograph of a thin section displaying this specific mineral assemblage (Plate 7f and 7g) shows wollastonite laths enclosed in bigger grains of poikiloblastic K-feldspar. Sericite is ubiquitious, in some places as a matrix mineral, in others as a pseudomorph after andalusite or sillimanite, or it may form an intimate intergrowth with wollastonite (Plate 7h). Apatite is a common mineral in the thin section and occurs preferably together with K-feldspar and sericite.

3.8.1 Inferred Mineral Reactions and Fluid Phase Compositions during Pro- and Retrograde Metamorphism

The mineral assemblage wollastonite- K-feldspar- muscovite- apatite shall be discussed by means of an isobaric T-X_{CO2} phase diagram (Fig. 24) which presents probable reactions that could have led to the mineral assemblage present. The reaction curves given in this diagram were calculated using the same criteria as explained in Chapter C 3.6.1. The thermodynamic data are taken from Table 2. Experiments concerning reactions 1 (Greenwood, 1967) and 2 (Chatterjee and Johannes, 1974) are in very good agreement with the calculated positions of these reactions. Reaction curve 3 has not yet been experimentally investigated.

The occurrence of wollastonite laths as inclusions in K-feldspar, and the absence of mica inclusions within wollastonite, makes it very probable that reaction 1: calcite + quartz = wollastonite + CO_2 occurred at lower temperatures than reaction 2: muscovite + quartz = K-feldspar + andalusite + H_2O or reaction 3: muscovite + wollastonite + CO_2 = K-feldspar + andalusite + calcite + H_2O. As can be seen in Figure 24, this is only possible at a low X_{CO2} (<0.19).

In order to describe a reaction path that led to the observed mineral assemblage, the process of buffering of the fluid phase has to be considered. The fluid phase is internally buffered if the system is completely closed. If the system is open or partly open, allowing e.g. diffusion or infiltration of a fluid phase, the fluid phase involved in devolatization reactions can be buffered externally. Internally and externally buffered systems represent only the extreme cases of which a combination is more probable to occur in natural metamorphic rocks. Mineral assemblages in relatively thin and alternating layers of changing composition, like water-bearing pelites and carbonates, are more likely to be subjected to external buffering, as the volatiles of different composition evolving in the different layers tend to pervade and therefore influence each other. Xenolith D is mineralogically rather inhomogeneous, and it is therefore to be expected that different fluids of different compositions developed at different stages of metamorphism and hence favour the assumption of externally buffered systems in this xenolith. Each system, though, contributes to the overall change of the fluid phase composition and becomes internally buffered, depending of the size of the system under consideration and the amount of the pervading fluids. From the mineralogical observations it is obvious that reaction 1 took place first. If internal buffering is assumed, the reaction path follows the reaction curve 1 with increasing temperature, until the invariant point is reached. As CO_2 is produced during the reaction, X_{CO2} increases. Sufficient quartz and calcite have to be assumed so that the system does not leave reaction curve 1 before the invariant point is reached. At a certain pressure, temperature and X_{CO2}, which is defined by the invariant point, all phases and reactions are in equilibrium. A further increase in temperature will involve all phases in the reactions intersecting the invariant point. The first phase being used up during these reactions defines the further reaction path. Seeing that the rocks under consideration do not contain any free quartz, it can be assumed that this phase was used up during reaction 1 and defines the reaction path to follow along reaction 3. As soon as one reactant of reaction 3, that is K-feldspar, andalusite or calcite, is used up, the reaction path goes straight up as no further CO_2 becomes evolved through reaction 3. If either quartz or calcite were used up in reaction 1 before the invariant point was reached, the reaction path would leave reac-

tion curve 1 at this specific moment to go straight up with increasing temperatures until it reaches reaction curve 2. From there it follows reaction curve 2 with increasing temperature in direction to lower X_{CO2} as water becomes evolved from this reaction until either muscovite or quartz is used up. This should occur at $X_{CO2} > 0$, because in a closed system CO_2, which evolved from reaction 1, dilutes the H_2O evolving from reaction 2. The shallow slope of reaction 2 at low X_{CO2} indicates a relatively high reaction rate with increasing temperature, which also increases the probability that either muscovite or quartz are used up before X_{CO2} becomes very low.

A different reaction path can be assumed if external buffering took place. Some fluids probably existed before reaction 1 occurs. The reaction path goes straight up with increasing temperature, intersecting reaction curves 1 and 2 while the external fluid phase becomes continuously enriched in CO_2. The originally carbonate-bearing sediments within the xenolith were the main suppliers of the fluids that evolved with increasing temperature. In Chapter B 7.1 it was shown that the fluid phase in carbonate-bearing rocks becomes enriched in CO_2 with increasing degrees of metamorphism.

The "real" position of the reaction path most probably lies between the externally and internally buffered paths (dashed line in Fig. 24). The kinks appearing at each intersection with a reaction curve represents a change of the fluid phase composition due to evolving CO_2 or H_2O which influences the infiltrating fluids. In this context it is noteworthy that even a small dilution of an internally buffered fluid phase by an infiltrating fluid phase of a different composition makes it improbable that the invariant point is intersected. At a defined pressure and temperature, the invariant point exists only at a certain X_{CO2}, that is the degrees of freedom are zero (Gibbs phase rule). As soon as the fluid phase composition changes e.g. by infiltration of another fluid phase of a different and variable composition, the degree of freedom increases by one. This gives the reaction path one additional degree of freedom, thereby preventing it from intersecting the invariant point, and moving through divariant $T\text{-}X_{CO2}$ spaces rather than along univariant reaction lines.

From the previous considerations it is very probable that the sequence of reactions that occurred during prograde metamorphism is representred by the dashed arrow in Figure 24. At elevated temperatures an increase in X_{CO2} leads to the occurrence of reaction 3: muscovite + wollastonite + CO_2 = K-feldspar + andalusite + calcite + H_2O. Andalusite most probably converted to pseudomorphic sillimanite at higher temperatures (>~650°C, Althaus, 1967; >~760°C, Richardson et al., 1969).

3.8.2 **Conclusions**

From the previous considerations the following conclusions can be drawn:

a) Wollastonite formed before K-feldspar at a low X_{CO2}.

b) Pseudomorphs of sericite after andalusite, which formed due to reaction 3, indicate an increase of X_{CO2} concomitant with an increase in temperature.

c) Sericite and apatite formed during retrograde metamorphism due to the influx of a water-rich fluid of post magmatic origin carrying alkalis and phosphorous.

D CHEMICAL AND GENETICAL RELATIONSHIPS BETWEEN THE DIFFERENT GROUPS OF XENOLITHS

This chapter aims to show the genetical and chemical relationship between the different xenoliths. There is a relatively strong mineralogical relationship between the marginal and the critical zone xenoliths on the one hand and between the upper zone xenoliths on the other hand. Even though these two groups are mineralogically quite distinct with respect to the kind and diversity of the present minerals, the main components forming the dominant mineral assemblages are quite similar. These are $CaO-MgO-SiO_2-CO_2$ in the marginal and critical zone xenoliths and $CaO-MgO-Al_2O_3-SiO_2-CO_2-H_2O$ in the upper zone xenoliths. Experiments provide very good evidence that the minerals and mineral assemblages found in the upper zone xenoliths can readily result from those encountered in the marginal and critical zone xenoliths by adding Al_2O_3 and H_2O to the system $CaO-MgO-SiO_2-CO_2$. The Al_2O_3 content depends on the original bulk composition, while H_2O was predominantly introduced from an external source, most probably in the form of postmagmatic fluids, during retrograde metamorphism.

1 Vesuvianite and Grandite as Alteration Product of Melilite

The most abundant minerals in the marginal and critical zone xenoliths are melilite (akermanite-rich), monticellite and clinopyroxene. The predominant minerals in the upper zone xenoliths are vesuvianite, garnet (grandite), clinopyroxene, melilite (gehlenite-rich) and wollastonite. Experiments carried out by Christie (1961), Ito and Arem (1971), Olesch (1978), Valley and Essene (1979) and Hochella et al. (1982) emphasize the genetical relationship of those minerals. Ito and Arem (1970, 1971) discussed the stability of vesuvianite and the kinetics of the following reactions, using vesuvianites of different composition:

a) vesuvianite = melilite + monticellite + wollastonite + H_2O, and

b) vesuvianite = hydrogarnet + diopside ($+CaSiO_4.nH_2O$ + xanthophyllite)

Hochella et al. (1982) state that a) is a continuous reaction in which idocrase and melilite + monticellite coexist over a temperature

range. This, together with the upper and lower stability limit of vesuvianite, is represented in Figure 25 (after Hochella et al., 1982). It has to be pointed out that the indicated high temperature assemblage wollastonite-melilite-monticellite-H_2O is metastable at temperatures >800°C as wollastonite and monticellite react to form akermanite (Chapter C 3.4). As akermanite only increases the Mg content in melilite, the high temperature assemblage is melilite and H_2O. Christie (1961) discussed the dependence of the decomposition of melilite with respect to its composition, and concluded that akermanite-rich melilite ($Ak_{>25}$) decomposes together with water to form vesuvianite and hydrogarnet, while gehlenite rich melilite ($Ge_{>75}$) reacts together with water to form vesuvianite, wollastonite and clinopyroxene.

Willemse and Bensch (1964) assumed the vesuvianite-garnetfels of the upper zone xenolith B to be either alteration products of akermanite and monticellite or due to lower metamorphic temperatures reached in the upper zone magma. The latter is improbable because within xenolith D the high-temperature minerals akermanite and monticellite coexist with vesuvianite-bearing mineral assemblages, which are stable only at much lower temperatures. This indicates that the xenoliths in the upper zone were penetrated by sufficient amounts of water-rich post magmatic fluids to bring about a substantial or complete alteration of the melilite-rich high temperature mineral assemblages.

Apart from the volatile content, the bulk composition of the xenoliths is also significant in determining the amount of vesuvianite and garnet which formed from the melilite-rich mineral assemblages. Willemse and Bensch (1964) state that xenolith B is richer in aluminium than the marginal zone xenoliths, and is reflected in the greater abundance of vesuvianite and garnet in the former. In contrast to xenolith B, aluminium-poor melilites are a major constituent in xenolith D. These melilites have even lower aluminium contents (Analysis Ma 16 in Table 11a) than those present in the marginal- and critical zone xenoliths (Table 1), which seems to be the main reason for the absence of any signs of alteration into vesuvianite-bearing assemblages. The presence of vesuvianite in different parts of xenolith D, however, strongly indicates that some aluminium-rich melilite was

present in this xenolith at high temperatures and this has subsequently altered into vesuvianite-bearing assemblages.

The low aluminium content in the melilites together with the percolating water-rich fluids seems to be a prerequisite for the reaction akermanite = wollastonite + monticellite (Chapter C 3.4), which can be observed very often in xenolith D, but is rather an exception in the marginal zone xenoliths A and absent in the critical zone xenolith C.

From the previous considerations it seems to be very likely that most of the assemblages involving vesuvianite, grandite, melilite, monticellite, wollastonite and clinopyroxene formed from melilite-rich rocks and a water-rich postmagmatic fluid during retrograde metamorphism. This is borne out by the described replacement textures in which vesuvianite replaces melilite (I15 in Table 1 and 1a, Plate 2d and 2e), or monticellite (Ma22 in Plate 6g, Chapter C 3.3). Garnet, clinopyroxene and xantophyllite appear often in symplectic textures together with vesuvianite, which appear, at least partly, to be due to replacement reactions (Chapters C 3.3 and C 2.7).

The above-mentioned experiments that involve vesuvianite indicate the presence of hydrogarnet rather than garnet as decomposition product of vesuvianite. Ito and Arem (1970, 1971) state that large amounts of ferric iron (several wt.%) in starting materials for idocrase synthesis resulted in run products dominated by iron-rich grossular. This could readily account for the stability of grandites instead of hydrogrossular. No experimental results on Fe-vesuvianite-andradite involving reactions are published, and from the observations in the thin sections it remains somewhat ambiguous whether the garnets formed after, together or prior to vesuvianite. The occurrence of melanite idioblasts together with vesuvianite, as described in Chapter C 2.6 and C 2.7, indicates an earlier formation of garnet. The assemblages involving less Ti- and Fe-rich grandites and vesuvianite often form symplectic textures. Ito and Arem (1970) state that less than one tenth of the Al sites of Mg-idocrase can be filled by Fe^{3+}, and that with further increase of ferric iron, idocrase begins to break down to an Fe^{3+}-rich grossular. As most of the analysed vesuvianites

from xenolith B and D have relatively high Fe^{3+} contents, it seems as if some of the grandites originated more or less together with vesuvianite during retrograde metamorphism. The absence of hydrogrossular is therefore purely due to the presence of Fe^{3+} in the vesuvianites and garnets.

2 Externally Controlled Parameters Necessary for the Formation of Vesuvianite and Grandite

Pure akermanite or Al-poor melilites do not decompose to vesuvianite as a certain Al-content is necessary to form vesuvianite. This alteration is possible only in the presence of a water-rich fluid. Olesch (1978) states that vesuvianite is stable only at $X_{CO2} \leq 0.5$.

Willemse and Bensch (1964) ascribe the different mineralogy of the monticellite-akermanite fels of the marginal zone xenoliths and the vesuvianite-garnet felses in the upper zone xenolith D to differences in the amount and composition of volatiles in the magmas. To account for the observed alterations and pseudomorphic replacement of melilite by fibrous idocrase (Chapter B 2.5) they concluded that the environment was rather dry during formation of the monticellite-akermanite assemblages and that hydroxyl only became available at a later stage. Even though some of the analysed melilites from the marginal zone xenoliths and especially from the critical zone xenoliths have considerable amounts of aluminium, the majority of the present melilites are unaltered. This could be due to the absence of significant amounts of postmagmatic fluids percolating through the xenoliths, or to a dominance of carbon dioxide in these fluids. The latter is less probable as the water content usually exceeds the carbon dioxide content in postmagmatic fluids.

Figure 26 schematically illustrates how the xenoliths in the marginal, critical and upper zones of the eastern Bushveld Complex relate to each other. While most of the minerals and mineral assemblages in upper zone xenolith D can be obtained by merely introducing water to marginal zone xenolith A, the upper zone xenolith B is additionally enriched in Al_2O_3. The critical zone xenolith C is enriched in MgO but

consists, like the marginal zone xenoliths, of "dry" mineral assemblages. In order to form the present mineral assemblages it can be assumed that in the upper zone sufficient water was present during cooling below 800°C to permit the formation of vesuvianite from melilite. In the marginal and critical zone cooling below 800°C took place under "drier" conditions.

3 Source of the Xenoliths

The discussion on where the xenoliths come from has to remain purely speculative. Willemse and Bensch (1964) assumed that they are of sedimentary origin. The Bushveld magmas intruded into sediments of the Transvaal Sequence and melted and assimilated those sediments which contained a high proportion of minerals or mineral assemblages which melt at relatively low temperatures, e.g. pelitic rocks or greywackes. The more refractory rocktypes, e.g. quartzites and calc-silicates, partly survived this melting process. This accounts for the quartzite xenoliths, which are quite abundant in the igneous rocks of the Bushveld Complex, as well as for the less abundant calc-silicate xenoliths.

Willemse and Bensch (1964) mentioned a difference in the bulk composition between the marginal and critical zone xenoliths on the one hand and the upper zone xenoliths on the other hand. This could indicate that the different Bushveld magmas intruded into or melted different stratigraphic levels of the sedimentary rocks. From Figure 26 it is obvious, though, that only a slight change of the original bulk composition together with different conditions during retrograde metamorphism results in an almost completely different mineralogy.

E SUMMARY AND CONCLUSIONS

Calc-silicate xenoliths in the eastern Bushveld Complex record a series of irreversible reactions which took place during devolatilization, as well as reactions that occurred during retrograde metamorphism in the presence of a H_2O-rich fluid phase.

The maximum pressure and temperature conditions that governed the reactions leading to the present high temperature mineral assemblages found in the marginal and critical zone xenoliths, were calculated. For this, an internally consistent set of thermodynamic data has been compiled and used to establish equilibrium conditions. These calculations, together with some textural features and the application of experimental results give relatively narrow constraints on the intrusion depths and temperature of the marginal and critical zone magmas. The lack of melting of the xenoliths indicates that maximum temperatures did not exceed 1400°C. This is supported by the mineral assemblages present in the marginal and critical zone xenoliths, which indicate temperatures lower than 1390°C and overload pressures during the respective intrusions of less than 3.1 (marginal zone) and 2.3 kbar (critical zone).

The presence of dehydroxylated Ba-rich phlogopite indicates temperatures higher than 1050°C and the occurrence of forsterite exsolutions in optically positive monticellite further indicates temperatures in excess of 1200°C.

The above conclusions are in very good agreement with the experimental work by Sharpe and Irvine (1983) who have shown that the Bushveld magma temperature was between 1200 and 1300°C. On the basis of these temperatures, the calculated overload pressure at the time of emplacement of the marginal zone was between 1.1 and 2.4 kbar, while that at the time of the intrusion of the critical zone was calculated as between 0.6 and 1.6 kbar. Because merwinite and periclase are absent in the marginal zone xenoliths, it can be concluded that the gabbronoritic magma of the marginal zone had a lower temperature than than the magma from which the feldspathic pyroxenite of the critical zone crystallized. This conclusion is also supported by the observa-

tion that the forsterite exsolutions in monticellite are much more abundant and also bigger in the critical zone xenoliths than in the marginal zone xenoliths. Assuming a temperature of 1200°C for the marginal zone magma and 1300°C for the critical zone magma, the pressure estimates overlap in the range 1.1 to 1.6 kbar, which is equivalent to intrusion depths of ca. 3.3 - 4.8 km.

Besides minor sediments, felsites are assumed to form the roof-rocks of the Bushveld Complex (e.g. von Gruenewaldt et al. 1985). For the felsites, which are regarded as volcanic precursor of the plutonic episodes, Twist (1985) suggest a thickness of ca. 3.5 km. This would mean that the felsites formed the main constituent of the roof-rocks at the time of the Bushveld intrusion. Apart from that, the pressure calculations also indicate that large volumes of Bushveld magma were only emplaced after formation of the metamorphic mineral assemblages in the critical and marginal zone xenoliths. Had the total magma column been in place at that time, an additional lithostatic pressure of at least 1 kbar (>3 km thick magma column) would have prevailed, which is not reflected in the mineral assemblages of the xenoliths. This strongly supports the hypothesis (Sharpe, 1985) that the main zone magma was emplaced after most of the critical zone had crystallized.

Previous estimates and calculations from metamorphic mineral assemblages indicate different overburden pressures reaching from ca. 2 to 5 kbar (Chapter 2). The reasons for the existence of this range rather than one unique pressure need to be further investigated. Nevertheless, it can be stated that the pressure estimates are higher than those calculated from the mineral parageneses and mineral reactions found in the investigated calc-silicate xenoliths. The solid-solid reactions used for the pressure calculations in the floor-rocks (Chapter 2) reflect the maximum overburden pressure of more or less the whole column of Bushveld rocks. Critical parageneses described in the present investigation mainly result from irreversible solid-fluid reactions occurring during the actual intrusion of the respective Bushveld magmas in which the xenoliths were included. The resulting high-temperature low-pressure mineral parageneses were 'frozen in' and have not been affected by subsequent changes of the P-

T conditions. This explains the relatively low pressures inferred from the critical mineral parageneses found in the investigated xenoliths.

Based on the observations and calculations a petrogenitic grid was constructed, that serves to predict the fate of siliceous dolomites under very extreme geological conditions.

The occurrence and stability of the high-temperature parageneses is partly controlled by a fluid phase, which was CO_2-rich during prograde metamorphism and H_2O-rich during retrograde metamorphism. Whether and in how far there is an interaction of this fluid phase with the coexisting mineral phases remains somewhat enigmatic. Further investigations are necessary to elucidate this problem.

The mineral assemblages found in the upper zone xenoliths are different from those of the marginal and critical zone xenoliths and the major minerals are vesuvianite, grandite and melilite. Microprobe analyses of different coloured Mg-Fe-vesuvianites, garnets of different composition, prehnite and xantophyllite show interesting variations in their chemical composition. Most of the minerals and mineral assemblges found in the upper zone xenoliths can theoretically be obtained by taking the bulk composition of the marginal zone xenoliths, enriching it to a certain extent in Al and subjecting such high-temperature assemblages to retrograde metamorphism. During this, H_2O-rich fluids had to be introduced to form the water-bearing minerals.

It appears very probable that the high temperature mineral-assemblages in the marginal and upper zone xenoliths were rather similar. Melilite and monticellite are the predominating minerals in the marginal zone xenoliths where absence of an appropriate fluid phase prevented these minerals from reacting to form vesuvianite or vesuvianite-bearing assemblages during retrograde metamorphism. Water-rich postmagmatic fluids probably percolated through the upper zone xenoliths which was, together with the presence of aluminium-bearing melilites, a main precondition for the formation of vesuvianite during retrograde metamorphism of melilite + H_2O ($T<800^oC$: Hochella et al., 1982; $T<700^oC$: Ito and Arem, 1970).

Two different kind of textures predominate in the marginal-, critical- and upper zone xenoliths. A granoblastic-polygonal texture results from prograde metamorphism and is typical of the high temperature mineral assemblages in the marginal and critical zone xenoliths. Symplectic textures and intimate intergrowths are less abundant in the marginal and critical zone xenoliths but characterize the mineral assemblages in the upper zone xenoliths and are ascribed to retrograde metamorphism.

Acknowledgements

I would like to pay tribute to the Director of the Bushveld Institute, Prof. G. von Gruenewaldt who provided me with the opportunity of undertaking this study and for his valuable contribution as co-supervisor during the final stages of completion of the thesis

I wish to express my deepest appreciation to the Council of Scientific and Industrial Research (C.S.I.R.) for financial support during the period August 1984 to April 1988.

Special thanks go to my supervisor Dr. C.J. Hatton for his substantial help in developing the applied computer programs and for his helpful criticism during the course of this investigation.

I also wish to thank Dr. M.R. Sharpe who gave me an extremely valuable introduction to the field relationships in the Bushveld Complex and who provided valuable assistance as co-supervisor of this project until his resignation from the Institute.

Miss H.E. Horsch sacrified many hours both on and off duty to guide me through the analytical procedures at the microprobe.

To Dr. G.T. Droop (University of Manchester) and Dr. S.L. Harley (Oxford University), I extend my grateful appreciation for their interest and helpful discussions during my investigation.

I wish to thank J. Nell who cordially handed to me some of his rock specimens to include them into my investigation.

I am also indebted to H.J. Schweitzer, M. Potgieter, Dr. R.K.W. Merkle, F.J. Reichhardt, Dr. D. Twist, H.J. Wilhelm, D. Harney and Dr. P.J. Hattingh for their stimulating interest and moral support.

Finally, I would like to thank L.J. Jacobs who prepared most of the thin sections used in this investigation.

References

Adams, G.E. and Bishop, F.C. (1985) An experimental investigation of thermodynamic properties and unit-cell parameters of forsterite-monticellite solid solutions. American Mineralogist 70, 714-722.

Althaus, E. (1967) The triple point andalusite-sillimanite-kyanite. An experimental and petrologic study. Contributions to Mineralogy and Petrology 16, 29-44.

Boettcher, A.L. (1970) The system $CaO-Al_2O_3-SiO_2-H_2O$ at high temperatures and pressures. Journal of Petrology 11, 337-379.

Bottinga, Y. and Richet, P. (1981) High pressure and temperature equation of state and calculation of the thermodynamic properties of gaseous carbon dioxide. American Journal of Science 281, 615-660.

Bowen, N.L. (1940) Progressive metamorphism of siliceous limestones and dolomite. Journal of Geology 68, 225-274.

Brousse, C., Newton, R.C. and Kleppa, O.J. (1984) Enthalpy of formation of forsterite, enstatite, akermanite, monticellite and merwinite at 1073°C determined by alkali borate solution calorimetry. Geochimica and Cosmochimica Acta 48, 1081-1088.

Bulatov, V.K. (1974) Experimental studies of mineral equilibria in high-temperature part of the system $CaO-MgO-SiO_2-CO_2-H_2O$. Geochimia 8, 1268-1271 (in Russian).

Burnham, C.W. (1959) Contact metamorphism of magnesian limestones at Crestmore, California. Bulletin of the Geological Society of America, 70, 879-920.

Burnham, C.W. (1979) The importance of volatile constituents. In: The Evolution of the Igneous Rocks, ed. H.S. Yoder, Princeton University Press.

Burnham, C.W., Holloway, J.R. and Davis, N.F. (1969) Thermodynamic properties of water to 1000°C and 10000 bars. Geological Society of America Special Paper 132.

Cameron, W.E. (1976) Coexisting sillimanite and mullite. Geological Magazine, 113, 497-515.

Carmichael, D.M. (1977) Chemical equilibria involving pure crystalline compounds. In H.J. Greenwood, Ed., MAC short course in application of thermodynamics to petrology and ore deposits. Mineralogical Association of Canada, 47-65.

Charlu, T.V., Newton, R.C. and Kleppa, O.J. (1981) Thermochemistry of synthetic $Ca_2Al_2SiO_7$ (gehlenite)-$Ca_2MgSi_2O_7$ (akermanite) melilites. Geochimica and Cosmochimica Acta 45, 1609-1617.

Chaterjee, N.D. and Johannes, W. (1974) Thermal stability and standard thermodynamic properties of synthetic $2M_1$-muscovite, $KAl_2[AlSi_3O_{10}(OH)_2$. Contributions to Mineralogy and Petrology 48, 89-114.

Chou, I. and Williams, R.J. (1977) Activity of H_2O in CO_2-H_2O at 600°C and pressure to 8 kilobars (abstract). Geological Society of America Annual Reports 9, 928.

_____ (1979) The activity of H_2O in supercritical fluids: H_2O-CO_2 at 600°C and 700°C at elevated pressures (abstract). Lunar and Planetary Science Conference, 10th, X, 201-203.

Christie O.H.J. (1961) On subsolidus relations of silicates. I. The lower break down temperature of the akermanite gehlenite mixed crystal series at moderate water pressue. Norsk Geologisk Tidsskrif 41, 225-269.

Christophe-Michel-Levy M. (1960) Reproduction artificelle de l'idocrase. Bulletin de la Societe Francaise de Mineralogie et de Crystallograpie 83, 23-25.

Coda, A., Della Giusta, A., Isetti, G. and Mazzi F. (1970) On the crystal structure of vesuvianite. Atti della Accademia delle Scienze dell'Instituto di Torino 105, 63-84.

Coetzee, G.L. (1970) The Rooiberg felsites series, north of Nylstrom. Geological Society of South Africa Special Publication, 1, 312-325.

Coombs, D.S., Ellis, A.J., Fyfe, W.S. and Taylor, A.M. (1959) The zeolite facies; with comments on the interpretation of hydrothermal syntheses. Geochimica and Cosmochimica Acta 17, 53.

Deer, W.A., Howie, R.A. and Zussman, J. (1961) Rock-Forming Minerals, Volume 3, Sheet Silicates. Longman, London.

Deer,W.A., Howie, R.A.and Zussman, J. (1975) An Introduction to the Rock-Forming Minerals. Longman, London.

Deer, W.A., Howie, R.A. and Zussman, J. (1982) Rock-Forming Minerals, Volume 1a, Orthosilicates. Longman, London.

Dixon B.E. and Kennedy W.Q. (1933) Optically uniaxial titanaugite from Aberdeenshire. Zeitschrift für Kristallographie 86, 112-120.

Edmister, W.C. (1968) Applied Hydrocarbon Thermodynamics, Part 32-Compressibility Factors and Fugacity Coefficients from the Redlich-Kwong Equation of State. Hydrocarbon Processing, 47, 9, 239-244.

Fein, J.B. and Walther J.V. (1987) Calcite solubility in supercritical CO_2-H_2O fluids. Geochimica and Cosmochimica Acta, 51 1665-1673.

Ferry, J.M. and Spear, F.S. (1978) Experimental calibration of the partitioning between biotite and garnet: Contributions to Mineralogy and Petrology 66, 113-117.

Fyfe, W.S., Price, N.J. and Thompson A.B. (1978) Fluids in the earth's crust. Developments in Geochemistry, 1. Elsevier.

Finger. L.W. (1972) The uncertainty in the calculated ferric iron content of a microprobe analysis. Carnegie Institute of Washington Yearbook 71, 600-603.

Flowers, G.C. (1979) Correction of Holloway's (1977) adaption of the modified Redlich-Kwong equation of state for calculation of fugacities of molecular species in supercritical fluids of geologic interest. Contributions to Mineralogy and Petrology 69, 315-318.

French, B.M. and Twist, D. (1983) Status of the Rooiberg felsites in the Bushveld Complex: A review. Institute for Geological Research on the Bushveld Complex, 39.

Ghent, E.D. (1976) Plagioclase-garnet-Al_2O_3-quartz: A potential geobarometer-geothermometer. American Mineralogist 61, 710-714.

Gordon, T.M. and Greenwood, H.J. (1971) The stability of grossularite in H_2O-CO_2 mixtures. American Mineralogist 56, 1674-1688.

Greenwood, H.J. (1967) Wollastonite: stability in H_2O-CO_2 mixtures and occurrence in contact-metamorphic aureole near Salmo, British Columbia Canada. American Mineralogist 52, 1669-1680.

Gruenewaldt, G. von (1977) The mineral resources of the Bushveld Complex. Minerals Science and Engineering 9, 83-95.

Gruenewaldt, G. von, Sharpe, M.R. and Hatton, C.J. (1985) The Bushveld Complex: introduction and review. Economic Geology 80, 803-812.

Guo Q. (1984) Topological relations in multisystems of more than n+3 phases. Journal of metamorphic Geology 2, 267-295.

Hall, A.L. (1911) Note on some remarkable xenoliths of altered shale from the norite of Potgietersrus and Mapoch's country. Transactions of the Geological Society of South Africa 14, 74-78.

Hall, A.L. and Nel, L.T. (1926) On an occurrence of corundum-sillimanite rock in the norite of the Bushveld igneous complex. Transactions of the Geological Society of South Africa 29, 1-16.

Hamilton, J. (1977) Sr-isotope and trace element studies of the Great Dyke and Bushveld mafic Phase and their relation to early Proterozoic magma genesis in Southern Africa. Journal of Pretrology 18, 24-52.

Harker, R.I. and Tuttle, O.F. (1956) The lower limit of stability of akermanite ($Ca_2MgSi_2O_7$). American Journal of Science 254, 468-478.

Hattingh, P.J. (1980) The structure of the Bushveld Complex in the Groblersdal-Lydenburg-Belfast area of the eastern Transvaa as interpreted from a regional gravity survey. Transactions of the Geological Society of South Africa 83, 125-133.

Harmer, R.E. and Sharpe, M.R. (1985) Field relations and strontium isotope systematics of the marginal rocks of the eastern Bushveld Complex. Economic Geology 80, 813-837.

Helgeson, H.C., Delany, J.M., Nesbitt, H.W. and Bird, D.K. (1978) Summary and critique of the thermodynamic properties of rock-forming minerals. American Journal of Science 278 A, 1-229.

Hemingway, B.S., Evans Jr., H.T., Nord Jr., G.L., Haselton Jr, H.T., Robie, R.A. and McGee, J.J. (1986) Akermanite: Phase transitions in heat capacity and thermal expansion, and revised thermodynamic data. Canadian Mineralogist 24, 425-434.

Hey, M.H. (1954) A new review of the chlorites. Mineralogical Magazine 30, 1954, 227-292.

Hochella M.F. jr., Liou, J.G., Keskinen M.J. and Kim H.S (1982) Synthesis and stability relations of magnesium idocrase. Economic Geology 77, 798-808.

Hoisch, T.D. (1985) The solid solution chemistry of vesuvianite. Contributions to Mineralogy and Petrology 89, 205-214.

Holland, T.J.B. (1981) Thermodynamics of simple mineral systems. In: Thermodynamics of Minerals and Melts, Newton, R.C., Navrotsky, A. and Wood, B.J., Springer Verlag, New-York.

Holloway, J.R. (1977) Fugacity and activity of molecular species in supercritical fluids. In: Thermodynamics in Geology, Fraser. D.G., Reidel Publishing Corporation, Holland.

Hoschek, G. (1974) Gehlenite stability in the system $CaO-Al_2O_3-SiO_2-H_2O-CO_2$. Contributions to Mineralogy and Petrology 47, 245-254.

Huckenholz, H.G., Hölzl E. and Lindhuber, W. (1975) Grossularite, its solidus and liquidus relations in the $CaO-Al_2O_3-SiO_2-H_2O$ system up to 10 kbar. Neues Jahrbuch der Mineralogie, Abhandlungen 124, 1-46.

Huckenholz, H.G., Lindhuber, W. and Springer, J. (1974) The join $CaSiO_3-Al_2O_3-Fe_2O_3$ of the $CaO-Al_2O_3-Fe_2O_3-SiO_2$ quaternary system. and its bearing on the formation of granditic garnets and fassaitic pyroxenes. Neues Jahrbuch der Mineralogie, Abhandlungen 121, 160-207.

Huggins, F.E, Virgo, D. and Huckenholz H.G. (1977) Titanium-containing silicate garnets. I. The distribution of Al, Fe^{3+}, and Ti^{4+} between octahedral and tetrahedral sites. American Mineralogist 62, 475-490.

Hulbert, L.J and Sharpe, M.R. (1981a) Metamorphics project. Institute for Geological Research on the Bushveld Complex, University of Pretoria, Annual Report 1980, 30-32.

Hulbert, L.J and Sharpe, M.R. (1981b) Stop 1: andalusite-biotite-cordierite-muscovite hornfels, Faugha Ballagh. In Vermaak, C.F and von Gruenewaldt, editors, Third international platinum symposium - excursion guidebook. Geological Society of South Africa, 39-41.

Human, D.R. (1975) The geology and metamorphic petrology of part of the basal argillaceous zone, Daspoort stage, Pretoria series on the farm Havercroft, north eastern Transvaal. Petros 6, 25-43.

Hunt, J.A. and Kerrick, D.M. (1977) The stability of sphene; experimental redetermination and geologic implications. Geochimica and Cosmochimica Acta 41, 279-288.

Ito, J. and Arem, J.E. (1970) Idocrase: synthesis, phase relations and crystal chemistry. American Mineralogist 55, 880-912.

Ito, J. and Arem, J.E. (1971) Idocrase: synthesis, phase relations and crystal chemistry. Mineralogical Society of Japan Special Papers 1, 63-66.

Joesten, R. (1974) Pseudomorphic replacement of melilite by idocrase in a zoned calc-silicate skarn, Christmas Mountains, Big Bend Region, Texas. American Mineralogist 59, 694-699.

Joubert, J. (1976) Gemetamorfoseerde karbonaatinsluitsels in die bosone van die Bosveldstollingskompleks, wes van Roossenekal, Transvaal. MSc thesis (unpublished) University of Pretoria.

Kerrick, D.M. and Jacobs, G.K. (1981) A modified Redlich-Kwong equation for H_2O, CO_2 and H_2O-CO_2 mixtures at elevated pressures and temperatures. American Journal of Science 281, 735-767.

Kushiro, I. (1964) Stability field of akermanite. Carnegie Institute of Washington Year Book 63, 84-86.

_____ and Yoder, H.S. (1964) Breakdown of monticellite and akermanite at high pressures. Carnegie Institute of Washington Year Book 63, 81-83.

Manning, P.G. (1975) Charge-Transfer processes and the origin of colour and pleochroism of some Ti-rich vesuvianites. Canadian Mineralogist 13, 110-116.

Manning, P.G. and Tricker, M.J. (1975) Optical-absorption and Mössbauer spectral studies of iron titanium site-populations in vesuvianites. Canadian Mineralogist 13, 259-265.

Miyashiro, A. (1973) Metamorphism and Metamorphic Belts. George Allen & Unwin, London.

Moore, P.B. and Araki, T. (1972) Atomic arrangement of merwinite, $Ca_3Mg[SiO_4]_2$, an unusual dense-packed structure of geophysical interest. American Mineralogist 57, 1355-1374.

Mostert, A.B (1982) The mineralogy, petrology and sulphide mineralization of the Plat Reef north-west of Potgietersrus, Transvaal, Republic of South Africa. Geological Survey of South Africa, Bulletin 72, 1-48.

Nell, J. (1985) The Bushveld metamorphic aureole in the Potgietersrus area: evidence for a two-stage metamorphic event. Economic Geology, 80, 1985.

Neuvonen, K.J. (1952a) Thermochemical investigation of the akermanite-gehlenite series. Bulletin de la Commission Geologique De Finlande 26, 5-50.

Neuvonen, K.J. (1952b) Heat of formation of merwinite and monticellite. American Journal of Science, (Bowen Volume), 373-380.

Nurse R.W. and Midgley H.G. (1953) Studies on the melilite solid solutions. Journal of the Iron and Steel Institute 174, 121-131.

Olesch, M. (1978) Obere thermische Stabilitat von Vesuvian (Idocrase) bis 2 Kbar und Vesuvian + Quarz bis 5 Kbar im System CaO-MgO-Al_2O_3-SiO_2-H_2O (abstract). Fortschritte der Mineralogie 56, 99.

Olesch, M. and Seifert, F. (1976) Stability and phase relations of trioctahedral calcium brittle micas in the system CaO-MgO-Al_2O_3-SiO_2-H_2O. American Mineralogist 60, 188-199.

Osborn E.F., Roeder P.L and Ulmer G.C. (1969) Phase equilibria at solidus temperatures in the quarternary system CaO-MgO-Al_2O_3-SiO_2, and their bearing on optimum composition of blast furnace slag and on slag properties. The Pennsylvania State University, Eart and Minneral Sciences Experimental Station Bulletin 85, 1-22.

Page, D.C. (1970) The mineralogy of South African Jade and the associated rocks in the district Rustenburg, Western Transvaal. MSc thesis (unpublished), University of Pretoria.

Philpotts, A.R., Pattison, E.F. and Fox, J.S. (1967) Kalsilite, diopside and melilite in a sedimentary xenolith from Brome Mountain, Quebec. Nature 214, 1322-1323.

Powell, R. (1978) Equilibrium Thermodynamics in Petrology. Harper and Row, London.

Powell, R. and Holland, T.J.B. (1985) An internally consistent thermodynamic dataset with uncertainties and correlations. Journal of Metamorphic Geology 3, 327-342.

Prausnitz, J.M. (1974) Molecular thermodynamics of fluid-phase equilibria, Prentice-Hall, New Jersey.

Råheim, A. and Green, D.H. (1974) Experimental determination of the temperature and pressure dependence of the Fe-Mg partition coefficient for coexisting garnet and clinopyroxene. Contributions to Mineralogy and Petrology 48, 179-203.

Redlich, O. and Kwong, J.N.S. (1949) An equation of state. Fugacities of gaseous solutions. Chemistry Reviews, 233-244.

Richardson, S.W., Gilbert, M.C. and Bell, P.M. (1969) Experimental determination of kyanite-andalusite and andalusite-sillimanite equilibria; The aluminum silicate triple point. American Journal of Science 267, 259-272.

Rhodes, R.C. (1974) Petrochemical characteristics of Bushveld Granite and Rooiberg felsite. Transactions of the Geological Society of South Africa 78, 93-98.

Robie, R.A. and Waldbaum D.R. (1978) Thermodynamic properties of minerals and related substances at 298.15K (25°C) and one atmosphere (1.013 bars) pressure and at higher temperatures. United States Geological Survey Bulletin 1452.

Roedder, E. (1984) Fluid inclusions. Reviews in Mineralogy, vol. 12.

Roseboom, E.H. Jr. and Zen, E-an (1982) Unary and binary multisystems, topological classification of phase diagrams and relation to Euler's theorem on polyhedra. American Journal of Science 282, 286-310.

Roy, D.M. and Roy, R. (1957) System CaO-Al_2O_3-SiO_2-H_2O. VI. The grossularite CaO.Al_2O_3.6H_2O join (abstract). Bulletin of the Geological Society of America 68, 1788-1789.

Rucklidge, J.C, Kocman V., Whitlow, S.H. and Gabe, E.J. (1975) The crystal structure of three Canadian vesuvianites. The Canadian Mineralogist 13, 15-21.

Santis, R. de, Breedveld, G.J.F. and Prausnitz, J.M. (1974) Thermodynamic properties of aqueous gas mixtures at advanced pressures. Industrial & Engineering Chemistry Process Design & Development 13, 374-377.

Saxena, S.K. (1973) Thermodynamics of Rock-Forming Crystaline Solutions. Springer Verlag.

Schmid, R. and Wood, B.J. (1976) Phase relationships in granulite metapelites from the Ivrea-Verbano zone (Northern Italy). Contributions to Mineralogy and Petrology 54, 255-279.

Schuiling, R.D. and Vink, B.W. (1967) Stability relations of some titanium-minerals (sphene, perovskite, rutile, anatase). Geochimica et Cosmochimica Acta 31, 2399-2411.

Seifert, F. (1974) Stability of sapphirine: a study of the aluminous part of the system $MgO-Al_2O_3-SiO_2-H_2O$. Journal of Geology 82, 173-204.

Sharp, W.E. and Kennedy G.C. (1965) The system $CaO-CO_2-H_2O$ in the two-phase region calcite + aqueous solution. Journal of Geology 73, 391-403.

Sharp, Z.D., Essene, E.J., Anovitz, L.M., Metz, G.W., Westrum Jr, E.F., Hemingway, B.S. and Valley, J.W. (1986) The heat capacity of a natural monticellite and phase equilibria in the system $CaO-MgO-SiO_2-CO_2$. Geochimica and Cosmochimica Acta 50, 1475-1484.

Sharpe, M. R. (1985) Strontium isotope evidence for preserved density stratification in the main zone of the Bushveld Complex, South Africa. Nature 316, 119-126.

Sharpe, M.R. and Förtsch, E. (1981) Grandite garnet in metamorphosed stromatolites from the Houtenbek Formation, eastern Transvaal. Transactions of the Geogical Society of South Africa 84, 245-250.

Sharpe M.R. and Irvine T.N. (1983) Melting relations of two Bushveld margin rocks and implications for the origin of chromite. Carnegie Institute of Washington Yearbook 82, 295-300.

Skinner, B.J. (1966) Thermal expansion. In: Handbook of Physical Constants (ed. Clark, S.P.) 75-96. Geological Society of America Memoir 97.

Shmonov, V.M. and Shmulovich, K.I. (1974) Molar volumes and equations of state for CO_2 between 100-1000°C and 2000-10000 bars. Dokladi Akademii Nauk SSSR 217, 935-938.

Slaughter, J., Kerrick, D.M., Wall, V.J. (1975) Experimental and thermodynamic study of equilibria in the system $CaO-MgO-SiO_2-H_2O-CO_2$. American Journal of Science 275, 143-162.

Speer, J.H and Ribbe, P.H. (1982) Miscalleneous Orthosilicates; in: Reviews in Mineralogy 5, 413-417.

Solie, D.N. and Su, S.C. (1987) An occurrence of Ba-rich micas from the Alaska Range. American Mineralogist, 72, 995-999.

Tilley, C.E. (1948) The gabbro-limestone contact zone of Camas Mòr, Muck, Inverness-shire. Bulletin de la Commission géologique de Finlande 140, 97-104.

Tracy, R.J. (1978) Monticellite marble at Cascade Mountain, Adirondack Mountains, New York. American Mineralogist, 63, 991-999.

Tröger, W.E. (1969) Optische Bestimmung der Gesteinsbildenden Minerale. Schweizerbart, 2. Auflage.

Turner, F.J. (1968) Metamorphic Petrology. McGraw-Hill, 1st edition.

Twist, D. (1985) Geochemical evolution of the Rooiberg silicic lavas in the Loskop Dam area, Southeast Bushveld. Economic Geology, 80, 1153-1165.

_____ and Harmer R.E. (1987) Geochemistry of contrasting siliceous magmatic suites in the Bushveld Complex: Genetic aspects and implication for tectonic discrimination diagrams. Journal of Vulcanology and Geothermal Research, 32, 83-98.

Valley, J.W. and Essene, E.J. (1980) Akermanite in the Cascade Slide Xenolith and its significance for regional metamorphism in the Adirondacks. Contributions to Mineralogy and Petrology 74, 143-152.

Walter, L.S. (1963a) Experimental studies on Bowen's decarbonation series. I; P-T univariant equilibria of the "monticellite" and "akermanite" reactions. American Journal of Science 261, 488-500.

_____ (1963b) Experimental studies on Bowen's decarbonation series. II; P-T univariant equilibria of the reaction forsterite + calcite = monticellite + periclase + CO_2. American Journal of Science 261, 773-779.

_____ (1966) Synthesis and composition of idocrase in the system $CaO-MgO-Al_2O_3-SiO_2-H_2O$. Geological Society of America Special Papers.

Wang, H.F. (1978) Elastic constants systematics. Physics and Chemistry of Minerals 3, 251-261.

Warner, R.D and Luth, W.C. (1973) Two-phase data for the join monticellite ($CaMgSiO_4$) - forsterite (Mg_2SiO_4): Experimental results and numerical analysis. American Mineralogist 58, 998-1008.

Weller, W.W, and Kelley, K.K. (1963) Low-temperature heat capacities and entropies at 298.15°K of akermanite, cordierite, gehlenite and merwinite: United States Bureau of Mines Report of Investigations 6343, 7.

Wells, P.R.A. (1979) Chemical and thermal evolution of Archean sialic crust, southern Greenland. Journal of Petrology 20, 187-226.

Willemse, J. and Bensch, J.J. (1964) Inclusions of original carbonate rocks in gabbro and norite of the eastern part of the Bushveld Complex. Transactions and Proceedings of the Geological Society of South Africa 67, 1-87.

Winkler, H.G.F. (1979) Petrogenesis of Metamorphic Rocks. Springer Verlag, 5th edition.

Willemse J. and Viljoen, E.A. (1970) The fate of argillaceous material in the gabbroic magma of the Bushveld Complex. Geological Society of South Africa Special Publication 1, 336-366.

Wohl, K. (1946) Thermodynamic evaluations of binary and ternary liquid systems. Transactions of the American Institute of Chemical Engineers 42, 215-249.

Wood, B.J. and Fraser D.G. (1976) Elementary Thermodynamics for Geologists. Oxford University Press.

Wyllie and Tuttle (1960) The system $CaO-CO_2-H_2O$ and the origin of carbonatites. Journal of Petrology 1, 1-46.

Yoder, H.S. (1968) Akermanite and related melilite-bearing assemblages. Carnegie Institute of Washington Yearbook 66, 471-477.

_____ (1973) Melilite stability and paragenesis. Fortschritte der Mineralogie 50, 140-173.

_____ and Eugster, H.P.(1955) Synthetic and natural muscovites. Geochimica and Cosmochimica Acta 8, 225-280.

Yoshii, M. and Maeda, K. (1975) Relations between barium content and the physical and optical properties in the manganoan phlogopite-kinoshitalite series. Mineralogical Journal 8, 58-65.

Zen, E-an. (1966) Construction of pressure-temperature diagrams for multicomponent systems after the method of Schreinemakers - a geometric approach. United States Geological Survey Bulletin 1225.

Zharikov, V.A, Shmulovich, K.I. and Bulatov, V.K. (1977) Experimental studies in the system $CaO-MgO-Al_2O_3-SiO_2-CO_2-H_2O$ and conditions of high temperature metamorphism. Tectonophysics 43, 145-162.

Table 1 Representative microprobe analyses (wt.% and atoms per formula unit) of merwinite, periclase, melilite, monticellite, clinopyroxene, olivine, spinel, kalsilite, larnite and Ba-rich phlogopite, occurring in xenoliths A and C.

	Mer.			Per.	Melilite							Monticellite					Clinopyroxene	
	Wi	Wia	Wib	Wi7	J8(1)	J8(2)	J6	J6a	I15	Wila	Wilb	J8	I3	Wil	Wi7	Wia	J8	J21
SiO_2	35.64	36.34	37.04	0.01	42.28	42.44	35.08	42.23	38.89	33.21	28.49	37.39	37.37	37.91	37.64	38.20	46.08	52.87
TiO_2	0.03	0.00	0.00	0.00	0.02	0.01	0.00	0.00	0.00	0.00	0.00	0.01	0.04	0.02	0.03	0.03	2.09	0.54
Al_2O_3	0.00	0.00	0.00	0.00	5.80	3.71	16.74	4.86	8.77	16.04	24.18	0.00	0.00	0.01	0.00	0.01	9.31	2.06
Cr_2O_3	0.01	0.03	0.00	0.03	0.00	0.00	0.00	0.00	0.01	0.02	0.00	0.03	0.01	0.02	0.01	0.00	0.00	0.05
Fe_2O_3*	0.00	0.00	0.00	0.00	0.00	0.00	0.00	0.00	0.00	0.00	0.00	0.00	0.00	0.00	0.00	0.00	1.40	0.00
FeO	0.30	0.39	0.36	3.54	0.69	0.83	0.61	0.85	0.31	0.68	0.79	4.01	1.37	0.60	0.61	0.51	2.21	1.49
MnO	0.01	0.00	0.00	0.12	0.03	0.00	0.04	0.03	0.00	0.01	0.01	0.29	0.10	0.31	0.31	0.18	0.05	0.03
MgO	11.60	11.62	12.01	96.23	10.90	11.84	7.11	11.70	10.23	7.91	4.68	22.20	25.31	25.48	25.70	25.91	13.44	16.88
CaO	52.19	50.89	49.95	0.00	38.94	39.85	40.06	39.99	41.06	41.59	41.66	35.82	35.84	35.71	35.73	35.13	25.48	25.83
Na_2O	0.00	0.03	0.01	0.00	1.06	1.08	0.30	0.31	0.27	0.04	0.04	0.00	0.01	0.02	0.00	0.00	0.00	0.00
K_2O	0.00	0.00	0.00	0.00	0.23	0.32	0.03	0.04	0.23	0.03	0.03	0.00	0.00	0.00	0.00	0.00	0.00	0.00
Total	99.78	99.30	99.37	99.93	99.95	100.08	99.98	100.01	99.77	99.53	99.88	99.75	100.05	100.07	100.01	99.97	100.06	99.75
Formula	8(O)			1(O)	7(O)							4(O)					(O)	
Si	1.97	2.01	2.03	0.00	1.91	1.93	1.59	1.91	1.78	1.53	1.31	1.00	0.98	0.99	0.99	1.00	1.69	1.93
Ti	0.00	0.00	0.00	0.00	0.03	0.00	0.00	0.00	0.00	0.00	0.00	0.00	0.00	0.00	0.00	0.00	0.06	0.01
Al	0.00	0.00	0.00	0.00	0.31	0.20	0.90	0.26	0.47	0.87	1.31	0.00	0.00	0.00	0.00	0.00	0.40	0.09
Cr^{3+}	0.00	0.00	0.00	0.00	0.00	0.00	0.00	0.00	0.00	0.00	0.00	0.00	0.00	0.00	0.00	0.00	0.00	0.00
Fe^{3+}*	0.00	0.00	0.00	0.00	0.00	0.00	0.00	0.00	0.00	0.00	0.00	0.00	0.00	0.00	0.00	0.00	0.04	0.00
Fe^{2+}	0.01	0.02	0.02	0.02	0.03	0.03	0.02	0.03	0.01	0.03	0.03	0.09	0.03	0.01	0.01	0.01	0.07	0.05
Mn	0.00	0.00	0.00	0.00	0.00	0.00	0.00	0.00	0.00	0.00	0.00	0.01	0.00	0.01	0.01	0.00	0.00	0.00
Mg	0.95	0.96	0.98	0.98	0.74	0.80	0.48	0.79	0.70	0.54	0.32	0.88	0.99	0.99	1.00	1.01	0.74	0.92
Ca	3.09	3.01	2.94	0.00	1.89	1.94	1.95	1.94	2.01	2.06	2.05	1.02	1.00	1.00	1.00	0.98	1.00	1.01
Na	0.00	0.00	0.00	0.00	0.09	0.10	0.03	0.03	0.02	0.00	0.00	0.00	0.00	0.00	0.00	0.00	0.00	0.00
K	0.00	0.00	0.00	0.00	0.01	0.02	0.00	0.00	0.01	0.00	0.00	0.00	0.00	0.00	0.00	0.00	0.00	0.00
Total	6.02	6.00	5.97	1.00	5.01	5.02	4.97	4.96	5.00	5.03	5.02	3.00	3.00	3.01	3.01	3.00	4.00	4.01
					Ak_{66}	Ak_{75}	Ak_{46}	Ak_{74}	Ak_{71}	Ak_{57}	Ak_{34}							

Table 1a

	Olivine						Spinel					Kals.	Lar.	Ba-Phl.			Ves
	J8	I3	J21	Wi1	Wi7	Wia(6)	J6	J8	Wi7	I3	Wia	J21	J8	J21	J6(a)	J6(b)	I15
SiO_2	41.87	41.83	41.35	42.32	42.07	41.93	0.04	0.05	0.04	0.00	0.03	37.84	35.73	36.74	31.21	31.67	36.39
TiO_2	0.00	0.00	0.00	0.00	0.00	0.00	0.09	0.02	0.46	0.11	0.65	0.00	0.00	0.00	3.33	3.30	0.00
Al_2O_3	0.01	0.02	0.02	0.01	0.01	0.00	67.25	66.13	61.26	70.01	61.79	31.13	0.07	15.86	18.91	18.50	10.02
Cr_2O_3	0.00	0.02	0.01	0.00	0.00	0.00	0.00	0.17	0.11	0.01	0.14	0.00	0.01	0.01	0.00	0.00	0.01
Fe_2O_3 *	0.20	1.30	0.95	0.53	0.66	0.67	3.44	4.66	10.93	1.12	9.74	0.00	0.00	1.42	2.54	2.34	0.57
FeO	3.24	0.00	4.07	0.00	0.00	0.00	3.97	3.87	0.40	1.51	0.85	0.46	0.18	0.00	0.00	0.00	0.00
MnO	0.30	0.09	0.18	0.27	0.28	0.27	0.11	0.20	0.12	0.02	0.20	0.02	0.00	0.02	0.04	0.04	0.00
MgO	53.95	55.97	53.02	57.33	56.88	56.82	25.31	25.15	27.37	27.17	27.02	0.00	0.00	25.70	23.03	23.66	9.73
CaO	0.40	0.87	0.36	0.47	0.37	0.39	0.05	0.04	0.00	0.01	0.00	0.01	63.54	0.00	0.04	0.17	38.58
BaO	0.00	0.00	0.00	0.00	0.00	0.00	0.00	0.00	0.00	0.00	0.00	0.00	0.00	7.21	12.69	14.60	0.00
Na_2O	0.00	0.00	0.00	0.00	0.00	0.00	0.00	0.00	0.00	0.00	0.00	0.00	0.00	0.00	0.03	0.05	0.00
K_2O	0.00	0.00	0.03	0.00	0.00	0.00	0.00	0.01	0.00	0.01	0.00	30.42	0.10	8.84	6.23	5.77	0.01
H_2O **														4.20	1.95		
Total	99.97	100.10	99.99	100.93	100.27	100.08	100.26	100.30	100.69	99.97	100.42	99.88	99.63	100.00	100.00	100.10	95.31
Formula	4(0)						4(0)					4(0)	4(0)	22(0) norm.			50 cat. norm.
Si	1.00	0.99	0.99	0.99	0.99	0.99	0.00	0.00	0.00	0.00	0.00	1.01	1.04	5.44	4.67	4.69	17.41
Ti	0.00	0.00	0.00	0.00	0.00	0.00	0.00	0.00	0.01	0.00	0.01	0.00	0.00	0.00	0.37	0.37	0.00
Al	0.00	0.00	0.00	0.00	0.00	0.00	1.93	1.91	1.78	1.98	1.80	0.97	0.02	2.78	3.34	3.31	5.65
Cr^{3+}	0.00	0.00	0.00	0.00	0.00	0.00	0.00	0.00	0.00	0.00	0.00	0.00	0.00	0.00	0.00	0.00	0.00
Fe^{3+} *	0.00	0.02	0.02	0.01	0.01	0.01	0.07	0.09	0.20	0.02	0.18	0.00	0.00	0.02	0.29	0.26	0.22
Fe^{2+}	0.06	0.00	0.08	0.00	0.00	0.00	0.08	0.08	0.01	0.03	0.02	0.01	0.00	0.00	0.00	0.00	0.00
Mn	0.01	0.00	0.00	0.01	0.00	0.00	0.00	0.00	0.00	0.00	0.00	0.00	0.00	0.00	0.00	0.00	0.00
Mg	1.92	1.97	1.90	1.99	1.99	1.99	0.92	0.92	1.00	0.97	0.99	0.00	0.00	5.67	5.13	5.22	6.94
Ca	0.01	0.02	0.01	0.01	0.01	0.01	0.00	0.00	0.00	0.00	0.00	0.00	1.95	0.00	0.01	0.03	19.77
Ba	0.00	0.00	0.00	0.00	0.00	0.00	0.00	0.00	0.00	0.00	0.00	0.00	0.00	0.42	0.74	0.85	0.00
Na	0.00	0.00	0.00	0.00	0.00	0.00	0.00	0.00	0.00	0.00	0.00	0.00	0.00	0.00	0.01	0.01	0.00
K	0.00	0.00	0.00	0.00	0.00	0.00	0.00	0.00	0.00	0.00	0.00	1.03	0.00	1.67	1.19	1.09	0.01
Total	3.00	3.00	3.00	3.01	3.00	3.00	3.00	3.00	3.00	3.00	3.00	3.02	3.01	16.00	15.75	15.83	50.00
(OH)														(0.00)	(1.94)	(0.00)	
(O_2)														(4.15)	(2.06)	(4.00)	

* Recalculated (Finger, 1972)
** Estimated to obtain 100 wt.%

Table 2 Thermodynamic properties

H: enthalpy of formation from elements at 1 bar and 298°K (cal $mole^{-1}$)
S: third law entropy at 1 bar and 298°K (cal $mole^{-1}$ $^{o}K^{-1}$)
V: molar volume at 1 bar and 298°K (cal bar^{-1})
a,b,c and d are molar heat capacity polynomial coefficients, where the heat capacity, $Cp=a+bt+ct^{-2}+dT^{-0.5}$.
AT: coefficient of thermal expansion multiplied by the molar volume (cal bar^{-1} $^{o}K^{-1}$)
PT: coefficient of isothermal compressibility multiplied by the molar volume (cal bar^{-2})

Mineral	H	S	V	a	b $x10^{-3}$	c $x10^{5}$	d	AT $x10^{-5}$	BP $x10^{-6}$
akermanite	-923777.0[a]	50.030	2.2180	60.090	11.400	-11.400	0.000	7.0985[b]	2.6291[c]
andalusite	-615866.0[a]	22.200	1.2316	41.311	6.293	-12.392	0.000	1.7208[d]	0.7409
calcite	-288772.0	22.150	0.8830	24.980	5.240	-6.200	0.000	2.1511[d]	1.2667[d]
diopside	-765598.0	34.200	1.5800	52.800	7.840	-15.740	0.000	5.2581[d]	1.3145[d]
dolomite	-556851.0	37.090	1.5384	41.557	23.952	-9.884	0.000	3.7285[d]	1.5774[d]
forsterite	-520000.0	22.750	1.0470	35.810	6.540	-8.520	0.000	3.8241[d]	0.7648[d]
grossular	-1583397.0	60.870	2.9948	104.017	17.013	-27.318	0.000	7.1702[d]	1.8881
gehlenite	-951665.0	48.100	2.1568	63.740	8.000	-15.120	0.000	5.4971[d]	1.9120[d]
kalsilite	-509408.0	31.850	1.4314	29.430	17.360	-5.320	0.000	3.5000[e]	2.9200[c]
K-feldspar	-949188.0	51.130	2.6021	76.617	4.311	-29.945	0.000	4.9200[e]	4.7800
leucite	-726255.0[f]	47.850[f]	2.1126[f]	35.470[f]	32.087[f]	-5.173[f]	0.000	6.0700[e]	4.2100[c]
monticellite	-537530.0[a]	26.400	1.2280	36.820	5.340	-8.000	0.000	4.6606[b]	1.1233[c]
merwinite	-1085060.0[g]	60.500	2.4950	72.970	11.960	-14.444	0.000	9.7275[b]	2.4857[c]
muscovite	-1427408.0[g]	68.800	3.3631	97.560	26.380	-25.440	0.000	10.7600[d]	3.8200[d]
periclase	-143800.0	6.440	0.2690	10.180	1.740	-1.480	0.000	1.0994[d]	0.1673[d]
perovskite	-396900.0[f]	22.380[f]	0.8037[f]	2.987[f]	10.793[f]	-15.062[f]	588.430[f]		
prehnite	-1482089.0	65.000	3.3540	91.600	37.820	-19.600	0.000	10.7600	3.8200
phlogopite	-1488067.0	76.100	3.5770	100.610	28.780	-21.500	0.000	11.4700[d]	5.9800[d]
rutile	-225801.0[f]	12.020[f]	0.4498[f]	15.076[f]	2.702[f]	-2.357[f]	1.342[f]		
sillimanite	-615099.0	23.130	1.1927	40.024	7.391	-11.674	0.000	1.7208[d]	0.7409
spinel	-546847.0	19.270	0.9491	36.773	6.415	-9.709	0.000	2.4618[d]	0.3824[d]
titanite	-621749.0[f]	30.880[f]	1.3301[f]	42.240[f]	5.701[f]	-9.538[f]	0.000		
wollastonite	-389810.0	19.600	0.9540	26.640	3.600	-6.520	0.000	2.3184[d]	1.1950[d]
CO_2	-94054.0	51.072	0.0000	10.570	2.100	-2.060	0.000	0.0000	0.0000
H_2O	-57796.0	45.104	0.0000	7.300	2.450	0.000	0.000	0.0000	0.0000

Sources: a) Brousse et al. (1984); b) Skinner (1966); c) estimated by method of Wang (1978) explained in Powell and Holland (1985); d) Powell and Holland (1985); e) estimated as explained in Powell and Holland (1985); f) Robie and Waldbaum (1978); g) adapted to experiments of Yoder (1968); all other data from Helgeson et. al (1978).

Table 3 Mineral assemblages of xenoliths from the marginal and critical zone of the Bushveld Complex

Mineral\Sample	J8	I3	I15	J6	J21	Wi1	Wi7	Wia
Assemblages	3\4	2	-	1	-	6	7	5\7
melilite	$X_{1,2}$		X_7	X_2		X_2		
monticellite	X_7	$X_{2,8}$		O_7		X_8	X	X_8
clinopyroxene	X_1				X			
olivine	X_1	O_6			X	O_6	X_9	X_6
spinel	O_3	O_3		$X_{2,3}$		O_3	O_3	$X_{3,10}$
phlogopite	O_{11}			O_4	X			
kalsilite					O_7			
wollastonite				O_7				
larnite	O_4							
merwinite						X_2		
periclase							O_{11}	O_{11}
brucite							X	X
calcite	O_5	X_5		X_5			O_5	X_5
vesuvianite			X_7					

X: Essential mineral O: Accessory mineral (<2vol%).
The assemblage numbers in the second line refer to Figure 2a and b.
Sample J8, I3, I15, J6, J21 : marginal zone; Wi1, Wi7, Wia: critical zone.
1: symplectic intergrowth; 2: polygonal grains; 3: inclusions in all phases except but calcite; 4: inclusions in melilite; 5: inclusions in melilite and monticellite; 6: as exsolutions in monticellite and intergranular; 7: decomposition product of melilite; 8: displays exsolutions of forsterite; 9: relict in brucite; 10: intergranular; 11: inclusions in brucite.

Table 4

High temperature reactions in the system $CaO-MgO-SiO_2-Al_2O_3-CO_2$ involving the solid phases akermanite (Ak), gehlenite (Ge), calcite (Cc), diopside (Di), forsterite (Fo), merwinite (Me), monticellite (Mo), periclase (Pe), wollastonite (Wo) and spinel (Sp). Numbers in parentheses designate the invariant points that are intersected by the respective reactions. Reactions that are stable over a realistic P-T range are designated with "x". Numbers in parentheses refer to the subsystems, in which the respective reaction occurs.

1)	x $Cc+Wo+Mo=Me+CO_2$	(4,7,18,40,43,54,88)
2)	x $Wo+Mo=Ak$	(4,5,9,12,19,21,80,81,84,89)
3)	x $2Wo+2Mo=Di+Me$	(5,7,14,41,43,50,86)
4)	x $Cc+Di=Wo+Mo+CO_2$	(7,11,21,43,47,57,78)
5)	$Mo+Di=2Wo+Fo$	(9,11,14,45,47,50,77,83)
6)	$3Cc+3Wo+Fo=2Me+3CO_2$	(17,18,20,53,54,56,76)
7)	$Cc+3Wo+Fo=2Ak+CO_2$	(10,17,19,92)
8)	$Cc+2Di=3Wo+Fo+CO_2$	(10,11,20,46,47,56,73)
9)	$3Wo+Fo+Me=3Ak$	(12,13,17,94)
10)	$Cc+Wo+Fo=2Mo+CO_2$	(11,18,19,47,54,55,79)
11)	$Me+3Di=6Wo+2Fo$	(13,14,20,49,50,56,74)
12)	x $Cc+Di=Ak+CO_2$	(2,3,6,10,16,21,28,30,34,91)
13)	x $3Mo+Di=2Ak+Fo$	(1,6,9,35)
14)	x $Di+Me=2Ak$	(1,2,3,5,13,16,28,29,33,85)
15)	x $Me+Fo=3Mo$	(1,8,12,14,15,18,23,25,31,37,44,48,50,51,61,93)
16)	$2Cc+Di=Me+2CO_2$	(2,3,7,8,16,20,27,28,36,38,39,43,44,52,64,75)
17)	x $Cc+Ak=Me+CO_2$	(2,3,4,15,16,17,22,24,28,87)
18)	x $Cc+Fo+Ak=3Mo+CO_2$	(6,15,19,26)
19)	x $2Cc+Di+Fo=3Mo+2CO_2$	(6,8,11,32,42,44,47)
20)	$3Wo+Fo=Di+Ak$	(9,10,13,82,90)
21)	$3Fo+Ak=2Di+3Pe$	(29,30,35,82,90)
22)	$Cc+2Fo=Di+3Pe+CO_2$	(27,30,32,66,73)
23)	$2Cc+2Fo=Ak+3Pe+2CO_2$	(22,26,30,92)
24)	$2Pe+Di+Me=4Mo$	(31,33,36,69,86)
25)	$Mo+Fo=Di+2Pe$	(31,32,35,71,77,83)
26)	$Me+4Fo=6Pe+3Di$	(27,29,31,65,74)
27)	$Cc+Pe+Di=2Mo+CO_2$	(32,34,36,70,78)
28)	x $Cc+Fo=Mo+Pe+CO_2$	(23,26,32,62,79)
29)	$Ak+Pe=2Mo$	(24,25,26,33,34,35,80,81,84,89)
30)	x $Cc+2Mo=Me+Pe+CO_2$	(23,24,36,60,88)
31)	x $3Cc+2Fo=Me+3Pe+3CO_2$	(22,23,27,58,76)
32)	$2Me+2Fo=3Pe+3Ak$	(22,25,29,94)
33)	$4Wo+2Pe=Me+Di$	(74,75,85,86)
34)	$3Wo+3Pe=Me+Fo$	(74,76,83,90)
35)	$Di+Pe=Wo+Fo$	(73,74,77,82)
36)	$2Wo+Pe=Ak$	(80,81,82,85,87,89,90,91,92)
37)	$Mo=Wo+Pe$	(77,78,79,80,81,83,84,86,88,89)
38)	$Cc+Di=Wo+2Pe+CO_2$	(73,75,78,91)
39)	$Cc+Fo=Wo+2Pe+CO_2$	(73,76,79,92)
40)	$Cc+Pe+2Wo=Me+CO_2$	(75,76,87,88)
41)	$2Ge+3Fo=Di+3Mo+2Sp$	(37,42,45,71)
42)	$2Ge+6Mo=3Me+Di+2Sp$	(37,38,41,69)
43)	$2Ge+2Fo=Me+Di+2Sp$	(37,49,52)
44)	$Di+Ge=Sp+3Wo$	(39,41,45,46,49,57)
45)	$2Mo+Ge=Me+Sp+Wo$	(40,41,48)
46)	$Fo+Ge=Mo+Sp+Wo$	(45,48,55)
47)	$2Fo+3Ge=Me+3Sp+3Wo$	(48,49,53)
48)	x $Cc+Ge+2Fo=Sp+3Mo+CO_2$	(42,55,62)
49)	$Cc+Sp+Di=Ge+Fo+CO_2$	(42,46,52,66)
50)	$3Cc+2Di+Sp=3Mo+Ge+CO_2$	(38,42,57,70)
51)	$Cc+Ge+3Mo=2Me+Sp+CO_2$	(38,40,51,60)
52)	$2Cc+Sp+3Wo=Ge+Me+2CO_2$	(39,40,53)
53)	$Cc+2Wo+Sp=Mo+Ge+CO_2$	(40,55,57)
54)	$Cc+2Sp+3Wo=2Ge+Fo+CO_2$	(46,53,55)
55)	$Cc+Ge+Fo=Me+Sp+CO_2$	(51,52,53,58)
56)	x $Me+Sp=Ge+Pe+Mo$	(60,61,69)
57)	x $3Ge+Fo+3Pe=3Sp+2Me$	(58,61,65)
58)	x $Sp+2Mo=Ge+Fo+Pe$	(61,62,71)
59)	$4Ge+Di+6Pe=4Sp+3Me$	(64,65,69)
60)	$Sp+2Di+3Pe=Ge+3Fo$	(65,66,71)
61)	$Ge+Di+3Pe=3Mo+Sp$	(69,70,71)
62)	$2Cc+Fo+Sp=Ge+3Pe+2CO_2$	(58,62,66)
63)	x $Cc+Me+2Sp=2Ge+3Pe+CO_2$	(58,60,64)
64)	$Cc+Mo+Sp=Ge+2Pe+CO_2$	(60,62,70)
65)	$3Cc+Di+2Sp=2Ge+3Pe+3CO_2$	(64,66,70)

Table 5 Reactions occuring in the subsystems 1-94

a) Subsystems in the system $CaO-MgO-SiO_2-CO_2$ involving the minerals akermanite (Ak), calcite (Cc), diopside (Di), forsterite (Fo), monticellite (Mo), merwinite (Me), wollastonite (Wo) and periclase (Pe) (subsystems involving periclase and wollastonite are omitted)

1) [Cc,Wo,Pe] stable

Di+Me=2Ak	[Mo][Fo]
3Mo+Di=2Ak+Fo	[Me]
Me+Fo=3Mo	[Ak][Di

2) [Fo,Wo,Pe] stable

Di+Me=2Ak	[Mo][Cc]
$Cc+Di=Ak+CO_2$	[Mo][Me]
$2Cc+Di=Me+2CO_2$	[Mo][Ak]
$Cc+Ak=Me+CO_2$	[Mo][Di]

3) [Fo,Mo,Pe] stable

Di+Me=2Ak	[Wo][Cc]
$Cc+Di=Ak+CO_2$	[Wo][Me]
$Cc+Ak=Me+CO_2$	[Wo][Di]
$2Cc+Di=Me+2CO_2$	[Wo][Ak]

4) [Fo,Di,Pe] stable

Wo+Mo=Ak	[Me][Cc]
$Cc+Wo+Mo=Me+CO_2$	[Ak]
$Cc+Ak=Me+CO_2$	[Wo][Mo]

5) [Cc,Fo,Pe] stable

2Wo+2Mo=Di+Me	[Ak]
Wo+Mo=Ak	[Me][Di]
Di+Me=2Ak	[Wo][Mo]

6) [Wo,Me,Pe] stable

3Mo+Di=2Ak+Fo	[Cc]
$Cc+Fo+Ak=3Mo+CO_2$	[Di]
$Cc+Di+Fo=Mo+CO_2$	[Ak]
$Cc+Di=Ak+CO_2$	[Mo][Fo]

7) (Fo,Ak,Pe) metastable

2Wo+2Mo=Di+Me	[Cc]
$2Cc+Di=Me+2CO_2$	[Wo][Mo]
$Cc+Di=Wo+Mo+CO_2$	[Me]
$Cc+Wo+Mo=Me+CO_2$	[Di]

8) (Wo,Ak,Pe) metastable

Me+Fo=3Mo	[Di][Cc]
$Cc+Di+Fo=3Mo+CO_2$	[Me]
$2Cc+Di=Me+2CO_2$	[Mo][Fo]

9) (Cc,Me,Pe) metastable

Wo+Mo=Ak	[Di][Fo]
3Mo+Di=2Ak+Fo	[Wo]
2Wo+Fo=Mo+Di	[Ak]
3Wo+Fo=Di+Ak	[Mo]

10) (Mo,Me,Pe) metastable

3Wo+Fo=Di+Ak	[Cc]
$Cc+2Di=3Wo+Fo+CO_2$	[Ak]
$Cc+3Wo+Fo=2Ak+CO_2$	[Di]
$Cc+Di=Ak+CO_2$	[Wo][Fo]

11) (Me,Ak,Pe) metastable

Mo+Di=2Wo+Fo	[Cc]
$2Cc+Di+Fo=3Mo+2CO_2$	[Wo]
$Cc+2Di=3Wo+Fo+CO_2$	[Mo]
$Cc+Di=Wo+Mo+CO_2$	[Fo]

12) (Cc,Di,Pe) metastable

3Wo+Fo+Me=3Ak	[Mo]
Me+Fo=3Mo	[Wo][Ak]
Wo+Mo=Ak	[Me][Fo]

13) (Cc,Mo,Pe) metastable

Me+3Di=6Wo+2Fo	[Ak]
3Wo+Fo=Ak+Di	[Me]
3Wo+Fo+Me=3Ak	[Di]
Di+Me=2Ak	[Fo][Wo]

14) (Cc,Ak,Pe) metastable

Me+3Di=6Wo+2Fo	[Mo]
2Wo+2Mo=Di+Me	[Fo]
Mo+Di=2Wo+Fo	[Me]
Me+Fo=3Mo	[Wo][Di]

15) (Wo,Di,Pe) stable

Me+Fo=3Mo	[Ak][Cc]
$Cc+Ak=Me+CO_2$	[Mo][Fo]
$Cc+Fo+Ak=3Mo+CO_2$	[Ak][Cc]

16) (Wo,Mo,Pe) stable

Di+Me=2Ak	[Fo][Cc]
$Cc+Ak=Me+CO_2$	[Di][Fo]
$Cc+Di=Ak+CO_2$	[Me][Fo]

17) (Di,Mo,Pe) metastable

3Wo+Fo+Me=3Ak	[Cc]
$3Cc+3Wo+Fo=2Me+3CO_2$	[Ak]
$Cc+3Wo+Fo=2Ak+CO_2$	[Me]
$Cc+Ak=Me+CO_2$	[Wo][Fo]

18) (Di,Ak,Pe) metastable

Me+Fo=3Mo	[Wo][Cc]
$3Cc+3Wo+Fo=2Me+3CO_2$	[Mo]
$Cc+Fo+Wo=2Mo+CO_2$	[Me]
$Cc+Wo+Mo=Me+CO_2$	[Fo]

19) (Me,Di,Pe) metastable

Wo+Mo=Ak	[Fo][Cc]
$Cc+Wo+Fo=2Mo+CO_2$	[Ak]
$Cc+Fo+Ak=3Mo+CO_2$	[Wo]
$Cc+3Wo+Fo=2Ak+CO_2$	[Mo]

20) (Mo,Ak,Pe) metastable

Me+3Di=6Wo+2Fo	[Cc]
$Cc+2Di=3Wo+Fo+CO_2$	[Me]
$2Cc+Di=Me+2CO_2$	[Wo][Fo]
$3Cc+3Wo+Fo=2Me+3CO_2$	[Di]

21) (Fo,Me,Pe) stable

Wo+Mo=Ak	[Di][Cc]
$Cc+Di=Wo+Mo+CO_2$	[Ak]
$Cc+Di=Ak+CO_2$	[Wo][Me]

22) (Di,Mo,Wo) metastable

2Me+2Fo=3Pe+3Ak	[Cc]
$Cc+Ak=Me+CO_2$	[Fo][Pe]
$3Cc+2Fo=Me+3Pe+3CO_2$	[Ak]
$2Cc+2Fo=Ak+3Pe+2CO_2$	[Me]

23) (Di,Ak,Wo) stable

Me+Fo=3Mo	[Pe][Cc]
$3Cc+2Fo=Me+3Pe+3CO_2$	[Mo]
$Cc+Fo=Mo+Pe+CO_2$	[Me]
$Cc+2Mo=Me+Pe+CO_2$	[Fo]

24) (Di,Fo,Wo) metastable

Ak+Pe=2Mo	[Me][Cc]
$Cc+Ak=Me+CO_2$	[Mo][Pe]
$Cc+2Mo=Me+Pe+CO_2$	[Ak]

25) (Cc,Di,Wo) metastable

Ak+Pe=2Mo	[Me][Fo]
Me+Fo=3Mo	[Ak][Pe]
2Me+2Fo=3Pe+3Ak	[Mo]

26) (Di,Me,Wo) metastable

Ak+Pe=2Mo	[Fo][Cc]
$Cc+Fo=Mo+Pe+CO_2$	[Ak]
$2Cc+2Fo=Ak+3Pe+2CO_2$	[Mo]

27) [Ak,Mo,Wo] stable

Me+4Fo=6Pe+3Di	[Cc]
$2Cc+Di=Me+2CO_2$	[Fo][Pe]
$Cc+2Fo=Di+3Pe+CO_2$	[Me]
$3Cc+2Fo=Me+3Pe+3CO_2$	[Di]

28) [Mo,Fo,Wo] stable

Di+Me=2Ak	[Pe][Cc]
$2Cc+Di=Me+2CO_2$	[Pe][Ak]
$Cc+Di=Ak+CO_2$	[Pe][Ak]
$Cc+Ak=Me+CO_2$	[Pe][Ak]

29) [Mo,Cc,Wo] metastable

Di+Me=2Ak	[Fo][Pe]
2Me+2Fo=3Pe+3Ak	[Di]
Me+4Fo=3Di+6Pe	[Ak]
2Di+3Pe=Ak+2Fo	[Me]

30) [Mo,Me,Wo] metastable

Ak+2Fo=2Di+3Pe	[Cc]
$Cc+2Fo=Di+3Pe+CO_2$	[Ak]
$2Cc+2Fo=Ak+3Pe+CO_2$	[Di]
$Cc+Di=Ak+CO_2$	[Fo][Pe]

31) [Cc,Ak,Wo] stable

2Pe+Di=Mo+Fo	[Me]
Fo+Me=3Mo	[Di][Pe]
2Pe+Di+Me=4Mo	[Fo]
6Pe+3Di=Me+4Fo	[Mo]

32) [Ak,Me,Wo] metastable

2Pe+Di=Mo+Fo	[Me]
$Cc+Di+Pe=2Mo+CO_2$	[Fo]
$2Cc+Di+Fo=3Mo+2CO_2$	[Pe]
$Cc+Fo=Mo+Pe+CO_2$	[Di]

33) [Cc,Fo,Wo] metastable

Pe+Ak=2Mo	[Di][Me]
Di+Me=2Ak	[Mo][Pe]
2Pe+Di+Me=4Mo	[Ak]

34) [Fo,Me,Wo] metastable

Pe+Ak=2Mo	[Di][Me]
$Cc+Di=Ak+CO_2$	[Pe][Mo]
$Cc+Di+Pe=2Mo+CO_2$	[Ak]

35) [Cc,Me,Wo] metastable

Pe+Ak=2Mo	[Di][Fo]
3Mo+Di=2Ak+Fo	[Pe]
2Fo+Ak=2Di+3Di	[Mo]
Mo+Fo=Di+2Pe	[Ak]

36) [Ak,Fo,Wo] metastable

2Pe+Di+Me=4Mo	[Cc]
$2Cc+Di=Me+2CO_2$	[Pe][Mo]
$Cc+2Mo=Me+Pe+CO_2$	[Di]
$Cc+Pe+Di=2Mo+CO_2$	[Me]

b) Subsystems in the system $CaO-MgO-SiO_2-Al_2O_3-CO_2$ involving the minerals calcite, diopside, forsterite, gehlenite (Ge), spinel (Sp), monticellite, merwinite, wollastonite and periclase (subsystems involving periclase and wollastonit are omitted)

37) [Cc,Wo,Pe] metastable

3Me+Di+2Sp=2Ge+6Mo	[Fo]
Me+Fo=3Mo	[Ge][Sp][Di]
Me+Di+2Sp=2Ge+2Fo	[Mo]
Di+3Mo+Sp=2Ge+3Fo	[Me]

38) [Fo,Wo,Pe] metastable

3Me+Di+2Sp=2Ge+6Mo	[Cc]
Cc+Ge+3Mo=2Me+Sp+CO_2	[Di]
2Cc+Di=Me+2CO_2	[Ge][Sp][Mo]
3Cc+2Di+Sp=3Mo+Ge+3CO_2	[Mo]

39) [Fo,Mo,Pe] metastable

Di+Ge=Sp+3Wo	[Me][Cc]
2Cc+Di=Me+2CO_2	[Ge][Sp][Wo]
2Cc+Sp+3Wo=Ge+Me+CO_2	[Di]

40) [Fo,Di,Pe] metastable

2Mo+Ge=Me+Sp+Wo	[Cc]
Cc+Ge+3Mo=2Me+Sp+CO_2	[Wo]
Cc+Wo+Mo=Me+CO_2	[Ge][Sp]
2Cc+Sp++3Wo=Ge+Me+2CO_2	[Mo]
Cc+2Wo+Sp=Mo+Ge+CO_2	[Me]

41) [Cc,Fo,Pe] metastable

Di+Ge=Sp+3Wo	[Mo][Me]
2Wo+2Mo=Di+Me	[Ge][Sp]
2Ge+6Mo=3Me+Di+2Sp	[Wo]
2Mo+Ge=Me+Sp+Wo	[Di]

42) [Wo,Me,Pe] metastable

2Ge+3Fo=Di+3Mo+2Sp	[Cc]
Cc+Ge+2Fo=Sp+3Mo+CO_2	[Di]
2Cc+Di+Fo=3Mo+2CO_2	[Ge][Sp]
3Cc+2Di+Sp=3Mo+Ge+3CO_2	[Fo]
Cc+Sp+Di=Ge+Fo+CO_2	[Mo]

43) [Fo,Ge,Sp,Pe] = 7) [Fo,Ak,Pe] metastable

44) [Wo,Ge,Sp,Pe] = 8) [Wo,Ak,Pe] metastable

45) [Cc,Me,Pe] metastable

Di+Ge=Sp+3Wo	[Fo][Cc]
Cc+Sp+Di=Ge+Fo+CO_2	[Wo]
Cc+2Sp+3Wo=2Ge+Fo+CO_2	[Di]
Cc+2Di=3Wo+Fo+CO_2	[Ge][Sp]

46) [Mo,Me,Pe] metastable

Di+Ge=Sp+3Wo	[Fo][Cc]
Cc+2Di=3Wo+Fo+CO_2	[Ge][Sp]
Cc+Sp+Di=Ge+Fo+CO_2	[Wo]
Cc+2Sp+3Wo=2Ge+Fo+CO_2	[Di]

47) [Me,Ge,Sp,Pe] = 11) [Me,Ak,Pe] metastable

48) [Cc,Di,Pe] metastable

Me+Fo=3Mo	[Ge][Sp][Wo]
2Mo+Ge=Me+Sp+Wo	[Fo]
2Fo+3Ge=Me+3Sp+3Wo	[Mo]
Fo+Ge=Mo+Sp+Wo	[Me]

49) [Cc,Mo,Pe] metastable

Di+Ge=Sp+3Wo	[Fo][Me]
Me+3Di=6Wo+2Fo	[Ge][Sp]
2Ge+2Fo=Me+Di+2Sp	[Wo]
2Fo+3Ge=Me+3Sp+3Wo	[Di]

50) [Cc,Ge,Sp,Pe] = 14) [Cc,Ak,Pe] metastable

51) [Wo,Di,Pe] metastable

Me+Fo=3Mo	[Ge,Sp,Cc]
Cc+Ge+2Fo=Sp+3Mo+CO_2	[Me]
Cc+Ge+Fo=Me+Sp+CO_2	[Mo]
Cc+Ge+3Mo=2Me+Sp+CO_2	[Fo]

52) [Wo,Mo,Pe] metastable

2Ge+2Fo=Me+Di+Sp	[Cc]
Cc+Ge+Fo=Me+Sp+CO_2	[Di]
2Cc+Di=Me+CO_2	[Ge][Sp]
Cc+Sp+Di=Ge+Fo+CO_2	[Me]

53) [Di,Mo,Pe] metastable

2Fo+3Ge=Me+3Sp+3Wo	[Cc]
Cc+Ge+Fo=Me+Sp+CO_2	[Wo]
3Cc+Fo+3Wo=2Me+3CO_2	[Ge][Sp]
2Cc+Sp+3Wo=Ge+Me+2CO_2	[Fo]
Cc+2Sp+3Wo=Ge+Fo+CO_2	[Me]

54) [Di,Ge,Sp,Pe] = 18) [Di,Ak,Pe] metastable

55) [Me,Di,Pe] metastable

Fo+Ge=Mo+Sp+Wo	[Cc]
Cc+Ge+2Fo=Sp+3Mo+CO_2	[Wo]
Cc+Wo+Fo=2Mo+CO_2	[Ge][Sp]
Cc+2Wo+Sp=Mo+Ge+CO_2	[Fo]
Cc+2Sp+3Wo=2Ge+Fo+CO_2	[Mo]

56) [Mo,Ge,Sp,Pe] = 20) [Mo,Ak,Pe] metastable

57) [Fo,Me,Pe] metastable

Di+Ge=Sp+3Wo	[Mo][Cc]
Cc+Di=Wo+Mo+CO_2	[Ge][Sp]
3Cc+2Di+Sp=3Mo+Ge+3CO_2	[Wo]
Cc+2Wo+Sp=Mo+Ge+CO_2	[Di]

58) [Di,Mo,Wo] stable

3Ge+Fo+3Pe=3Sp+2Me	[Cc]
Cc+Ge+Fo=Me+Sp+CO_2	[Pe]
Cc+Me+2Sp=2Ge+3Pe+CO_2	[Fo]
3Cc+2Fo=Me+3Pe+3CO_2	[Ge][Sp]
2Cc+Fo+Sp=Ge+3Pe+2CO_2	[Me]

59) [Di,Sp,Ge,Wo] = 23) [Di,Ak,Wo] stable

60) [Di,Fo,Wo] metastable

Me+Sp=Ge+Pe+Mo	[Cc]
Cc+Me+2Sp=2Ge+3Pe+CO_2	[Mo]
Cc+Mo+Sp=Ge+2Pe+CO_2	[Me]
Cc+2Mo=Me+Pe+CO_2	[Ge][Sp]
Cc+Ge+3Mo=2Me+Sp+CO_2	[Pe]

61) [Cc,Di,Wo] stable

Sp+2Mo=Ge+Fo+Pe	[Me]
3Ge+Fo+3Pe=3Sp+2Me	[Mo]
Me+Sp=Ge+Pe+Mo	[Fo]
Me+Fo=3Mo	[Ge][Sp][Pe]

62) [Di,Me,Wo] stable

Sp+2Mo=Ge+Fo+Pe	[Cc]
Cc+Ge+2Fo=Sp+3Mo+CO_2	[Pe]
Cc+Fo=Mo+Pe+CO_2	[Ge][Sp]
2Cc+Fo+Sp=Ge+3Pe+2CO_2	[Mo]
Cc+Mo+Sp=Ge+2Pe+CO_2	[Fo]

63) [Ge,Sp,Mo,Wo] = 27) [Ak,Mo,Wo] stable

64) [Mo,Fo,Wo] metastable

4Ge+Di+6Pe=4Sp+3Me	[Cc]
Cc+Me+2Sp=2Ge+3Pe+CO_2	[Di]
3Cc+Di+2Sp=2Ge+3Pe+3CO_2	[Me]

65) [Cc,Mo,Wo] metastable

Sp+2Di+3Pe=Ge+3Fo	[Me]
4Ge+Di+6Pe=4Sp+3Me	[Fo]
3Ge+Fo+3Pe=3Sp+2Me	[Di]
2Ge+2Fo=Me+Di+2Sp	[Pe]

66) [Mo,Me,Wo] metastable

Sp+2Di+3Pe=Ge+3Fo	[Cc]
Cc+2Fo=Di+3Pe+CO_2	[Ge][Sp]
2Cc+Fo+Sp=Ge+3Pe+2CO_2	[Di]
3Cc+Di+2Sp=2Ge+3Pe+3CO_2	[Fo]

67) [Cc,Ge,Sp,Wo] = 31) [Cc,Ak,Wo] stable

68) [Ge,Sp,Me,Wo] = 32) [Ak,Me,Wo] metastable

69) [Cc,Fo,Wo] metastable

Ge+Di+3Pe=3Mo+Sp	[Me]
Me+Sp=Ge+Pe+Mo	[Di]
2Ge+6Mo=3Me+Di+2Sp	[Pe]
4Mo=2Pe+Di+Me	[Ge][Sp]
4Ge+Di+6Pe=4Sp+3Me	[Me]

70) [Fo,Me,Wo] metastable

Ge+Di+3Pe=3Mo+Sp	[Cc]
Cc+Mo+Sp=Ge+2Pe+CO_2	[Di]
3Cc+Di+2Sp=2Ge+3Pe+CO_2	[Mo]
3Cc+2Di+Sp=3Mo+Ge+3CO_2	[Pe]
Cc+Pe+Di=2Mo+CO_2	[Ge][Sp]

71) [Cc,Me,Wo] metastable

Ge+Di+3Pe=3Mo+Sp	[Fo]
Sp+2Mo=Ge+Fo+Pe	[Di]
2Ge+3Fo=Di+3Mo+2Sp	[Pe]
Sp+2Di+3Pe=Ge+3Fo	[Mo]
Mo+Fo=2Pe+Di	[Ge][Sp]

72) [Ge,Sp,Fo,Wo] = 36) [Ak,Fo,Wo] metastable

c) Additional metastable subsystems in the system $CaO-MgO-SiO_2-CO_2$ involving the minerals wollastonite and periclase

73) [Mo,Ak,Me] metastable

Di+Pe=Wo+Fo	[Cc]
$Cc+2Di=3Wo+Fo+CO_2$	[Pe]
$Cc+Di=Wo+2Pe+CO_2$	[Fo]
$Cc+Fo=Wo+2Pe+CO_2$	[Di]
$Cc+2Fo=Di+3Pe+CO_2$	[Wo]

74) [Cc,Mo,Ak] metastable

Di+Pe=Wo+Fo	[Me]
4Wo+2Pe=Me+Di	[Fo]
Me+4Fo=6Pe+3Di	[Wo]
Me+3Di=6Wo+2Fo	[Pe]
3Wo+3Pe=Me+Fo	[Di]

75) [Mo,Ak,Fo] metastable

4Wo+2Pe=Me+Di	[Cc]
$2Cc+Di=Me+2CO_2$	[Wo][Pe]
$Cc+Di=Wo+2Pe+CO_2$	[Me]
$Cc+Pe+2Wo=Me+CO_2$	[Di]

76) [Mo,Ak,Di] metastable

3Wo+3Pe=Me+Fo	[Cc]
$3Cc+2Fo=Me+3Pe+3CO_2$	[Wo]
$Cc+Fo=Wo+2Pe+CO_2$	[Me]
$Cc+Pe+2Wo=Me+CO_2$	[Fo]
$3Cc+3Wo+Fo=2Me+3CO_2$	[Pe]

77) [Cc,Ak,Me] metastable

Mo=Wo+Pe	[Di][Fo]
Mo+Di=2Wo+Fo	[Pe]
Mo+Fo=Di+2Pe	[Wo]
Di+Pe=Wo+Fo	[Mo]

78) [Ak,Me,Fo] metastable

Mo=Wo+Pe	[Cc][Di]
$Cc+Di=Wo+Mo+CO_2$	[Pe]
$Cc+Pe+Di=2Mo+CO_2$	[Wo]
$Cc+Di=Wo+2Pe+CO_2$	[Mo]

79) [Ak,Me,Di] metastable

Mo=Wo+Pe	[Cc][Fo]
$Cc+Wo+Fo=2Mo+CO_2$	[Pe]
$Cc+Fo=Mo+Pe+CO_2$	[Wo]
$Cc+Fo=Wo+2Pe+CO_2$	[Mo]

80) [Cc,Me,Fo] metastable

Mo=Wo+Pe	[Ak][Di]
Wo+Mo=Ak	[Pe][Di]
2Mo=Ak+Pe	[Wo][Di]
2Wo+Pe=Ak	[Mo][Di]

81) [Cc,Me,Di] metastable

Wo+Mo=Ak	[Pe][Fo]
Mo=Wo+Pe	[Ak][Fo]
2Mo=Ak+Pe	[Wo][Fo]
2Wo+Pe=Ak	[Mo][Fo]

82) [Cc,Me,Mo] metastable

2Wo+Pe=Ak	[Di][Fo]
3Wo+Fo=Di+Ak	[Pe]
3Fo+Ak=2Di+3Pe	[Wo]
Di+Pe=Wo+Fo	[Ak]

83) [Cc,Me,Ak] metastable

Mo=Wo+Pe	[Di][Fo]
Mo+Di=2Wo+Fo	[Pe]
Di+Pe=Wo+Fo	[Mo]
Mo+Fo=Di+2Pe	[Wo]

84) [Cc,Fo,Di] metastable

Mo=Wo+Pe	[Ak][Me]
Wo+Mo=Ak	[Pe][Me]
2Mo=Ak+Pe	[Wo][Me]
2Wo+Pe=Ak	[Mo][Me]

85) [Cc,Fo,Mo] metastable

4Wo+2Pe=Me+Di	[Ak]
2Wo+Pe=Ak	[Me][Di]
Di+Me=2Ak	[Wo][Pe]

86) [Cc,Fo,Ak] metastable

4Wo+2Pe=Me+Di	[Mo]
Mo=Wo+Pe	[Me][Di]
2Wo+2Mo=Di+Me	[Pe]
2Pe+Di+Me=4Mo	[Wo]

87) [Fo,Di,Mo] metastable

2Wo+Pe=Ak	[Cc][Me]
$Cc+Pe+2Wo=Me+CO_2$	[Ak]
$Cc+Ak=Me+CO_2$	[Pe][Wo]

88) [Fo,Di,Ak] metastable

Mo=Wo+Pe	[Cc][Me]
$Cc+Pe+2Wo=Me+CO_2$	[Mo]
$Cc+Wo+Mo=Me+CO_2$	[Pe]
$Cc+2Mo=Me+Pe+CO_2$	[Wo]

89) [Fo,Di,Me] metastable

Mo=Wo+Pe	[Ak][Cc]
Wo+Mo=Ak	[Pe][Cc]
2Mo=Ak+Pe	[Wo][Cc]
2Wo=Pe+Ak	[Mo][Cc]

90) [Cc,Mo,Me] metastable

Di+Pe=Wo+Fo	[Ak]
3Wo+Fo=Di+Ak	[Pe]
3Fo+Ak=2Di+3Pe	[Wo]
2Wo+Pe=Ak	[Di][Fo]

91) [Mo,Me,Fo] metastable

2Wo+Pe=Ak	[Cc][Di]
$Cc+Di=Ak+CO_2$	[Wo][Pe]
$Cc+Di=Wo+2Pe+CO_2$	[Ak]

92) [Mo,Me,Di] metastable

2Wo+Pe=Ak	[Cc][Fo]
$Cc+3Wo+Fo=2Ak+CO_2$	[Pe]
$Cc+Fo=Wo+2Pe+CO_2$	[Ak]
$2Cc+2Fo=Ak+3Pe+2CO_2$	[Wo]

93) [Cc,Ak,Di] metastable

3Wo+3Pe=Me+Fo	[Mo]
Mo=Wo+Pe	[Me][Fo]
Me+Fo=3Mo	[Pe][Wo]

94) [Cc,Di,Mo] metastable

3Wo+3Pe=Me+Fo	[Ak]
2Wo+Pe=Ak	[Me][Fo]
3Wo+Fo+Me=3Ak	[Pe]
2Me+2Fo=3Pe+3Ak	[Wo]

Table 6 Listing of high-temperature reactions and authors, who experimentally investigated the P-T locations of these reactions.

a)	$Cc + Di = Ak + CO_2$	(Walter, 1963a; Yoder, 1973; Zharikov et al., 1977)
b)	$2Cc + Di + Fo = 3Mo + 2CO_2$	(Walter, 1963a; Zharikov et al. 1977)
c)	$Cc + Fo + Ak = 3Mo + CO_2$	(Walter, 1963a)
d)	$Cc + Ak = Me + CO_2$	(Bulatov, 1974; Zharikov et al., 1977)
e)	$Cc + Fo = Mo + Pe + CO_2$	(Walter, 1963b; Bulatov, 1974; Zharikov et al., 1977)
f)	$3Mo + Di = 2Ak + Fo$	(Walter, 1963; Yoder, 1968)
g)	$Wo + Mo = Ak$	(Harker and Tuttle, 1956; Yoder, 1968)
h)	$2Wo + 2Mo = Di + Me$	(Yoder, 1968)
i)	$Di + Me = 2Ak$	(Kushiro and Yoder, 1964; Yoder, 1975)
j)	$Me + Fo = 3Mo$	(Yoder, 1968 and 1973)

Table 7 Representative microprobe analyses (wt.% and atoms per formula unit) of clinopyroxene, orthopyroxene, olivine and plagioclase occurring in the gabbronorite and the metasomatic reaction seam (Figure 19 A and B).

	Clinopyroxene			Opx.	Ol.	Plagioclase	
	J1	J2	J3	J1	J3	J1	J2
SiO_2	52.80	52.65	47.99	54.47	41.34	48.08	46.47
TiO_2	0.35	0.49	0.37	0.21	0.00	0.01	0.01
Al_2O_3	1.31	2.29	8.43	0.75	0.00	32.38	32.92
Cr_2O_3	0.24	0.03	0.00	0.11	0.02	0.01	0.01
Fe_2O_3 *	0.00	0.00	3.16	0.00	0.00	0.00	0.00
FeO	7.34	5.44	1.13	18.19	8.87	0.48	0.19
MnO	0.18	0.17	0.06	0.37	0.51	0.00	0.00
MgO	14.94	15.78	13.47	25.40	49.35	0.20	0.02
CaO	22.49	22.75	25.03	0.75	0.12	16.18	16.92
BaO	0.00	0.00	0.00	0.00	0.00	0.02	0.00
Na_2O	0.00	0.00	0.09	0.01	0.00	2.02	0.02
K_2O	0.00	0.00	0.01	0.00	0.01	0.15	0.13
Total	99.65	99.60	99.74	100.27	100.22	99.53	96.70
Formula	6(O)			6(O)	4(O)	8(O)	5 cat. norm.
Si	1.96	1.94	1.78	1.98	1.01	2.22	2.23
Ti	0.01	0.01	0.00	0.01	0.00	0.00	0.00
Al	0.06	0.10	0.37	0.03	0.00	1.76	1.86
Cr^{3+}	0.01	0.00	0.00	0.00	0.00	0.00	0.00
Fe^{3+} *	0.00	0.00	0.09	0.00	0.00	0.00	0.00
Fe^{2+}	0.23	0.17	0.03	0.55	0.18	0.02	0.01
Mn	0.01	0.01	0.00	0.01	0.01	0.00	0.00
Mg	0.83	0.87	0.73	1.38	1.79	0.01	0.00
Ca	0.89	0.90	0.99	0.03	0.00	0.80	0.88
Ba	0.00	0.00	0.00	0.00	0.00	0.00	0.00
Na	0.00	0.00	0.01	0.00	0.09	0.18	0.01
K	0.00	0.00	0.00	0.00	0.00	0.01	0.01
Total	4.00	4.00	4.00	3.99	2.99	5.00	5.00

* Recalculated (Finger, 1972)
J1: minerals in gabbronorite; J2 and J3: minerals in metasomatic reaction seam.

Table 8 Mineral assemblages of xenoliths B (Av) and D (Ma), situated in the upper zone of the Bushveld Complex

Mineral\Sample	Av2	Av3	Av4	Av6	Av8	Av15	Av19	Ma2b	Ma9	Ma10	Ma13	Ma16	Ma22
vesuvianite		X_4	X_3		X_{10}	X_{10}	X_{10}	X_{10}					X_{10}
garnet			X_2	X_8	X_{10}	X_{10}	X_{10}	X_{10}		X_{10}			X_{10}
wollastonite	X_1	X_4		X_8							X_{11}	X_{10}	
clinopyroxene	X_1		X_7	X_8		X_9		X_{10}	$X_{1,8}$	X_8			
K-feldspar											X_1		
muscovite										X_{10}	X_{10}		
prehnite										X_{10}			
xantophyllite													X_{10}
chlorite							X_9	O					
titanite	$X_{2,5}$												
calcite	$X_{3,6}$		O			O		X_{10}	X_{10}		O		O
apatite		O									X		
magnetite							X		X_{10}				
monticellite												X_{10}	X_{10}
akermanite												X_{10}	
perovskite									X_{10}				
spinel									X_{10}				

X: Essential mineral O: Accessory mineral (<2vol%)
Sample Av2, Av3, Av4, Av6, Av15, Av18 : xenolith B; Ma2b, Ma9, Ma10, Ma13, Ma16, Ma22 : xenolith D
1: poikiloblastic; 2: idioblastic; 3: xenoblastic; 4: graphic intergrowth; 5: as inclusions in clinopyroxene or wollastonite; 6: as inclusions in wollastonite; 7: fibrous; 8: granoblastic; 9: granular; 10: intimately intergrown or symplectic; 11: as inclusions in K-feldspar.

Table 9 Representative microprobe analyses (wt.% and atoms per formula unit) of clinopyroxene, garnet, wollastonite, apatite, plagioclase, vesuvianite, chlorite and magnetite occurring in xenolith B

	Clinopyroxene			Garnet					Wollastonite		Apat.	Vesuvianite						Chlor.	Mag.
	Av4	Av6	Av15	Av4	Av6	Av8	Av15	Av19	Av3	Av6	Av3	Av32	Av33	Av4	Av8	Av21	Av19	Av19	Av18
SiO_2	54.29	51.90	55.16	28.03	38.23	32.29	34.48	31.51	50.51	51.06	2.30	35.51	34.53	36.01	35.38	34.84	36.27	33.98	0.13
TiO_2	0.00	0.00	0.00	11.89	0.21	6.77	4.08	6.95	0.00	0.00	0.00	0.00	0.00	0.01	0.50	1.03	0.86	0.01	2.07
Al_2O_3	0.09	0.00	0.01	4.05	16.07	7.73	8.20	5.96	0.17	0.00	0.01	12.25	12.11	12.12	13.88	14.75	11.67	10.85	1.32
Cr_2O_3	0.00	0.00	0.00	0.00	0.00	0.00	0.00	0.00	0.01	0.01	0.00	0.00	0.00	0.00	0.00	0.00	0.00	0.02	0.00
Fe_2O_3*	0.00	0.00	0.00	21.64	9.15	17.99	18.05	20.25	0.00	0.00	0.00	6.52	6.73	6.41	6.17	7.15	5.88	0.00	62.69
FeO	0.27	9.90	0.43	0.00	0.00	0.00	0.00	0.00	0.07	0.39	0.03	0.00	0.00	0.00	0.00	0.00	0.00	1.07	31.31
MnO	1.52	0.85	0.90	0.07	0.33	0.20	0.25	0.08	0.03	0.24	0.00	0.25	0.29	0.27	0.13	0.06	0.14	0.24	1.03
MgO	16.86	10.21	26.26	0.48	0.00	0.58	0.50	0.39	0.03	0.01	0.03	4.17	4.06	4.77	6.02	2.57	5.73	34.60	0.48
CaO	26.12	24.83	0.00	33.95	36.51	33.81	34.10	34.07	48.49	48.11	52.48	36.71	36.19	36.05	33.84	35.71	34.18	0.11	0.00
BaO	0.00	0.00	0.00	0.07	0.02	0.03	0.03	0.07	0.04	0.00	0.00	0.00	0.00	0.00	0.00	0.00	0.00	0.01	0.00
Na_2O	0.00	0.01	0.00	0.00	0.00	0.00	0.00	0.00	0.00	0.00	0.00	0.00	0.00	0.11	0.16	0.06	0.18	0.01	0.00
K_2O	0.00	0.32	0.00	0.00	0.00	0.00	0.00	0.00	0.01	0.01	0.00	0.00	0.00	0.00	0.00	0.00	0.00	0.02	0.00
Total	99.15	97.71	100.54	100.18	100.52	99.40	99.69	99.24	99.66	99.83	54.85	95.41	93.91	95.75	96.08	96.17	94.91	80.92	99.03**
Formula	6(O)			24(O)					6(O)		10 cat. norm.	50 cat. norm.						20 cat. norm.	3 cat. norm.
Si	1.99	2.01	1.99	4.71	5.91	5.30	5.61	5.25	1.98	1.99	0.39	17.64	17.46	17.82	17.28	17.31	18.01	6.82	0.01
Ti	0.00	0.00	0.00	1.51	0.02	0.84	0.50	0.87	0.00	0.00	0.00	0.00	0.00	0.00	0.18	0.39	0.33	0.00	0.06
Al	0.00	0.00	0.00	0.80	2.92	1.50	1.58	1.17	0.03	0.00	0.00	7.16	7.23	7.08	7.98	8.63	6.83	2.57	0.06
Cr^{3+}	0.00	0.00	0.00	0.00	0.00	0.00	0.00	0.00	0.00	0.00	0.00	0.00	0.00	0.00	0.00	0.00	0.00	0.00	0.00
Fe^{3+} *	0.00	0.00	0.00	2.74	1.06	2.22	2.21	2.54	0.00	0.00	0.00	2.45	2.55	2.38	2.26	2.69	2.21	0.00	1.81
Fe^{2+}	0.01	0.32	0.01	0.00	0.00	0.00	0.00	0.00	0.00	0.01	0.01	0.00	0.00	0.00	0.00	0.00	0.00	0.18	1.00
Mn	0.05	0.03	0.03	0.01	0.04	0.03	0.04	0.01	0.00	0.01	0.00	0.12	0.12	0.09	0.06	0.03	0.06	0.04	0.03
Mg	0.92	0.59	0.96	0.12	0.00	0.14	0.12	0.10	0.00	0.00	0.01	3.08	3.07	3.51	4.37	1.91	4.23	10.36	0.03
Ca	1.03	1.03	1.02	6.11	6.04	5.96	5.95	6.09	2.01	2.00	9.59	19.55	19.58	19.12	17.69	19.02	18.16	0.02	0.00
Ba	0.00	0.00	0.00	0.00	0.00	0.00	0.00	0.00	0.00	0.00	0.00	0.00	0.00	0.00	0.00	0.00	0.00	0.00	n.d.
Na	0.00	0.00	0.00	0.00	0.00	0.00	0.00	0.00	0.00	0.00	0.00	0.00	0.00	0.00	0.18	0.02	0.18	0.00	n.d.
K	0.00	0.00	0.00	0.00	0.00	0.00	0.00	0.00	0.00	0.00	0.00	0.00	0.00	0.00	0.00	0.00	0.00	0.00	n.d.
Total	4.00 diop.	3.98 salite	4.01 diop.	4.96 And 84 Gr 16 Pyr 0	5.00 And 27 Gr 73 Pyr 0	5.02 And 68 Gr 31 Pyr 1	5.03 And 63 Gr 36 Pyr 1	5.02 And 74 Gr 26 Pyr 0	4.02	4.01	10.00	50.00	50.00	50.00	50.00	50.00	50.00	20.00 penn.	3.00

* Fe_2O_3 recalculation for water-free silicates after Finger (1972); for vesuvianite after Manning and Tricker (1975); for magnetite, assuming stoichiometric composition.

** plus traces of V_2O_5

Table 10 Vesuvianite analyses from different localities.

Red vesuvianites (xenolith B):

Av32: $(Ca_{19.55}Na_{0.00})(Mg_{3.08}Mn_{0.12}Fe^{3+}_{2.45}Ti_{0.00}Al_{6.80})(Al_{0.36}Si_{17.64})$
X=19.55 Y=12.45 Z=18.00

Av33: $(Ca_{19.58}Na_{0.00})(Mg_{3.07}Mn_{0.12}Fe^{3+}_{2.55}Ti_{0.00}Al_{6.69})(Al_{0.54}Si_{17.46})$
X=19.58 Y=12.43 Z=18.00

Av4: $(Ca_{19.12}Na_{0.00})(Mg_{3.51}Mn_{0.09}Fe^{3+}_{2.38}Ti_{0.00}Al_{6.90})(Al_{0.18}Si_{17.82})$
X=19.12 Y=12.88 Z=18.00

Av21: $(Ca_{19.02}Na_{0.02})(Mg_{1.91}Mn_{0.03}Fe^{3+}_{2.69}Ti_{0.39}Al_{7.94})(Al_{0.69}Si_{17.31})$
X=19.04 Y=12.96 Z=18.00

Green-yellowish vesuvianites (xenolith B):

Av8: $(Ca_{17.69}Na_{0.18})(Mg_{4.37}Mn_{0.06}Fe^{3+}_{2.26}Ti_{0.18}Al_{7.26})(Al_{0.72}Si_{17.28})$
X=17.87 Y=14.13 Z=18.00

Av19: $(Ca_{18.16}Na_{0.18})(Mg_{4.23}Mn_{0.06}Fe^{3+}_{2.21}Ti_{0.33}Al_{6.83})(Al_{0.00}Si_{18.01})$
X=18.34 Y=13.66 Z=18.00

Reddish vesuvianites (xenolith D):

Ma2a: $(Ca_{19.04}Na_{0.00})(Mg_{2.77}Mn_{0.00}Fe^{2+}_{1.51}Ti_{1.36}Al_{7.32})(Al_{0.12}Si_{17.88})$
X=19.04 Y=12.96 Z=18.00

Ma2b: $(Ca_{18.98}Na_{0.00})(Mg_{2.29}Mn_{0.00}Fe^{3+}_{2.12}Ti_{0.00}Al_{8.52})(Al_{0.00}Si_{18.09})$
X=18.98 Y=12.93 Z=18.09

Ma22: $(Ca_{19.10}Na_{0.00})(Mg_{2.86}Mn_{0.00}Fe^{3+}_{0.95}Ti_{0.32}Al_{8.77})(Al_{0.44}Si_{17.56})$
X=19.10 Y=12.90 Z=18.00

Honey-yellow vesuvianites (locality A):

I15: $(Ca_{19.77}K_{0.01})(Mg_{6.94}Mn_{0.00}Fe^{3+}_{0.22}Ti_{0.00}Al_{5.06})(Al_{0.59}Si_{17.41})$
X=19.78 Y=12.22 Z=18.00

Table 11 Representative microprobe analyses (wt.% and atoms per formula unit) of clinopyroxene, garnet, wollastonite, K-feldspar, perovskite, spinel, apatite, vesuvianite, prehnite, chlorite, muscovite, xantophyllite, monticellite and melilite, occurring in xenolith D

	Clinopyroxene					Garnet			Wollastonite		K-feld.	Perovs.	Spinel		
	Ma2b	Ma9	Ma13	Ma10a	Ma10b	Ma2b	Ma10a	Ma22	Ma13	Ma16	Ma13	Ma9	Ma9	Ma22a	Ma22b
SiO_2	54.66	38.50	52.22	46.18	48.35	38.76	38.04	36.47	50.80	51.23	65.56	0.00	0.01	0.00	0.00
TiO_2	0.00	3.98	0.12	1.60	0.79	1.30	0.02	2.21	0.07	0.01	0.01	58.39	0.04	0.00	0.00
Al_2O_3	0.21	13.19	0.85	4.57	3.11	17.30	21.28	12.02	0.03	0.07	18.54	0.18	61.55	64.76	59.60
Cr_2O_3	0.02	0.01	0.01	0.00	0.00	0.00	0.00	0.00	0.02	0.00	0.00	0.00	0.25	0.15	0.20
Fe_2O_3 *	0.00	9.11	1.63	3.51	2.56	3.66	0.00	14.64	0.00	0.00	0.00	0.00	8.36	0.88	9.72
FeO	1.30	0.00	6.68	11.49	11.37	1.43	1.17	0.42	0.97	0.00	0.08	0.65	7.79	11.33	8.37
MnO	0.07	0.02	0.16	0.19	0.19	0.02	0.07	0.17	0.14	0.00	0.00	0.00	0.18	0.08	0.11
MgO	17.18	9.68	12.98	8.65	9.25	0.55	0.02	0.32	0.06	0.09	0.00	0.00	22.09	22.48	21.50
CaO	26.07	24.98	24.83	22.71	23.28	37.33	37.31	33.81	47.58	47.67	0.04	41.12	0.00	0.00	0.00
BaO	0.00	0.00	0.00	0.00	0.00	0.00	0.00	0.00	0.00	0.00	0.00	0.21	0.00	0.00	0.00
Na_2O	0.00	0.00	0.16	0.00	0.00	0.00	0.00	0.00	0.00	0.00	0.25	0.00	0.00	0.00	0.00
K_2O	0.00	0.00	0.00	0.01	0.04	0.00	0.01	0.00	0.00	0.00	15.23	0.00	0.00	0.00	0.00
Total	99.51	99.47	99.64	98.91	98.94	100.35	97.92	100.06	99.67	99.07	99.71	100.55	100.27	99.68	99.50
Formula	6(O)					24(O)			6(O)		8(O)	6(O)	4(O)		
Si	2.00	1.47	1.96	1.80	1.86	5.91	5.86	5.78	1.98	1.99	3.02	0.00	0.00	0.00	0.00
Ti	0.00	0.11	0.00	0.05	0.02	0.15	0.00	0.27	0.00	0.00	0.00	1.98	0.00	0.00	0.00
Al	0.01	0.59	0.04	0.21	0.14	3.11	3.86	2.25	0.00	0.00	1.01	0.01	1.83	1.90	1.80
Cr^{3+}	0.00	0.00	0.00	0.00	0.00	0.00	0.00	0.00	0.00	0.00	0.00	0.00	0.01	0.00	0.01
Fe^{3+} *	0.00	0.26	0.05	0.10	0.10	0.42	0.15	1.75	0.00	0.00	0.00	0.00	0.16	0.02	0.19
Fe^{2+}	0.04	0.00	0.21	0.38	0.37	0.18	0.00	0.06	0.03	0.00	0.00	0.02	0.16	0.24	0.18
Mn	0.00	0.00	0.00	0.01	0.01	0.00	0.01	0.02	0.01	0.00	0.00	0.00	0.01	0.00	0.00
Mg	0.94	0.55	0.73	0.50	0.53	0.13	0.01	0.08	0.00	0.01	0.00	0.00	0.83	0.84	0.82
Ca	1.02	1.02	1.00	0.95	0.96	6.10	6.16	5.75	1.99	1.99	0.02	1.99	0.00	0.00	0.00
Ba	0.00	0.00	0.00	0.00	0.00	0.00	0.00	0.00	0.00	0.00	0.00	0.00	0.00	0.00	0.00
Na	0.00	0.00	0.01	0.00	0.00	0.00	0.00	0.00	0.00	0.00	0.02	0.00	0.00	0.00	0.00
K	0.00	0.00	0.00	0.00	0.00	0.00	0.00	0.00	0.00	0.00	0.89	0.00	0.00	0.00	0.00
Total	4.01	4.00	4.00	4.00	3.99	16.00	16.05	15.96	4.01	3.99	4.96	4.00	3.00	3.00	3.00
	diop.	Ti-aug.	salite	Fe-sal.	Fe-sal.	And 15	And 4	And 47							
						Gr 82	Gr 96	Gr 52							
						Pyr 1	Pyr 0	Pyr 1							
						Alm 2	Alm 0	Alm 0							

Table 11a

	Apatite	Vesuvianite			Prehnite			Chlor.	Muscovite		Xantophyllite		Monticellite		Melilite
	Mal3	Ma2a	Ma2b	Ma22	Mala	Malb	Mal0	Ma2b	Mal3	Mal0	Ma22a	Ma22b	Mal6	Ma22	Mal6
SiO_2	0.18	35.79	36.99	35.72	44.08	41.92	42.88	33.26	47.86	48.26	17.48	14.53	36.37	37.03	43.25
TiO_2	0.00	3.63	0.00	0.92	0.03	0.05	0.00	0.00	0.00	0.00	0.04	0.01	0.00	0.00	0.00
Al_2O_3	0.00	12.63	14.77	15.91	24.31	23.21	24.70	15.97	37.10	36.92	40.67	44.11	0.00	0.02	2.07
Cr_2O_3	0.00	0.02	0.00	0.02	0.00	0.01	0.00	0.02	0.00	0.00	0.03	0.26	0.02	0.01	0.00
Fe_2O_3 *	0.00	0.00	5.67	2.49	0.00	0.00	0.00	0.00	0.00	0.00	0.00	0.00	0.00	0.00	0.00
FeO	0.03	3.62	0.00	0.00	2.33	4.85	0.18	0.69	0.20	0.60	1.75	1.92	2.85	4.63	1.44
MnO	0.01	0.00	0.00	0.00	0.02	0.02	0.00	0.05	0.01	0.00	0.01	0.01	0.10	0.12	0.04
MgO	0.00	3.73	3.15	3.89	1.65	3.03	0.00	33.16	0.00	0.00	20.11	18.75	23.55	22.15	12.47
CaO	53.24	35.58	36.22	36.28	23.01	19.56	26.33	0.09	0.48	0.58	12.28	13.30	36.05	36.06	40.42
BaO	0.00	0.00	0.00	0.00	0.00	0.00	0.00	0.00	0.03	0.00	0.00	0.01	0.00	0.00	0.02
Na_2O	0.00	0.00	0.00	0.00	0.23	0.35	0.10	0.00	0.56	0.05	0.08	0.00	0.00	0.00	0.67
K_2O	0.00	0.00	0.00	0.00	0.01	0.02	0.07	0.01	8.63	11.03	0.02	0.00	0.01	0.00	0.09
Total	53.46	95.00	96.80	95.23	95.67	93.02	94.26	83.25	94.87	97.45	92.47	92.90	98.95	100.02	100.47
Formula	10 cat. norm.	50 cat. norm.			14 cat. norm.			20 cat. norm.	14 cat. norm.		16 cat. norm.		4(0)		7(0)
Si	0.03	17.88	18.10	17.56	6.04	5.89	5.97	6.51	6.42	6.31	2.54	2.10	0.98	0.99	1.97
Ti	0.00	1.36	0.00	0.32	0.00	0.01	0.00	0.00	0.00	0.00	0.01	0.00	0.00	0.00	0.00
Al	0.00	7.44	8.52	9.21	3.92	3.85	4.05	3.68	5.86	5.69	6.96	7.53	0.00	0.00	0.11
Cr^{3+}	0.00	0.00	0.00	0.00	0.00	0.00	0.00	0.00	0.00	0.00	0.00	0.03	0.00	0.00	0.00
Fe^{3+} *	0.00	0.00	2.12	0.92	0.00	0.00	0.00	0.00	0.00	0.00	0.00	0.00	0.00	0.00	0.00
Fe^{2+}	0.01	1.51	0.00	0.00	0.27	0.57	0.02	0.11	0.02	0.07	0.21	0.23	0.06	0.10	0.06
Mn	0.00	0.00	0.00	0.00	0.00	0.00	0.00	0.01	0.00	0.00	0.00	0.00	0.00	0.00	0.00
Mg	0.00	2.77	2.29	2.86	0.34	0.63	0.00	9.67	0.00	0.00	4.35	4.05	0.94	0.88	0.84
Ca	9.96	19.04	18.98	19.10	3.37	2.95	3.92	0.02	0.07	0.08	1.91	2.06	1.03	1.03	1.97
Ba	0.00	0.00	0.00	0.00	0.00	0.00	0.00	0.00	0.00	0.00	0.00	0.00	0.00	0.00	0.00
Na	0.00	0.00	0.00	0.00	0.06	0.10	0.03	0.00	0.15	0.01	0.02	0.00	0.00	0.00	0.06
K	0.00	0.00	0.00	0.00	0.00	0.00	0.01	0.00	1.48	1.84	0.00	0.00	0.00	0.00	0.00
Total	10.00	50.00	50.00	50.00	14.00	14.00	14.00	20.00 pennin.	14.00	14.00	16.00	16.00	3.01	3.00	5.01

* Fe_2O_3 recalculation: for water-free silicates after Finger (1972); for vesuvianites after Manning and Tricker (1975); for all other OH-bearing minerals, assuming Fe_{tot}=FeO.

Explanation of Plates 1 to 7

Abbreviations

ak: melilite (akermanite); ap: apatite; br: brucite; cc: calcite; Fe-br: ferrobrucite; ge: melilite (gehlenite); gr: garnet (grandite); ks: kalsilite; mo: monticellite; ol: olivine (forsterite); opx: orthopyroxene; px: clinopyroxene; pe: periclase; per: perovskite; phl: (Ba-rich) phlogopite; sp: spinel; ti: titanite; ves: vesuvianite; wo: wollastonite; xa: xantophyllite;
Nic. +: crossed Niccols; Nic. //: parallel Niccols.
The localities of the samples refer to Figure 1.

Scale

If not differently indicated, the bar in the lower right corner of each microphotograph indicates 0.40 mm.

Plate 1

a) Banded akermanite-monticellite-clinopyroxenefels from a marginal zone xenolith on the farm Hendriksplaats. Locality A.

b) Banded calc-silicates. Locality A.

c) Coarse-grained clinopyroxene (above hammer) abutting fine-grained gabbronorite (below hammer). Locality A.

d) Clinopyroxene developed at the xenolith-gabbronorite contact of a calc-silicate xenolith from locality A.

e) Forsterite exsolutions in monticellite. Sample I3, locality A, Nic. //.

f) Exsolutions of diopside (?) in akermanite. Sample J6, locality A, Nic. +.

g) Exsolutions of diopside (?) in akermanite. Sample J6, locality A, Nic. +.

h) Ba-rich phlogopite as inclusion in akermanite. Sample J6, locality A. Nic. +.

Plate 1

a

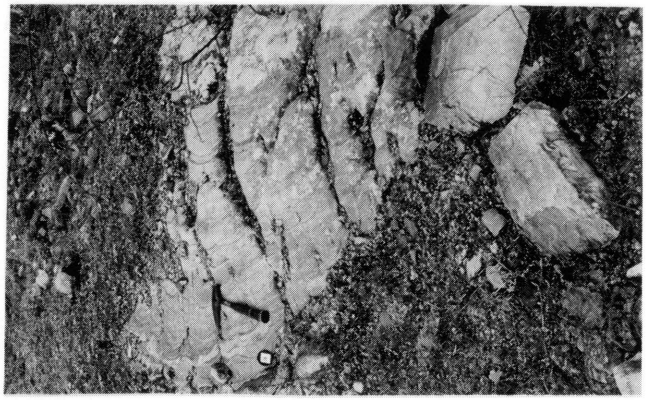

b

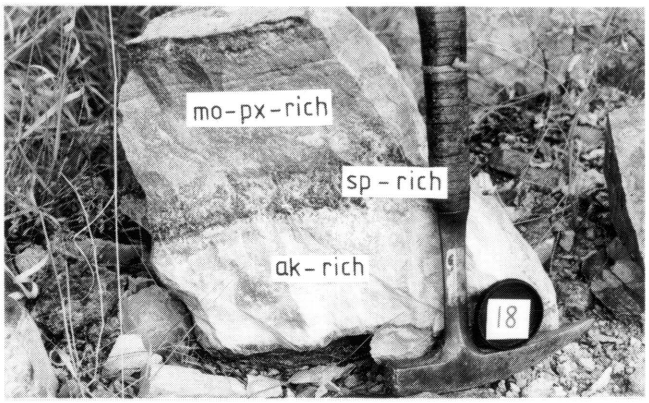

c

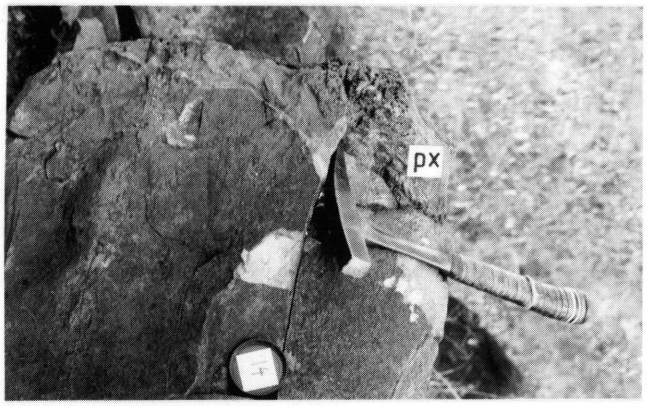

d

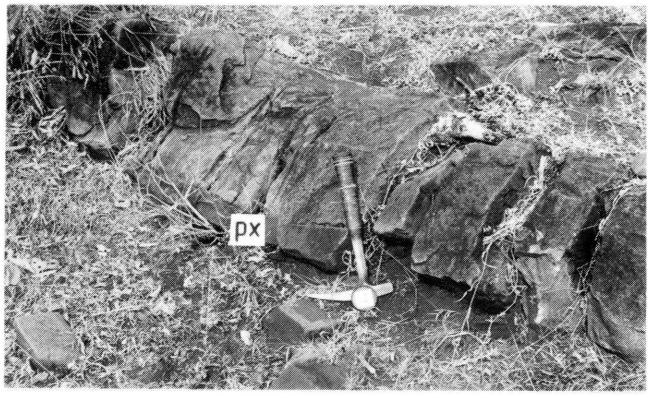

e

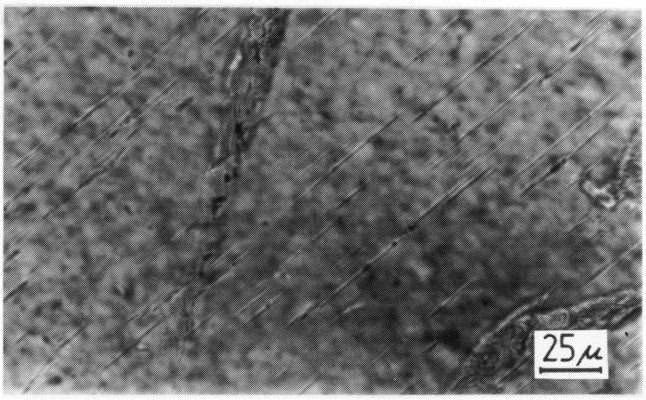

f

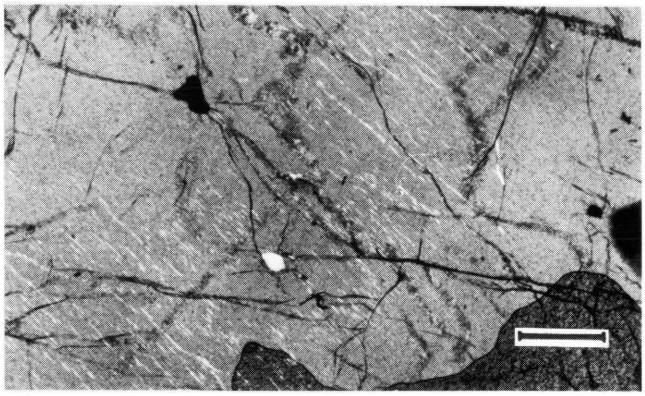

g

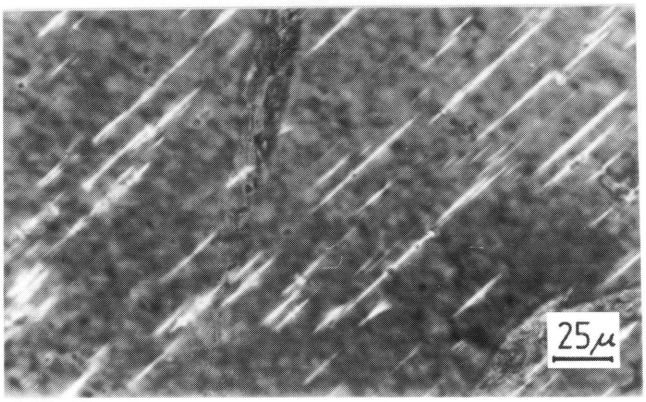

h

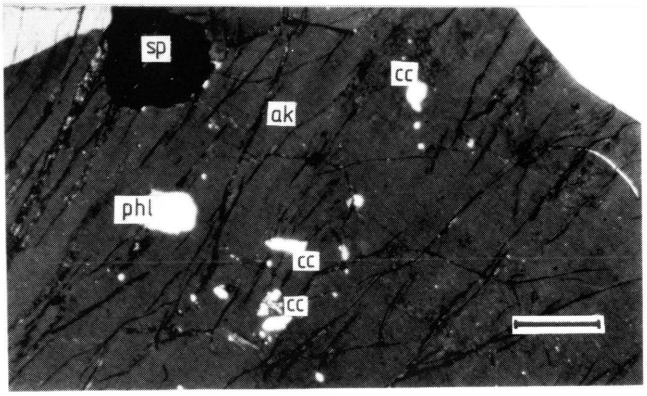

Plate 2

a) Ba-rich phlogopite associated with akermanite, monticellite, wollastonite and clinopyroxene. Symplectic-dactylitic intergrowth of wollastonite and monticellite as alteration product of akermanite (lower left corner). Sample J 11, locality A, Nic. +.

b) Symplectic mineral assemblage clinopyroxene-olivine-kalsilite (left half) adjacent to a very fine-grained mineral assemblage Ba-rich phlogopite-clinopyroxene-olivine-kalsilite-wollastonite. Sample J21, locality A, Nic. +.

c) Mineral assemblage Ba-rich phlogopite-clinopyroxene-olivine-kalsilite. Sample J21, locality A, Nic. +.

d) Fibrous vesuvianite replacing Al-rich melilite and Al-rich cores of zoned melilite grains. Sample I15, locality A, Nic. +.

e) The same as 2d but Nic. //. Vesuvianite (dark grey) replacing melilite (light grey).

f) Periclase, partly replaced by brucite, in monticellite. The dark grey grains represent Fe-rich spinels. Brucite is partly replaced by ferrobrucite along grain boundaries. Monticellite shows expansion cracks due to the increase in volume during the reaction periclase + H_2O = brucite. Sample Wia, xenolith C, Nic. //.

g) Forsterite exsolutions in monticellite (Black grains are spinel). Sample Wi, xenolith C, Nic. +.

h) Stringers of olivine exsolutions including small grains of spinel. The host mineral is monticellite. The relatively big grain in the lower left corner is also spinel. Sample Wi, xenolith C, Nic. +.

Plate 2

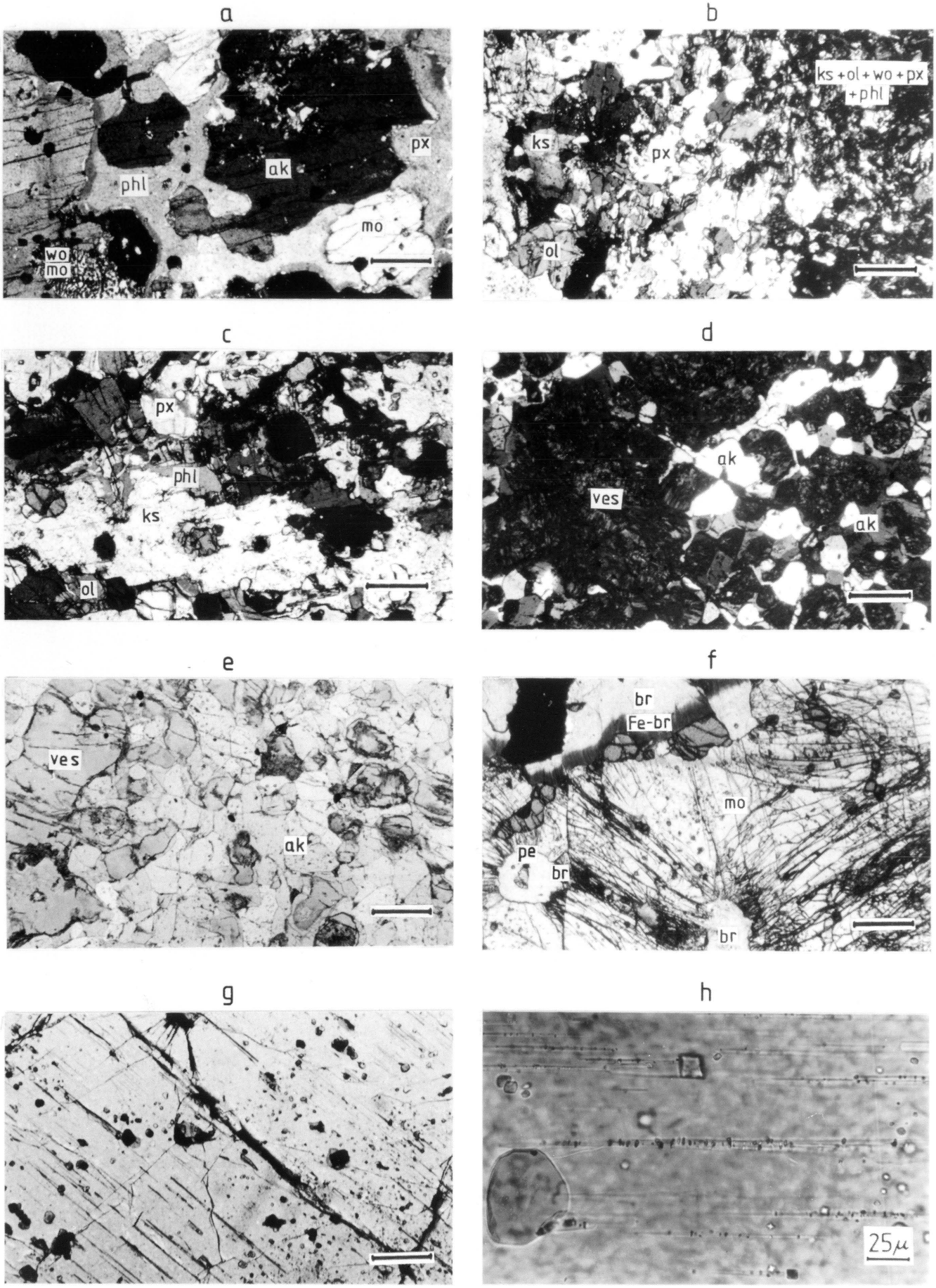

Plate 3

a) Mineral assemblage merwinite-monticellite-gehlenite. Merwinite displays polysynthetic twin lamellae. Gehlenite is partly altered to vesuvianite. Sample Wil, xenolith C, Nic. +.

b) Mineral assemblage merwinite-monticellite-gehlenite. Merwinite shows two systems of polysynthetic twin lamellae ('fishbone' pattern). Melilite is strongly zoned with a gehlenite-rich core becoming akermanite-richer towards the rim. The change from optically negative gehlenite to optically positive akermanite causes the optically isotropic (black) rim. Sample Wil, xenolith C, Nic. +.

c) Merwinite with 'lamellae' of merwinite with slightly different composition. Sample Wil, xenolith C, Nic. //.

d) Polygonal poikiloblastic monticellite with small spinel inclusions (dark grains), and coarser grained spinel stringers along monticellite grain boundaries. Sample WiE, xenolith C, Nic. //.

e) Zoned melilite with gehlenite-rich core and akermanite-rich rim. The change of the optical sign from gehlenite to akermanite, at ca. Ak_{60}, causes the optically isotropic (black) region in melilite. The small white inclusions consist of calcite and Ba-rich phlogopite. Sample J6, locality A, Nic. +.

f) Akermanite, partly altered to wollastonite and monticellite (upper right corner), with clinopyroxene (inclusions and interstitial). Sample J2, locality A, Nic. +.

g) Polygonal-granoblastic textured akermanite and monticellite both of which contain small calcite inclusions. Sample J2, locality A, Nic. +.

h) Polygonal-granoblastic textured monticellite with calcite inclusions (white specks) and interstitial olivine. Sample I3, locality A, Nic. +.

Plate 3

a

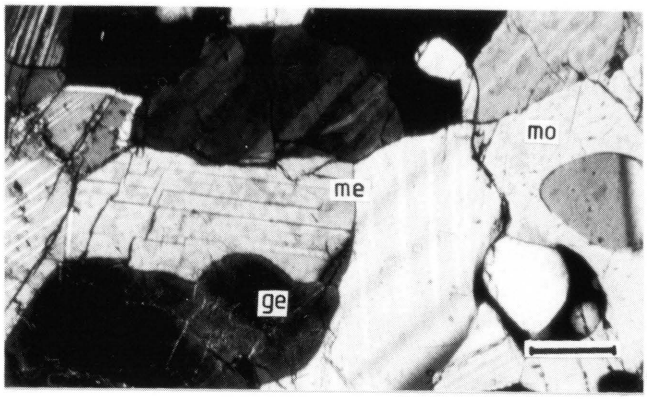

b

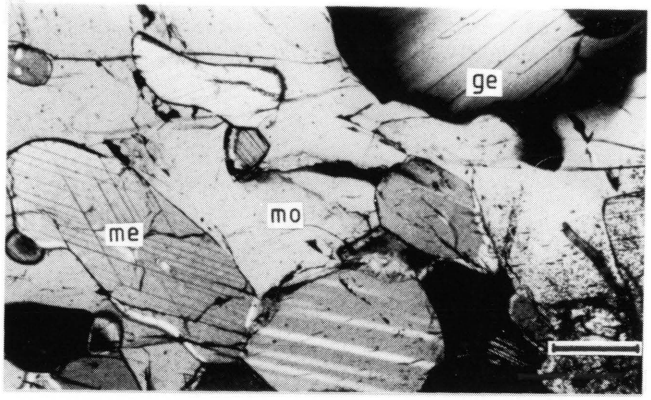

c

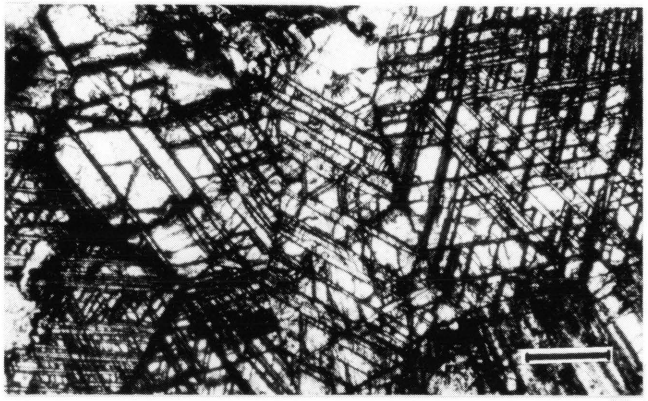

d

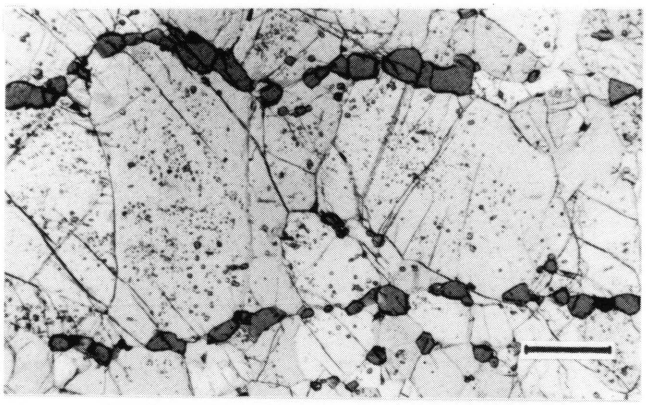

e

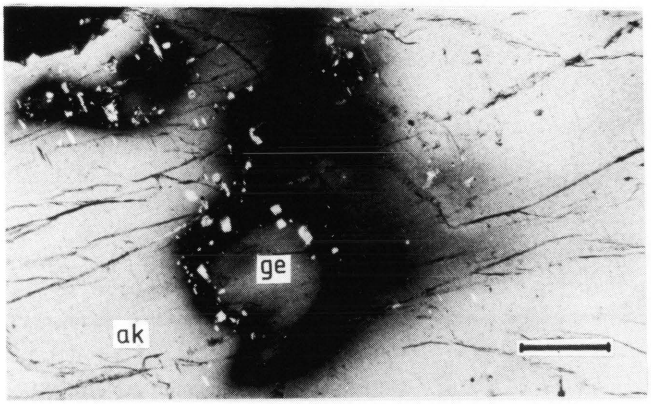

f

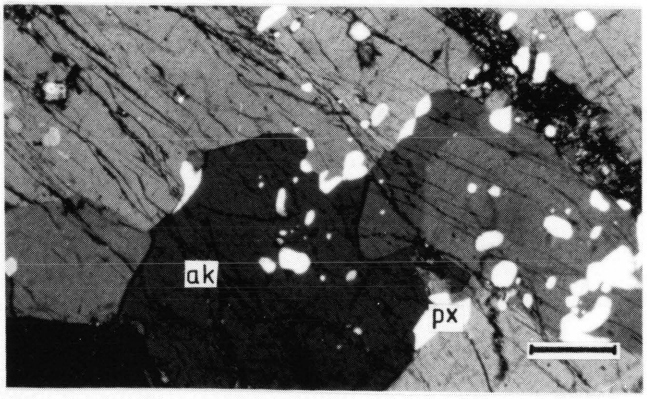

g

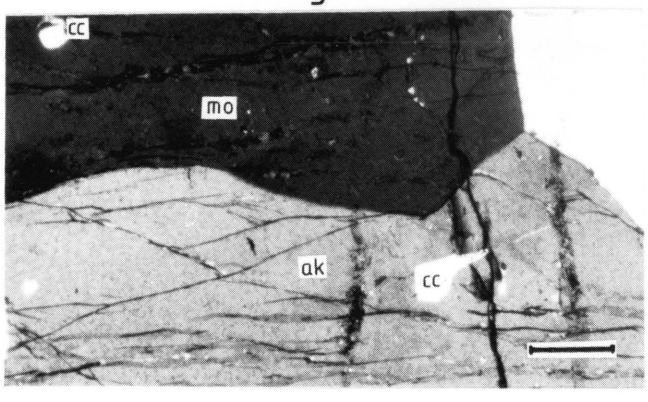

h

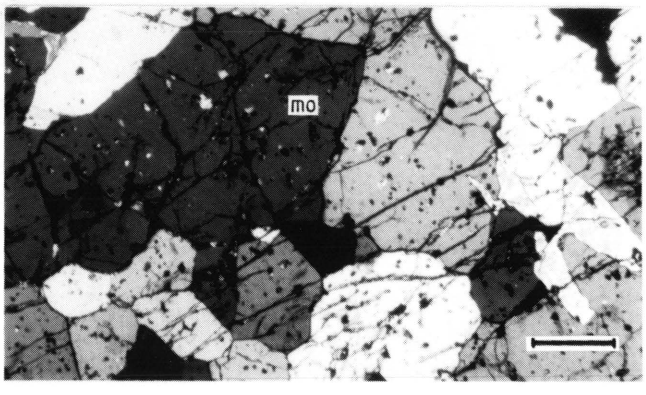

Plate 4

a) Symplectic intergrowth of olivine, clinopyroxene and monticellite. The small inclusions in olivine consist of spinel. This texture is caused by the retrograde reaction akermanite + forsterite = monticellite + diopside. Sample J8, locality A, Nic. +.

b) Slab of gabbronorite (black) intrusive into akermanite-monticellitefels. A narrow dark brown seam consists mainly of metasomatic clinopyroxene between the gabbronorite and the calc-silicates.

c) Gabbronorite of the marginal zone in contact with pure akermanitefels without any intervening metasomatic clinopyroxene seam.

d) Gabbronorite consisting of orthopyroxene, clinopyroxene and plagioclase. Sample J1, locality A, Nic. +.

e) Clinopyroxene of the metasomatic interaction seam between gabbronorite and xenolith displaying a disequilibrium texture, together with plagioclase. Sample J13, locality A, Nic. +.

f) Granoblastic-polygonal clinopyroxene with olivine from the metasomatic reaction seam. Sample J11, locality A, Nic. +.

g) Boulders of vesuvianite-grossularitefels on the farm Avontuur (xenolith B) in the upper zone of the eastern Bushveld Complex.

h) Symplectic intergrowth of vesuvianite (white) and garnet (grey) abutting against a Ti-poor magnetite. Sample Av10, xenolith B, Nic. //.

Plate 4

a

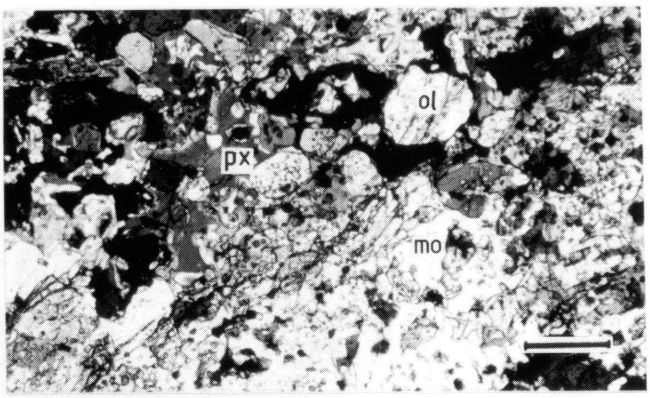

b

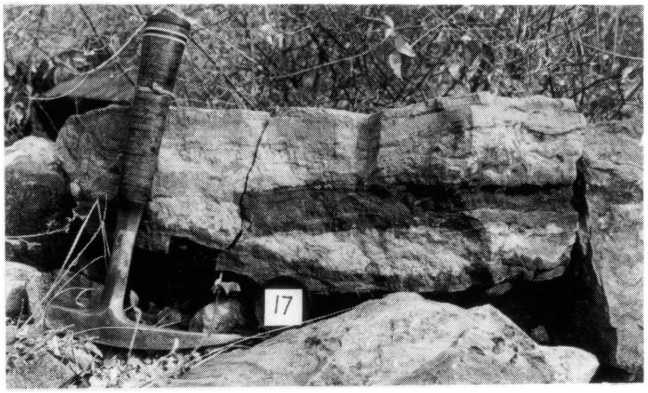

c

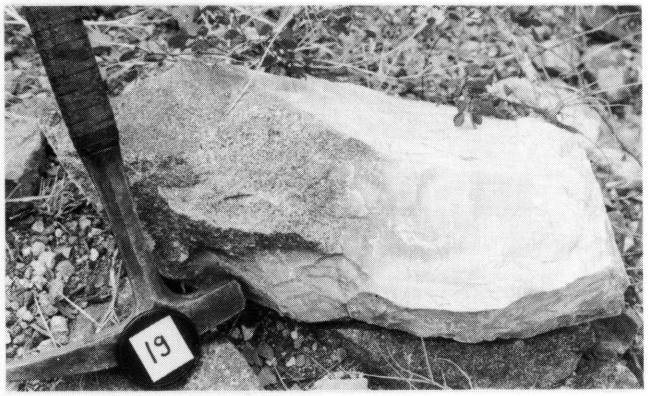

d

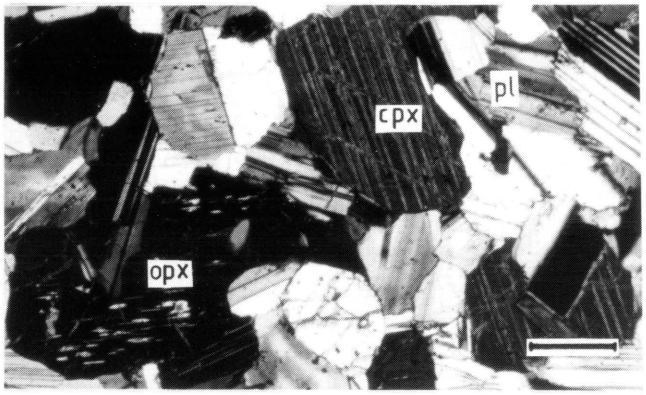

e

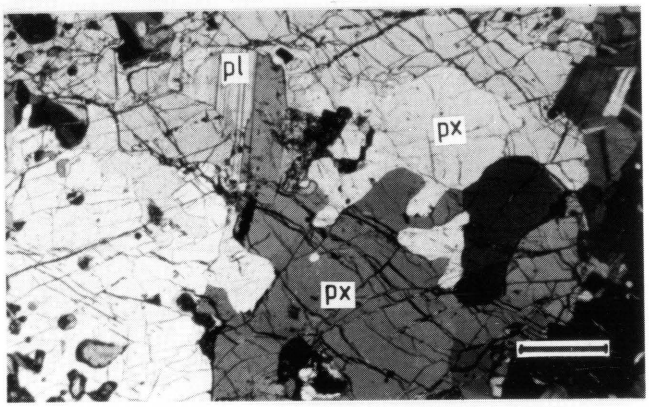

f

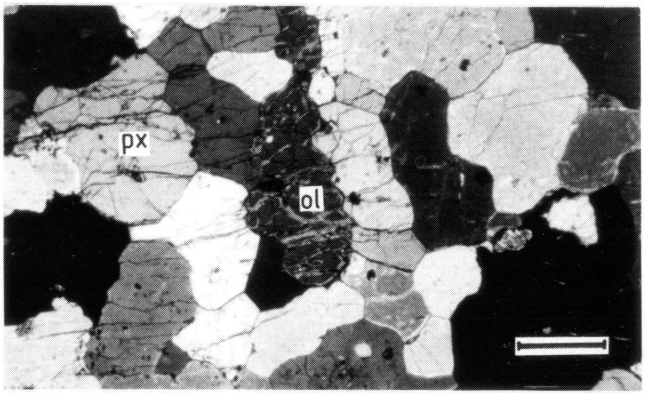

g

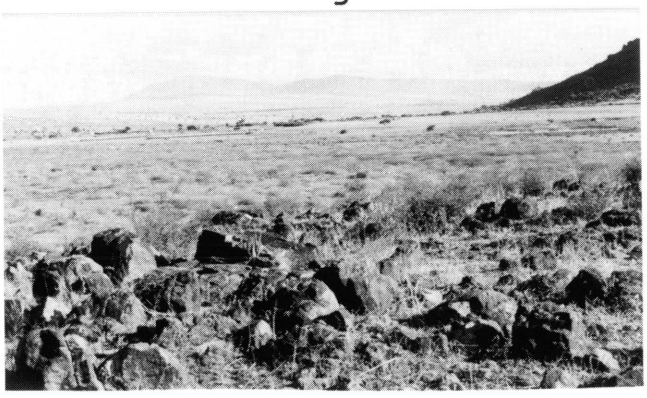

h

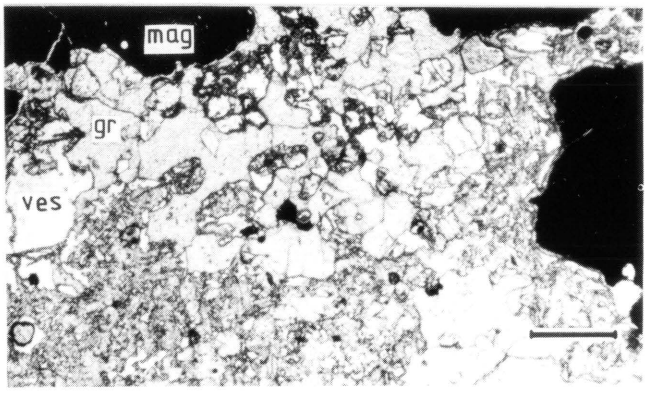

Plate 5

a) Mineral assemblage vesuvianite-garnet (melanite)-diopside. Fibrous diopside is interstitial. Melanite has a dark brown colour in the thin section. Sample Av4, xenolith B, Nic. partly +.

b) Polygonal garnet with interstitial vesuvianite in calc-silicate xenolith B. Sample Av8, Nic +.

c) Intimate intergrowth of clinopyroxene (greyish-white) and vesuvianite and garnet (both black). Sample Av15, xenolith B, Nic. +.

d) Graphic textured wollastonite (white) and vesuvianite (dark grey and black). Sample Av3, xenolith B, Nic. +.

e) Mineral assemblage wollastonite-clinopyroxene-garnet. Sample Av6, xenolith B, Nic. partly +.

f) Titanite idioblasts in wollastonite and clinopyroxene. Calcite exists as inclusions in wollastonite. Sample Av2, xenolith B, Nic. +.

g) Titanite idioblasts in wollastonite (black) with relict calcite (white). Sample Av2, xenolith B, Nic. +.

h) Calc-silicates of xenolith D (in front) are relatively resistant to weathering and form a prominent feature in the upper zone magnetitegabbro. The ridge in the background consists of recrystallized felsite of the Rooiberg Group which constitutes the roof of the Bushveld Complex in this area.

Plate 5

a

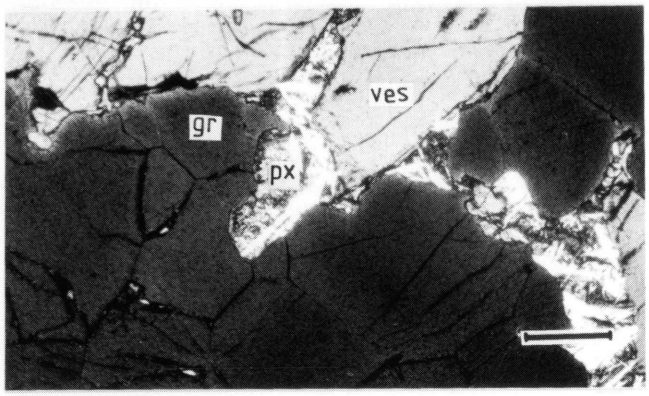

b

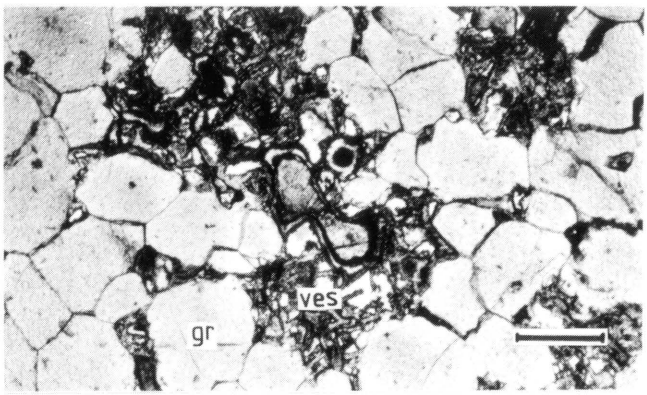

c

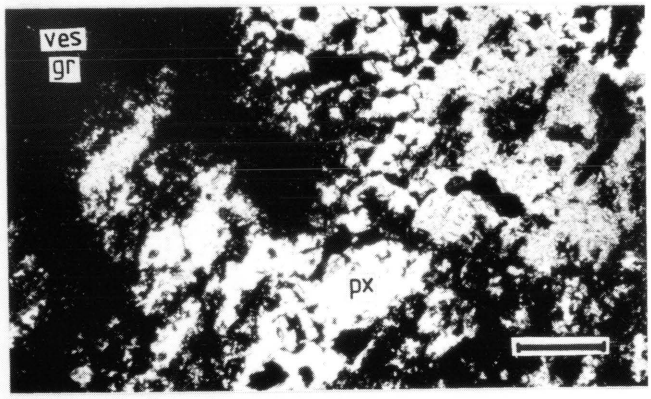

d

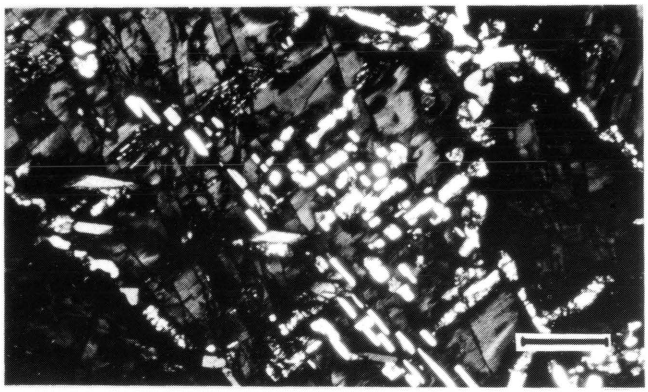

e

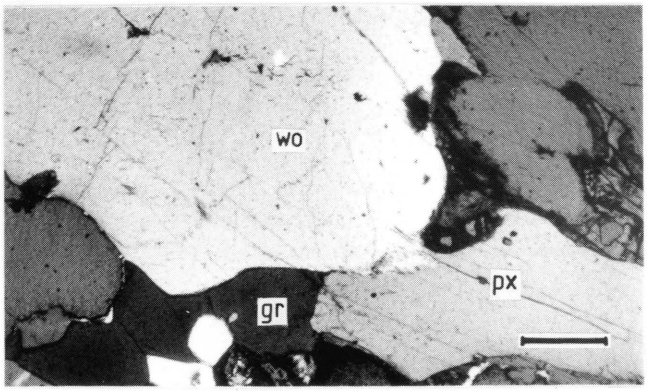

f

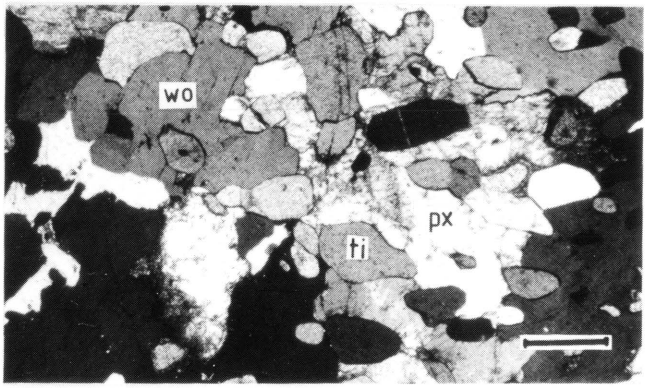

g

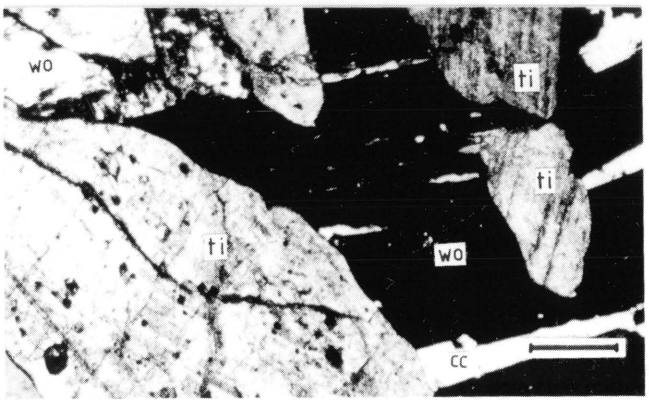

h

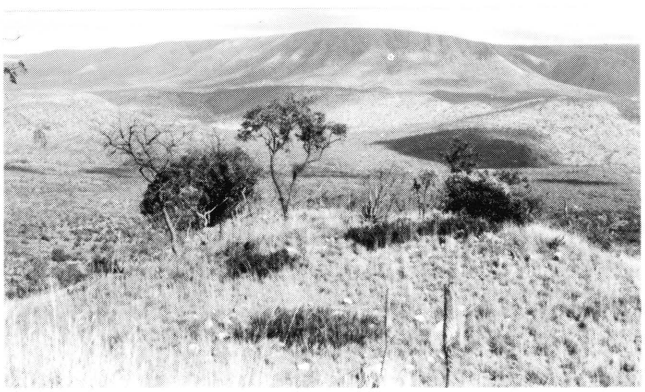

Plate 6

a) Fibrous and granular diopside (greyish-white) together with vesuvianite and garnet (black) on the farm Luipershoek. Sample Ma2b, xenolith D, Nic. +.

b) Mineral assemblage vesuvianite-grossular-diopside-calcite. In the photomicrograph grossular and vesuvianite are black and dark grey, respectively. Calcite and diopside appear white and light grey, respectively. Sample Ma2b, xenolith D, Nic. partly +.

c) Symplectic intergrowth of vesuvianite, grossular, clinopyroxene and calcite. Sample Ma6a, xenolith D, Nic. partly +.

d) Mineral assemblage vesuvianite-grossular-xantophyllite-calcite. Xantophyllite is fibrous and intimately intergrown with vesuvianite and garnet (dark grey and black). Sample Ma22, xenolith D, Nic. +.

e) Mineral assemblage vesuvianite-grossular-monticellite-xantophyllite-spinel. Xantophyllite is fibrous and intimately intergrown with vesuvianite and garnet (black). Sample Ma22, xenolith D, Nic. +.

f) The same as 6e but Nic. //.

g) Grossular and vesuvianite (black) replacing monticellite (white) along fractures and grain boundaries. Sample Ma22, xenolith D, Nic. +.

h) Polygonal-granoblastic akermanite partly replaced by a symplectic intergrowth of wollastinite and monticellite. Sample Ma16, xenolith D, Nic. +.

Plate 6

a

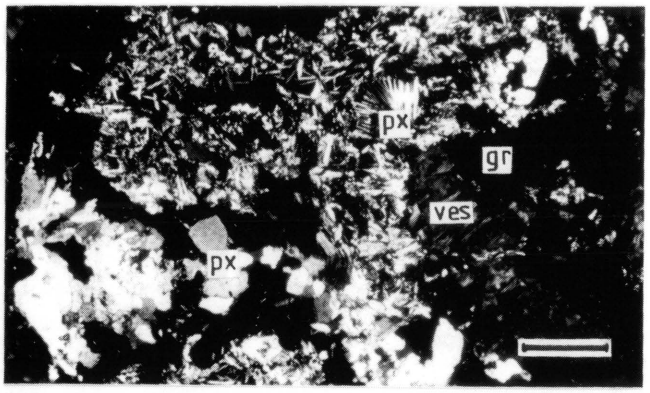

b

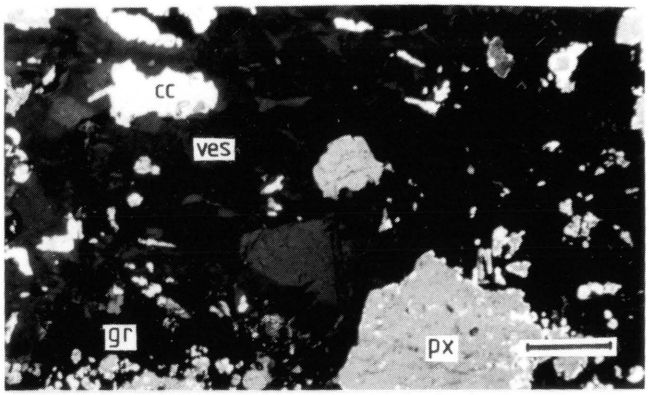

c

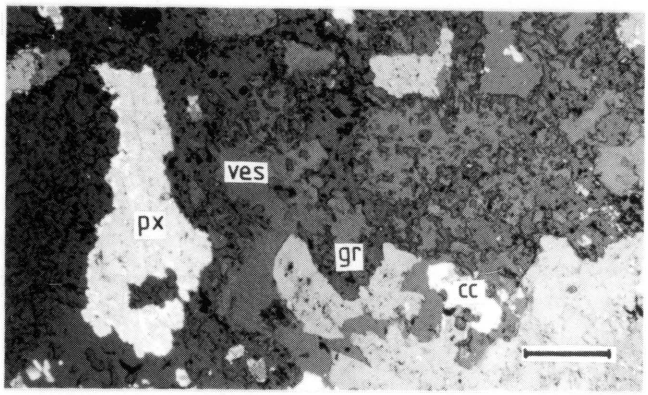

d

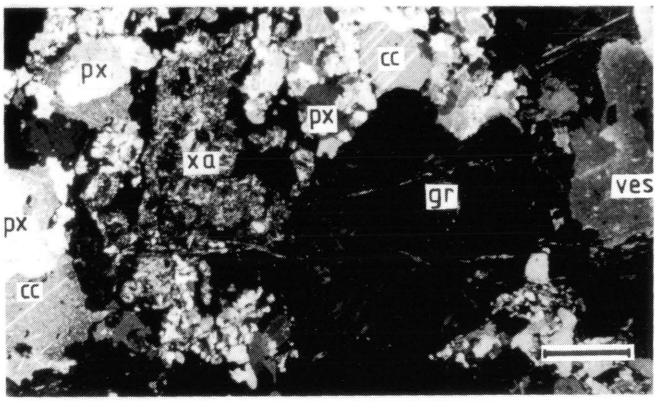

e

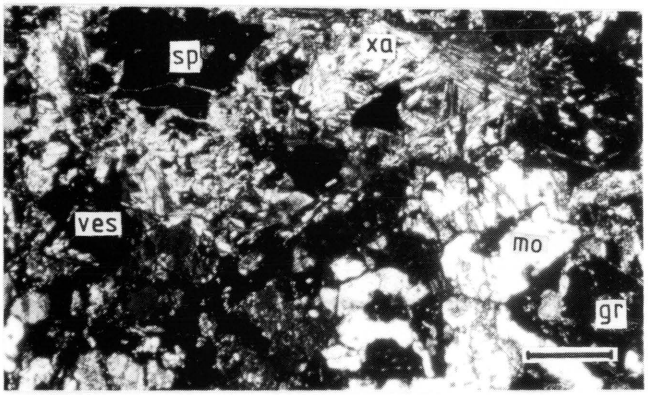

f

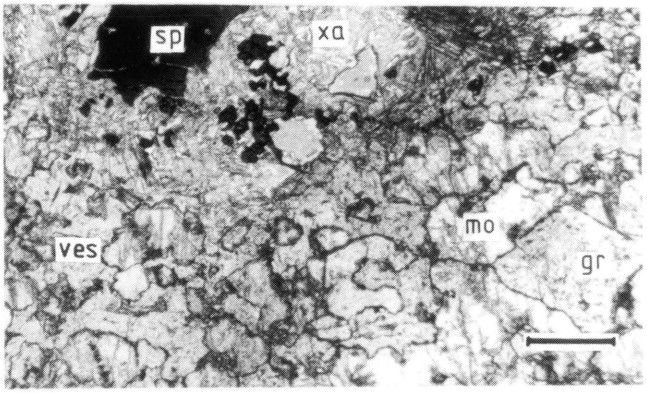

g

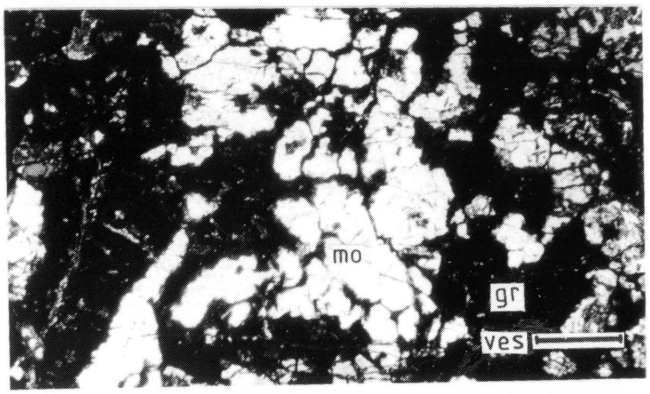

h

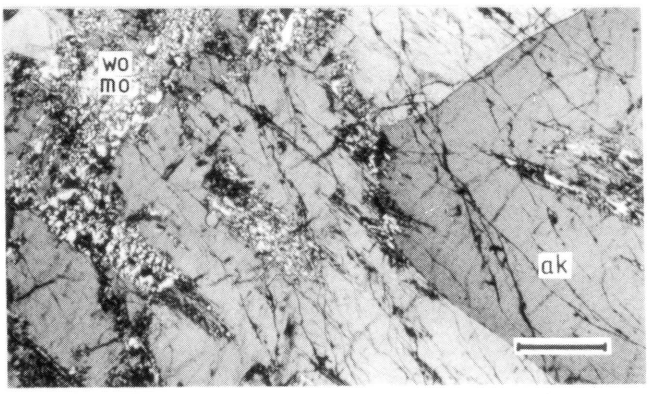

Plate 7

a) Replacement of akermanite, showing subgrain boundaries, by monticellite and wollastonite. Sample Ma2a, xenolith D, Nic. +.

b) Wollastonite-monticellitefels (white), including stringers of spinel (black), besides akermanitefels (grey). Xenolith D.

c) Symplectic textured calcite, perovskite, magnetite and spinel, included in magnetite which is surrounded by titanaugite. Due to the high Ti content the titanaugite (ca. 4 wt.%) is optically uniaxial. Sample Ma9, xenolith D, Nic. partly +.

d) Subidioblastic hydrogrossular nodules (black), partly pseudomorphously replaced by prehnite, in clinopyroxene. Sample Ma10, xenolith D, Nic. +.

e) Graphic texture of hydrogrossular, prehnite and clinopyroxene. Sample Ma10, xenolith D, Nic. +.

f) Wollastonite laths (white) in poikiloblastic K-feldspar (grey), sericite (fine-grained black and white aggregates). Apatite idioblast in the lower right corner. Sample Ma13, xenolith D, Nic. +.

g) The same as in 7f but Nic. //. Wollastonite and apatite have a higher relief than K-feldspar. Sericite aggregates appear grey in the photomicrograph.

h) Pseudomorphic replacement of andalusite by sericite (centre) with a corona of a fine-grained intergrowth of sericite and wollastonite. Laths of wollastonite in K-feldspar appear white in the photomicrograph. Sample Ma13, xenolith D, Nic. +.

Plate 7

a

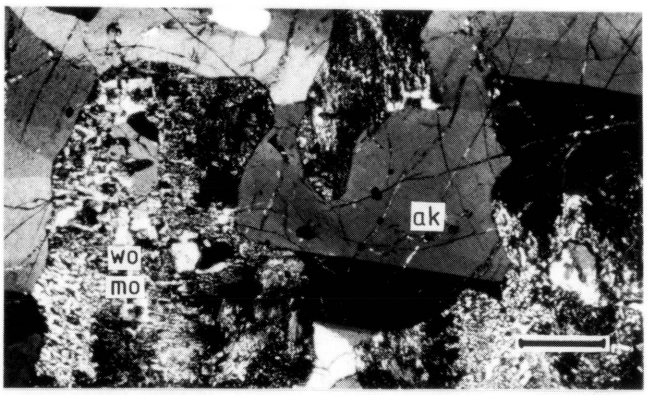

b

c

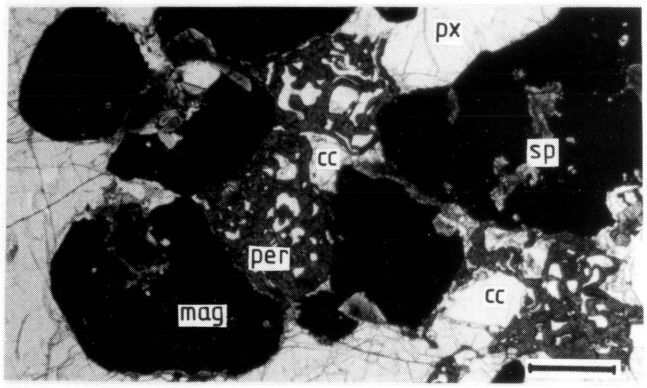

d

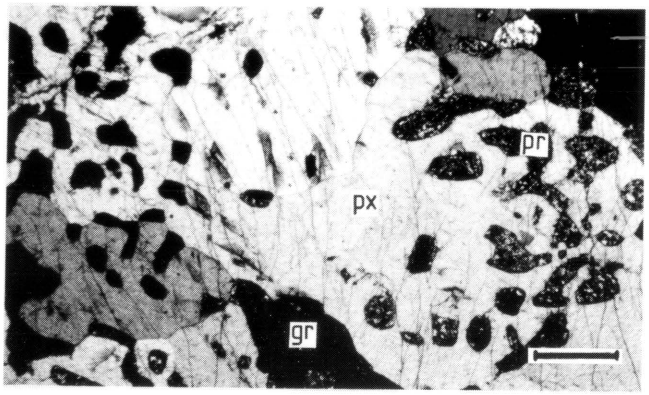

e

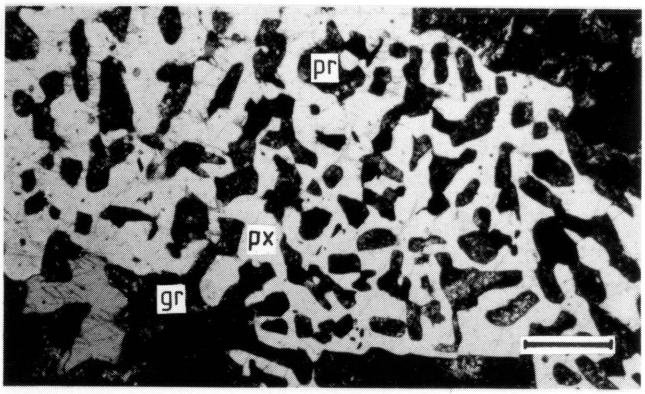

f

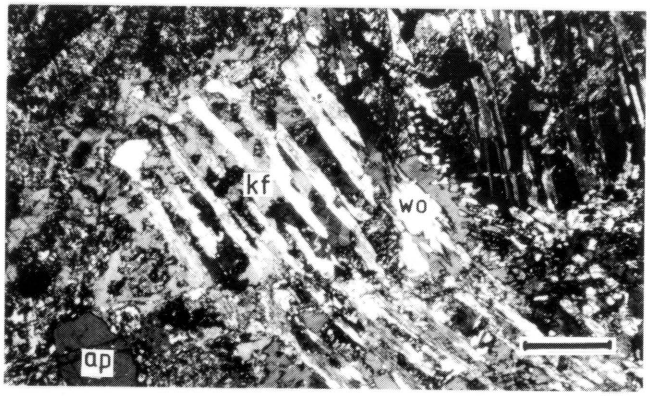

g

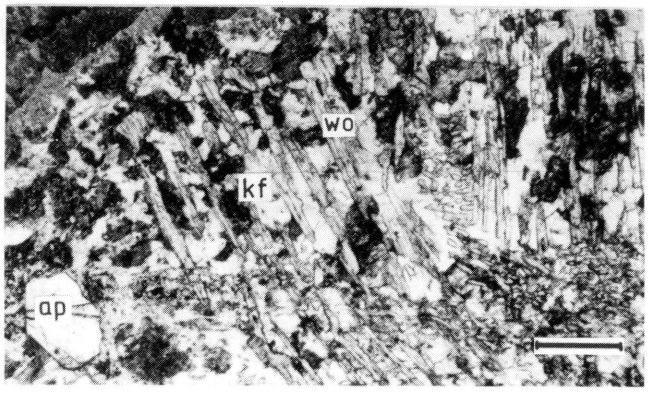

h

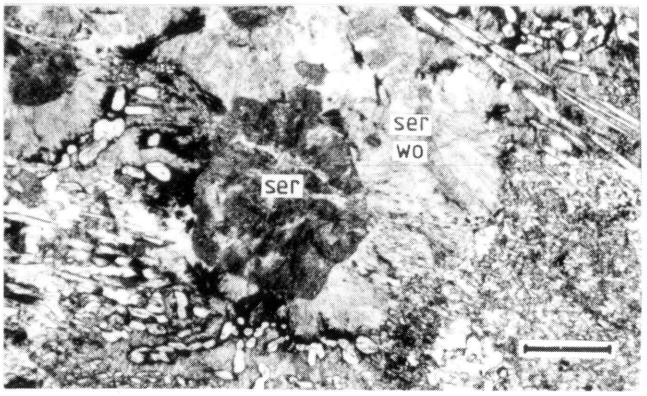

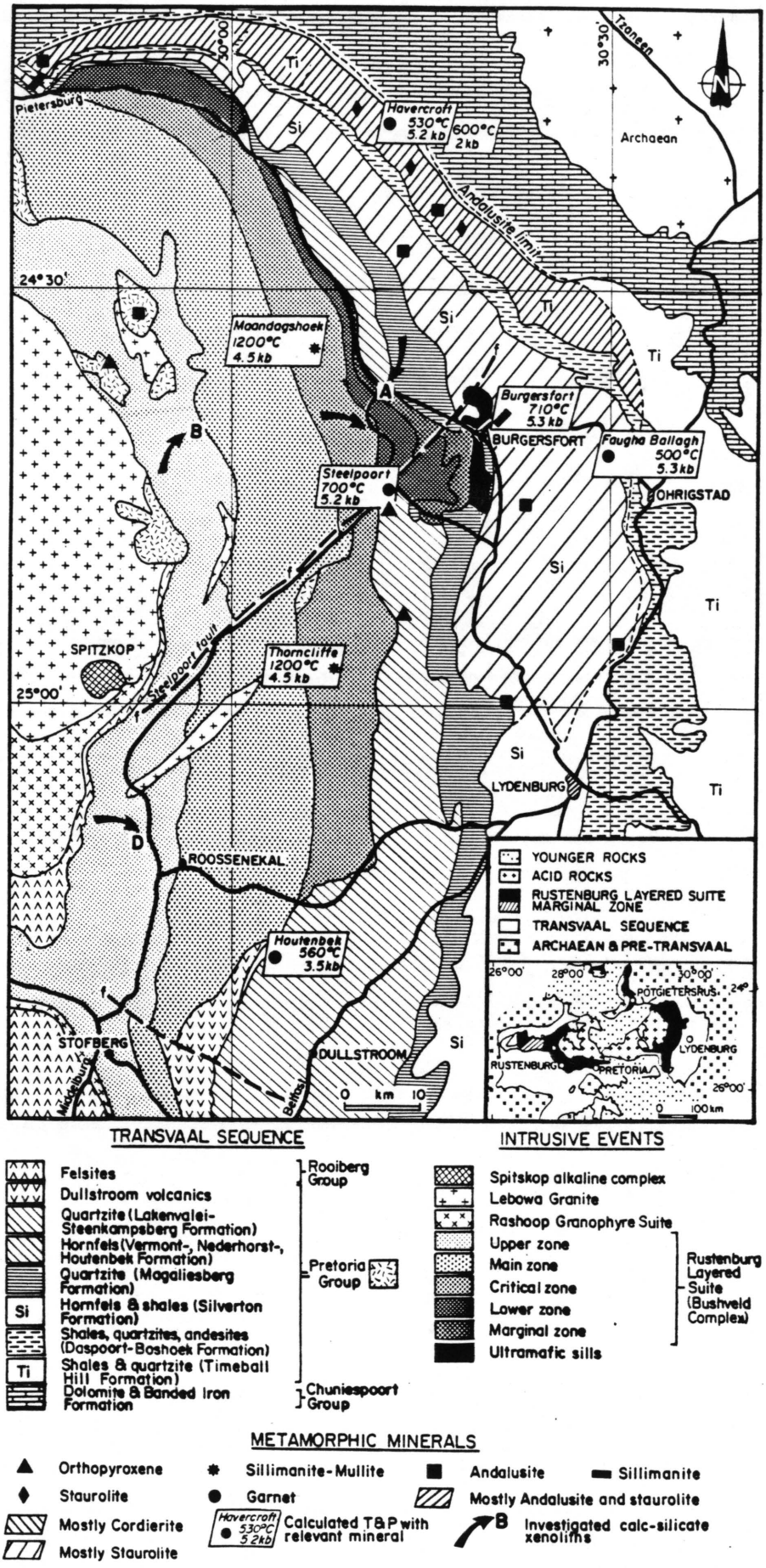

Fig. 1 Simplified map of the eastern Bushveld Complex and the metamorphic aureole (modified after Hulbert and Sharpe 1981a). The arrows indicate the localities of the xenoliths studied in this investigation.

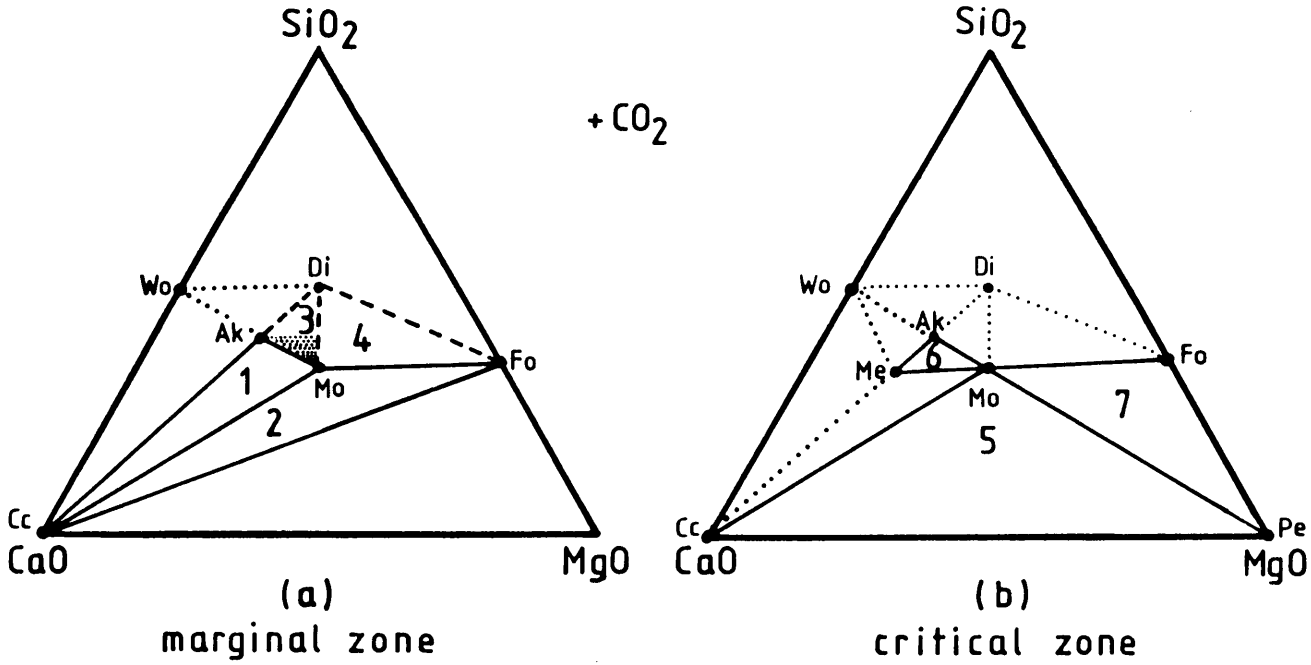

Fig. 2 Compositional triangles showing the important mineral phases and the dominant mineral assemblages occurring in the marginal zone xenoliths (a) and the critical zone xenolith (b). Assumed bulk composition of the marginal zone xenoliths are indicated by the shaded area in the centre of the triangle in Figure 2a. The numbers 1 - 6 refer to observed mineral assemblages. Solid and dashed lines connect minerals which occurred during prograde and retrograde metamorphism, respectively. Minerals assemblages connected by dotted lines were not observed. Ak: akermanite; Cc: calcite; Di: diopside; Fo: forsterite; Me: merwinite; Mo: monticellite; Pe: periclase; Wo: wollastonite

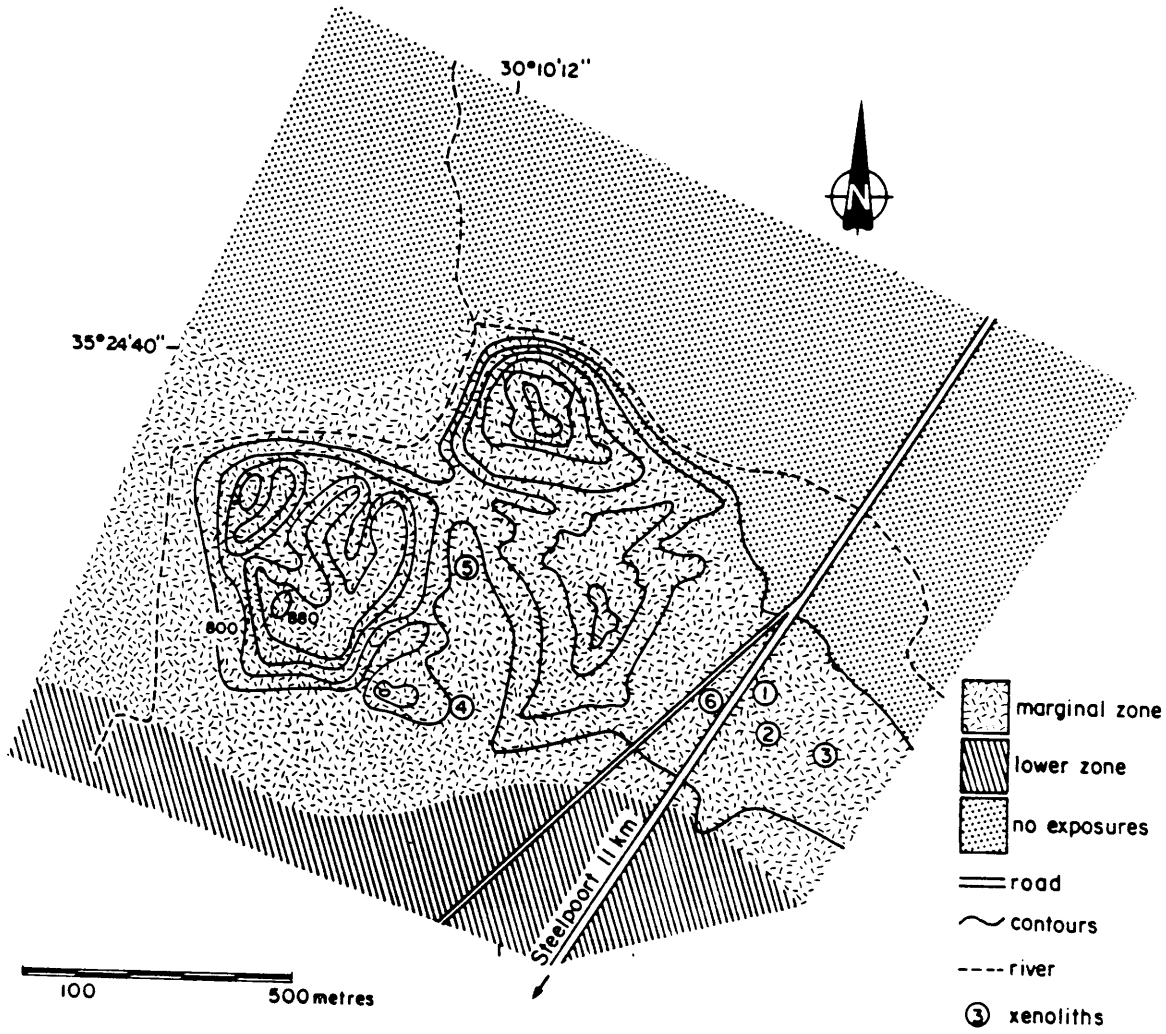

Fig. 3 Locality map of the described xenoliths in the marginal zone of the eastern Bushveld Complex on the farm Hendriksplaats (locality A in Figure 1).

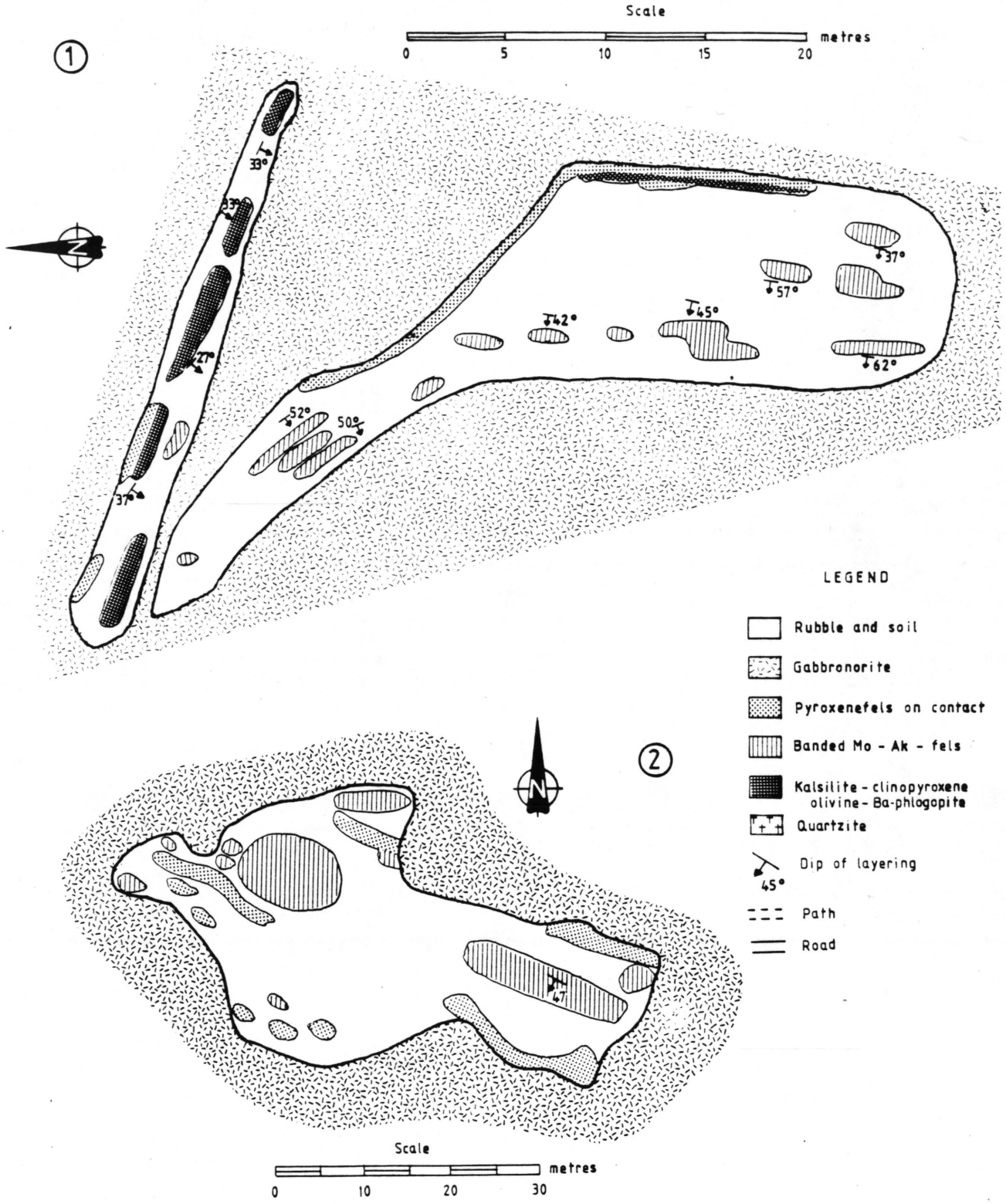

Fig. 4A Maps of the marginal zone xenoliths. The numbers of the xenoliths refer to the numbers in Figure 3.

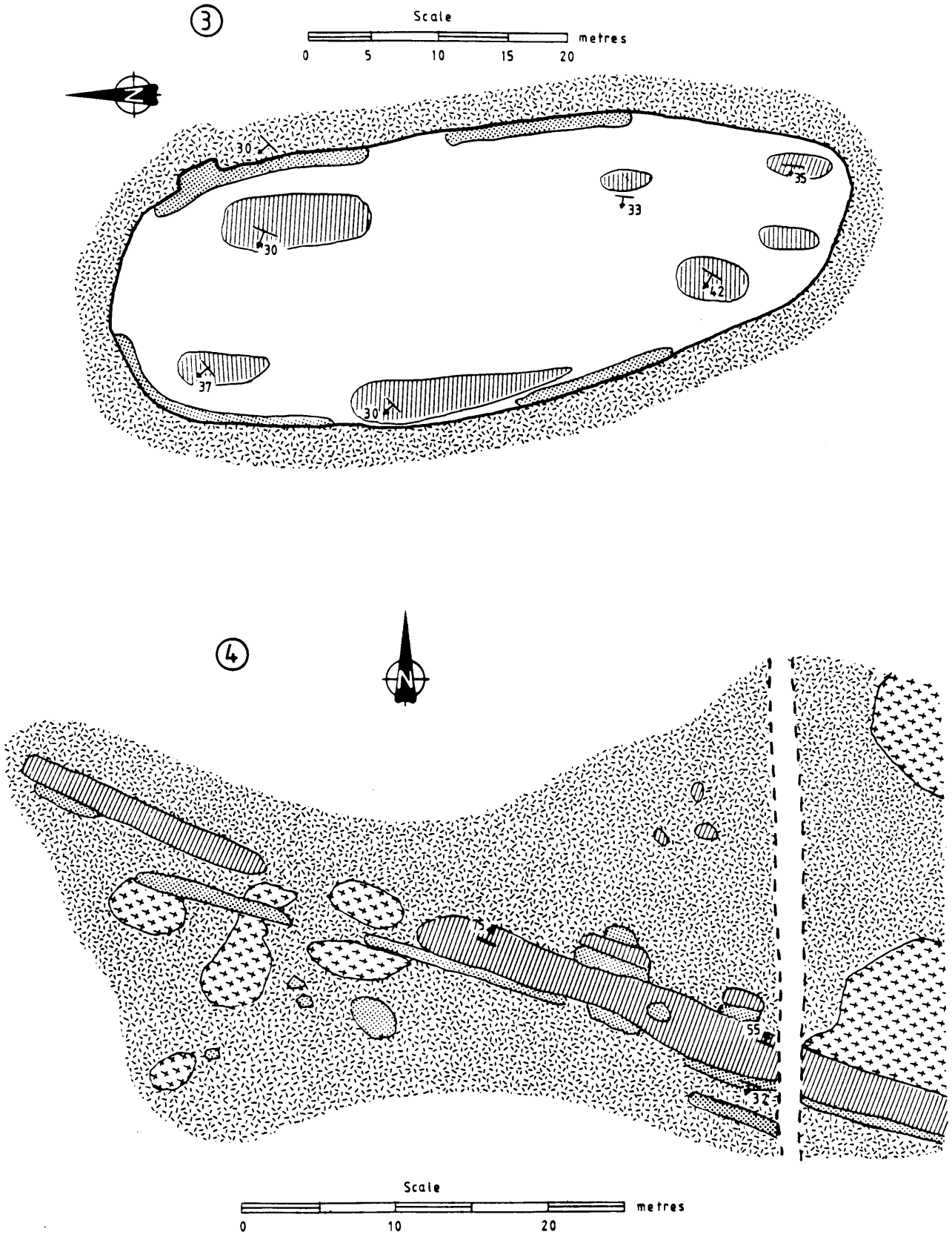

Fig. 4B Maps of the marginal zone xenoliths. The numbers of the xenoliths refer to the numbers in Figure 3. Legend as for Figure 4a.

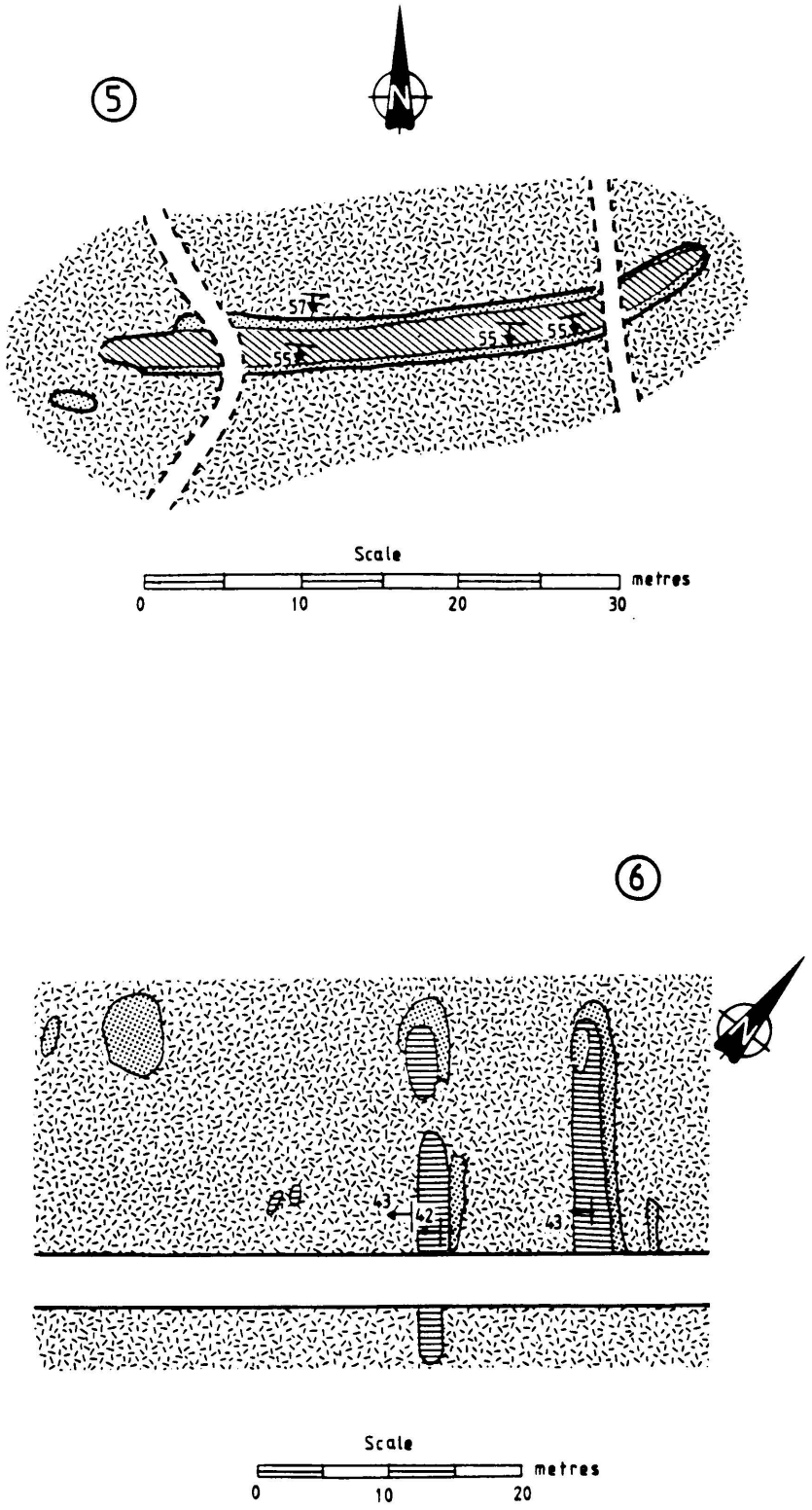

Fig. 4C Maps of the marginal zone xenoliths. The numbers of the xenoliths refer to the numbers in Figure 3. Legend as for Figure 4a.

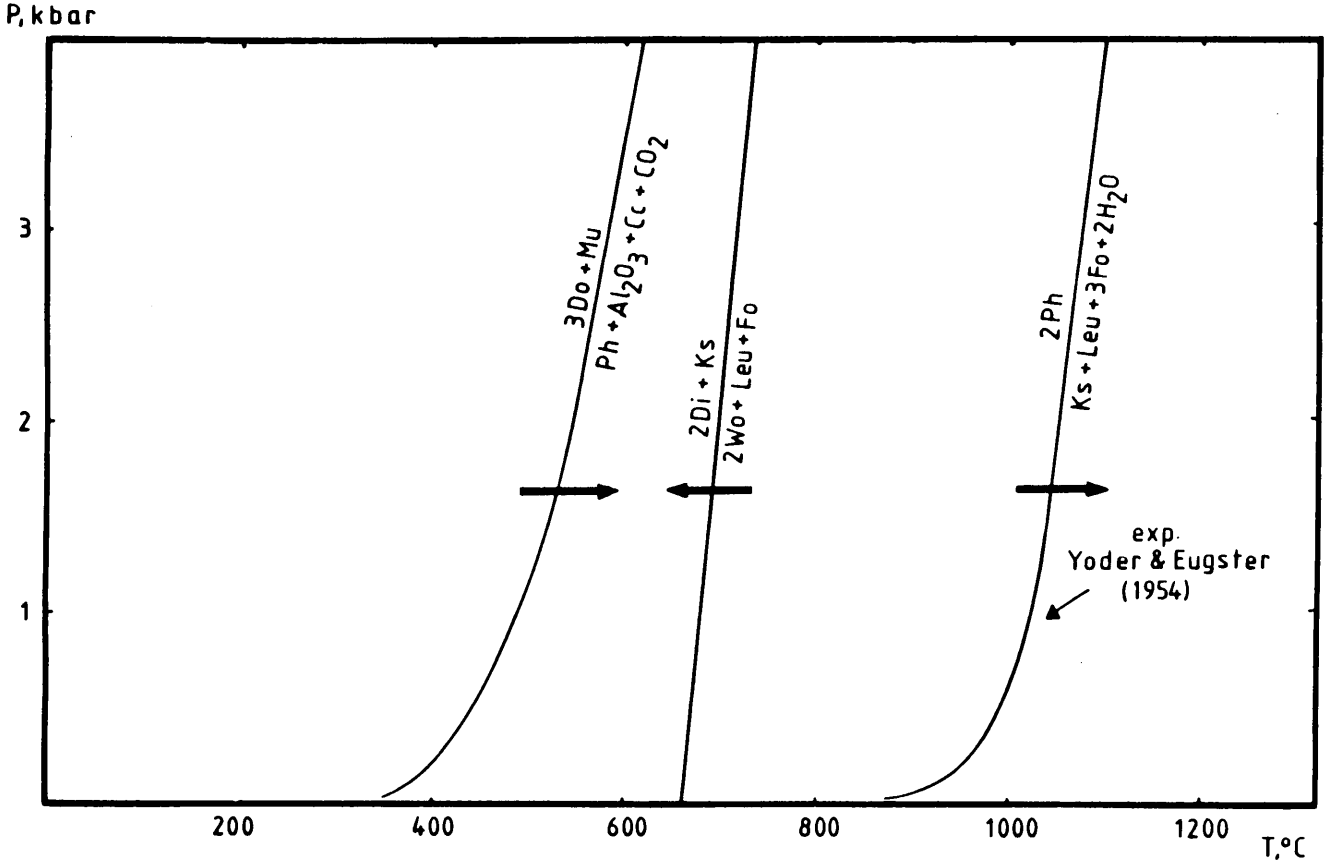

Fig. 5 P-T diagram showing the reactions that result in the mineral assemblage phlogopite-kalsilite-forsterite-diopside-wollastonite.

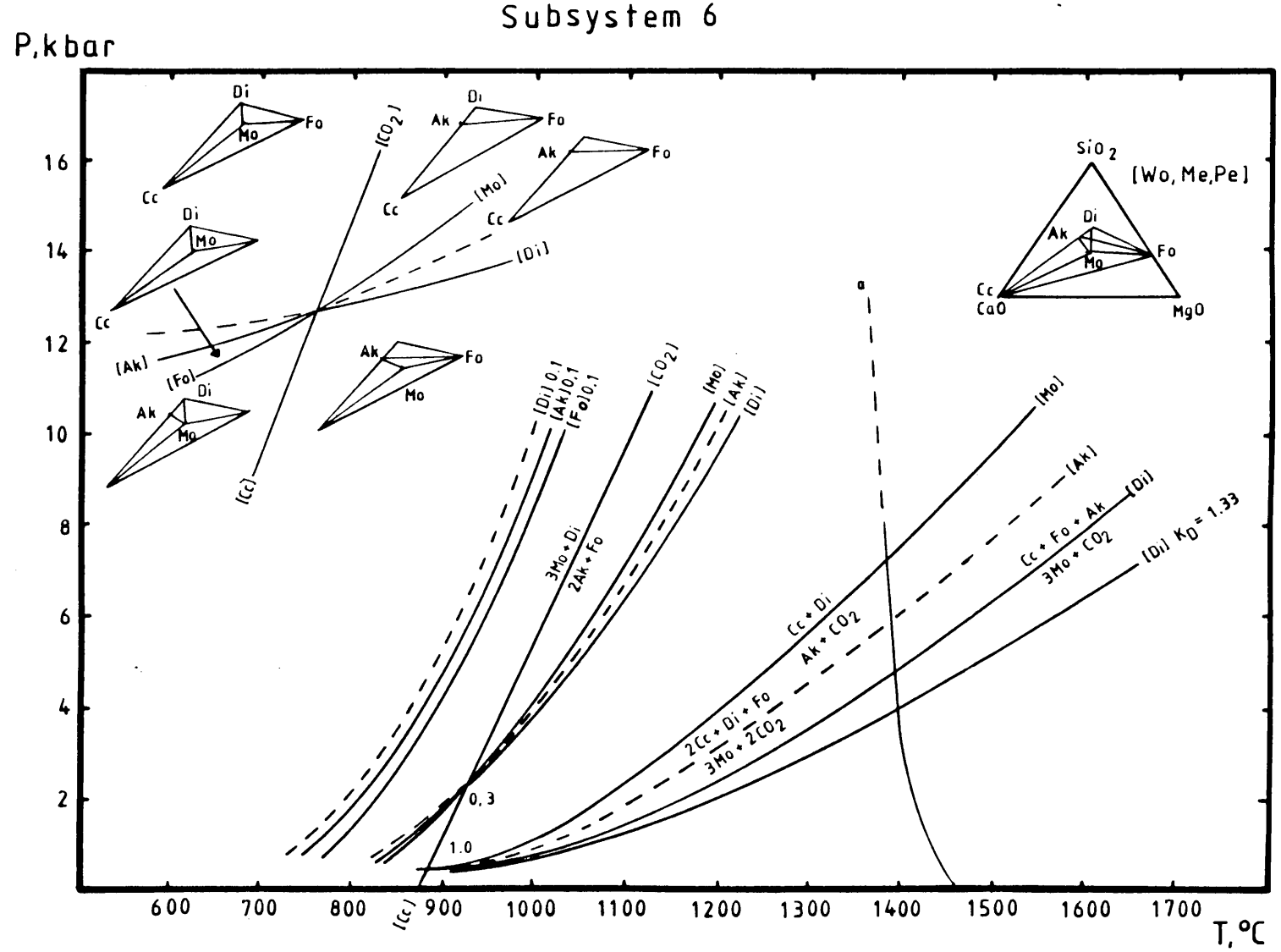

Fig. 6 P–T–X_{CO2} (X_{CO2} =0.1; 0.3; 1.0) diagram showing mineral reactions that led to the mineral assemblages found in the marginal zone xenoliths. Curve "a" indicates the begin of melting in the CO_2 saturated system (Yoder, 1968). The position of reaction [Di] is also given for K_D=1.33 which is due to solid solution between akermanite and gehlenite (Ak_{75}). Subsystem number refers to Table 5.

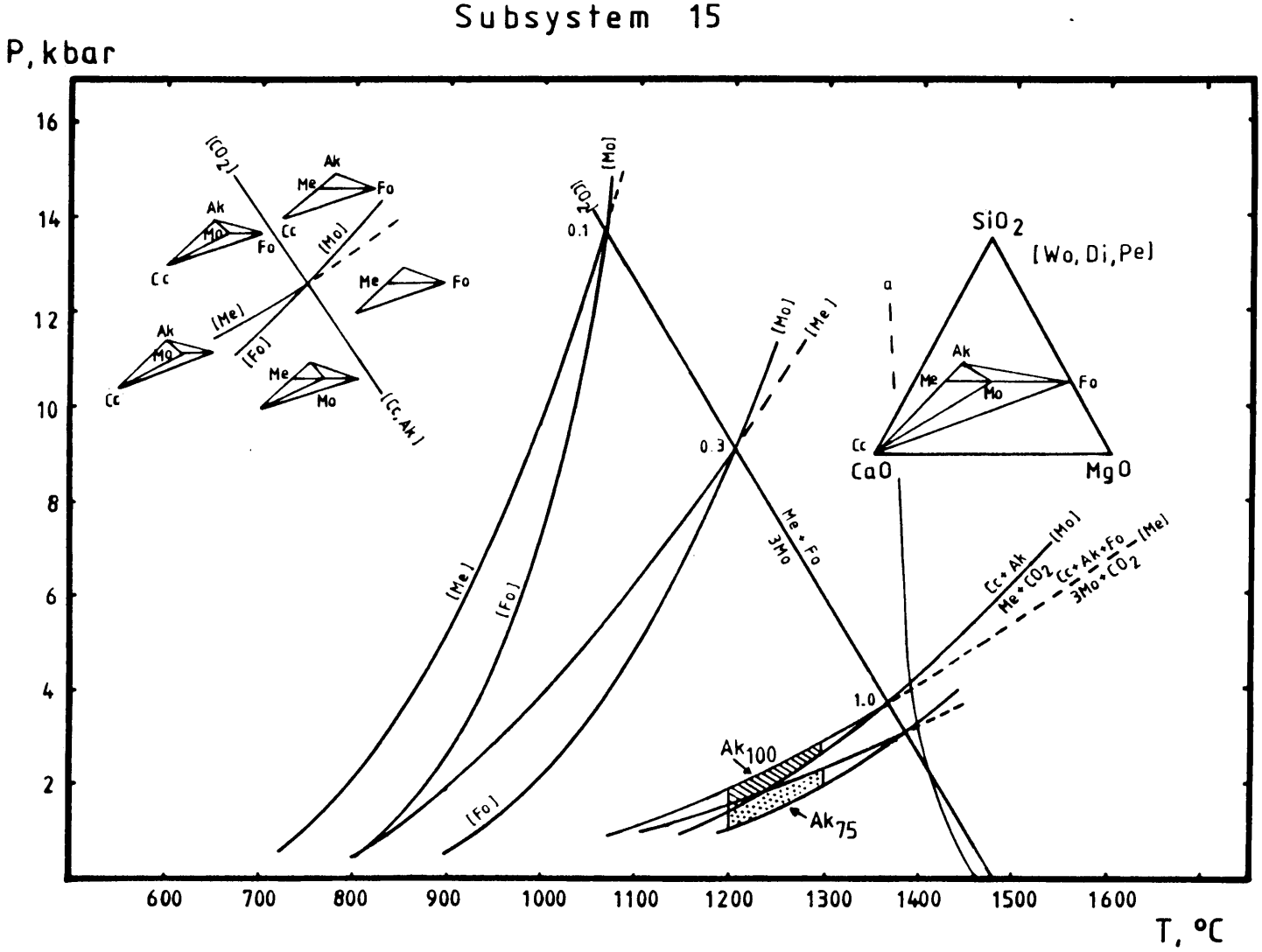

Fig. 7 P-T-X_{CO2} diagram (X_{CO2}=0.1; 0.3; 1.0) indicating the P-T conditions during the intrusion of the marginal zone magma (hatched field: Ak_{100}; dotted field: Ak_{75}). Subsystem number refers to Table 5.

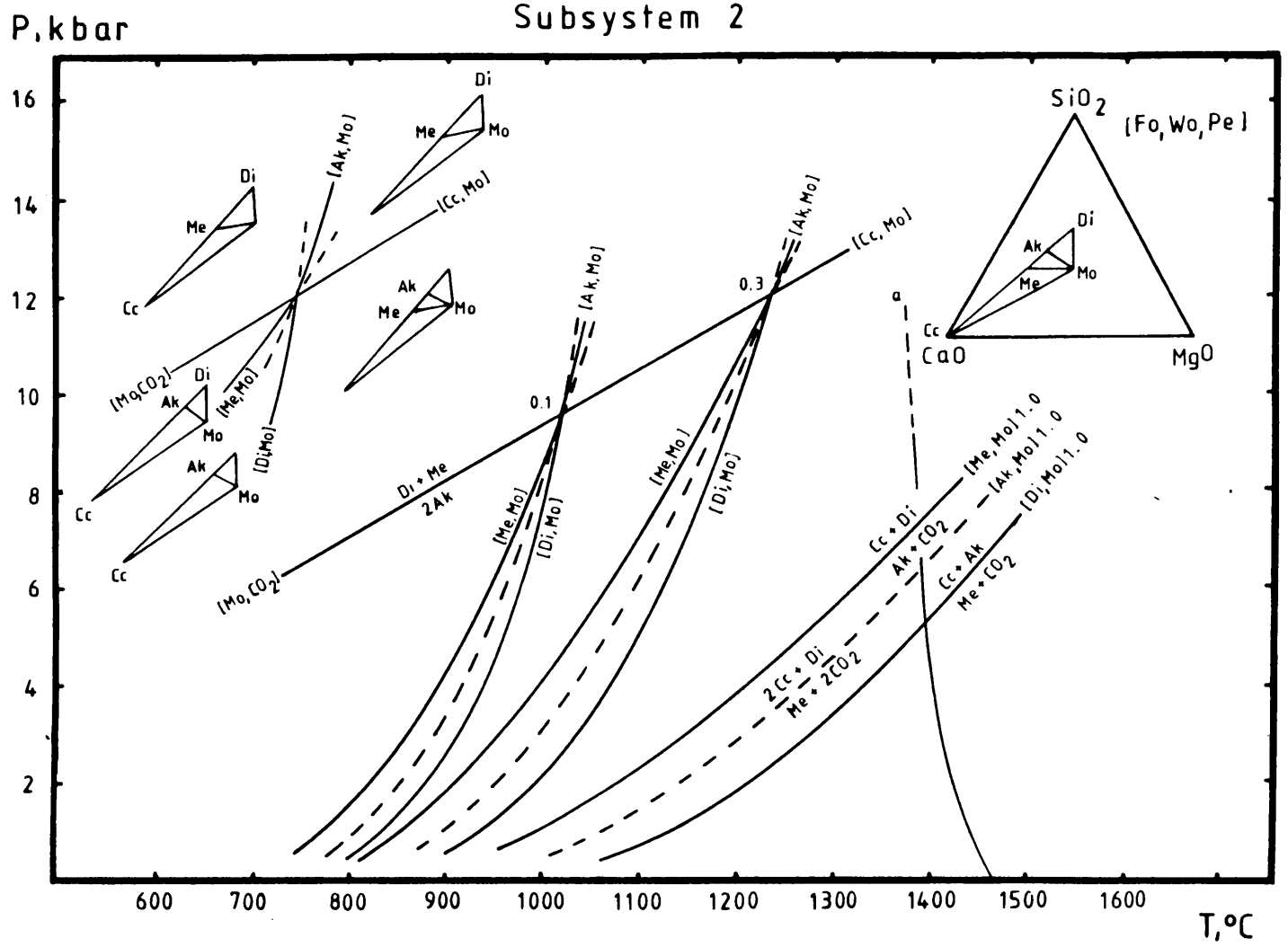

Fig. 8 P-T-X_{CO2} diagram (X_{CO2}=0.1; 0.3; 1.0) showing mineral reactions that led to the formation of akermanite and merwinite in the critical zone xenolith. Subsystem number refers to Table 5.

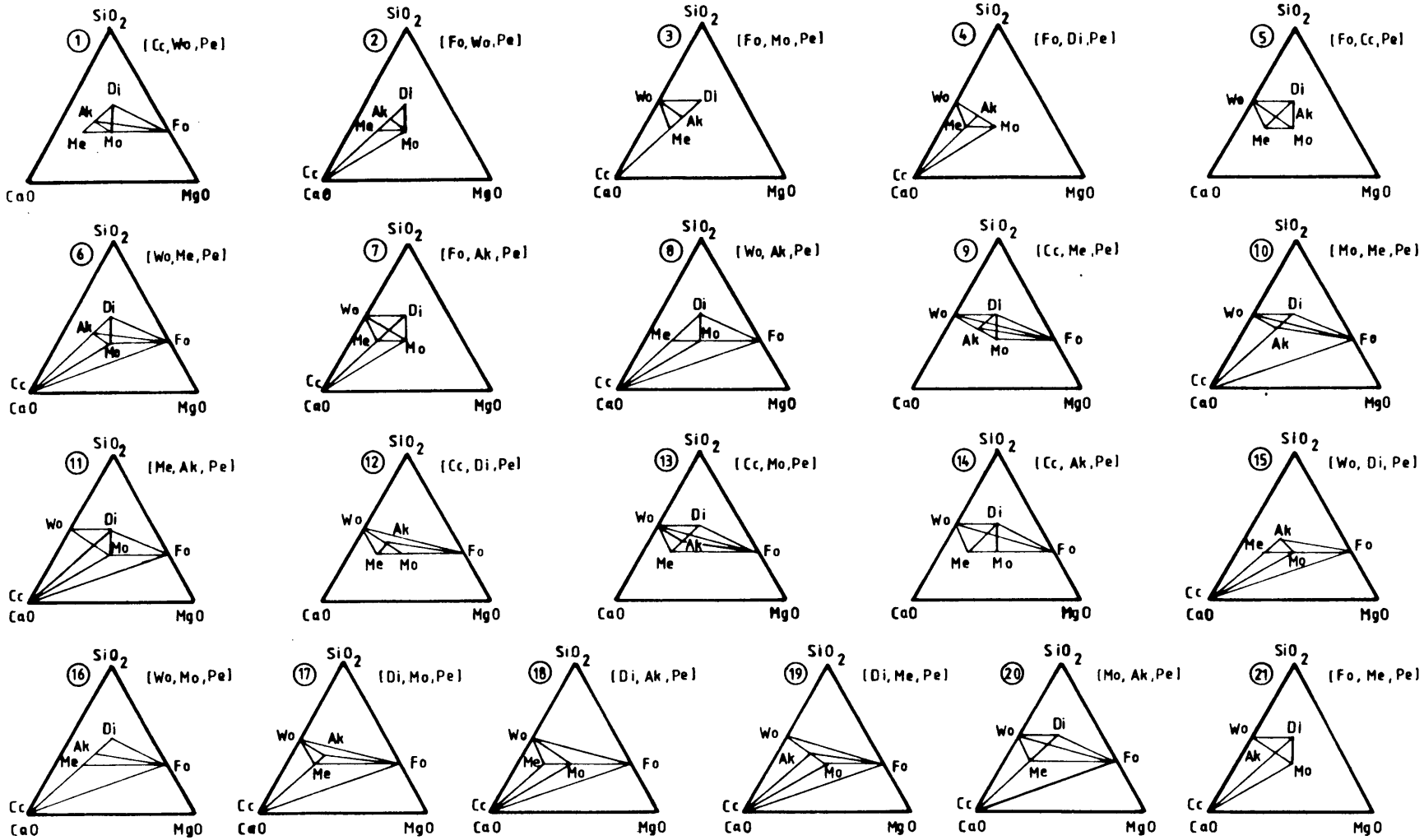

Fig. 9 Subsystems comprising all possible stable and metastable mineral assemblages in the system $CaO-MgO-SiO_2-CO_2$ with respect to the phases calcite, akermanite, monticellite, diopside, forsterite and merwinite. Reactions for each subsystem are listed in Table 5.

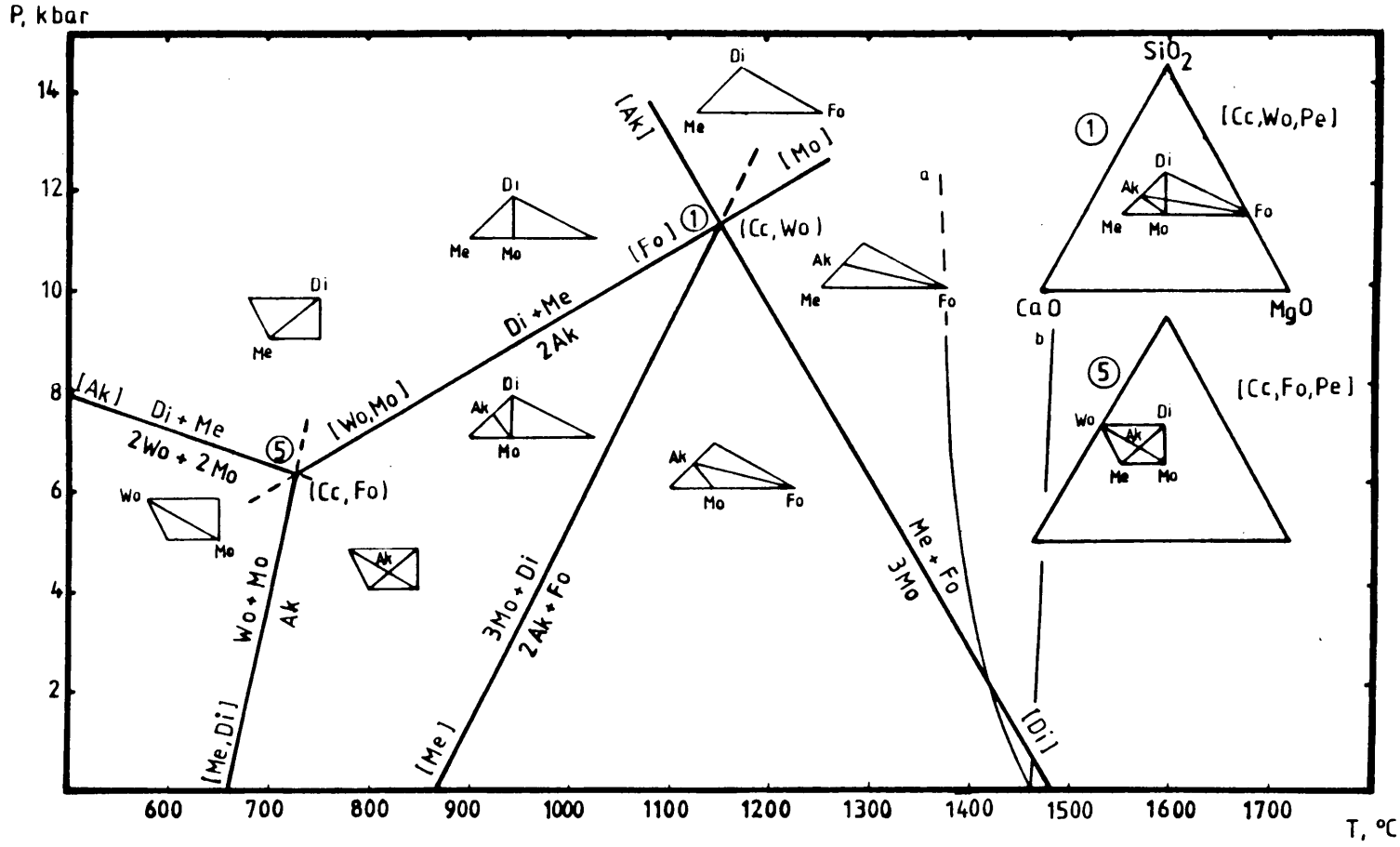

Fig. 10 Possible solid-solid reactions in the system CaO-MgO-SiO_2 comprising the phases akermanite, monticellite, diopside, forsterite, wollastonite and merwinite. Curve "a" and curve "b" indicate the begin of melting of akermanite in the presence of excess CO_2 (Yoder, 1973) and in a dry system (Kushiro, 1964), respectively. Subsystem numbers refer to Table 5.

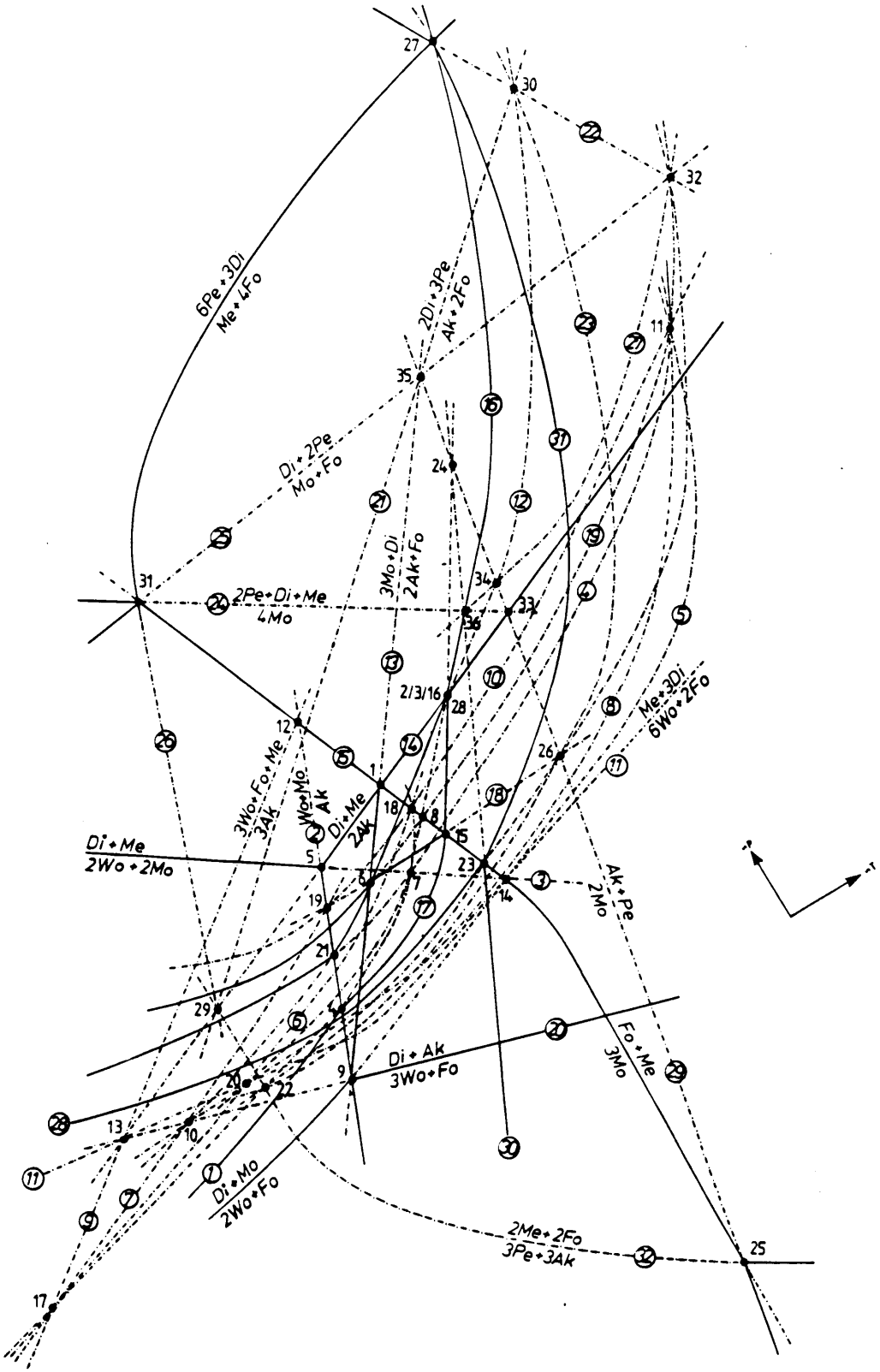

Fig. 11 Inferred petrogenetic grid for the system CaO-MgO-SiO_2-CO_2 including the phases akermanite, calcite, diopside, forsterite, merwinite, monticellite, wollastonite and periclase. The reaction numbers refer to Table 4, and the invariant points are designated by numbers that refer to Table 5.

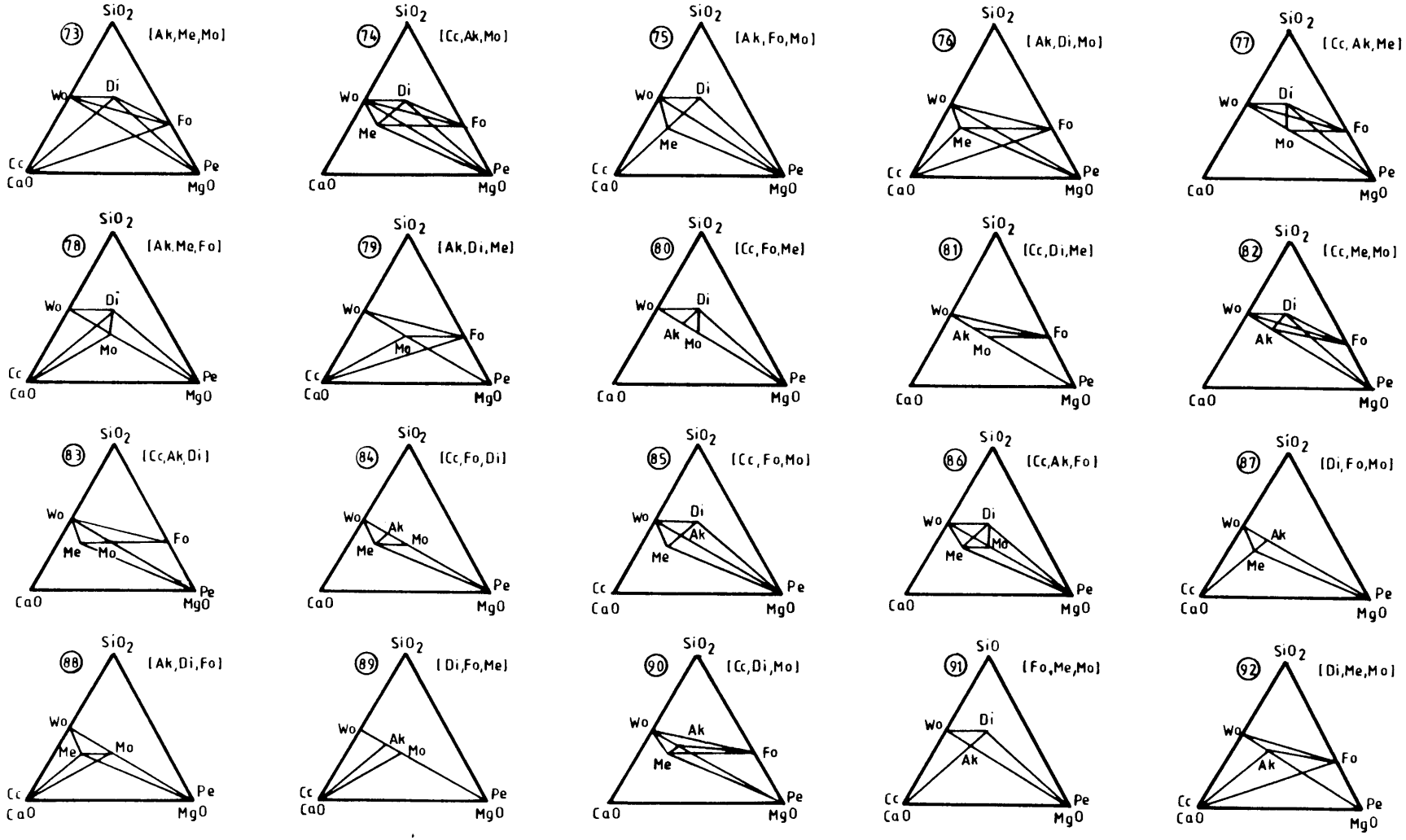

Fig. 12 Possible (metastable) subsystems (73-92) in which periclase and wollastonite occur together. The subsystems comprise the components CaO-MgO-SiO_2-CO_2 and the mineral phases calcite, akermanite, monticellite, diopside, forsterite, merwinite, wollastonite and periclase. Reactions for each subsystem are listed in Table 5.

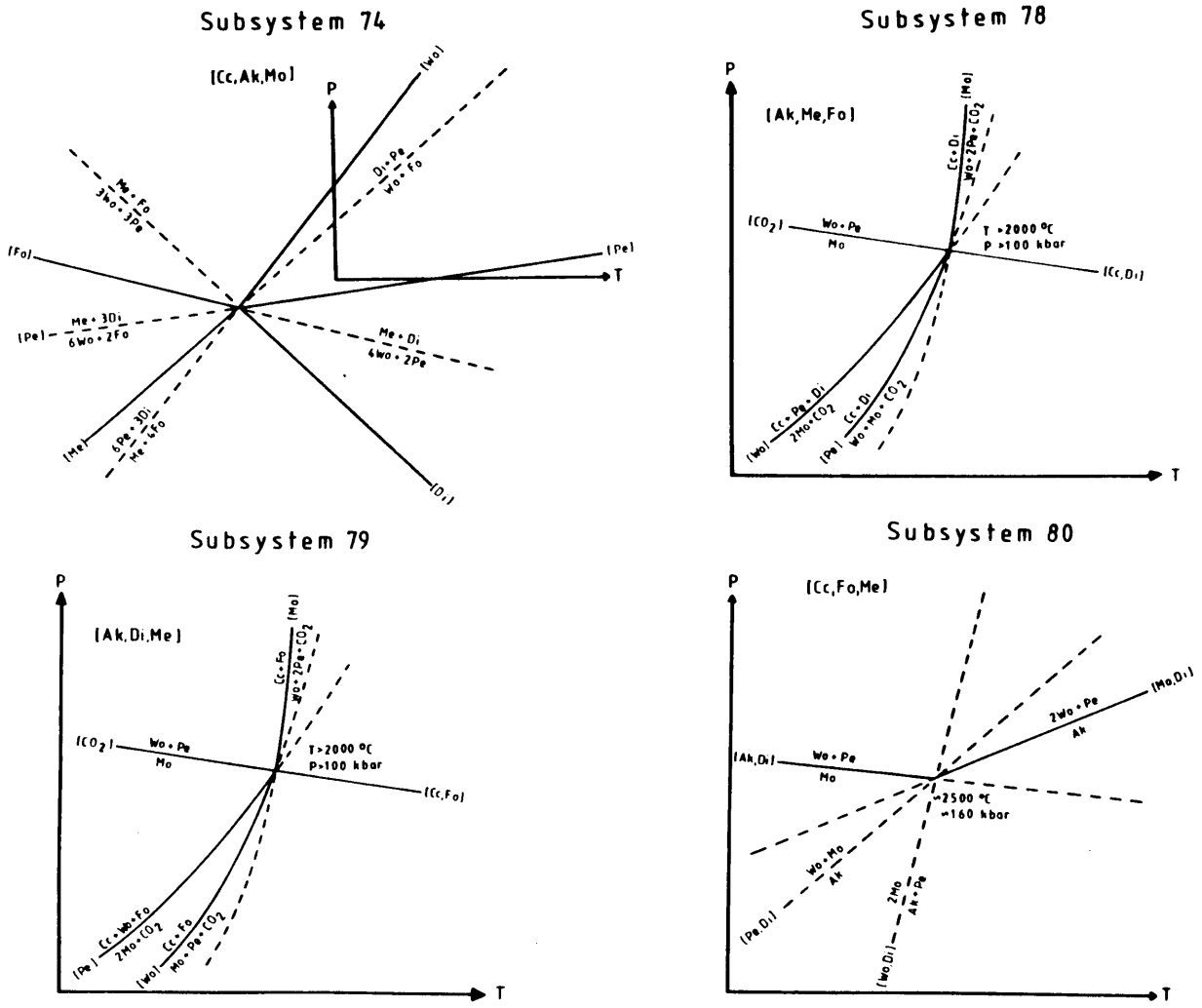

Fig. 13A Four of the eight (metastable) subsystems involving periclase and wollastonite. None of the reactions involving periclase and wollastonite simultaneously are stable over the complete possible P-T range.

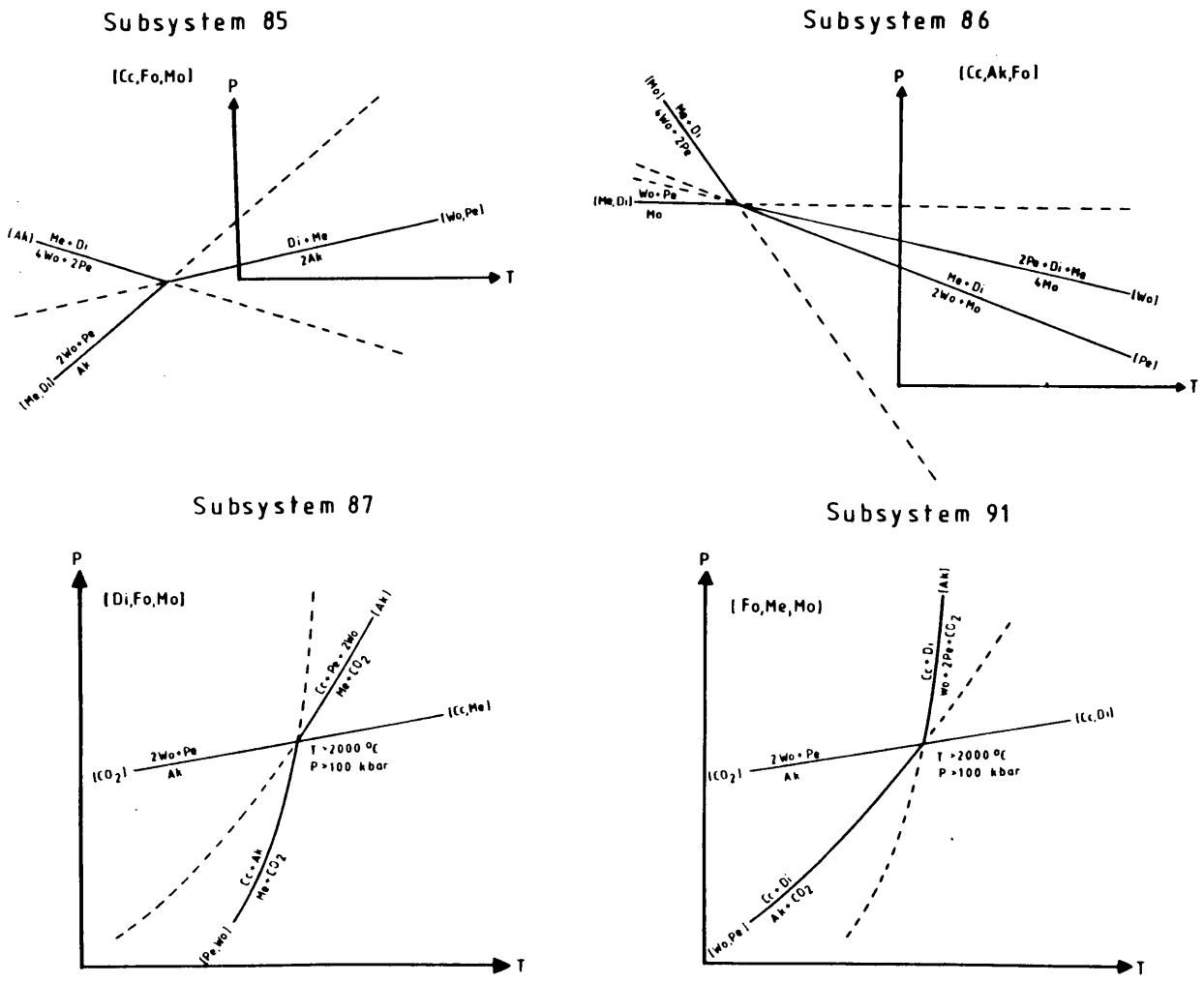

Fig. 13B The other four (metastable) subsystems involving periclase and wollastonite. None of the reactions involving periclase and wollastonite simultaneously are stable over the complete possible P-T range.

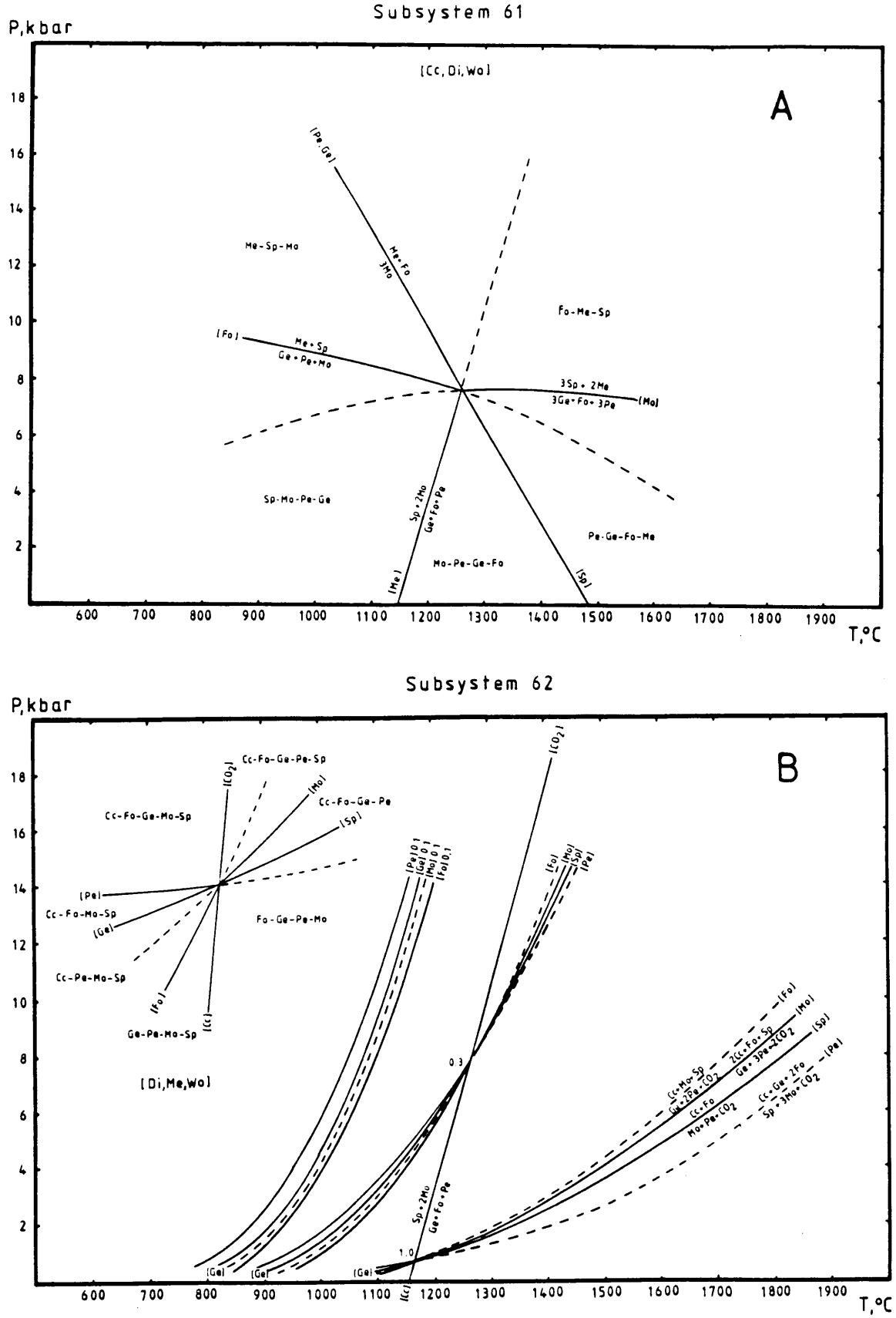

Fig. 14A+B The two inferred stable subsystems in the system CaO-MgO-SiO_2-Al_2O_3 that account for the very high temperature formation of spinel in calc-silicates. The reacting phases are calcite, forsterite, gehlenite, monticellite, merwinite, periclase, and spinel. Subsystem number refers to Table 5.

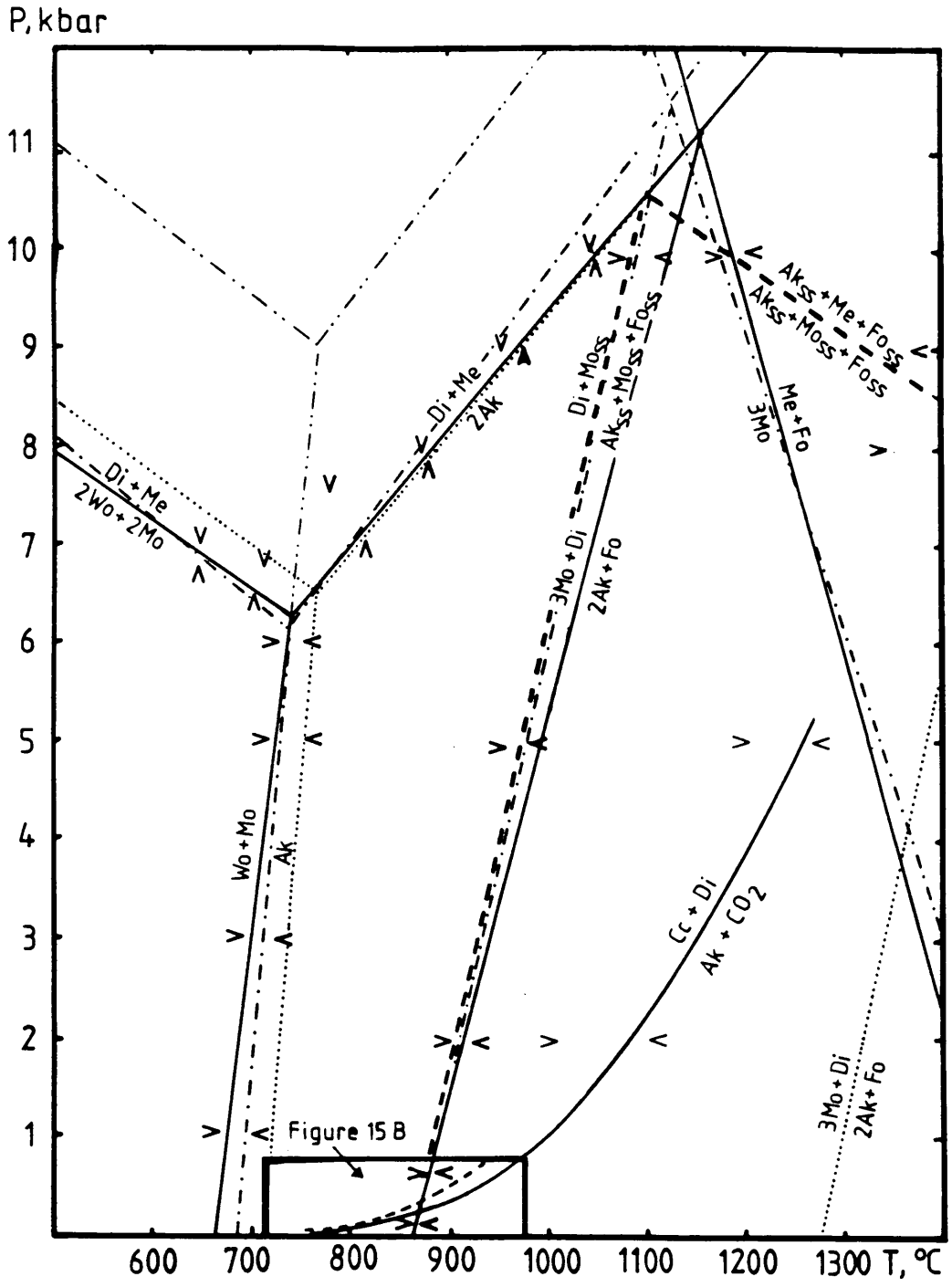

Fig. 15A

V
Λ — experimental brackets involving 'pure' minerals, or solid solutions (Yoder 1968, 1973)

calculated after:

..... Helgeson et al. (1978)

—·—·— Sharp et al. (1986) and Hemingway et al. (1986)

—··—··— Brousse et al. (1984)

——— Brousse et al. (1984) with corrected H°_{298} for merwinite

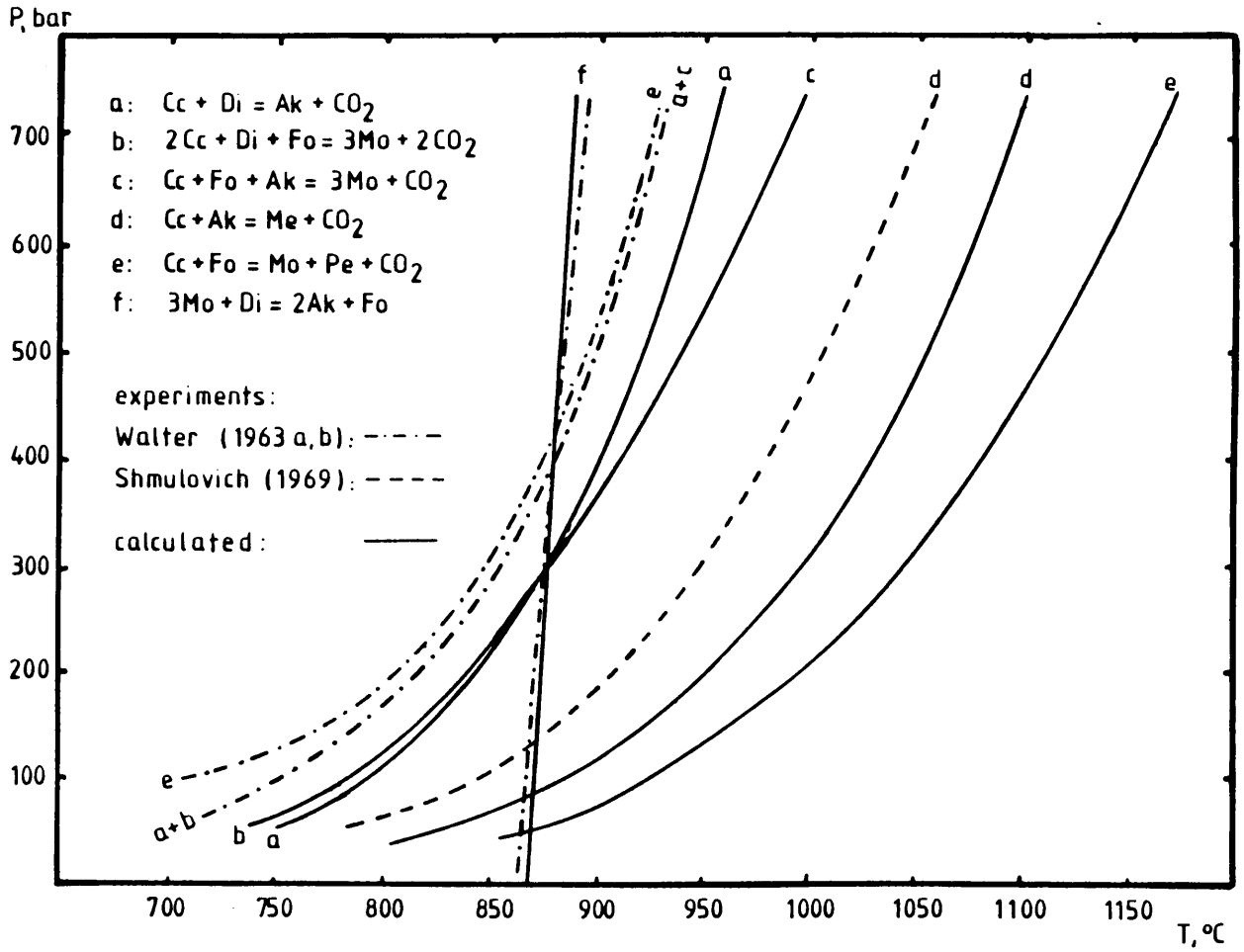

Fig. 15B

Fig. 15A+B Comparison of experimental with calculated results of reactions involving akermanite, calcite, diopside, forsterite, merwinite, monticellite, periclase and wollastonite and carbon dioxide.

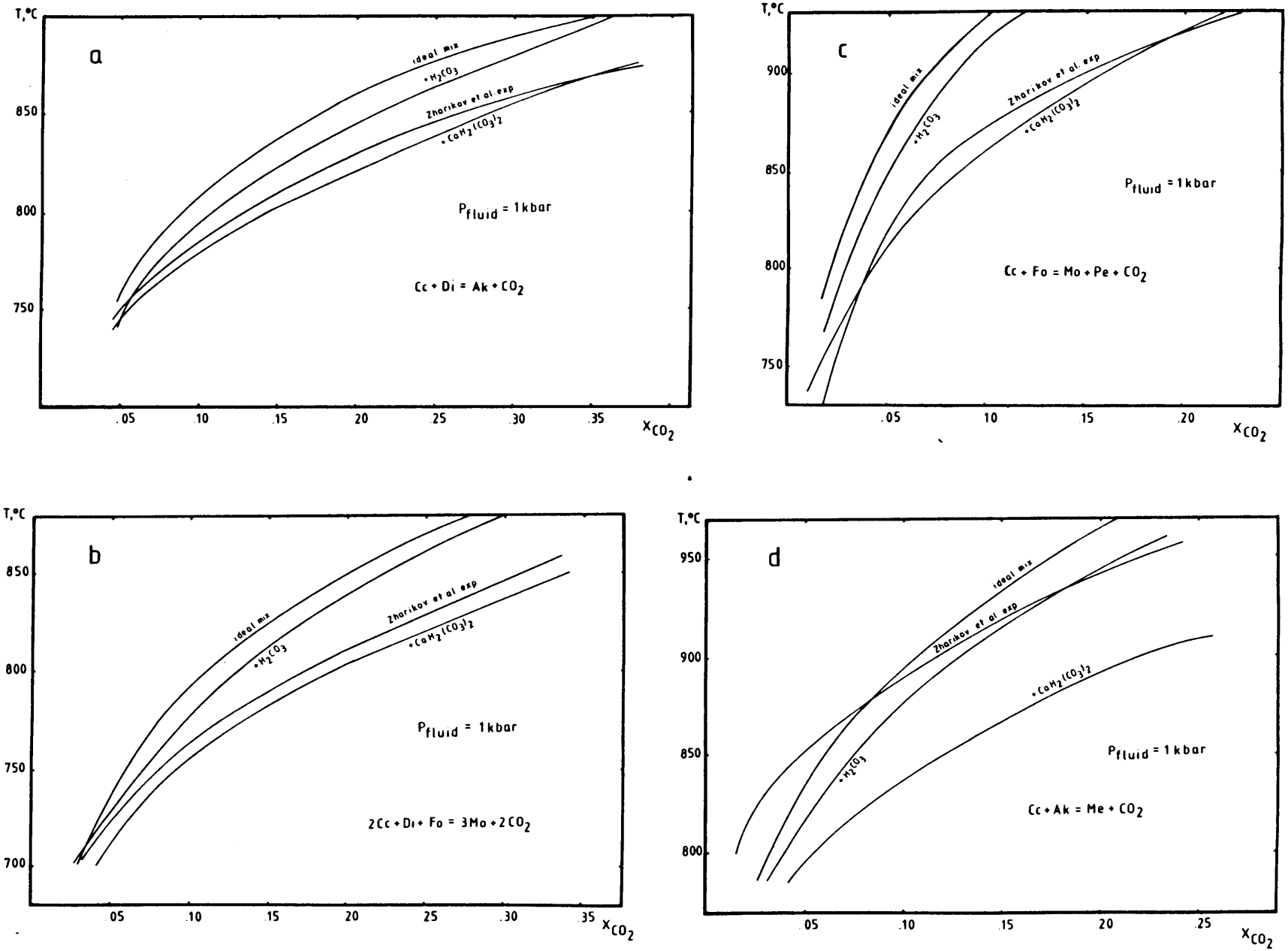

Fig. 16A-D Comparison of experimental results (Zharikov et al. 1977) with recalculations of the reaction equilibria at different X_{CO2}. The calculations were carried out by assuming either ideal mixing or non-ideal mixing that involves H_2CO_3 and $CaH_2(CO_3)$.

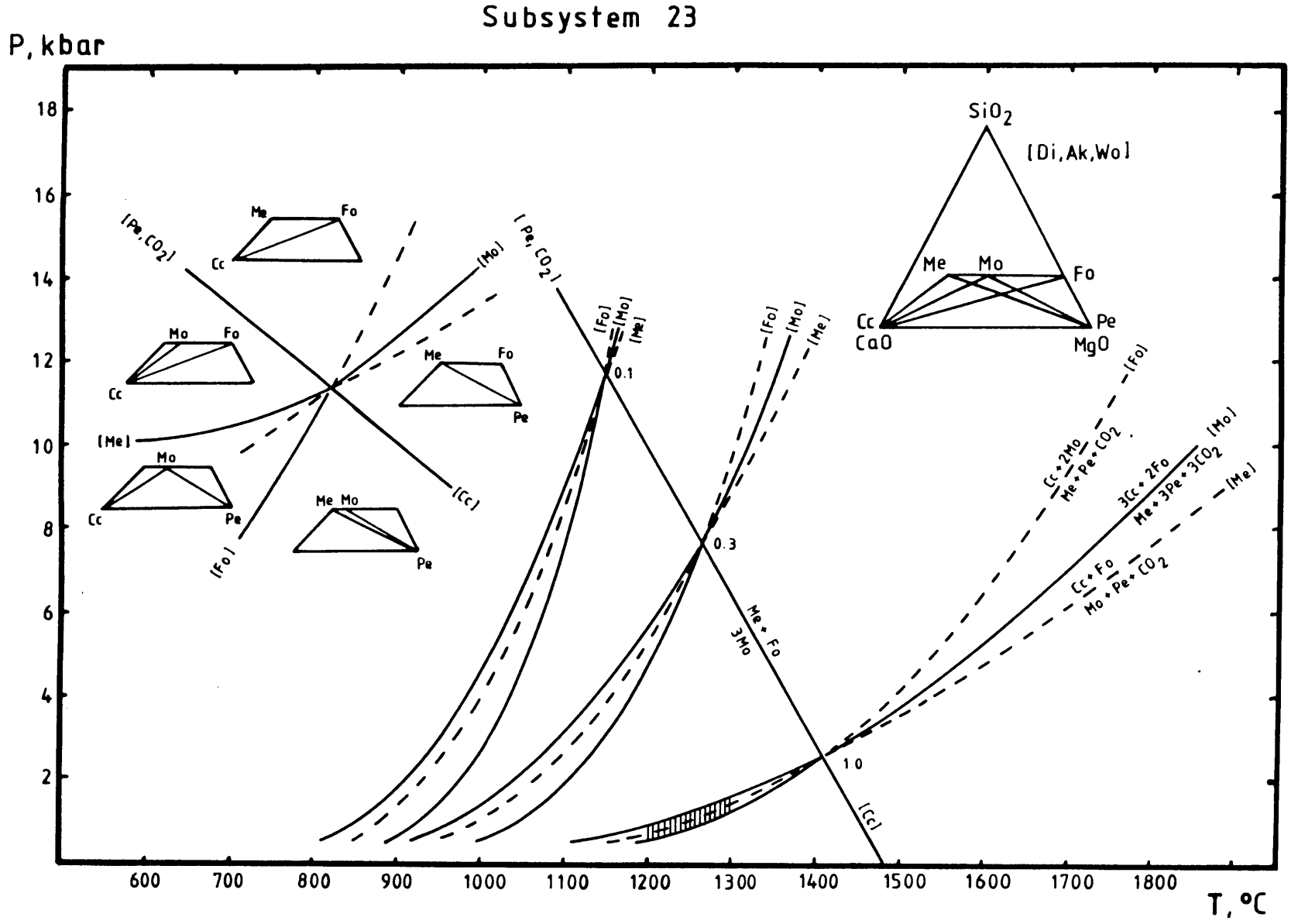

Fig. 17 P-T-X_{CO2} diagram outlining the P-T conditions during the emplacement of the critical zone magma intrusion (hatched field). Subsystem number refers to Table 5.

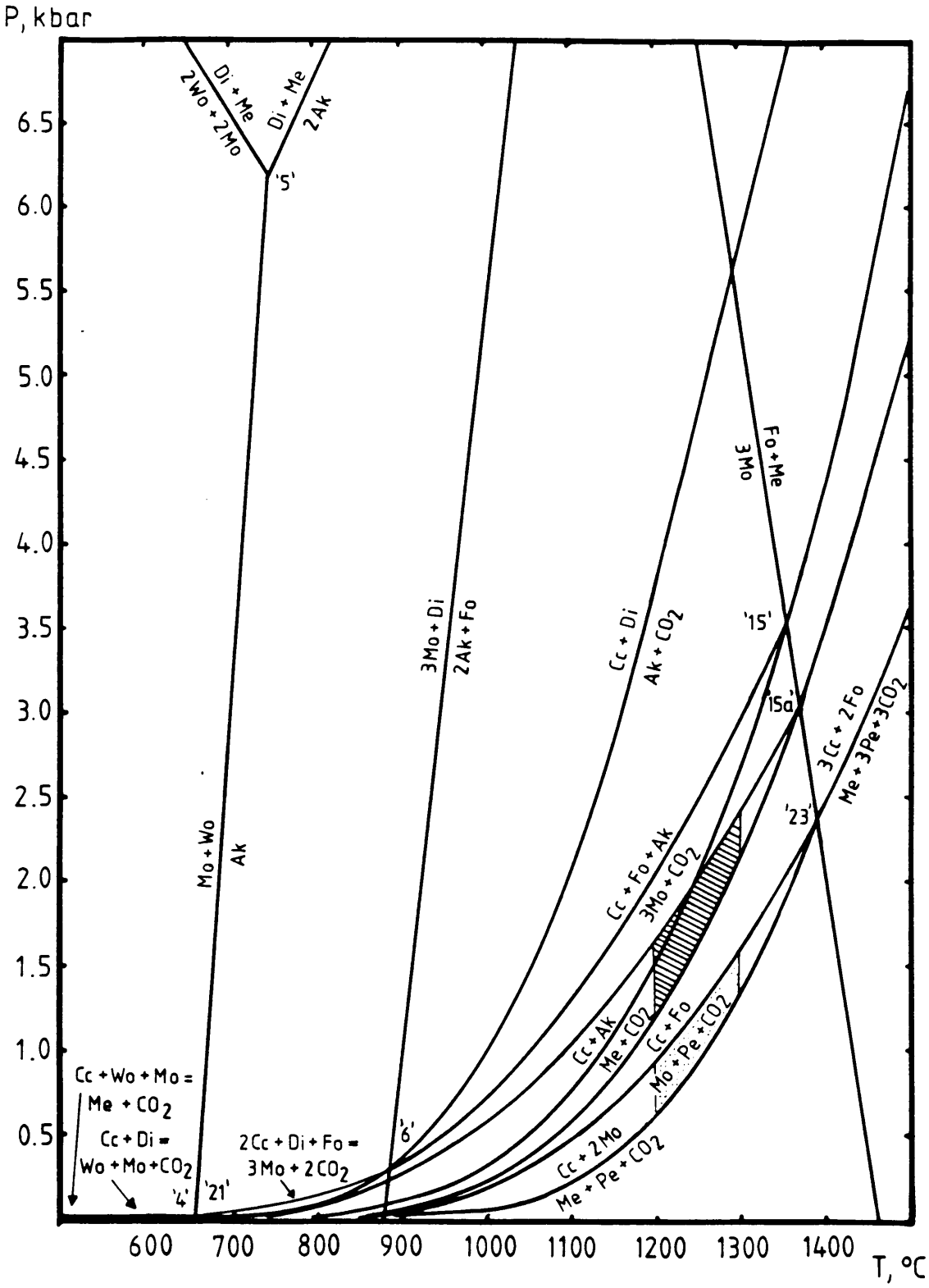

Fig. 18 Summary of decarbonation reactions that serve to give P-T constraints on the formation of critical mineral assemblages in the marginal and critical zone xenoliths ($P=P_{CO2}$). The numbers refer to the invariant points (subsystems) in Figure 11. Invariant point 15 and 15a are calculated for different ak_{ss} (15: ak_{100}; 15a: ak_{75}). The dashed and the dotted areas indicate the conditions of the emplacement af the marginal and critical zone, respectively.

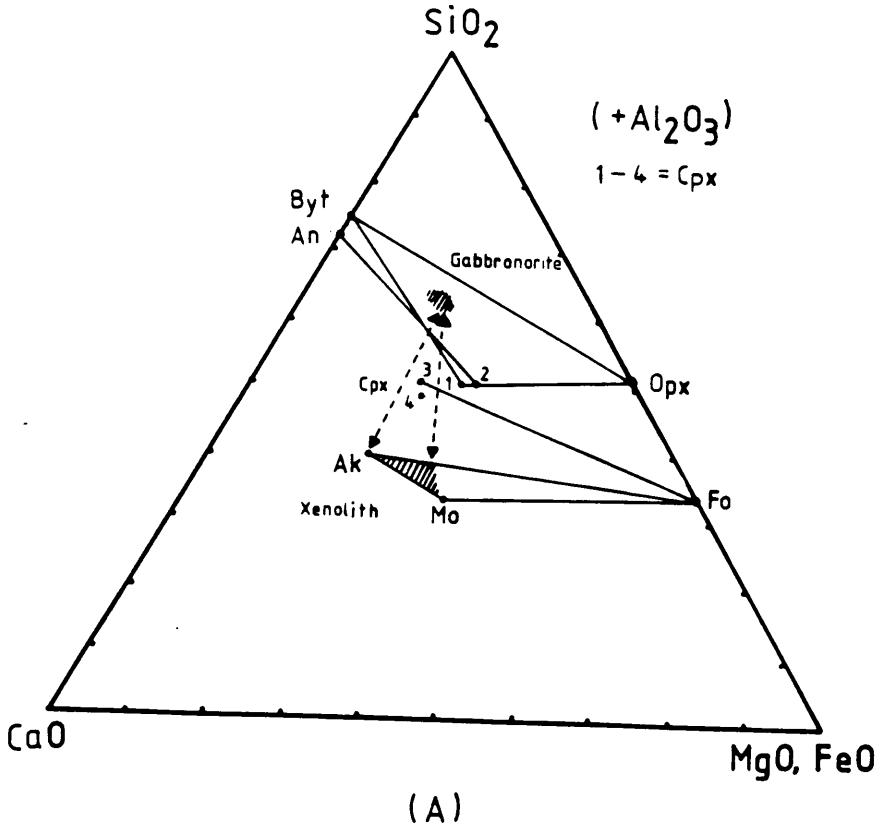

(A)

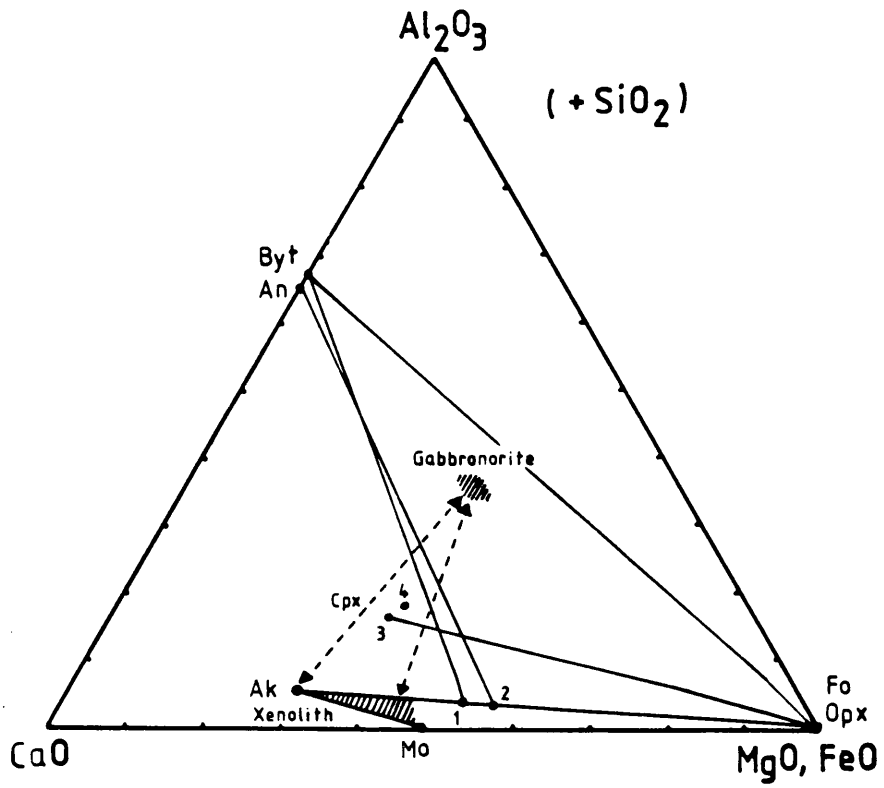

(B)

Fig. 19A+B Two compositional triangles displaying the chemical potential gradient between the gabbronorite (upper hatched field in both diagrams) and the marginal zone xenoliths (lower hatched field in both diagrams). The numbers in the centre of Fig. 19A+B refer to different clinopyroxenes (1: cpx in gabbronorite; 2, 3: metasomatic cpx; 4: cpx in xenolith).

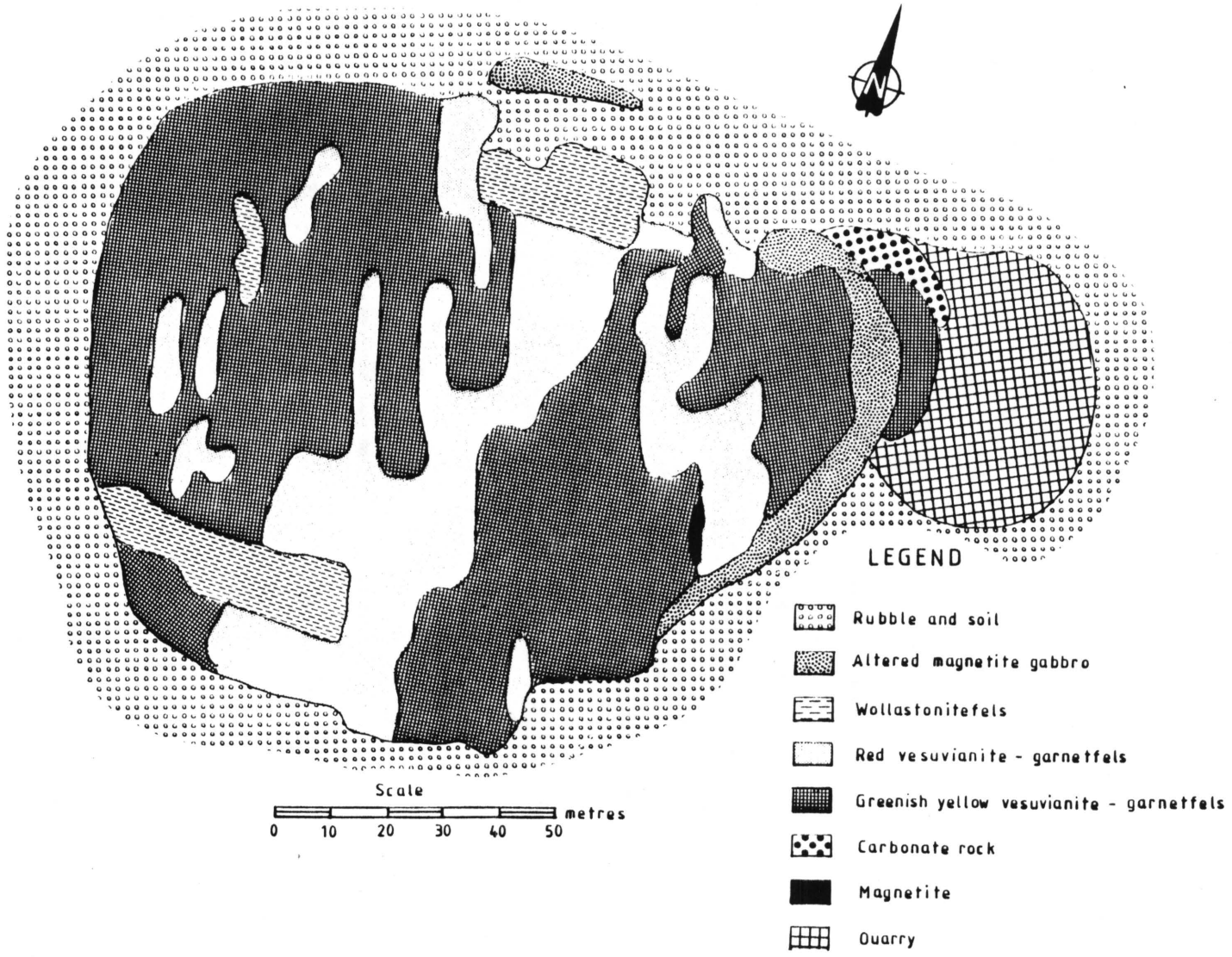

Fig. 20 Map of xenolith B in the upper zone.

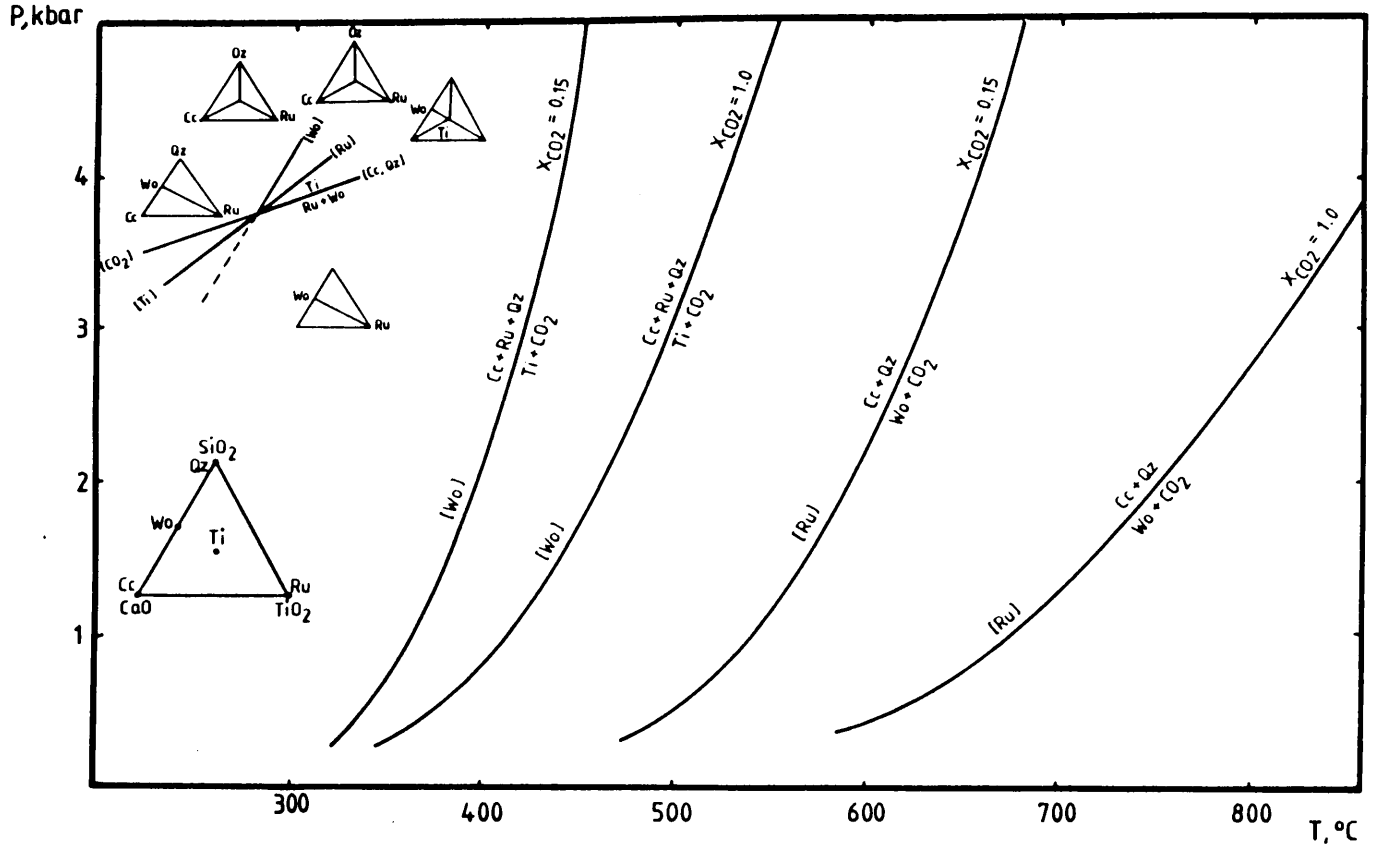

Fig. 21 P-T-X_{CO2} diagram showing reactions at different X_{CO2} that led to the mineral paragenesis calcite-titanite-wollastonite.

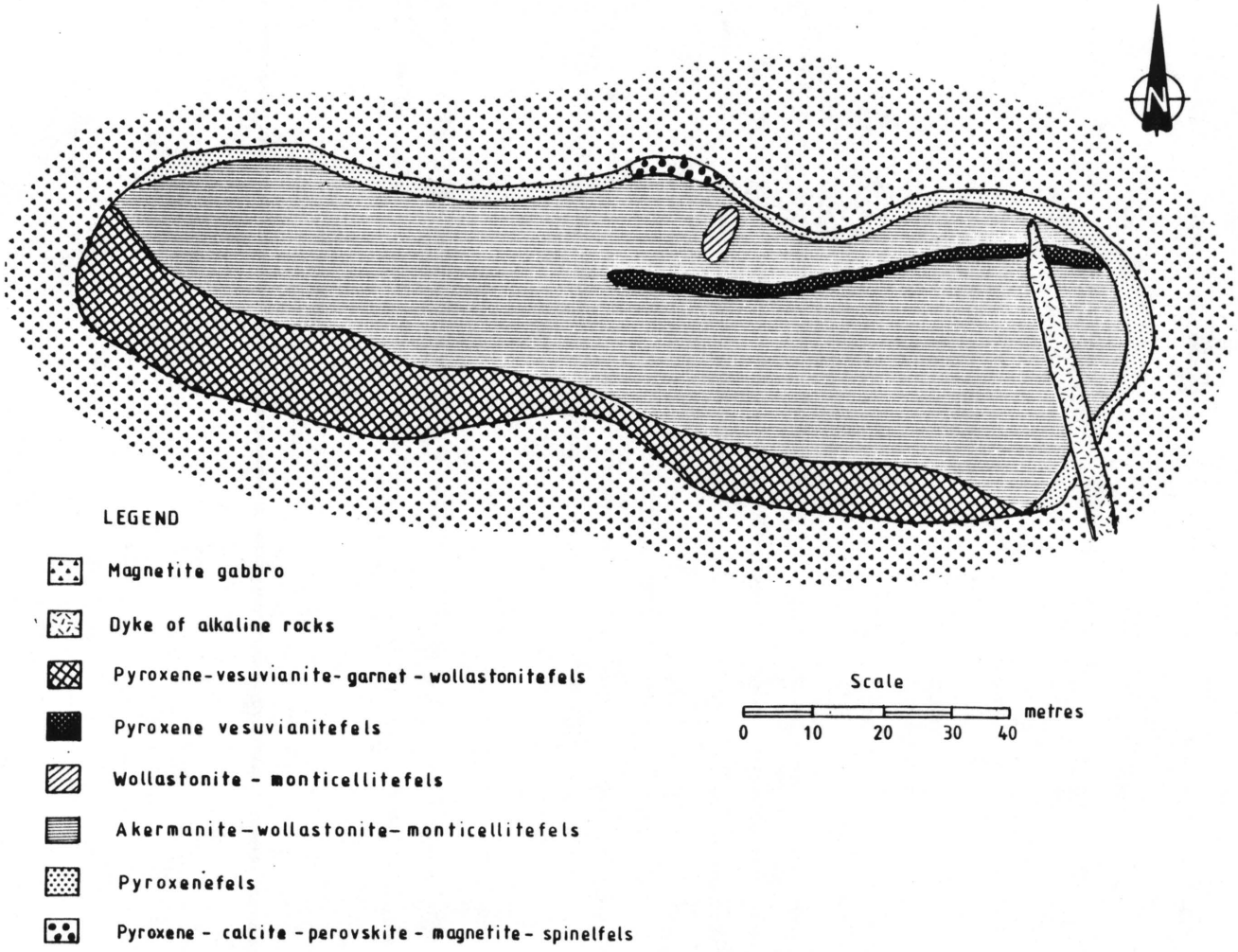

Fig. 22 Map of xenolith D in the upper zone.

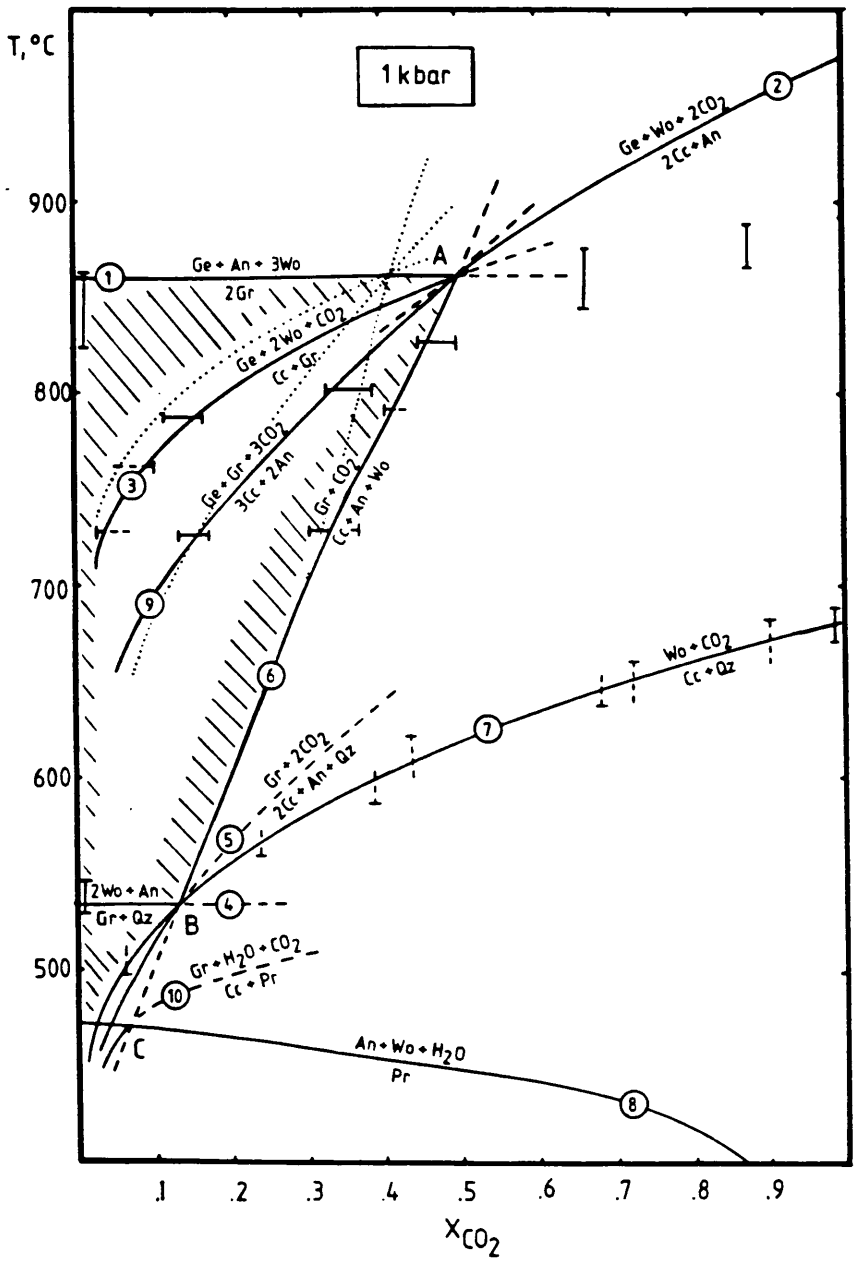

Fig. 23 $T\text{-}X_{CO2}$ positions of reactions used for the discussion on the stability of grossular, hydrogrossular and prehnite. The semi-hatched filed outlines the stability field of grossular. The reaction curves were calculated by using the thermodynamic data in Table 2 assuming non-ideal mixing of H_2O and CO_2 (solid lines) and ideal mixing (dotted lines). The solid bars indicate the experimentally determined brackets of reversed reactions, the dashed bars result from reactions that have not been reversed; reaction 1: Boettcher (1970) and Huckenholz et al. (1975); reaction 2, 3, 9: Hoschek (1974); reaction 4: Hoschek (1974) and Huckenholz et al. (1975); reaction 6: Hoschek (1974) and Zharikov et al. (1977); reaction 7: Greenwood (1967).

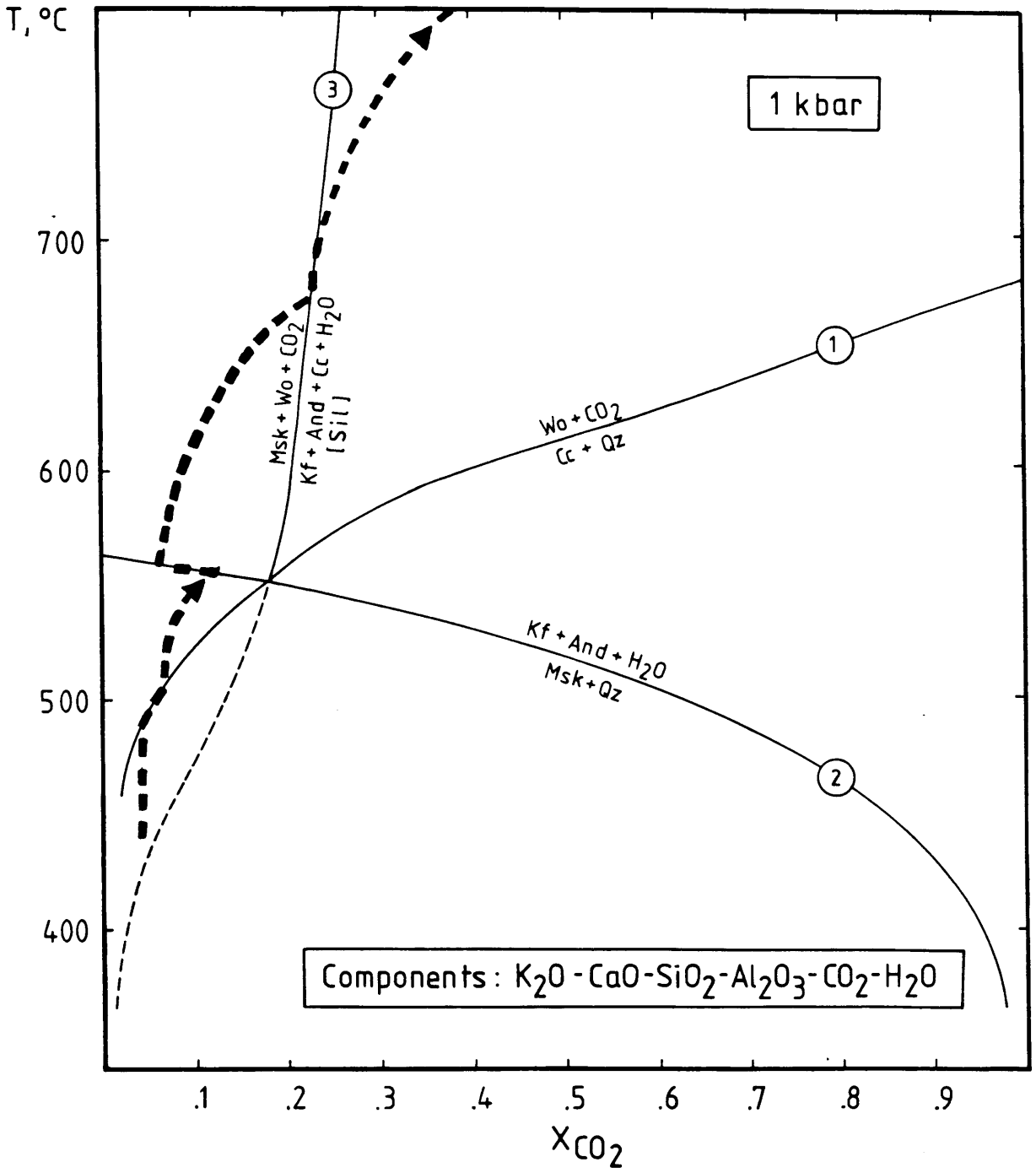

Fig. 24 Reactions explaining the mineral assemblage K-feldspar-wollastonite-sericite (-apatite). The arrow indicates the assumed reaction path reflecting a combination of internal and external buffering during prograde metamorphism. The dashed part of reaction 3 is metastable.

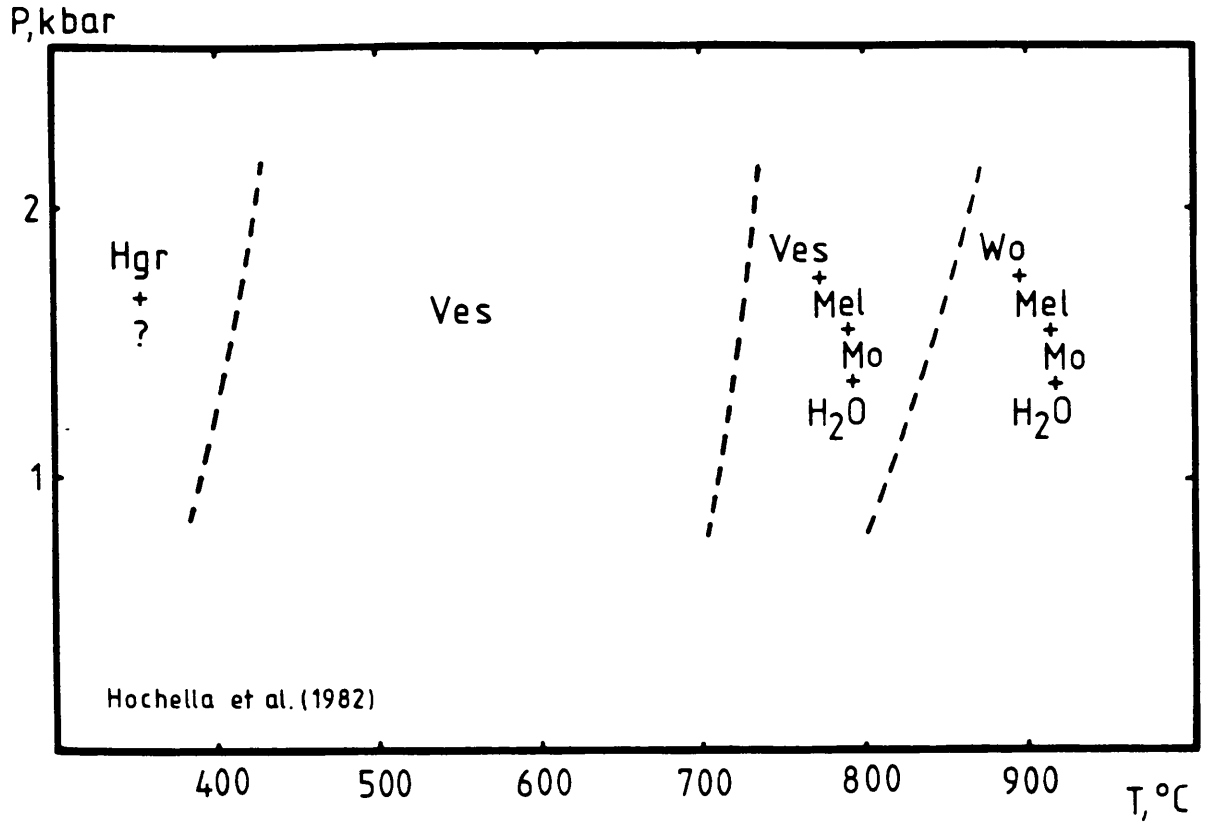

Fig. 25 Experimentally determined stability limits of vesuvianite, hydrogrossular, melilite, monticellite and wollastonite (Hochella et al. 1982).

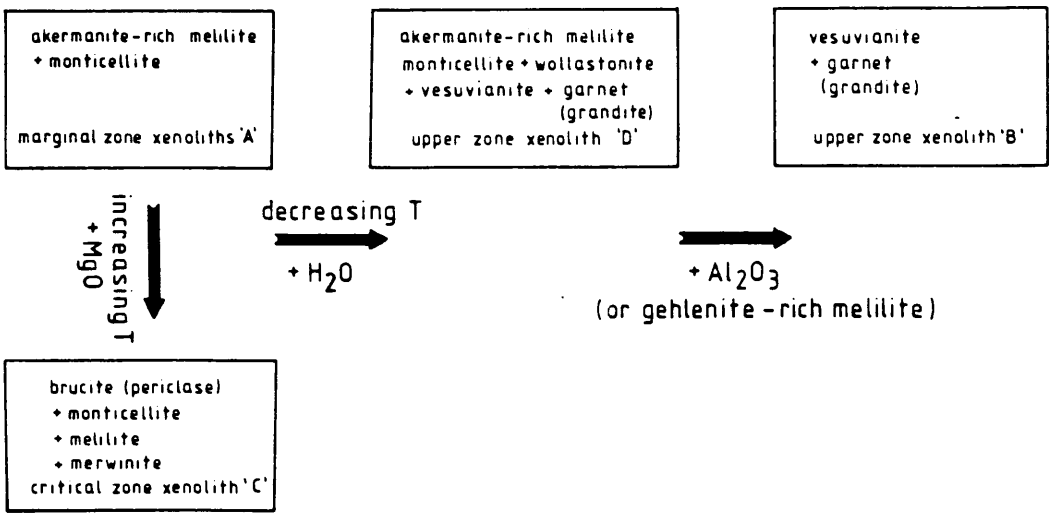

Fig. 26 Relationship between the marginal-, critical- and upper zone xenoliths.

Appendix I

Operating Conditions for Microprobe Analyses

All microprobe analyses were carried out on a JEOL 733 Superprobe with a wavelength dispersive system. The accelerating voltage was 20 kV, and the probe current (measured and monitored on a Faraday cage) was $2*10^{-7}$ A.

For the analyses of the silicates the pure oxides of the elements Al, Mg, Ti, Cr and Mn were used as standards, whereas the minerals hematite, albite, quartz, sanidine, wollastonite and BaF_2 were used as standards for Fe, Na, Si, K, Ca and Ba, respectively.

As the analysed phlogopites are relatively rich in Ba (max. 18.91 wt.%), it was necessary to consider the interference of the Ba-peaks on the Al- and Ti-peaks. The interference of Ba-L_{a1} and Ba-L_{a2}(3^{rd} order peaks) on Al-K_a were calculated to be 0.7 wt.% Al_2O_3 (measured on pure BaF_2 ≙ ca. 87.5 wt.% BaO), whereas the interference of Ba-L (1^{st} order peak) on Ti-K_a was calculated to be ca. 3 wt.% TiO_2.

The magnetites were analysed for Mg, Cr, V, Al, Ti, Mn, Fe, Si and Ca. Hematite, quartz and wollastonite served as standards for Fe, Si and Ca, and for the other elements pure oxides were used as standards. The analyses obtained were then recalculated to give values for Fe^{3+}, assuming stoichiometry. The effect of interference between the Ti-K_β X-ray emission line and the V-K_a line was also taken into account.

APPENDIX II

Fortran Computer Programs to calculate the Equilibrium Reactions at different X_{H2O} and X_{CO2}

Calculation Methods

Two FORTRAN computer programs (GG2 and GG5) are given in this appendix. These programs differ with respect to the calculations of the activities of CO_2 and H_2O in fluid mixtures.

The fundamental equations used to calculate equilibrium reactions are taken from Carmichael (1983) and have been extended by the constants e and d in the heat capacity term (Equation 1 to 10). A summary of calculations used in GG2 and GG5 is given in equation 1 to 34 below.

For a closed system the variation of G with P and T is given by

(1) $$dG=VdP-SdT.$$

From this it follows that the isothermal variation of G with P and the isobaric variation of G with T is

(2) $$(\partial G/\partial P)_T=V$$

and

(3) $$(\partial G/\partial P)_P=-S$$

The entropy is a function of temperature and can be expressed by means of a polynomial term (Holland, 1981)

(4) $$C_{p(1,T)}=a+bT+cT^{-2}+dT^{-0.5}+eT^2$$

where $C_{p(1,T)}$ stands for the isobaric heat capacity at 1 bar at a temperature T, and a,b,c,d and e are constants, which are different for each phase. As $C_{p(1,T)}$ generally converges towards $\rightarrow\infty$ and not

towards zero at T-0°K, this term shall be applied only for T>298°K. Carmichael (1983) uses an indefinite integral in order to calculate the molar entropy $S_{(1,T)}$. Applied to (4) this is

$$(5) \qquad S_{(1,T)}=\int[(a+bT+cT^{-2}+dT^{-0.5}+eT^{2})/T]dT$$
$$= r+a\ln T+bT-0.5cT^{-2}-2dT^{-0.5}+0.5eT^{2}$$

where 'r' is the integration constant that serves to fit the function $S_{(1,T)}$ to the known $S_{(1,298)}$. For 298.15°K this constant is

$$(6) \qquad r=S_{(1,298)}-5.6967a-298.15b+5.6247x10^{-6}c+0.1158d-4.4446x10^{4}e.$$

The molar entropy change in a reaction is given by

$$(7) \qquad \Delta S_{(1,T)}=r+\Delta a\ln T+\Delta bT-0.5\Delta cT^{-2}-2\Delta dT^{-0\ 5}+0.5\Delta eT^{2}$$

where

$$(8) \quad r=\Delta S_{(1,298)}-5.6967\Delta a-298.15\Delta b+5.6247x10^{-6}\Delta c+0.1158\Delta d-4.4446x10^{4}\Delta e.$$

After substitution of G and S in (3) by $\Delta G_{(1,T)}$ and $\Delta S_{(1,T)}$, and using (7) for $S_{(1,T)}$,

$$(9) \qquad \Delta G_{(1,T)}=-\int(r+\Delta a\ln T+\Delta bT-0.5\Delta cT^{-2}-2\Delta dT^{-0.5}+0.5\Delta eT^{2})dT$$
$$=\theta+(\Delta a-r)T-\Delta aT\ln T-0.5\Delta bT^{2}-0.5\Delta cT^{-1}+4\Delta dT^{0.5}-\Delta eT^{3}/6$$

where $\Delta G(1,T)$ is the change of the molar Gibbs free energy of a reaction and

$$(10) \qquad \theta=\Delta G_{(1,298)}+298.15r+1400.6\Delta a+44446.7\Delta b+0.001677\Delta c$$
$$-69.0681\Delta d+4.4173x10^{6}\Delta e$$

The integration constant 'θ' fits $G_{(1,T)}$ to the known $G_{(1,298)}$.

In order to obtain the change of the molar Gibbs free energy of reaction at different pressures $G_{(P,T)}$, a term describing the change in free energy due to the change of the molar volume of solid phases

in the reaction

$$(11) \qquad \int_1^P \Delta V_{s(P,T)} = \Delta V_{s(1,298)}(P-1) + [1 + \Delta A(T-298) - \Delta B(0.5)P]$$

and an equivalent for a fluid phase

$$(12) \qquad \int_1^P \Delta V_{f(P,T)} = RT \ln f_i \sum_i$$

has to be added, where A and B are constant values expressing the thermal expansions and isobaric compressibilities for endmembers of solids, and 'f_i' refers to the fugacity of the 'i'th component in the fluid phase. Hence,

$$(13) \qquad \Delta G_{(P,T)} = \Delta G_{(1,T)} + \Delta V_{s(1,298)}(P-1) + (1 + \Delta A(T-298) - \Delta B(0.5)P + RT\Delta \ln f_i \sum_i$$

Because the solids participating in an equilibrium reaction are often solid solutions and the fluid phase may be a mixture of several components, terms that are functions of the activities of the respective phases have to be included to obtain the molar chemical potential:

$$(14) \qquad \Delta\mu_{(P,T)} = \Delta G_{(P,T)} + RT\ln X_{CO2} + RT\ln\gamma_{CO2} + RT\ln X_{H2O} + RT\ln_{H2O} + RT\ln K_s$$

where γ_i is the activity coefficient of component i and $RT\ln\gamma$ is given in equation (16). The mole fractions of the components of a binary fluid consisting of CO_2 and H_2O are designated by X_{CO2} and X_{H2O}, respectively. The activity A of the ith phase is given by the relation

$$(15) \qquad RT\ln A_i = RT\ln X_i + RT\ln\gamma_i$$

In program GG2 the activities of CO_2 and H_2O have been calculated by using relatively simple polynomial terms proposed by Powell and Holland (1985). These authors have taken the activity data of Kerrick and Jacobs (1981) and made a fit to their results using a pressure and temperature dependent subregular solution model. The activity coefficient γ of a component i (and j) in a binary fluid can be calculated from the term

(16) $RT\ln\gamma_i=(X_i)(X_j)[W_i+2(W_j-W_i)X_i]$ (Wohl, 1946).

Powell and Holland (1985) derive values of W_{H2O} and W_{CO2} as linear functions of pressure and temperature. The parameters derived for the range 2-10 kbar and 400-800°C are (Option 1)

(17) $$W_{H2O}=8.3-0.007T+0.26P$$

and

(18) $$W_{CO2}=17.8-0.014T+0.38P$$

and for pressures lower than 1.5 kbar they are (Option 2)

(19) $$W_{CO2}=25-0.025T$$

and

(20) $$W_{H2O}=1.08-0.012T$$

in kJ $mole^{-1}$, with T in K and P in kbar. Because the computer programs work with calories and bars, these terms are devided by 0.004184 in the program. Besides the subregular mixing models (Option 1 and 2) two further options (3 and 4) can be chosen in GG2. Option 3 applies an ideal mixing model while option 4 is proposed in connection with high temperature reactions (>600°C) involving calcite H_2O and CO_2 (Chapter B 7.2.).

In program GG2 the fugacities have been calculated after Holland and Powell (1985) using a low order polynomial term (Holland, 1981):

(21) $$RT\ln f=a+bT+cT^2$$

where a, b and c are functions of pressure. Powell and Holland (1985) fitted this term to the fugacity data of H_2O of Burnham, Holloway and Davis (1968) and to CO_2 data of Shmonov and Shmulovich (1974) and Bottinga and Richet (1981).

In contrast to Program GG2, GG5 calculates the fugacities of H_2O and CO_2 with the modified Redlich-Kwong (MRK) equation given by Prausnitz (1974). A program written by Holloway (1976) and corrected by Flowers (1979) has been applied in the subroutines of GG5.

Holloway (1976) used the method of Edmister (1968) to calculate compressibility factors, activity- and fugacity coefficients.

The modified Redlich-Kwong equation for the fugacity coefficient of the ith component of a mixture of nonpolar molecules is given by Prausnitz (1974) as

$$(22)\quad \ln(k)_i=\ln(V/(V-b))+(b_i i/(V-b))-(2\sum_{j=1}^{i} a_{i,j}X_j/bRT^{3/2})(\ln((V+b)/V)) +(ab_i/b^2RT^{3/2})(\ln(V+b)/V)-b/(V+b))-\ln(PV/RT)$$

where $k_{i,j}(i\neq j)$ is the fugacity coefficient, R designates the gas constant (82.057 cm^3bar/deg mol), V represents the molar volume, T stands for the temperature and a and b correspond to pressure-independent and composition-dependent terms that are (Redlich and Kwong, 1949)

$$(23)\quad a=\sum_{i=1}^{i}\sum_{j=1}^{j} a_{i,j}X_iX_j$$

and

$$(24)\quad b=\sum_{i=1}^{i} b_iX_i$$

where X_i and X_j refer to the mole fractions of the components in the gas mixture. The interaction coefficient for the two components is given by $a_{i,j}$, and b_i stands for the b coefficient for the ith gas. In the case of an interaction of unlike nonpolar molecules the term $a_{i,j}$ can be assumed to be (Redlich and Kwong, 1949)

$$(25)\quad a_{i,j}=(a_ia_j)^{1/2}.$$

The coefficients a_i and a_j can be expressed as (de Santis et al. 1974)

$$(26)\quad a_i=a_i^o+a_i(T)$$

and

$$(27)\quad a_j=a_j^o+a_j(T)$$

where a_i^o and a_j^o refer to temperature-independent dispersion forces and $a_i(T)$ and $a_i(T)$ correspond to temperature functions providing data for

intermolecular attraction due to hydrogen bonds, permanent dipoles, and quadrupoles. For CO_2 and H_2O the respective terms are

(28) $$a^{o}_{CO2}=46\times10^{6},$$

(29) $$b_{CO2}=29.7,$$

(30) $$a_{CO2}(T)=73.03\times10^{6}-71400.T+21.57T^{2}$$

and

(31) $$a^{o}_{H2O}=35\times10^{6},$$

(32) $$b_{H2O}=14.6,$$

(33) $$a_{H2O}(T)=166.8\times10^{6}-193080.T+186.4T^{2}-0.071288T^{3}.$$

By taking into account that some species like H_2O and CO_2 form complexes, the cross interaction coefficient can be expressed as (de Santis et al. 1974)

(34) $$a_{H2O,CO2}=(a^{o}_{H2O}a^{o}_{CO2})^{1/2}+0.5R^{2}T^{5/2}K$$

where K is equilibrium constant for the reaction $H_2O+CO_2=H_2CO_3$.

As in program GG2, several options with respect to different mixing models are available in GG5. In program GG5 they are designated as

a) Nonideal mixing with formation of hydrocarbon acid (modified Redlich-Kwong equation),
b) Nonideal mixing model; probably due to additional formation of $Ca[H_2(CO_3)_2]$,
c) Ideal mixing.

When applying the computer programs the superfluous options have to be 'commented out'. Options b and c in GG5 are equal to options 3 and 4 in GG2.

Range of Applicability for GG2 and GG5

The two FORTRAN programs GG2 and GG5 calculate reaction equilibria for solid-solid and solid-fluid reactions with respect to a binary fluid consisting of H_2O and CO_2. An advantage of GG2 is that it can readily be run with a Personal Computer, because it is shorter than GG5 and applies less intricate calculations. Powell and Holland

(1985) stated that the parameters for the mixing of binary fluids consisting of H_2O and CO_2 are reliable only for temperatures between 400 and 800°C and pressures lower than 10 kbar. For pressures lower than 1 kbar the results also deviate increasingly from those obtained by GG5, which applies the MRK. Holloway (1976) suggests that the MRK can be used to estimate the fugacity of CO_2, H_2O, H_2, CO and CH_4 in multispecies fluids at temperatures from about 450 to 1800°C and at pressures from 0.5 to about 40 kbar. In simple binary fluids consisting of H_2O and CO_2 the pressure range is even greater (1 bar to 100 kbar) while temperatures should not be lower than 400°C to gain reliable results. Because of the amount of calculation steps and for compiling reasons, it is advisable to use a 'Mainframe' computer to run GG5.

Graphical Explanation of Computing Steps

Figures A and B graphically approach to explain the principles applied in the programs, in order to calculate the equilibrium conditions of mineral reactions with or without the involvement of a fluid phase. The variables are P, T and X_{CO2}. Before the programs are executed it is necessary to define the starting and end temperatures and pressures, the temperature- and pressure steps, and the equilibrium constant K for the solid phases involved in the reaction. The latter is commonly 1 for pure phases. At equilibrium the change of the chemical potential $\Delta\mu_{(P,T)}=0$. In the programs, $\Delta\mu_{(P,T)}$ are referred to as GG and GH, respectively (Figure A). The variable used by the programs is X_{CO2}. With increasing X_{CO2}, a point will be surpassed, where $\Delta\mu_{(P,T)}=0$. In order to approach this specific value, the programs start with a low X_{CO2} (=0.001) and increases it stepwise. Before each step, GG is computed and compared with GH, which differs from GG by the stepwidth RINC (ΔX_{CO2}). The latter is 0.1 at the beginning (N=0). The lower and upper boundary of each X_{CO2}-step is expressed as LXCO2 and UXCO2, and can be attributed to GG and GH, respectively. As soon as a GG and GH have different signs, the last step becomes reversed, to define a new starting value and RINC of X_{CO2}. At N=1, the stepwidth is defined by RINC=0.01. This continues until RINC=10^{-6} at N=5. The resulting value for X_{CO2}, at which equilibrium ($\Delta\mu_{(P,T)}=0$) is reached,

lies between LXCO2 and UXCO2, which differ only by a very small X_{CO2} value (10^{-6}). In the next step, the temperature is increased by the defined temperature step (TSTEP) and the calculations are repeated until the defined temperature range (TSTART and TEND) is covered. Then, the pressure (PSTART) is increased by the defined pressure step (PSTEP) and the calculations for GG and GH at different temperatures start again, until the end pressure (PEND) is reached.

The computing procedure of a devolatization reaction in which CO_2 and H_2O becomes evolved is shown in Figure A and B. The solid curve in Figure B illustrates the equilibrium conditions at a fixed pressure with T and X_{CO2} as variables. After an increase of the equilibrium temperature with increasing X_{CO2} the equilibrium temperature decreases, after a maximum temperature (T2 in Figure B) has been reached. Above this maximum temperature GG and GH always have the same signs. After passing this point, the programs calculate the equilibrium composition of the fluid phase at decreasing temperatures. It is obvious from Figure B that different X_{CO2} values can be reached at the same equilibrium temperature, as the ascending and declining slope of the equilibrium curve lie in the same temperature range. At declining temperatures, RINC does not start at X_{CO2}=0.001 but at the last calculated UXCO2 value that resulted from a change of sign of GG and GH (dashed line in Figure B). This avoids double crossing of the equilibrium curve in Figure B, which is necessary because each equilibrium calculation can produce only one LXCO2 and UXCO2.

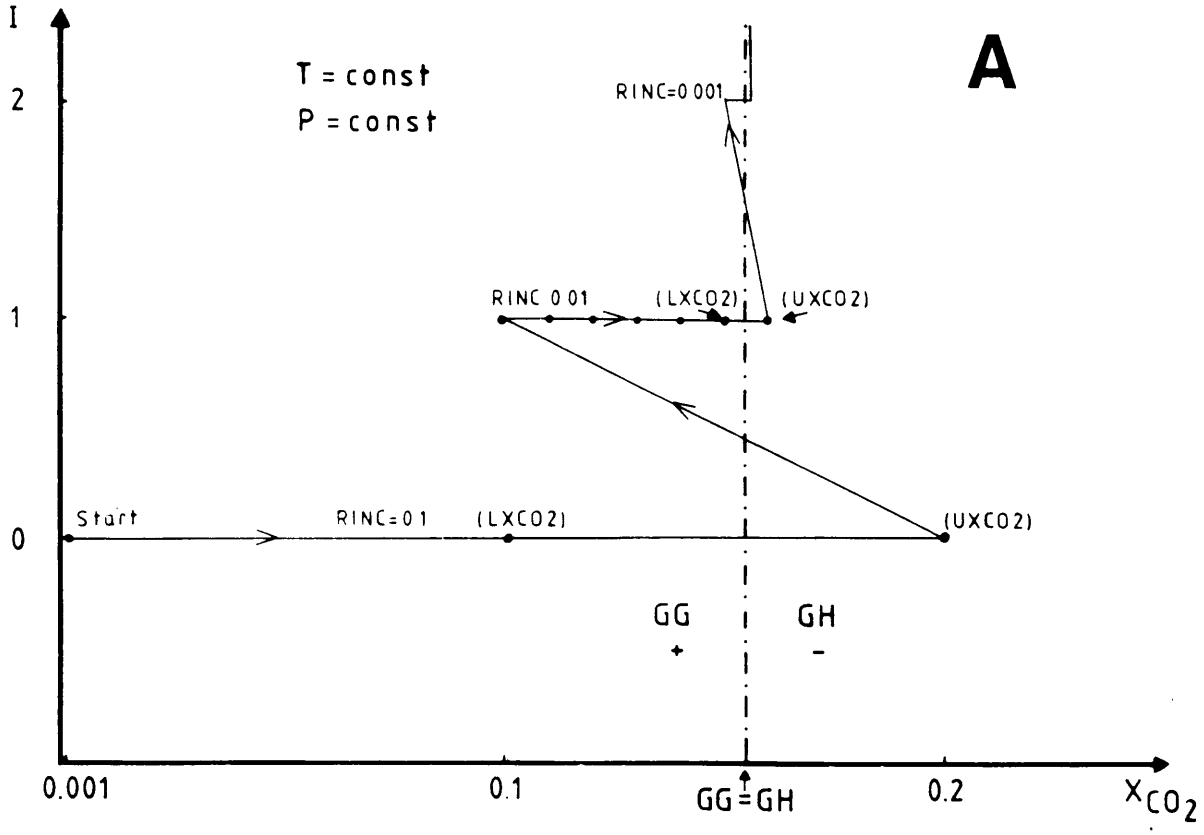

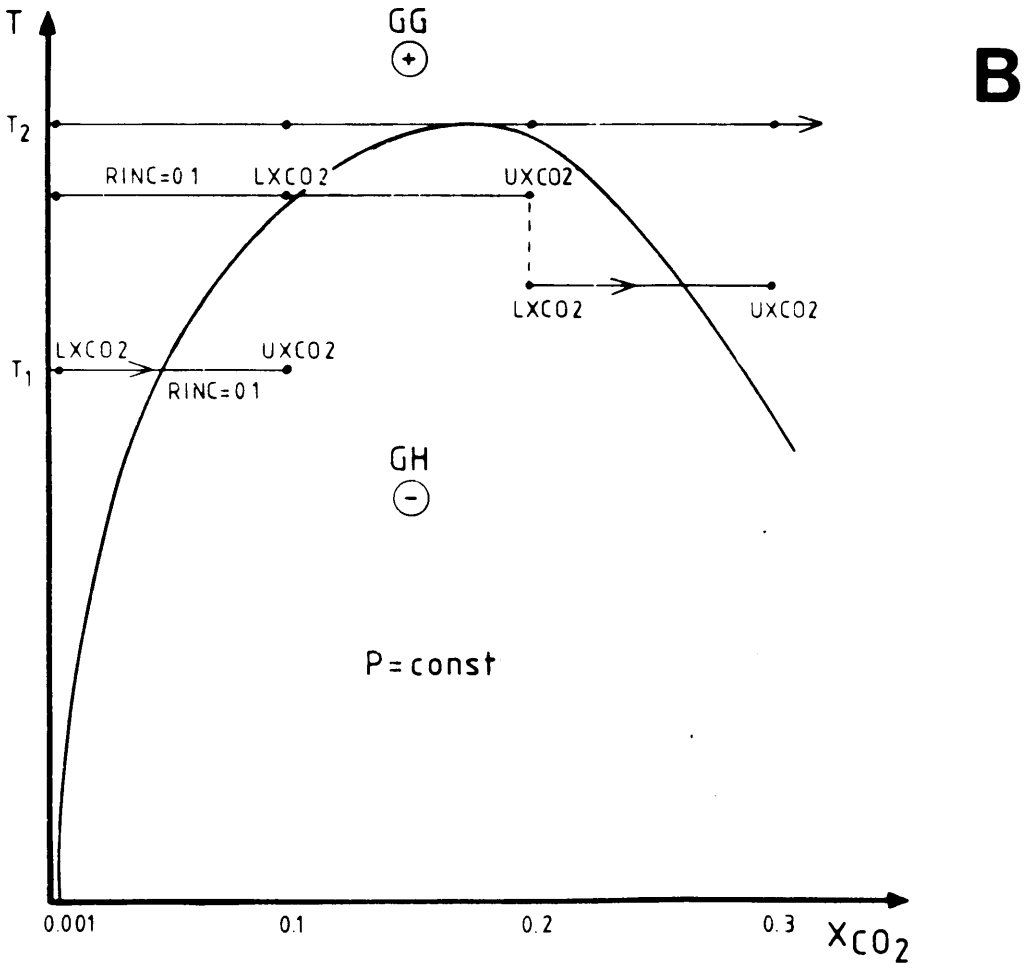

```
type work.for
$NOFLOATCALLS
C-----------------------------------------------------------------------C
C   COMPUTER PROGRAM GG2 FORTRAN                                        C
C   COMPILED BY T. WALLMACH, DR. C.J., HATTON & R. KEABLE               C
C   SYMBOL LIST                                                         C
C   RIC            INTEGRATION CONSTANT (r)                             C
C   S              ENTROPY AT 1 BAR and 298.15°K                        C
C   TK             TEMPERATURE IN KELVIN                                C
C   THE            THETA (Θ)                                            C
C   A,B,C,D,E,     CONSTANTS A,B,C,D,E, IN SPECIFIC HEAT EQUATION       C
C   AT             THERMAL EXPANSION COEFFICIENT MULTIPLIED BY V(MOL)C
C   BP             COMPRESSIBILITY COEFFICIENT MULTIPLIED BY V(MOL)     C
C   WA             MOLES OF H2O INVOLVED IN REACTION                    C
C   CO             MOLES OF CO2 INVOLVED IN REACTION                    C
C   GO             GIBBS FREE ENERGY OF REACTION AT 298.15°K            C
C   G              GIBBS FREE ENERGY EXCLUDING X_CO2 and X_H2O          C
C   GG AND GH      GIBBS FREE ENERGY INCLUDING X_CO2 and X_H2O          C
C   V              MOLAR VOLUME OF SOLIDS OF REACTION FOR SOLIDS        C
C   FFCO2          FUGACITY OF CO2=RT*LN(FCO2) AFTER                    C
C                  HOLLAND AND POWELL (1985)                            C
C                  (DIVIDED BY 0.004184 TO CONVERT KJ TO CAL)           C
C   FFH2O          FUGACITY OF H2O=RT*LN(FH2O)                          C
C                  HOLLAND AND POWELL (1985)                            C
C                  (DIVIDED BY 0.004184 TO CONVERT KJ TO CAL)           C
C   XCO2           MOLE FRACTION OF CO2                                 C
C   XH2O           MOLE FRACTION OF H2O ASSUMED=1-XCO2                  C
C   K              EQUILIBRIUM CONSTANT                                 C
C   R              GAS CONSTANT = 1.987 CAL/°K                          C
C   INPUT          S,A,B,C,D,E,AT,BP,K,WA,CO,STEMP(STARTING TEMP),TSTEP C
C                  (TEMPERATURE STEP),SPRESS(STARTING PRESSURE)         C
C   MATRIX         IS P = 1 TO 10000 BAR; T = 400 TO 800°K              C
C-----------------------------------------------------------------------C
      IMPLICIT REAL*8 (A-H,O-Z)
      IMPLICIT INTEGER (I-N)
      REAL*8 K,LXCO2
      DIMENSION AA(20,40),BB(10)
      CHARACTER*20 NAME(40)
      CHARACTER*1 YES,ANS
      DATA YES/'Y'/
      OPEN(1,FILE='LPT1:')
      OPEN(2,FILE='THERM.DAT',STATUS='OLD')
      J=0
      J=J+1
      READ(2,1000,END=200)(AA(I,J),I=1,10),NAME(J)
1000  FORMAT(F10.0,6F10.4/3F10.4,10X,A20)
      GOTO 11
200   WRITE(*,30)
30    FORMAT(' INPUT K (THE REACTION COEFFICIENT)  '\)
      READ(*,350)K
350   FORMAT(F9.3)
      WRITE(*,4000)
4000  FORMAT(1H ,'INPUT THE NUMBER OF WATER MOLECULES IN THE REACTION
     * '\)
      READ(*,350)WA
      WRITE(*,450)
450   FORMAT(' INPUT THE NUMBER OF THE CO MOLECULES IN THE REACTION
```

```
     * ´\)
       READ(*,350)CO
       WRITE(*,5000)
5000   FORMAT(´ INPUT STARTING TEMPERATURE (DEG. C) ´\)
       READ(*,350)STEMP
       WRITE(*,550)
550    FORMAT(´ INPUT TEMPERATURE INCREMENT (5.,10.,20.,40.,50.) ´\)
       READ(*,350)TSTEP
       WRITE(*,600)
600    (´ INPUT STARTING PRESSURE (BARS)) ´\)
       READ(*,350)SPRESS
       WRITE(*,650)
650    FORMAT(´ INPUT FINAL PRESSURE (BARS) ´\)
       READ(*,350)EPRESS
       WRITE(*,700)
700    FORMAT(´ INPUT PRESSURE INCREMENT (BARS) ´\)
       READ(*,350)PSTEP
       WRITE(*,*)
       WRITE(*,10)
10     FORMAT(7X,´PHASE NUMBER´,4X,´PHASE´)
       WRITE(*,*)
       DO 40 I=1,J-1
       WRITE(*,20)I,NAME(I)
20     FORMAT(11X,I3,8X,A20)
40     CONTINUE
       DO 9000 I=1,10
9000   BB(I)=0.0
       WRITE(*,*)
       WRITE(*,4500)
4500   FORMAT(´ DO YOU WANT A HARDCOPY OF THIS LIST (Y OR N) ´\)
       READ(*,4600)ANS
4600   FORMAT(A1)
       IF(ANS.EQ.YES)CALL HARD(NAME,J)
       WRITE(*,*)
       WRITE(*,5005)
5005   FORMAT(´ YOU MUST NOW INPUT THE PHASES IN YOUR REACTION´,\
    *,´ WHEN YOU NO LONGER WISH TO ADD ANY MORE PHASES TO THE´,\
    *,´ REACTION INPUT A ZERO AS THE PHASE NUMBER´)
       WRITE(*,*)
1      CONTINUE
       WRITE(*,*)
       WRITE(*,5010)
5010   FORMAT(1H ,´INPUT PHASE NUMBER (DECIMAL POINT NOT NEEDED) ´\)
       READ(*,5100)NUMBER
5100   FORMAT(I2)
       IF(NUMBER.EQ.0) GOTO 3
       WRITE(*,*)
       WRITE(*,5200)
5200   FORMAT(´ HOW MANY MOLECULES OF THIS PHASE ARE THERE IN THE
    *REACTION ´\)
       READ(*,5300)COEFF
5300   FORMAT(F5.3)
       DO 2000 I=1,10
       BB(I)=BB(I)+COEFF*AA(I,NUMBER)
2000   CONTINUE
       GOTO 1
3      CONTINUE
```

```
        H=BB(1)
        S=BB(2)
        V=BB(3)
        A=BB(4)
        B=BB(5)
        C=BB(6)
        D=BB(7)
        E=BB(8)
        AT=BB(9)
        BP=BB(10)
        R=1.9872
C-------------CALCULATE RIC GIVEN S,A,B,C,D AND E
        RIC=S-5.697*A-0.29815*B+5.6247E-1*C+0.1158*D-4.4446E-2*E
C-------------CALCULATE THE GIVEN GO,RIC,A,B,C,D AND E
        GO=H-298.15*S
        THE=GO+298.15*RIC+1400.6*A+44.4467*B+167.7*C
     *-69.0681*D+4.4173*E
        P=1.0
        TK=298.15
C-------------CARMICHAEL (1977), P.63
        G=THE+(A-RIC)*TK-A*TK*(ALOG(TK))-0.0005*B*TK*TK-50000.0
     **C/TK+4.0*D*SQRT(TK)-E(TK*TK*TK)/6.0E+6+V(P-1.0)
        WRITE(1,6010)TK,P,G
6010    FORMAT(' TK=',F8.2,'  P=',F12.2,'  G=',F16.0)
C-------------CALCULATION OF CO2 FUGACITY FROM HOLLAND (1985)
        P=SPRESS
        TK=STEMP
        UXCO2=0.0
        WRITE(*,*)
8700    WRITE(*,8000)
8000    FORMAT(' YOU MUST CHOOSE THE FOLLOWING MODELS')
        WRITE(*,*)
        WRITE(*,8100)
8100    FORMAT(' (1)--IRREGULAR MIXING P < 1.5 KB')
        WRITE(*,*)
        WRITE(*,8200)
8200    FORMAT(' (2)--IRREGULAR MIXING P > 1.5 KB')
        WRITE(*,*)
        WRITE(*,8300)
8300    FORMAT(' (3)--IDEAL MIXING - P INDEPENDENT')
        WRITE(*,*)
        WRITE(*,8400)
8400    FORMAT(' (4)--PROPOSED MODEL FOR T > 900 DEG K')
        WRITE(*,*)
        WRITE(*,8500)
8500    FORMAT(' INPUT THE NUMBER OF YOUR CHOICE (DECIMAL POINT NOT NEED
     *ED) '\)
        READ(*,8600)IH
8600    FORMAT(I2)
99      CONTINUE
        UXCO2=0.0
C       P+PSTEP
        IF(P.GT.EPRESS) GOTO 999
        IDECRE=0
        TK=STEMP-TSTEP
        IF(TSTEP.EQ.5.) LIM=300
        IF(TSTEP.EQ.10.) LIM=100
```

```
      IF(TSTEP.EQ.20.) LIM=80
      IF(TSTEP.EQ.40.) LIM=40
      IF(TSTEP.EQ.50.) LIM=24
      WRITE(1,2500) I,IOUT,IDECRE
      L=0
100   L=L+1
      IF(IDECRE.EQ.0) TK=TK+TSTEP
      IF(IDECRE.EQ.1) TK=TK-TSTEP
      FFCO2=0.0
      CALL FF(TK,P,FFCO2)
      IF(IDECRE.EQ.0) XCO2=0.001
      IF(IDECRE.EQ.1) XCO2=UXCO2
      CALL WATER(TK,P,FFH2O)
      XH2O=1.001-XCO2
      PV=P*(V+(AT/1.0E+5)*(TK-298.15)-(BP/1.0E+6)*P/2.)
      GSTOP=G
      G=THE+(A-RIC)*TK-A*TK*(ALOG(TK))-0.0005*B*TK*
     *TK-50000.0*C/TK+4.0*D*SQRT(TK)-E(TK*TK*TK)/6.0E+6+CO2
     **(FFCO2)+PV+WA*(FFH2O)
      IF(G.GT.0.0.AND.GSTOP.LT.0.0.AND.RINC.EQ.0.1.AND.
     *IOUT.EQ.11.AND.IDECRE.EQ.1) GOTO 25
      GOTO 26
25    P=P+PSTEP
      GOTO 99
26    IF(G.LT.0.0.AND.GSTOP.GT.0.0.AND.RINC.EQ.0.1.AND.IOUT.EQ.11.
     *AND.IDECRE.EQ.1) GOTO 27
      GOTO 28
27    P=P+PSTEP
      GOTO 99
28    WRITE(1,6020)TK,P,G,FFCO2,FFH2O
6020  FORMAT(' TK=',F7.1,' P=',F7.1,' G=',F8.0,' RTLNFCO2=',F8.1
     *' RTLNFH2O=',F8.1)
      IF(XH2O.LT.0.0)XH2O=1.0D-9
      IF(XCO2.LT.0.0)XCO2=1.0D-9
      IF(IH.GT.4) GOTO 8700
      IF(IH.EQ.1) CALL IRREG(GG,CO,WA,R,TK,XCO2,XH2O,WCO2,WH2O,K,G)
      IF(IH.EQ.2) CALL IRREG2(GG,CO,WA,R,TK,XCO2,XH2O,WCO2,WH2O,K,G,P)
      IF(IH.EQ.3) CALL REG(GG,CO,WA,R,TK,XCO2,XH2O,WCO2,WH2O,K,G)
      IF(IH.EQ.4) CALL PROP(GG,CO,WA,R,TK,XCO2,XH2O,WCO2,WH2O,K,G)
      RINC=0.1
      N=0
400   CONTINUE
      IOUT=1
      DO 300 I=1,10
      XCO2=XCO2+RINC
      XH2O=1.001-XCO2
      IF(XH2O.LT.0.0)XH2O=1.0D-9
      IF(XCO2.LT.0.0)XCO2=1.0D-9
      IF(IH.EQ.1) CALL IRREGA(GH,CO,WA,R,TK,XCO2,XH2O,WCO2,WH2O,K,G)
      IF(IH.EQ.2) CALL IRREG2A(GH,CO,WA,R,TK,XCO2,XH2O,WCO2,WH2O,K,G,P)
      IF(IH.EQ.3) CALL REGA(GH,CO,WA,R,TK,XCO2,XH2O,WCO2,WH2O,K,G)
      IF(IH.EQ.4) CALL PROPA(GH,CO,WA,R,TK,XCO2,XH2O,WCO2,WH2O,K,G)
      IF(GH.GT.0.0.AND.GG.LT.0.0) GOTO 901
      IF(GG.GT.0.0.AND.GH.LT.0.0) GOTO 901
      GG=GH
      IOUT=IOUT+1
300   CONTINUE
```

```
        IF(I.EQ.IOUT.AND.RINC.EQ.0.1.AND.UXCO2.GT.0.0) IDECRE=1
        WRITE(1,2500)I,IOUT,IDECRE,RINC
2500    FORMAT(' I=',I2,3X,' IOUT=',I2,3X,'IDECRE=',I2,'   RINC=',F9.7)
500     CONTINUE
        IF(TK.EQ.STEMP.AND.L.NE.1) GOTO 130
        GOTO 135
130     P=P+PSTEP
        GOTO 99
135     IF(L.NE.LIM) GOTO 100
        P=P+PSTEP
        IF(P.LT.EPRESS) GOTO 99
        GOTO 999
901     UXCO2=XCO2
        LXCO2=XCO2-RINC
        XCO2=LXCO2
        N=N+1
        IF(N.EQ.1) RINC=0.01
        IF(N.EQ.2) RINC=0.001
        IF(N.EQ.3) RINC=0.0001
        IF(N.EQ.4) RINC=0.00001
        IF(N.EQ.5) GOTO 911
        GOTO 400
911     WRITE(1,6040)UXCO2,LXCO2,RINC,I
6040     FORMAT(69X,'UXCO2=',F9.7,' LXCO2=',F9.7,'RINC=',F9.7,' I=',I2)
        IF(UXCO2.GE.1.0) P=P+PSTEP
        IF(UXCO2.GE.1.0) GOTO 99
        GOTO 500
999     STOP
        END
C
C
C**************************SUBROUTINE CO2*****************************
C
        SUBROUTINE FF(TK,P,FFCO2)
        IMPLICIT REAL*8 (A-Z)
        P=P/1000.
        A=-9.429+2.6209*P-0.011704*P*P
        B=0.12722+0.11587/P-0.02725/(P*P)-0.14323/DSQRT(P)
        C=-6.806E-07-2.3744E-07*P-5.677E-06/DSQRT(P)
        FFCO2=A+B*TK+C*TK*TK
        FFCO2=FFCO2/0.004184
        P=P*1000.
        RETURN
        END
C
C
C
C**************************SUBROUTINE WATER************************
C
C
        SUBROUTINE WATER(TK,P,FFH2O)
        IMPLICIT REAL*8 (A-Z)
        P=P/1000.
        A=-38.61+1.3854*P-0.001228*P*P
        B=0.12716+0.03977/P-0.0078802/(P*P)-0.041436/DSQRT(P)
        C=-9.8194E-06+6.5419E-08*P+1.3849-06/(P*P)-1.39E-05/DSQRT(P)
        FFH2O=A+B*TK+C*TK*TK
```

```
        FFH2O=FFH2O/0.004184
        P=P*1000.
        RETURN
        END
C
C
C
C**************************SUBROUTINE IRREG************************
C
C
        SUBROUTINE IRREG(GG,CO,WA,R,TK,XCO2,XH2O,WCO2,WH2O,K,G)
C-------IRREGULAR MIXING MODEL (POWELL&HOLLAND 1985 P<1.5 KBAR)------
        IMPLICIT REAL*8 (A-Z)
        WCO2=(25.0-0.025*TK)/0.004184
        WH2O=(1.08-0.012*TK)/0.004184
        GG=G+CO*R*TK*(DLOG(XCO2))+WA*R*TK*(DLOG(XH2O))+
     *CO*(XH2O*XH2O*(WCO2+2.*(WH2O-WCO2)*XCO2))+
     *WA*(XCO2*XCO2*(WH2O+2.*(WCO2-WH2O)*XH2O))+
     *R*TK*(DLOG(K))
        RETURN
        END
C
C
C**************************SUBROUTINE IRREG2************************
C
C
        SUBROUTINE IRREG2(GG,CO,WA,R,TK,XCO2,XH2O,WCO2,WH2O,K,G,P)
C-------IRREGULAR MIXING MODEL (POWELL&HOLLAND 1985 P>1.5 KBAR)------
        IMPLICIT REAL*8 (A-Z)
        WCO2=(17.8-0.014*TK+0.38*P/1000.)/0.004184
        WH2O=(8.3-0.007*TK+0.26*P/1000.)/0.004184
        GG=G+CO*R*TK*(DLOG(XCO2))+WA*R*TK*(DLOG(XH2O))+
     *CO*(XH2O*XH2O*(WCO2+2.*(WH2O-WCO2)*XCO2))+
     *WA*(XCO2*XCO2*(WH2O+2.*(WCO2-WH2O)*XH2O))+
     *R*TK*(DLOG(K))
        RETURN
        END
C
C
C**************************SUBROUTINE REG***************************
C
C
        SUBROUTINE REG(GG,CO,WA,R,TK,XCO2,XH2O,WCO2,WH2O,K,G)
C-------IDEAL MIXING MODEL : P INDEPENDENT--------------------------
        IMPLICIT REAL*8 (A-Z)
        GG=G+CO*R*TK*(DLOG(XCO2))+WA*R*TK*(DLOG(XH2O))+
     *R*TK*(DLOG(K))
        RETURN
        END
C
C
C**************************SUBROUTINE PROP**************************
C
C
        SUBROUTINE PROP(GG,CO,WA,R,TK,XCO2,XH2O,WCO2,WH2O,K,G)
C-------PROPOSED FOR TK>900 DEG K : P INDEPENDENT--------------------
        IMPLICIT REAL*8 (A-Z)
```

```
      GG=G+CO*R*TK*(DLOG(XCO2))+WA*R*TK*(DLOG(XH2O))+
     *(CO*(51.0-0.053*TK)*(XH2O*XH2O)/0.004184)+
     *(WA*(51.0-0.053*TK)*(XCO2*XCO2)/0.004184)+
     *R*TK*(DLOG(K))
      RETURN
      END

C
C
C*************************SUBROUTINE PROPA*************************
C
C
      SUBROUTINE PROPA(GH,CO,WA,R,TK,XCO2,XH2O,WCO2,WH2O,K,G)
C-------THIS SUBROUTINE USES SLIGHTLY DIFFERENT NUMBERS (GH) TO PROP--
      IMPLICIT REAL*8 (A-Z)
      GH=G+CO*R*TK*(DLOG(XCO2))+WA*R*TK*(DLOG(XH2O))+
     *(CO*(51.0-0.053*TK)*(XH2O*XH2O)/0.004184)+
     *(WA*(51.0-0.053*TK)*(XCO2*XCO2)/0.004184)+
     *R*TK*(DLOG(K))
      RETURN
      END
C
C
C*************************SUBROUTINE IRREGA************************
C
C
      SUBROUTINE IRREGA(GH,CO,WA,R,TK,XCO2,XH2O,WCO2,WH2O,K,G)
C-------THIS USES SLIGHTLY DIFFERENT VALUES (GH) TO IRREG-----------
      IMPLICIT REAL*8 (A-Z)
      WCO2=(25.0-0.025*TK)/0.004184
      WH2O=(1.08-0.012*TK)/0.004184
      GH=G+CO*R*TK*(DLOG(XCO2))+WA*R*TK*(DLOG(XH2O))+
     *CO*(XH2O*XH2O*(WCO2+2.*(WH2O-WCO2)*XCO2))+
     *WA*(XCO2*XCO2*(WH2O+2.*(WCO2-WH2O)*XH2O))+
     *R*TK*(DLOG(K))
      RETURN
      END
C
C
C*************************SUBROUTINE IRREG2A***********************
C
C
      SUBROUTINE IRREG2A(GH,CO,WA,R,TK,XCO2,XH2O,WCO2,WH2O,K,G,P)
C-------THIS USES SLIGHTLY DIFFERENT VALUES (GH) TO IRREG2----------
      IMPLICIT REAL*8 (A-Z)
      WCO2=(17.8-0.014*TK+0.38*P/1000.)/0.004184
      WH2O=(8.3-0.007*TK+0.26*P/1000.)/0.004184
      GH=G+CO*R*TK*(DLOG(XCO2))+WA*R*TK*(DLOG(XH2O))+
     *CO*(XH2O*XH2O*(WCO2+2.*(WH2O-WCO2)*XCO2))+
     *WA*(XCO2*XCO2*(WH2O+2.*(WCO2-WH2O)*XH2O))+
     *R*TK*(DLOG(K))
      RETURN
      END
```

```
C
C
C*************************SUBROUTINE REGA*************************
C
C
        SUBROUTINE REG(GH,CO,WA,R,TK,XCO2,XH2O,WCO2,WH2O,K,G)
C-------THIS USES SLIGHTLY DIFFERENT VALUES (GH) TO REG--------------
        IMPLICIT REAL*8 (A-Z)
        GH=G+CO*R*TK*(DLOG(XCO2))+WA*R*TK*(DLOG(XH2O))+
     *R*TK*(DLOG(K))
        RETURN
        END
C
C
C*************************SUBROUTINE HARD*************************
C
C
        SUBROUTINE HARD(NAME,J)
        INTEGER
        CHARACTER*20 NAME(40)
        WRITE(1,4700)
4700    FORMAT(7X,'PHASE NUMBER',4X,'PHASE')
        WRITE(1,*)
        DO 4750 I=1,J-1
        WRITE(1,4800)I,NAME(I)
4800    FORMAT(11X,I3,8X,A20)
4750    CONTINUE
        WRITE(1,4900)
4900    FORMAT(//)
        RETURN
        END
```

CREATION OF DATA FILE (THERM.DAT) AS SHOWN IN THE FOLLOWING EXAMPLE

```
  -923777.   50.0300    2.2180   60.0900   11.4000  -11.4000    0.0000
    0.0000    7.0985    2.6291          AKERMANITE
```

THE SEQUENCE FROM THE FIRST VALUE IN THE FIRST ROW TILL THE LAST VALUE
IN THE SECOND ROW ARE:

```
     H,S,V,A,B(*0.001),C(*100000),D,E(*0.000001),AT(*10E-8),BP(*10E-9)
```

```
C-----------------------------------------------------------------C
C                COMPUTER PROGRAM GG5 FORTAN                      C
C                COMPILED BY DR C.J.HATTON & T WALLMACH           C
C                UNITS: CALORIES, DEGREES KELVIN, BAR             C
C                USE TEMPORARY DATA FILE 'FILE FT01F001'          C
C                INPUT IN FILE 'GP FORTRAN' THEN WATFIV GP        C
C                OUTPUT IN FILE 6                                 C
C   SYMBOL LIST                                                   C
C   RIC          INTEGRATION CONSTANT (r)                         C
C   S            ENTROPY AT 1 BAR and 298.15°K                    C
C   TK           TEMPERATURE IN KELVIN                            C
C   THE          THETA (Θ)                                        C
C   A,B,C,D,E    CONSTANTS A,B,C,D,E IN SPECIFIC HEAT EQUATION    C
C   AT           THERMAL EXPANSION COEFFICIENT MULTIPLIED BY V(MOL) C
C   BP           COMPRESSIBILITY COEFFICIENT MULTIPLIED BY V(MOL) C
C   WA           MOLES OF H2O INVOLVED IN REACTION                C
C   CO           MOLES OF CO2 INVOLVED IN REACTION                C
C   GO           GIBBS FREE ENERGY OF REACTION AT 298.15°K        C
C   G            GIBBS FREE ENERGY EXCLUDING XCO2 and XH2O        C
C   GG AND GH    GIBBS FREE ENERGY INCLUDING XCO2 and XH2O        C
C   V            MOLAR VOLUME OF SOLIDS OF REACTION FOR SOLIDS    C
C   FFCO2        FUGACITY OF CO2=RT*LN(FCO2) AFTER                C
C                HOLLAND AND POWELL (1985)                        C
C                (DIVIDED BY 0.004184 TO CONVERT KJ TO CAL)       C
C   FFH2O        FUGACITY OF H2O=RT*LN(FH2O)                      C
C                HOLLAND AND POWELL (1985)                        C
C                (DIVIDED BY 0.004184 TO CONVERT KJ TO CAL)       C
C   XCO2=X(1)    MOLE FRACTION OF CO2                             C
C   XH2O=X(5)    MOLE FRACTION OF H2O ASSUMED=1-XCO2              C
C   K            EQUILIBRIUM CONSTANT                             C
C   R            GAS CONSTANT = 1.987 CAL/°K                      C
C   INPUT        S,A,B,C,D,E,AT,BP,K,WA,CO,STEMP(STARTING TEMP),TSTEP C
C                (TEMPERATURE STEP),SPRESS(STARTING PRESSURE)     C
C   MATRIX       IS P = 1 TO 100000 BAR; T = 400 TO 1800°K        C
C   X,GAM,PUREG  MOLE FRACTION, FUGACITY COEFFICIENT IN MIXTURE,  C
C                AND FUGACITY COEFFICIENT OF PURE PHASE FOR       C
C                CARBON DIOXIDE, CARBON MONOXIDE, METHANE HYDROGEN C
C                AND WATER. FOR PROGRAM GRAPHITE (HOLLOWAY)       C
C-----------------------------------------------------------------C
      REAL LXCO2,K
      REAL X(5),GAM(5),PUREG(5)
C--SET G TO 0.0 SO THAT FIRST CHECK ON G AND GSTOP WILL ALLOW IT TO---
C--CONTINUE. G CHANGES SIGN WHEN XCO2 IS 1----------------------------
      G=0.0
      DO 1 I=1,5
      X(I)=0.0
      GAM(I)=0.0
    1 PUREG(I)=0.0
      R=1.9872
      READ(3,3000)H,S,V,A,B,C,D,E,AT,BP,K,WA,CO,STEMP,TSTEP,SPRESS,
     *            EPRESS,PSTEP
 3000 FORMAT(F10.0,5F10.6,F10.2/3F10.6,5F9.3,3F9.1)
C--D.M. CARMICHAEL(1978),P.63-----------------------------------------
C--CALCULATE RIC WITH GIVEN S,A,B,C,D AND E--------------------------
      RIC=S-5.697*A-0.29815*B+5.6247E-1*C+0.1158*D-4.4446E-2*E
C--CALCULATE THE GIVEN GO,RIC,A,B,C,D AND E--------------------------
      GO=H-298.15*S
```

```
      THE=GO+298.15*RIC+1400.6*A+44.4467*B+167.7*C
     *-69.0681*D+4.4173*E
      P=SPRESS
C--THE PRESSURE LOOP BEGINS HERE-------------------------------------
   99 CONTINUE
   98 G=-G
      UXCO2=0.0
C--IDECRE = 0 FOR INCREASING TEMPERATURE-----------------------------
      IDECRE=0
      P=P=PSTEP
      IF(P.GT.EPRESS) GOTO 999
      TK=STEMP
      WRITE(6,2500) I,IOUT,IDECRE
C--THE TEMPERATURE LOOP STARTS HERE----------------------------------
      DO 100 IT=1,500
      IF(IDECRE.EQ.0) TK=TK+TSTEP
      IF(IDECRE.EQ.1) TK=TK-TSTEP
      IF(IDECRE.EQ.0) X(1)=0.001
      IF(IDECRE.EQ.1) X(1)=UXCO2
C--UXCO2 IS XCO2 AFTER INCREMENT SO FOR DECLINING TEMPERATURE---------
C--START WITH UXCO2--------------------------------------------------
      X(5)=1.0-X(1)
      ITNUM=0
      CALL RKMIX(ITNUM,TK,P,X,GAM,PUREG)
      PV=P*(V+(AT/1.0E+5)*(TK-298.15)-(BP/1.0E+6)*P/2.)
      FFCO2=R*TK*ALOG(PUREG(1)*P)
      FFH2O=R*TK*ALOG(PUREG(5)*P)
      GSTOP=G
      G=THE+(A-RIC)*TK-A*TK*(ALOG(TK))-0.0005*B*TK*
     * TK-50000.0*C/TK+4.0*D*SQRT(TK)-E(TK*TK*TK)/6.0E+6+CO
     * *(FFCO2)+PV+WA*(FFH2O)+R*TK*(ALOG(K))
      IF(G.GT.0.0.AND.GSTOP.LT.0.0.AND.IOUT.EQ.11.AND.RINC.EQ.0.1.
     * AND.IDECRE.EQ.1) GOTO 99
      IF(G.LT.0.0.AND.GSTOP.GT.0.0.AND.IOUT.EQ.11.AND.RINC.EQ.0.1.
     * AND.IDECRE.EQ.1) GOTO 99
      WRITE(6,6020)TK,G,P,GXSCO2,GXSH2O,FFCO2,FFH2O
 6020 FORMAT(' TK=',F7.1,' P=',F7.1,' G=',F8.0,'  GXSCO2=',F8.1,
     * ' GXSH2O=',F8.1,' FFCO2=',F8.1,' FFH2O=',F8.1)
      IF(X(5).LT.0.0) X(5)=1.0E-9
      IF(X(1).LT.0.0) X(1)=1.0E-9
C--INITIALISE THE CO2 LOOP-------------------------------------------
C--------------------------------------------------------------------
C--NONIDEAL MIXING AFTER THE MODIFIED REDLICH-KWONG EQUATION----------
C--WITH FORMATION OF HYDROCARBON ACID---------------------------------
C     GXSCO2= R*TK*ALOG(GAM(1)/PUREG(1))
C     GXSH2O= R*TK*ALOG(GAM(5)/PUREG(5))
C--NONIDEAL REGULAR MIXING MODEL; FORMATION OF CA(H2(CO3)2)-----------
      GXSCO2= ((51.0-0.053*TK)*(X(5)*X(5))/0.004184)
      GXSH2O= ((51.0-0.053*TK)*(X(1)*X(1))/0.004184)
C--IDEAL MIXING------------------------------------------------------
C     GXSCO2=0.0
C     GXSCO2=0.0
C--------------------------------------------------------------------
      GG=G+CO*R*TK*(ALOG(X(1)))+WA*R*TK*(ALOG(X(5)))+
     *   CO*GXSCO2+WA*GXSH2O
      RINC=0.1
      N=0
```

```
C--THE CO2 LOOP BEGINS HERE-----------------------------------------
  400 CONTINUE
      IOUT=1
C--THE LOOP TO FIND THE PARTICULAR DECIMAL PLACE BEGINS HERE----------
      DO 300 I=1,10
      X(1)=X(1)+RINC
      X(5)=1.0001-X(1)
      IF(X(5).LT.0.0) X(5)=1.0E-9
      IF(X(1).LT.0.0) X(1)=1.0E-9
      CALL RKMIX(ITNUM,TK,P,X,GAM,PUREG)
C-------------------------------------------------------------------
C--NONIDEAL MIXING AFTER THE MODIFIED REDLICH AND KWONG EQUATION------
C--WITH FORMATION OF HYDROCARBON ACID---------------------------------
C     GXSCO2= R*TK*ALOG(GAM(1)/PUREG(1))
C     GXSH2O= R*TK*ALOG(GAM(5)/PUREG(5))
C--NONIDEAL REGULAR MIXING MODEL; FORMATION OF CA(H2(CO3)2)-----------
      GXSCO2= ((51.0-0.053*TK)*(X(5)*X(5))/0.004184)
      GXSH2O= ((51.0-0.053*TK)*(X(1)*X(1))/0.004184)
C--IDEAL MIXING-----------------------------------------------------
C     GXSCO2=0.0
C     GXSCO2=0.0
C-------------------------------------------------------------------
      GH=G+CO*R*TK*(ALOG(X(1)))+WA*R*TK*(ALOG(X(5)))+
     *   CO*GXSCO2+WA*GXSH2O
      IF(GH.GT.0.0.AND.GG.LT.0.0) GOTO 901
      IF(GG.GT.0.0.AND.GH.LT.0.0) GOTO 901
      GG=GH
      IOUT=IOUT+1
C--THE LOOP TO FIND THE PARTICULAR DECIMAL PLACE ENDS HERE------------
  300 CONTINUE
      IF(I.EQ.IOUT.AND.RINC.EQ.0.1.AND.UXCO2.GT.0.0) IDECRE=1
  500 CONTINUE
      IF(TK.EQ.STEMP) GOTO 98
C--THE '100' TEMPERATURE LOOP ENDS HERE------------------------------
  100 CONTINUE
      IF(P.LT.EPRESS) GOTO 98
      GOTO 999
  901 UXCO2=X(1)
      LXCO2=X(1)-RINC
      X(1)=LXCO2
      N=N+1
      IF(N.EQ.3) GOTO 911
      RINC=10.0**(-N-1)
C--THE CO2 LOOP ENDS HERE-------------------------------------------
      GOTO 400
C--THE CO2 LOOP ENDS HERE AFTER FINDING XCO2 TO 4 DECIMAL PLACES------
  911 WRITE(6,6040) UXCO2,LXCO2,RINC,I
 6040 FORMAT(T69,'UXCO2=',F5.3,' LXCO2=',F5.3,' RINC=',F9.7,' I=',
     * I2)
      IF(UXCO2.GE.1.0) GOTO 99
      GOTO 500
  999 STOP
      END
C----------------------------SUBROUTINE-------------------------------
      SUBROUTINE RKMIX(ITNUM,T,P,Y,GAM,PUREG)
C--CALCULATION OF FLUID MIXTURE PROPERTIES USING DE SANTIS AND OTHERS
C  (1974) MODIFICATION OF THE REDLICH-KWONG EQUATION.
```

```
C  THIS PROGRAM FOR USE WITH PROGRAM GRAPHITE.
C  P IS IN ATMOSPHERES, T IS IN DEG. CELSIUS, Y(I) IS THE
C  MOLE FRACTION. GAM(I) IS THE FUGACITY COEFFICIENT FOR
C  MIXTURES (=FUGACITY(I)/TOTAL PRESSURE).
C  WRITTEN BY JOHN R. HOLLOWAY
C-----------------------------------------------------------------
      REAL A(5), B(5), Y(5), ASUM(5), BSUM(5), GAM(5), PUREG(5)
C--SPECIES ORDER IS CO2, CO, CH4, H2, H2O----------------------------
C--REDLICH-KWONG A AND B PARAMETERS----------------------------------
      DATA A/46.E6,16.98E6,31.59E6,3.56E6,35.E6/
      DATA B/2.97E1,2.738E1,2.9703E1,1.515E1,1.46E1/
      DATA MIXNUM/5/
C--DEFINE THE GAS CONSTANT IN CM3*ATM*DEG-1*MOLE-1.------------------
      R=82.057
      TCEL=T-273.15
      IF(ITNUM.GT.0.) GOTO 110
      R2T=R*R*T**2.5
      RT=R*T**1.5
C--AH2OM AND ACO2M ARE A(T) FUNCTIONS DEFINED BY DESANTIS AND--------
C--OTHERS (1974)-----------------------------------------------------
      AH2OM=166.8-.19308*TCEL+.1864E-3*TCEL*TCEL-.71288E-7*TCEL**3
      IF(TCEL.GT.1200.) AH2OM=140.-0.050*TCEL
      AH2OM=AH2OM*10.E5
      ACO2M=73.03-.0714*TCEL +2.157E-5*TCEL*TCEL
      ACO2M=ACO2M*10.E5
      XK=EXP(-11.071+(5953./T)-(2.746E6/(T*T))+(4.646E8/(T*T*T)))
      CO2H2O=XK*0.5*R2T
      CO2H2O=CO2H2O+SQRT(A(1)*A(5))
  110 CONTINUE
      K=1
      ASUM(K)=0.0
      BSUM(K)=0.0
C--CALC COMPOSITION DEPENDENT TERMS----------------------------------
      DO 101 I=1,MIXNUM
      BSUM(K)=BSUM(K)+B(I)*Y(I)
      DO 101 J=1,MIXNUM
      IF(I.EQ.J) GOTO 140
      IF(I.EQ.5.AND.J.EQ.1.) GOTO 150
      IF(I.EQ.1.AND.J.EQ.5.) GOTO 150
      ASUM(K)=ASUM(K)+Y(I)*Y(J)*SQRT(A(I)*A(J))
      GOTO 101
  140 CONTINUE
      IF(I.NE.5.) GOTO 141
      ASUM(K)=ASUM(K)+Y(I)*Y(J)*AH2OM
      GOTO 101
  141 IF(I.NE.1.) GOTO 142
      ASUM(K)=ASUM(K)+Y(I)*Y(J)*ACO2M
      GOTO 101
  142 ASUM(K)=ASUM(K)+Y(I)*Y(J)*A(I)
      GOTO 101
  150 ASUM(K)=ASUM(K)+Y(I)*Y(J)*CO2H2O
  101 CONTINUE
      AMIX=SQRT(ASUM(K)/(BSUM(K)*RT)
      BMIX=BSUM(K)/(R*T)
C--CALCULATION OF PRESSURE DEPENDANT TERMS---------------------------
      CALL REDKW(T,P,BMIX,A2BMIX,FP,Z)
C--CALCULATE V-------------------------------------------------------
```

```
      VOL=R*T*Z/P
      CHI1=ALOG(VOL/(VOL-BSUM(1)))
      CHI2=ALOG((VOL+BSUM(1))/VOL)
      CHI3=BSUM(1)/(VOL+BSUM(1))
      DO 202 J=1, MIXNUM
      AA=A(J)
      BB=B(J)
      IF(J.EQ.1.) AA=ACO2M
      IF(J.EQ.5.) AA=AH2OM
      A2B=AA/(BB*RT)
      BBB=BB/(R*T)
      CHI5=BB/(VOL-BSUM(1))
      CHI6=(ASUM(1)*BB)/(RT*BSUM(1)**2)
      ATOP=0.0
      DO 119 KK=1,MIXNUM
      Z1=A(J)
      Z2=A(KK)
      QQQ=SQRT(Z1*Z2)
      IF(KK.EQ.1.AND.J.EQ.5.OR.KK.EQ.5.AND.J.EQ.1.)QQQ=CO2H2O
      IF(KK.EQ.1.AND.J.EQ.1.)QQQ=ACO2M
      IF(KK.EQ.5.AND.J.EQ.5.)QQQ=AH2OM
      ATOP=ATOP+Y(KK)*QQQ
  119 CONTINUE
      CHI7=(2.0*ATOP)/(RT*BSUM(1))
      PHI=CHI1+CHI5-CHI7*CHI2+CHI6*(CHI2-CHI3)-ALOG(Z)
      PHI=EXP(PHI)
      IF(ITNUM.GT.0.0) GOTO 201
      CALL REDKW(T,P,BBB,A2B,FP,ZPURE)
      PUREG(J)=FP
  201 GAM(J)=PHI
  202 CONTINUE
      RETURN
      END
C
C
C*******************************SUBROUTINE*****************************
      SUBROUTINE REDKW(T,P,B,A2B,FP,Z)
C--A SUBROUTINE TO CALCULATE COMPRESSIBILITY FACTOR AND FUGACITY------
C  COEFFICIENT WITH THE REDLICH-KWONG EQUATION FOLLOWING THE METHOD
C  OF EDMISTER(1968). T IS IN KELVIN, P IS IN ATMOSPHERES, FP IS THE
C  FUGACITY COEFFICIENT (=FUGACITY/TOTAL PRESSURE)
C  WRITTEN BY JOHN HOLLOWAY(1973)
C  THIS IS A SOLUTION FOR A SUPERCRITICAL FLUID AND
C  RETURNS A VALUE OF 1.0 FOR FP WHEN ANY ARGUMENTS OUT OF RANGE.
C-----------------------------------------------------------------------
      BP=B*P
      TH=1./3.
      IF(A2B.LE.0.0) A2B=0.001
      RR=-A2B*BP*BP
      QQ=BP*(A2B-BP-1.01)
      XN=(QQ/3.)+RR-(2./27.)
      XM=QQ-1./3.
      ARG=((XN*XN)/4.)+(XM*XM*XM/27.)
      IF(ARG.GT.0.0) GOTO 5
      IF(ARG.LT.0.0) GOTO 15
      FP=1.0
      Z=1.0
```

```
      RETURN
   15 COSPHI=SQRT((XN*XN/4.)/(-XM*XM*XM/27.))
      IF(XN.GT.0.0) COSPHI=-COSPHI
      TANPHI=SQRT(1.-COSPHI*COSPHI)/COSPHI
      PHI=ATAN(TANPHI)/3.0
      FAC=2.*SQRT(-XM/3.)
      R1=FAC*COS(PHI)
      R2=FAC*COS(PHI+120.)
      R3=FAC*COS(PHI+240.)
      PHI=3.*PHI
C--SQRT FOR LARGEST ROOT-----------------------------------------------
      RH=R2
      IF(R1.GT.R2) RH=R1
      IF(R3.GT.RH) RH=R3
      Z=RH+TH
      GOTO 20
    5 X=SQRT(ARG)
      F=1.0
      XN2=-XN/2
      XMM=XN2+X
      IF(XMM.LT.0.0) F=-1.0
      XMM=F*((F*XMM)**TH)
      F=1.0
      XNN=XN2-X
      IF(XNN.LT.0.0) F=-1.0
      XNN=F*((F*XNN)**TH)
      Z=XMM+XNN+TH
   20 ZBP=2-BP
      IF(ZBP.LT.0.00001) ZBP=0.00001
      BPZ=1.+BP/Z
      FP=Z-1.-ALOG(ZBP)-A2B*ALOG(BPZ)
      IF(FP.LT.-50..OR.FP.GT.50.) FP=0.000001
      FP=EXP(FP)
      RETURN
      END
```

```
C-----------------------------------------------------------------------C
C  COMPUTER PROGRAM GP FORTRAN                                          C
C  THE PROGRAM CALCULATES THE STANDARD STATE FREE ENERGY OF A           C
C  REACTION. GIVEN THE REACTION COEFFICIENTS. COEFFICIENTS OF           C
C  REACTANTS GET NEGATIVE SIGN AND PRODUCTS GET POSITIVE SIGN           C
C  THE DATA MATRIX IS A SERIES OF H,S,V,A,B,C,D,E,AT,BP,RNUMBER         C
C  FOR NN COMPONENTS                                                    C
C-----------------------------------------------------------------------C
      REAL AA(10,29),BB(10),K
      J=0
   11 J=J+1
      READ (1,1000,END=999)(AA(I,J),I=1,10)
      WRITE(2,1000)(AA(I,J),I=1,10)
 1000 FORMAT (F10.0,6F10.4/3F10.4)
      GOTO 11
  999 READ (5,5000)K,WA,CO,STEMP,TSTEP,SPRESS,EPRESS,PSTEP
 5000 FORMAT(/8F9.3)
      DO 100 I=1,10
```

```
  100 BB(I)=0.0
    1 CONTINUE
      READ(5,5010,END=300)COEFF,NUMBER
 5010 FORMAT(F6.3,I4)
      DO 200 I=1,10
      BB(I)=BB(I)+COEFF*AA(I,NUMBER)
  200 CONTINUE
      GOTO 1
  300 WRITE(3,3000)BB,K,WA,CO,STEMP,TSTEP,SPRESS,EPRESS,PSTEP
 3000 FORMAT (F10.0,5F10.6,F10.2/3F10.6/5F9.3,3F9.1)
      STOP
      END
```

GP FORTRAN

```
C$ENTRY
  ---K---  ---WA---  ---CO---  --STEMP-  --TSTEP-  -SPRESS-  -EPRESS-  -PSTEP-
   1.0       0.0       1.0      1000.0     10.0      0.0      8000.0   2000.0
-1.0      2
-1.0      3
 1.0      1
 1.0      23
```

THE INPUT EXAMPLE IS FOR REACTION: CALCITE+DIOPSIDE=AKERMANITE+CO2
THE COEFFICIENTS ON THE LEFT HAND SIDE OF THE REACTION GET NEGATIVE SIGN. THE COEFFICENTS ON THE RIGHT HAND SIDE GET POSITIVE SIGN.
THE NUMBER REFERS TO THE POSITION OF THE PHASE IN THE DATA FILE (AKERMANITE = 1).
THE DATA FOR THE TEMPORARY DATA FILE FT01FF001 CAN BE TAKEN FROM TABLE 2, E.G.:

```
   -923777.    50.0300     2.2180    60.0900    11.4000  -11.4000       0.00
     0.0000     7.0985     2.6291              AKERMANITE
    .......    .......    ......    .......    .......   .......       ....
    .......    .......    ......              xxxxxxxxxx
```

APPENDIX III

P-T-X_{CO2} Diagrams for Subsystems 1-72

Subsystems 1-72 illustrates 72 invariant points given in Table 5a and b. The subsystem numbers refer to the numbers in Table 5a and b. The invariant points as well as the position of the equilibrium reactions are shown at different pressures, temperatures and carbon dioxide molefractions (X_{CO2} = 0.1; 0.3; 1). Water has been assumed to be the diluent for $X_{CO2} < 1$. The data for the calculations have been taken from Table 2 using the computer program GG5 (Appendix II). The relativ positions of the reaction curves used in the petrogenetic grid shown in Figure 11 is based on these calculations. The derivation and construction of the subsystems is explained and discussed in Chapter B 5. Involved minerals: Ak: akermanite; Cc: calcite; Di: diopside; Fo: forsterite; Ge: gehlenite; Mo: monticellite; Me: merwinite; Pe: periclase; Sp: spinel; Wo: wollastonite.

Subsystems 1+5

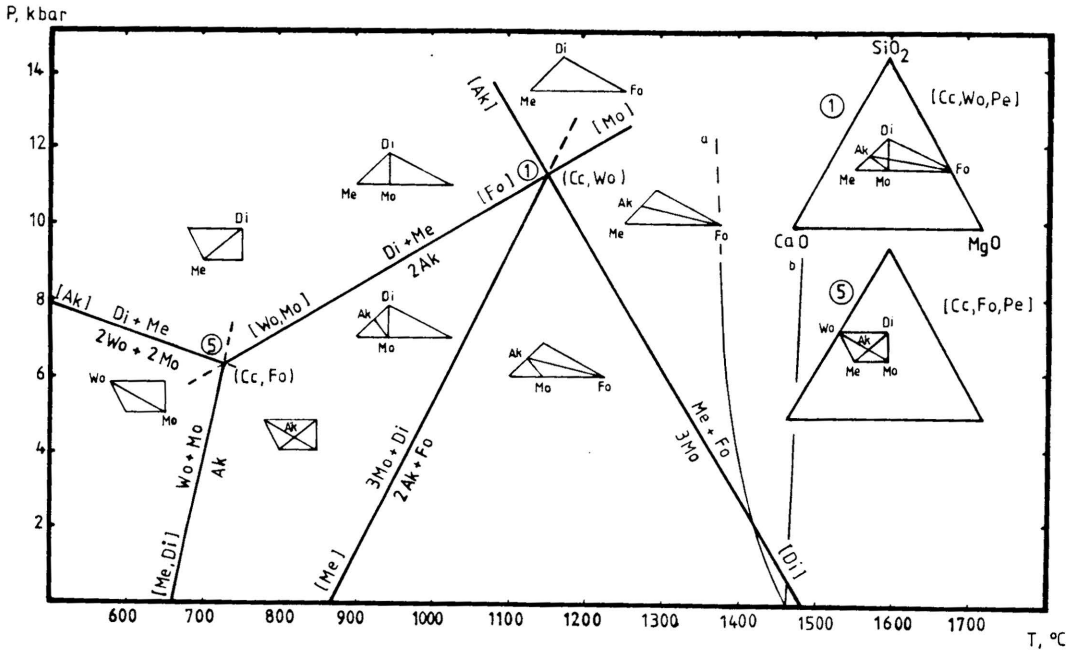

Subsystem 2

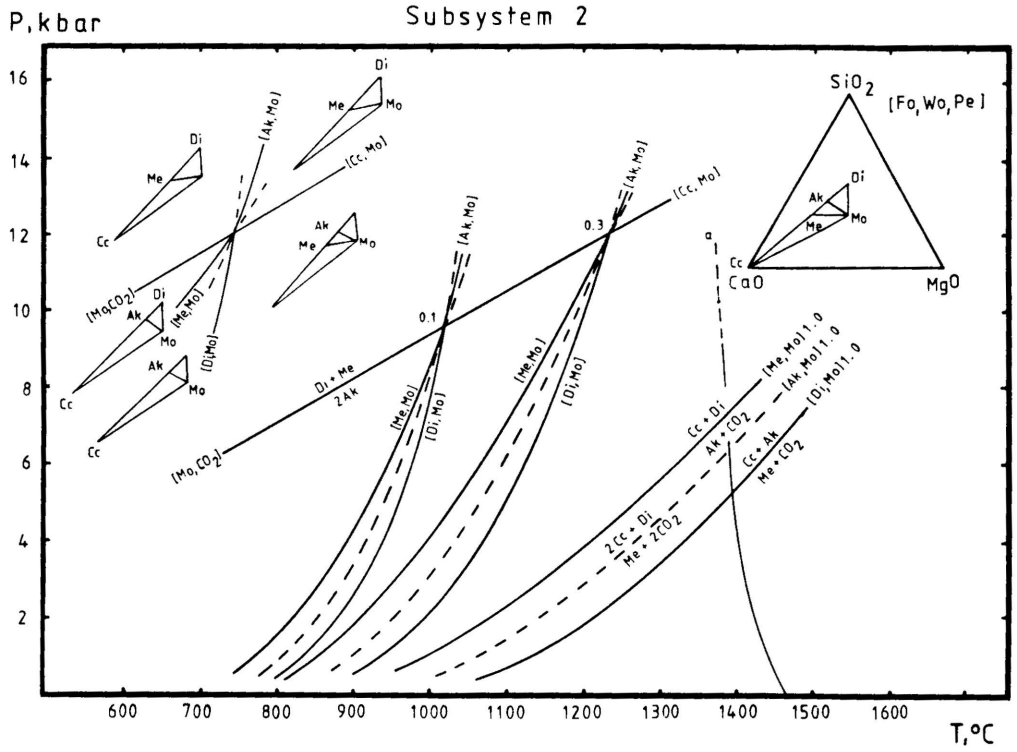

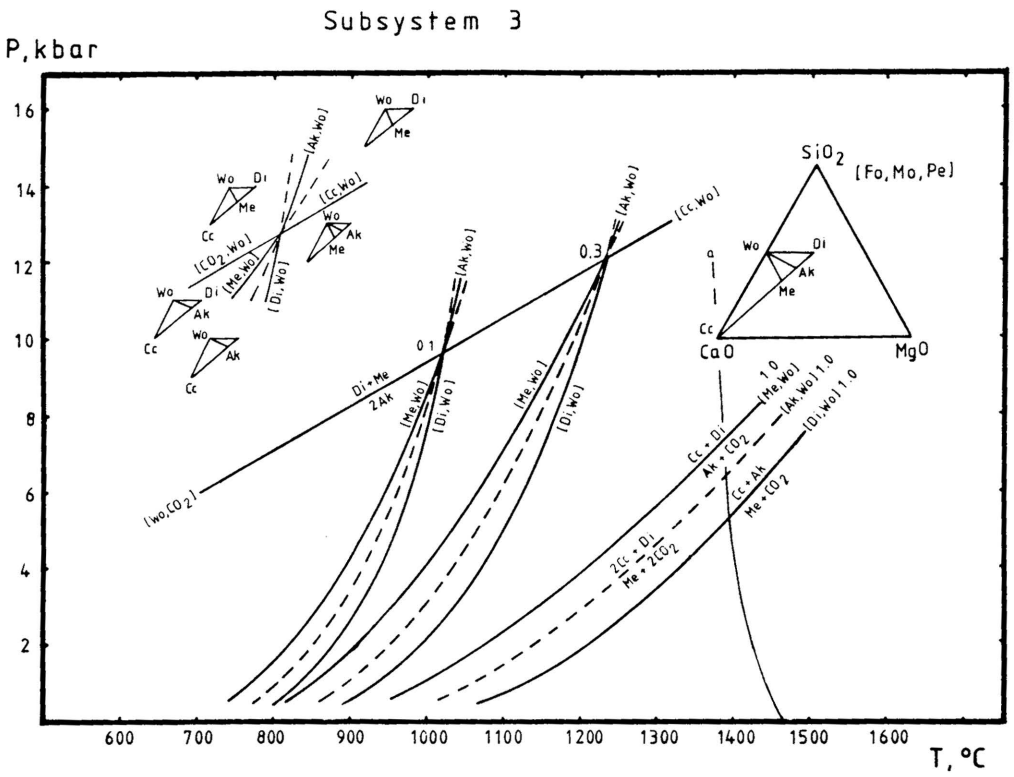

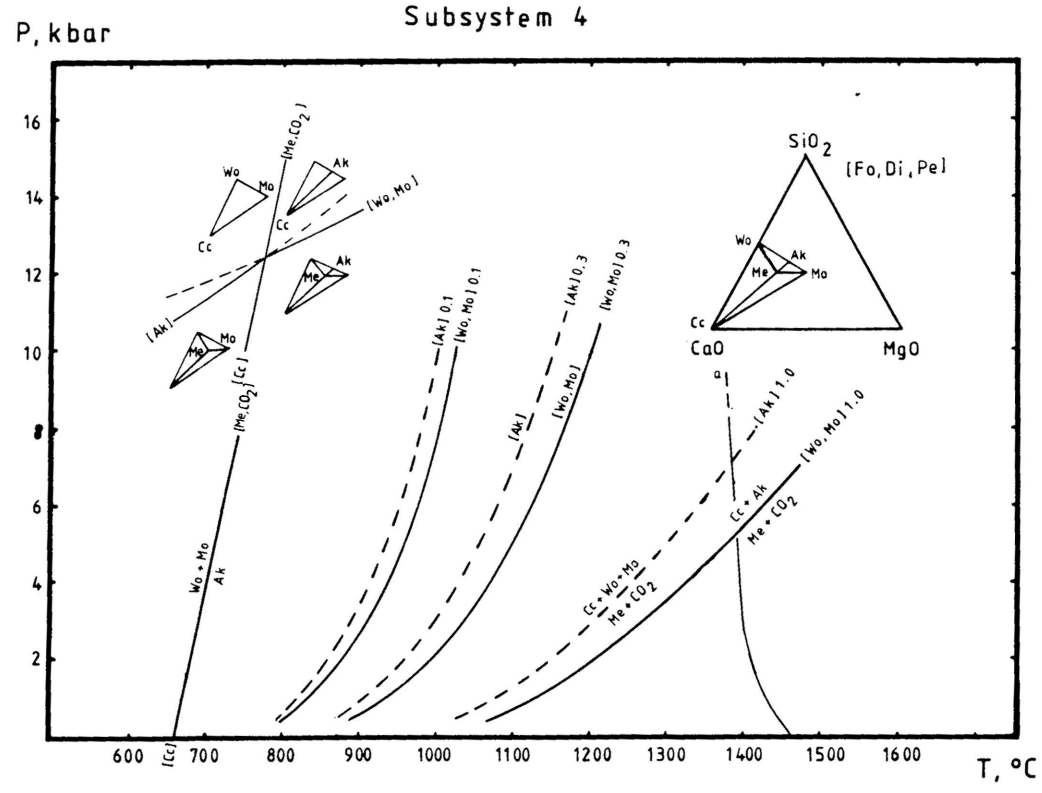

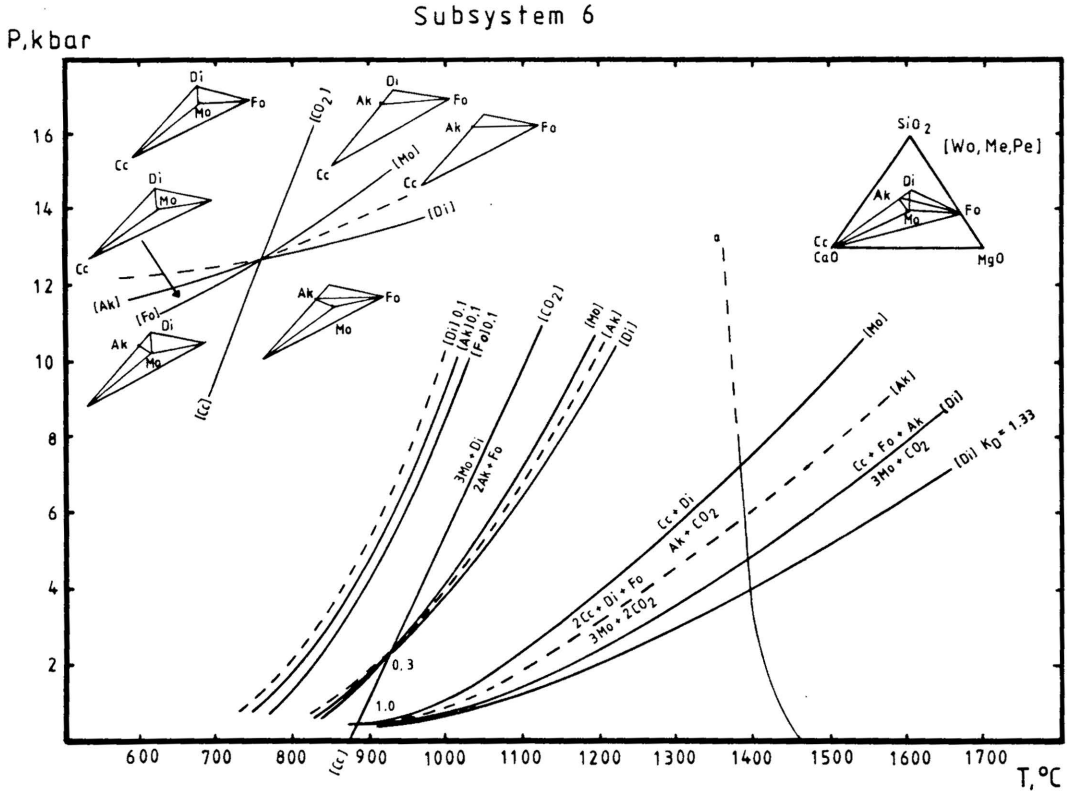

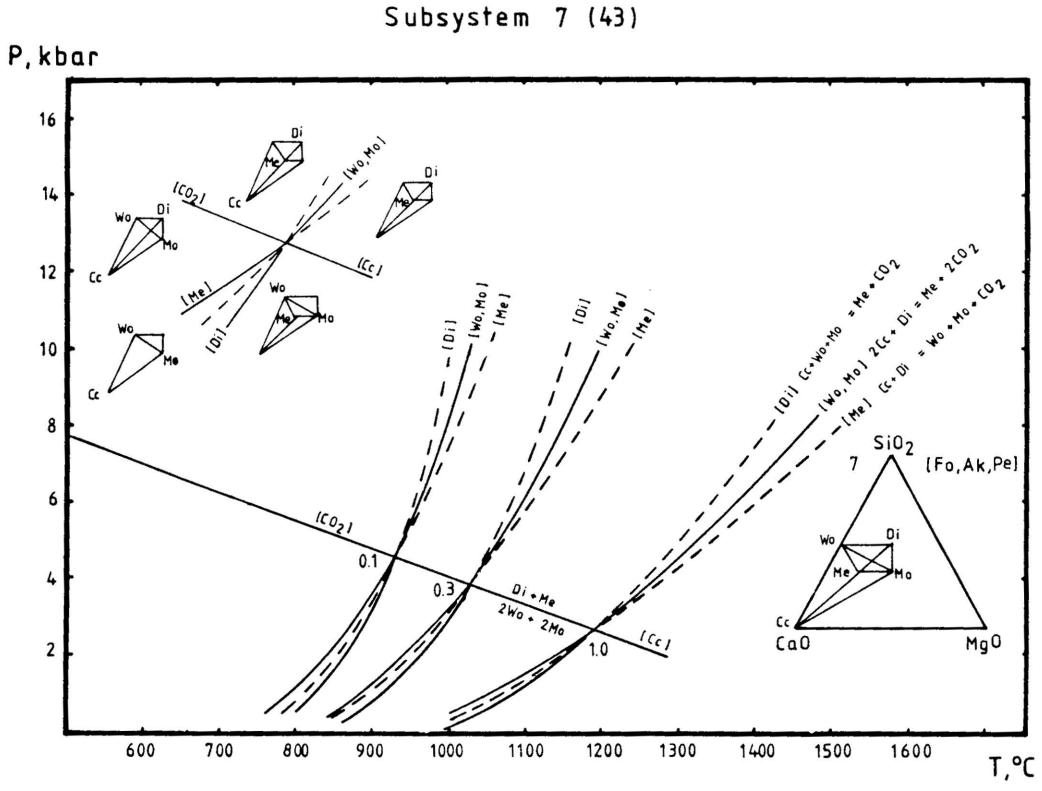

Subsystem 8 (44)

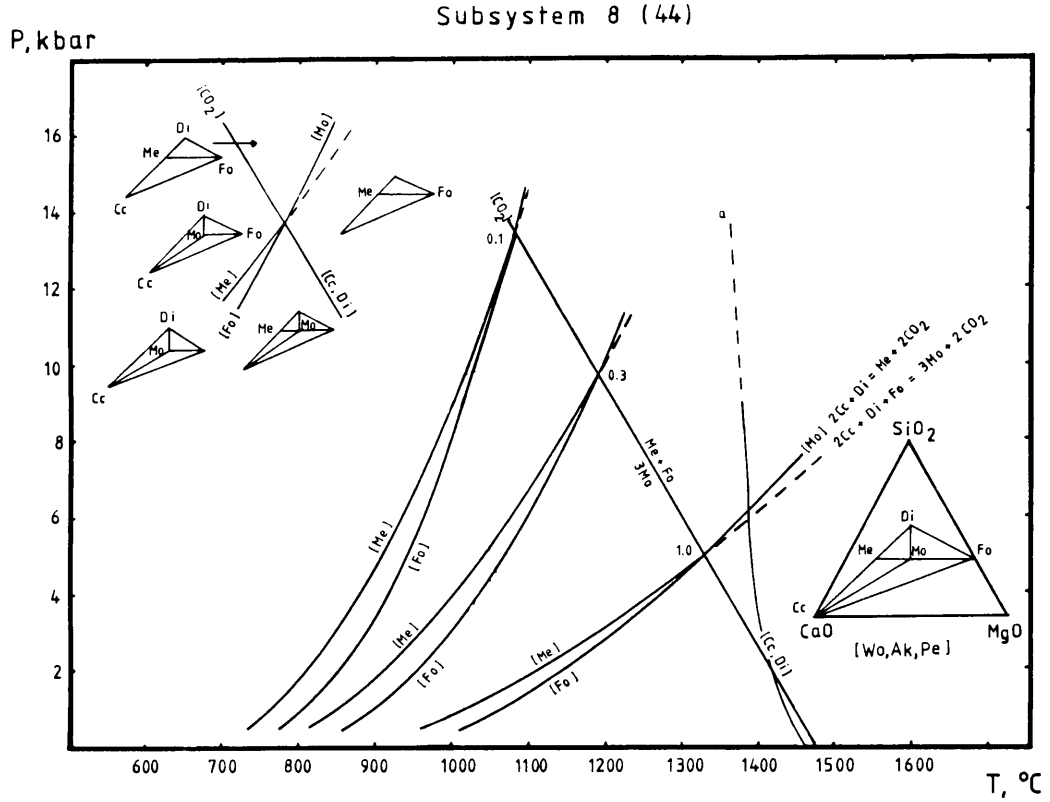

Subsystem 9

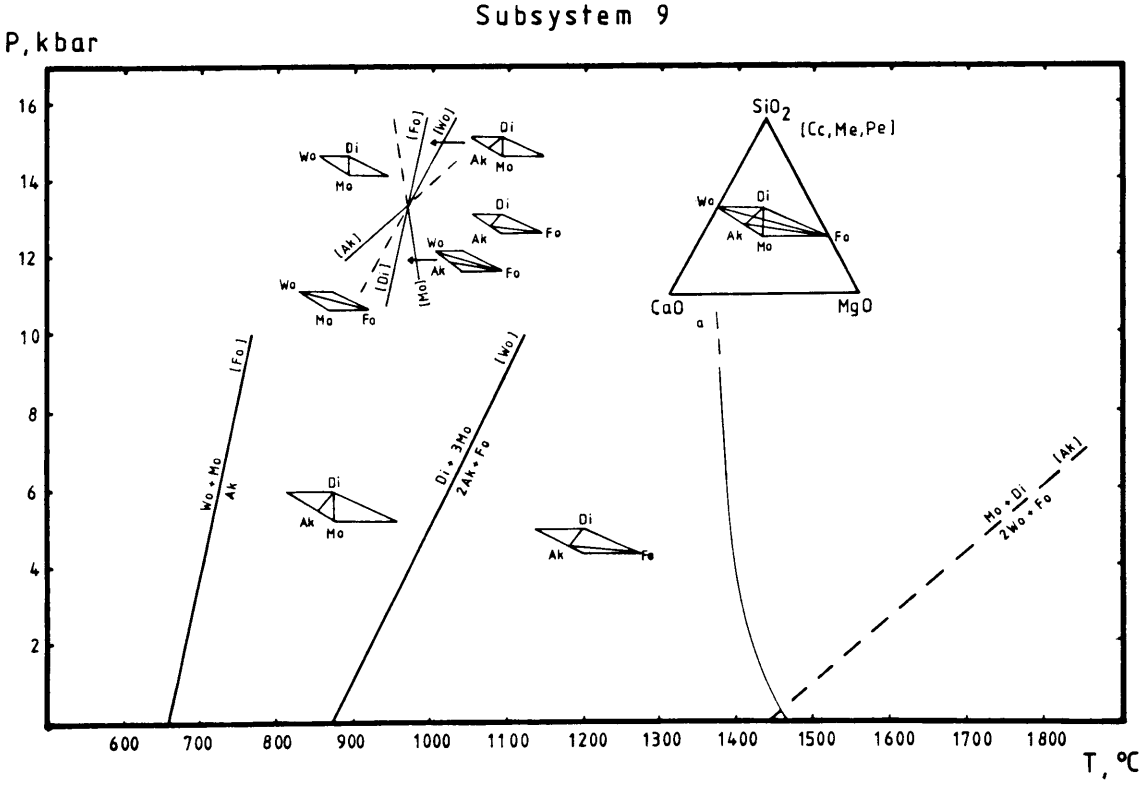

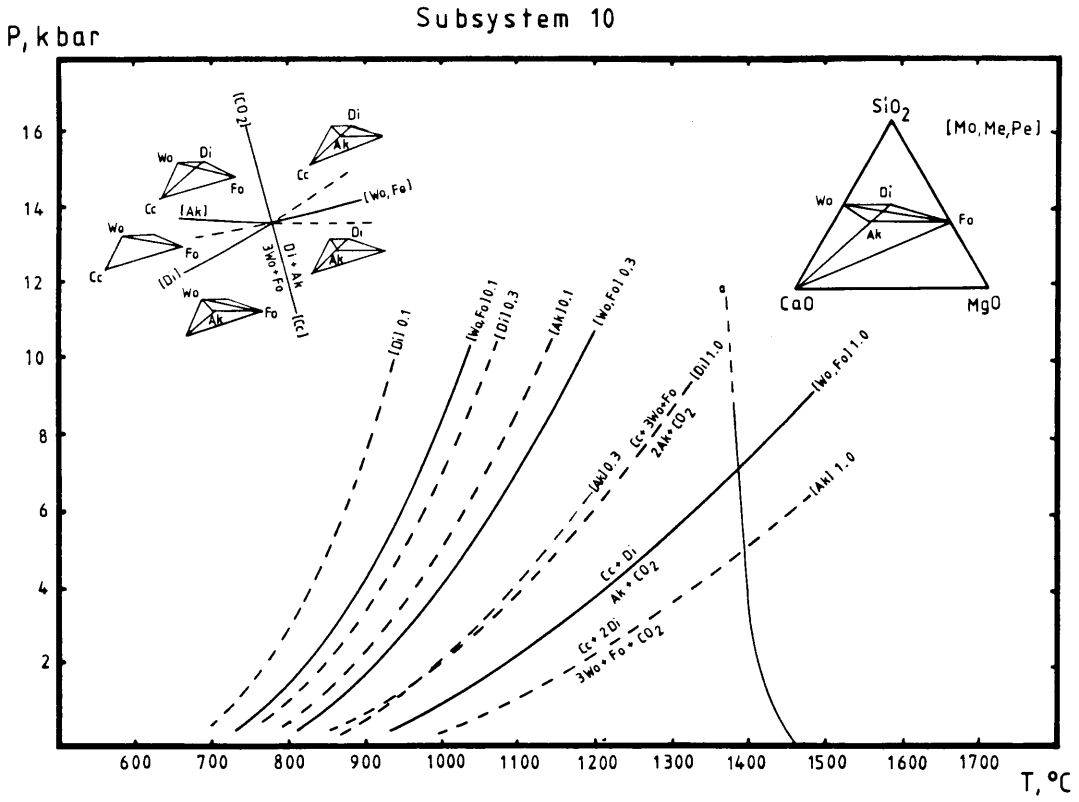

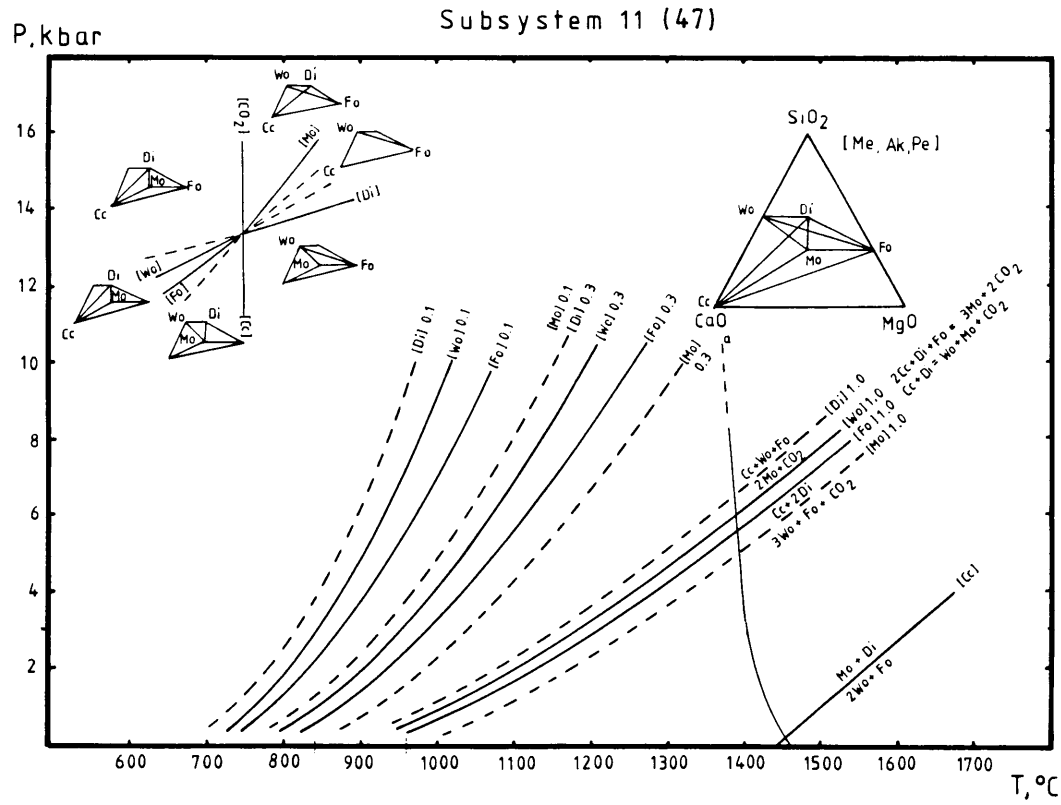

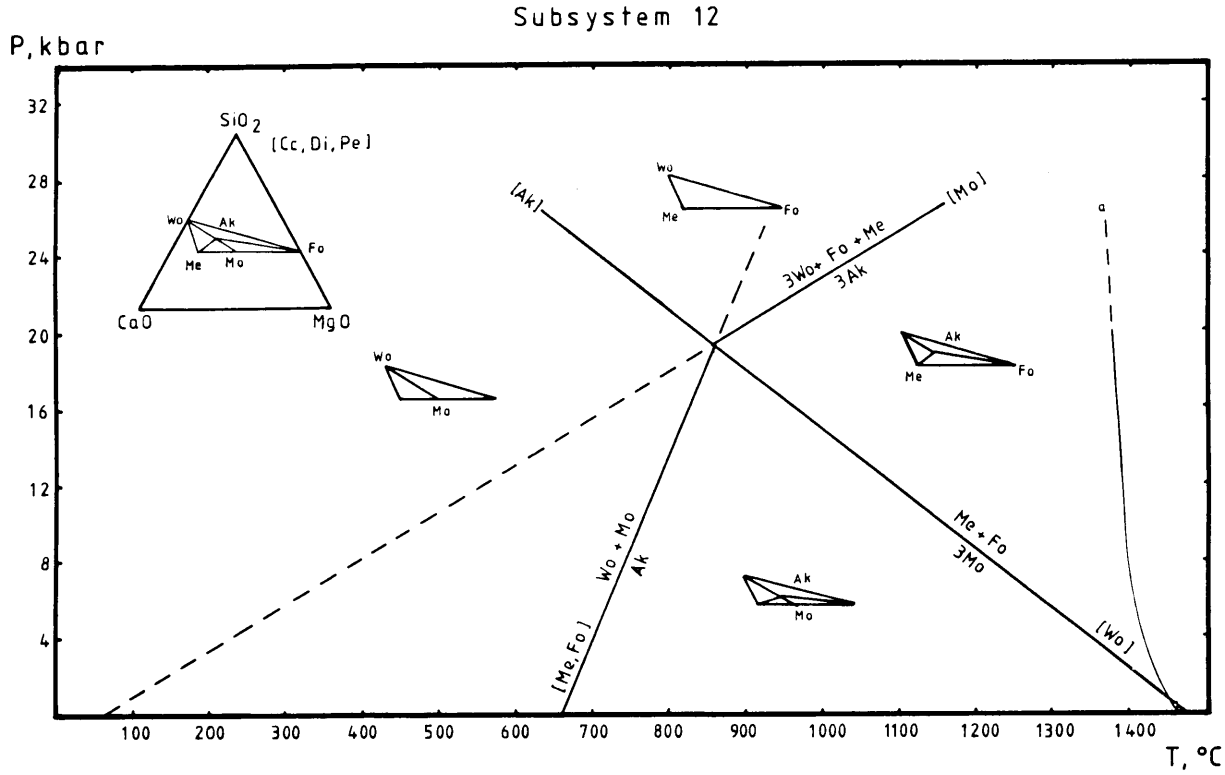

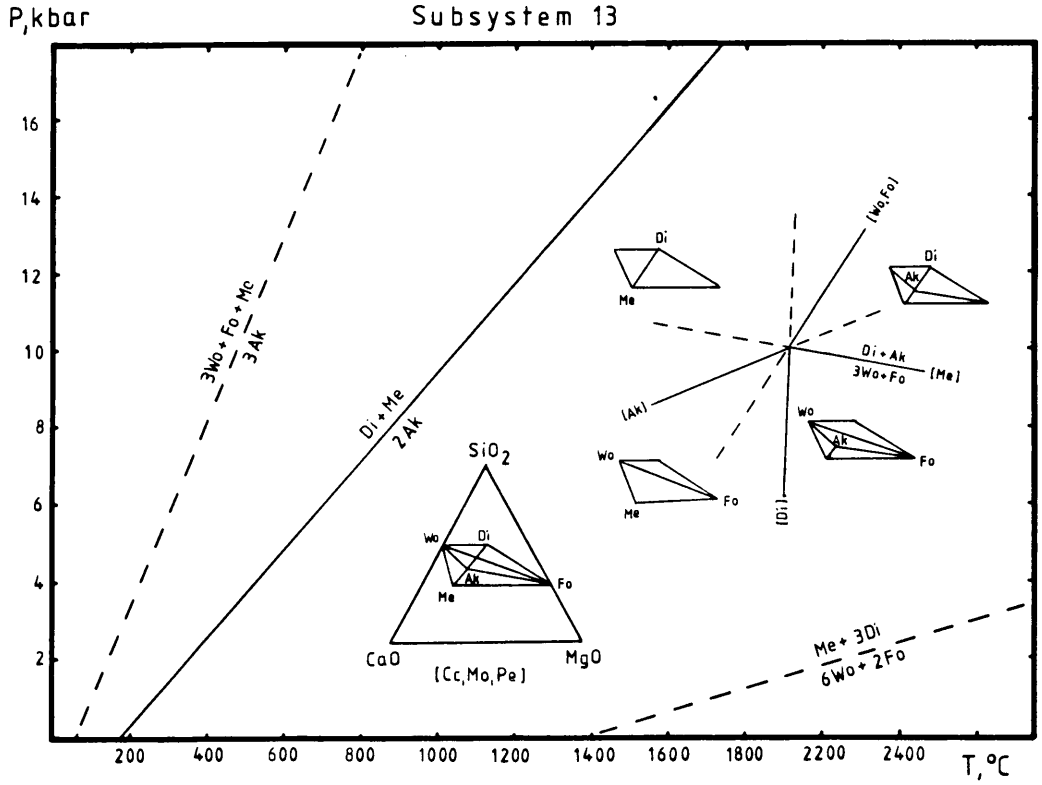

Subsystem 14 (50)

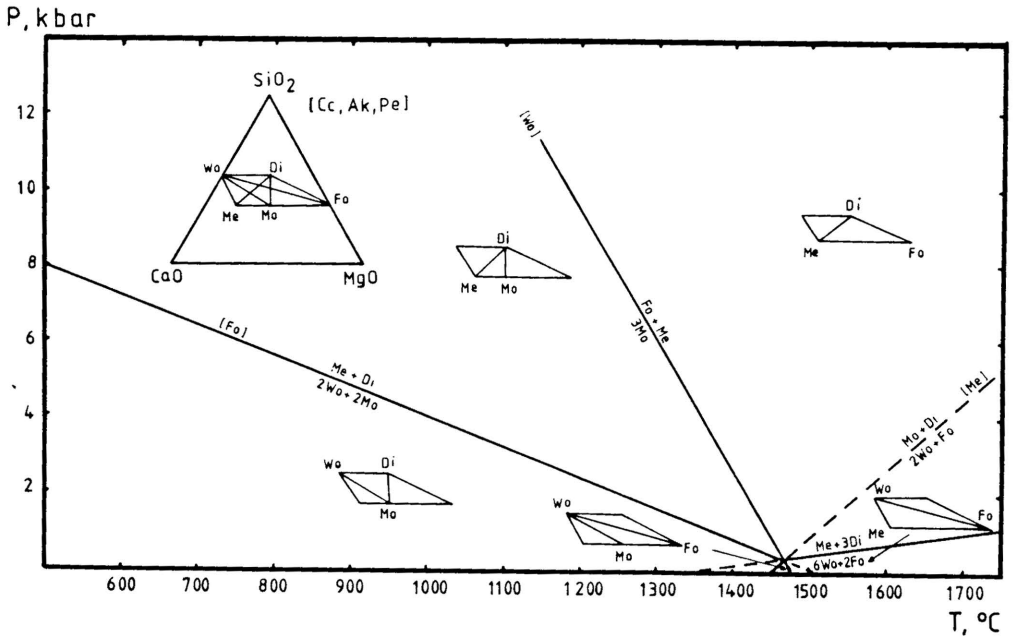

Subsystem 15

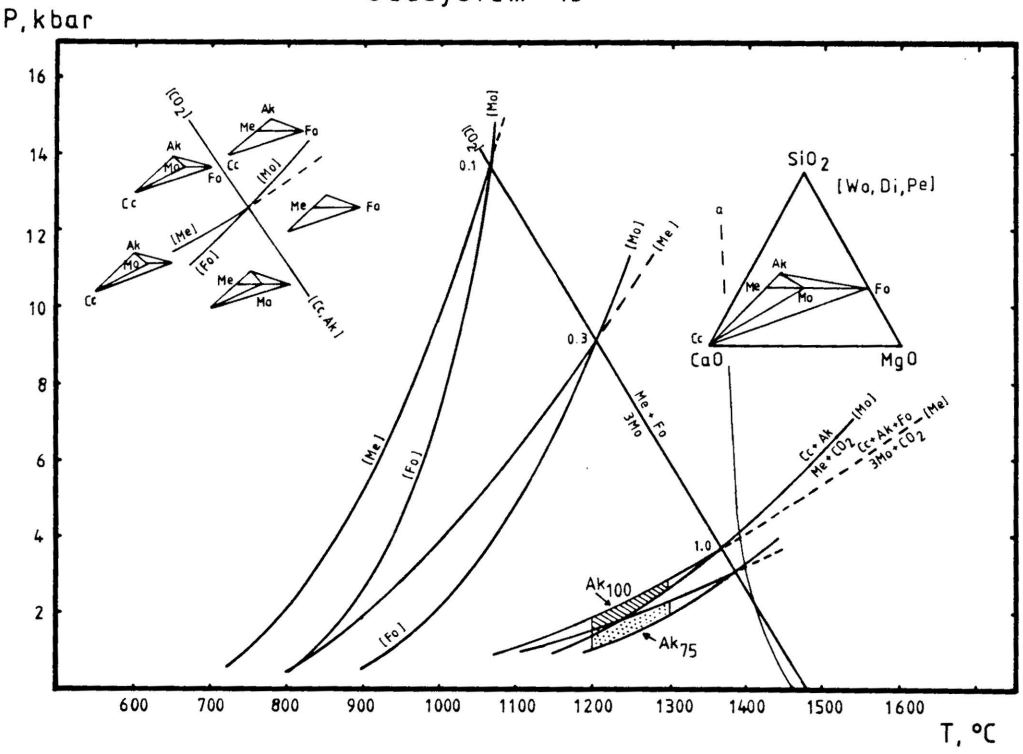

Subsystem 16

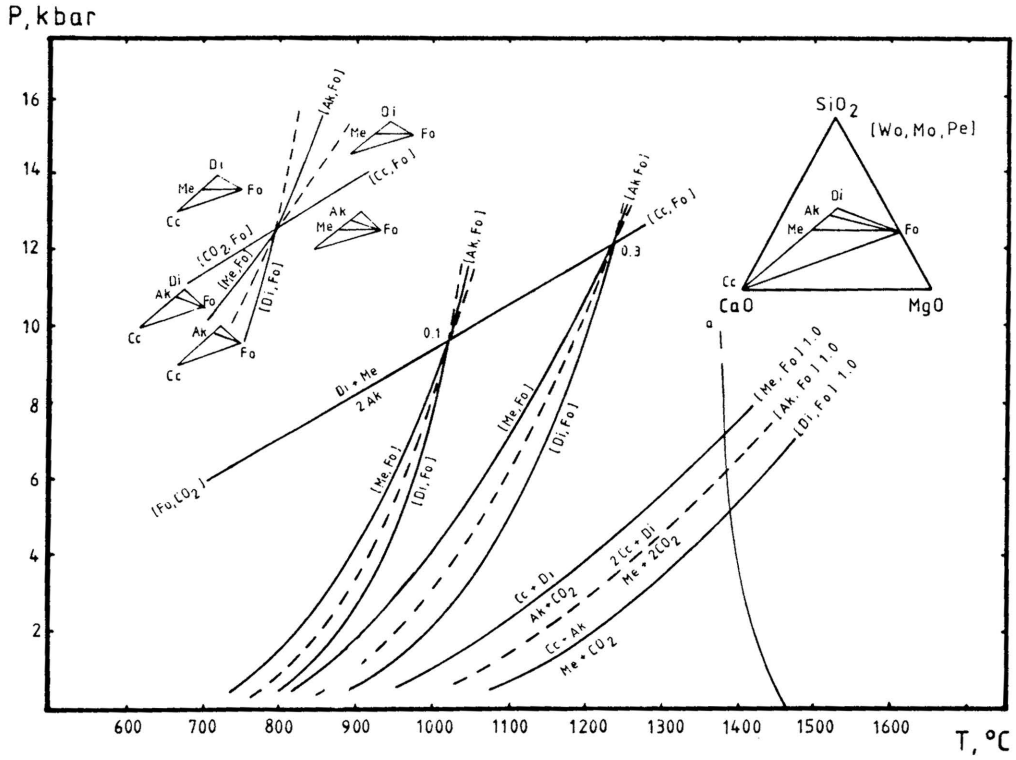

Subsystem 17

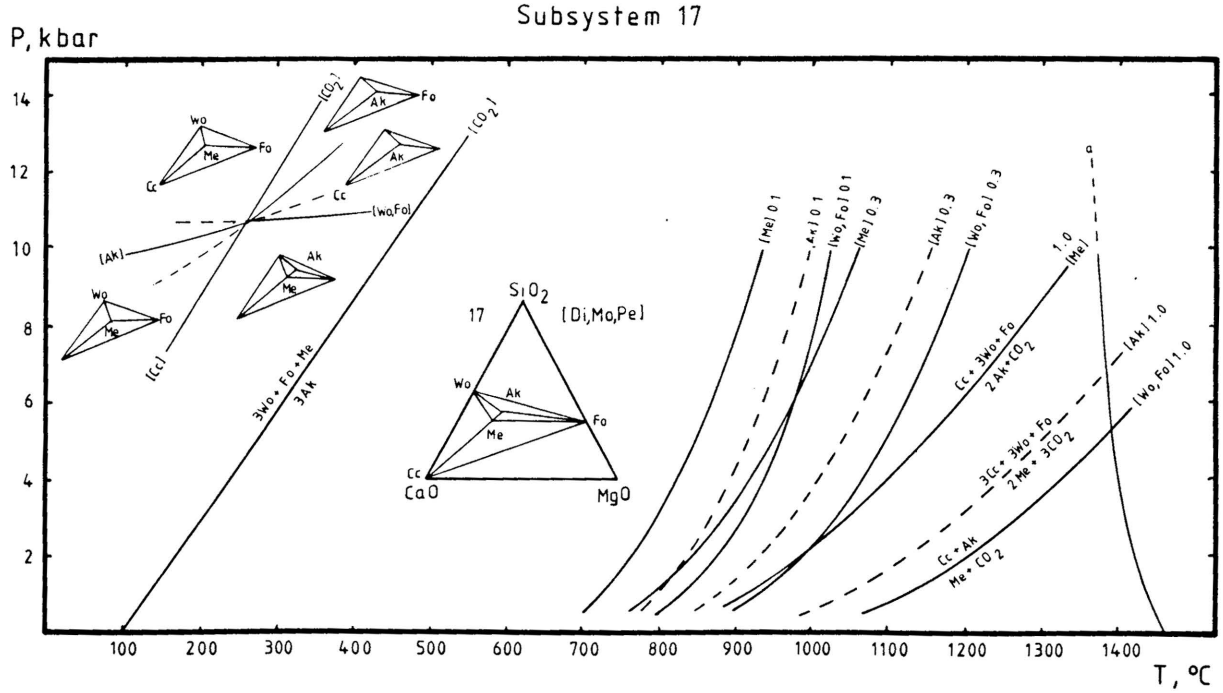

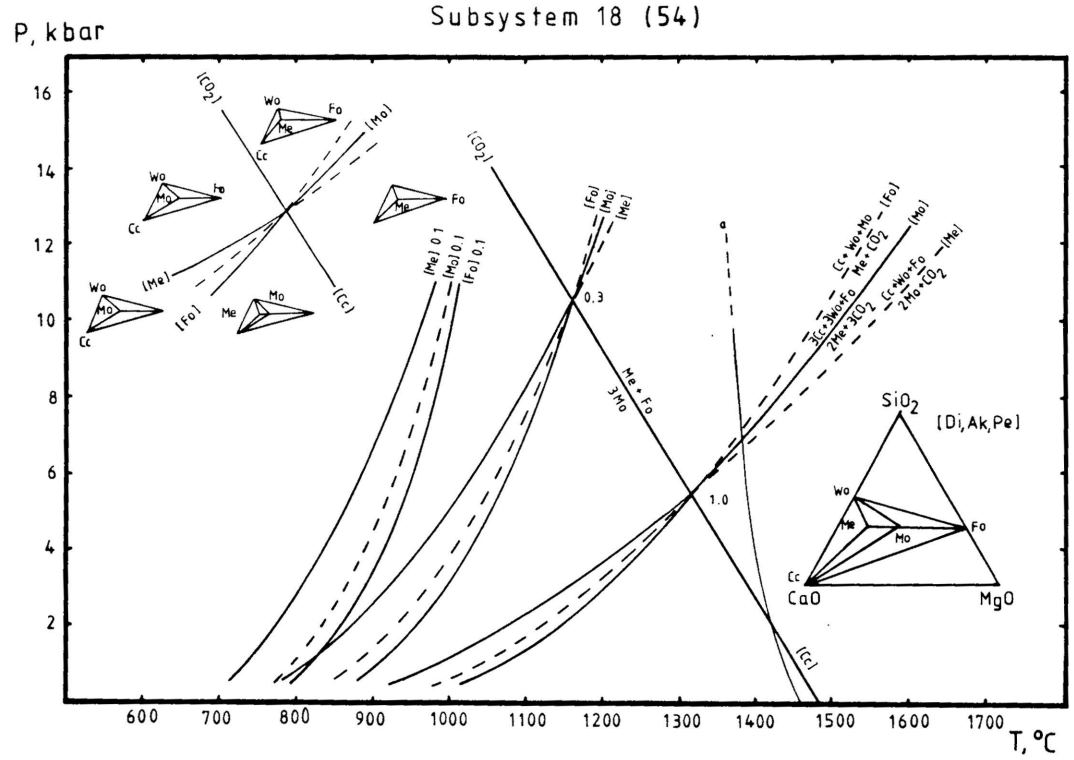

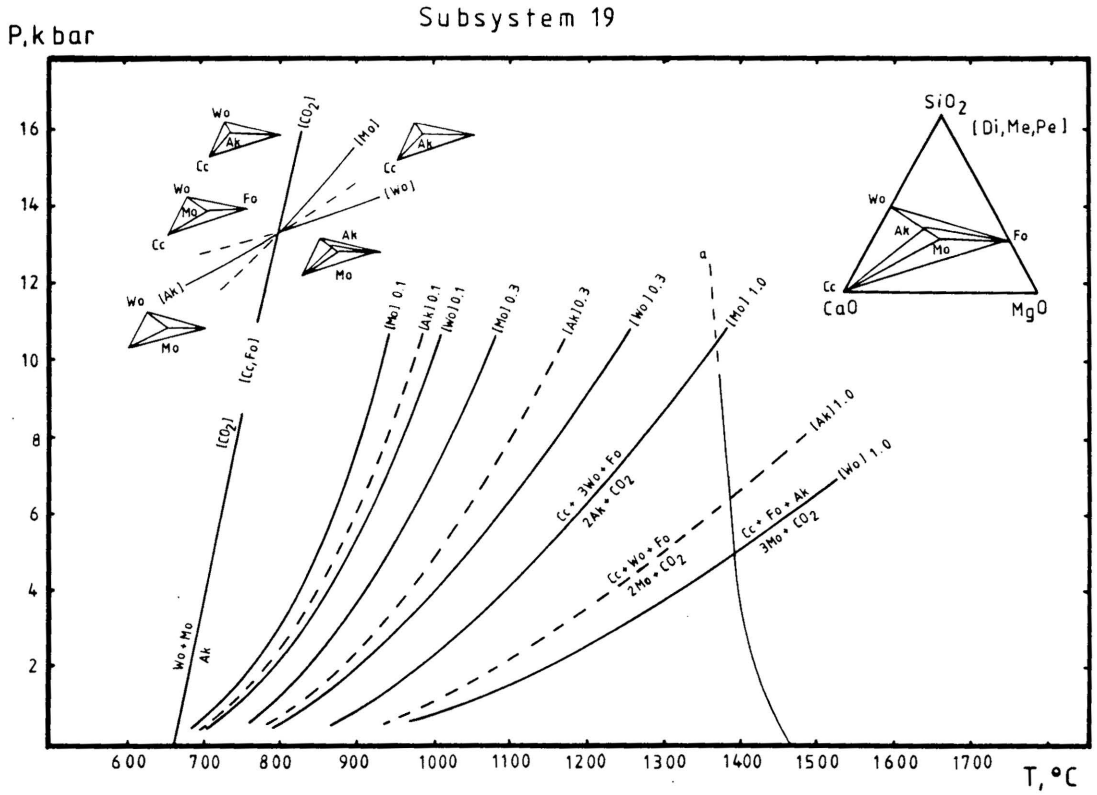

Subsystem 20 (56)

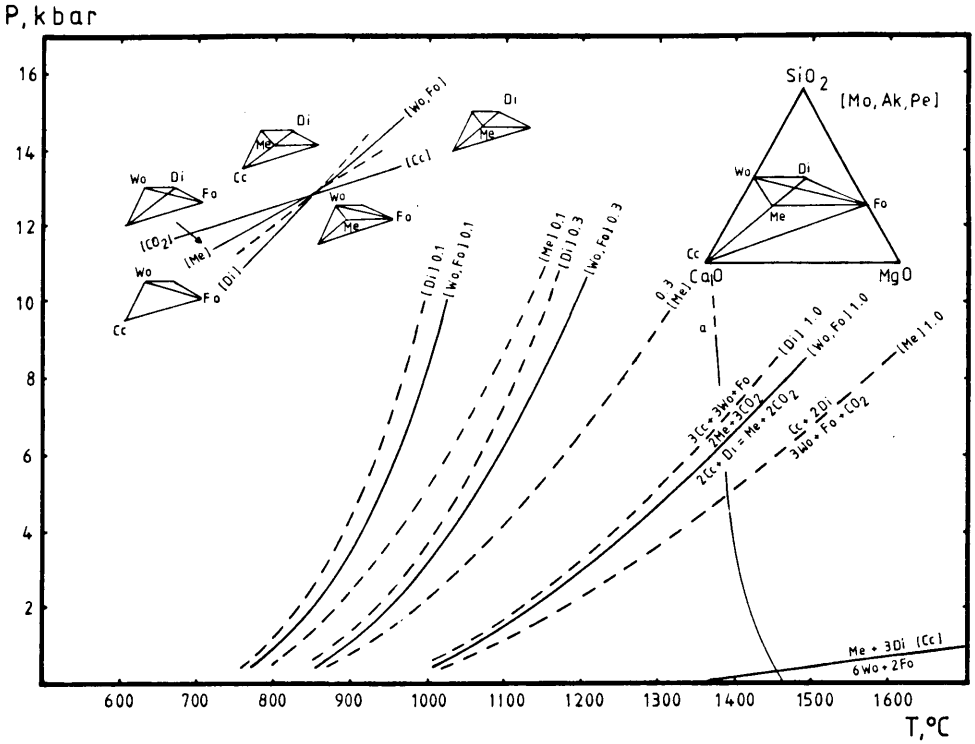

Subsystem 21

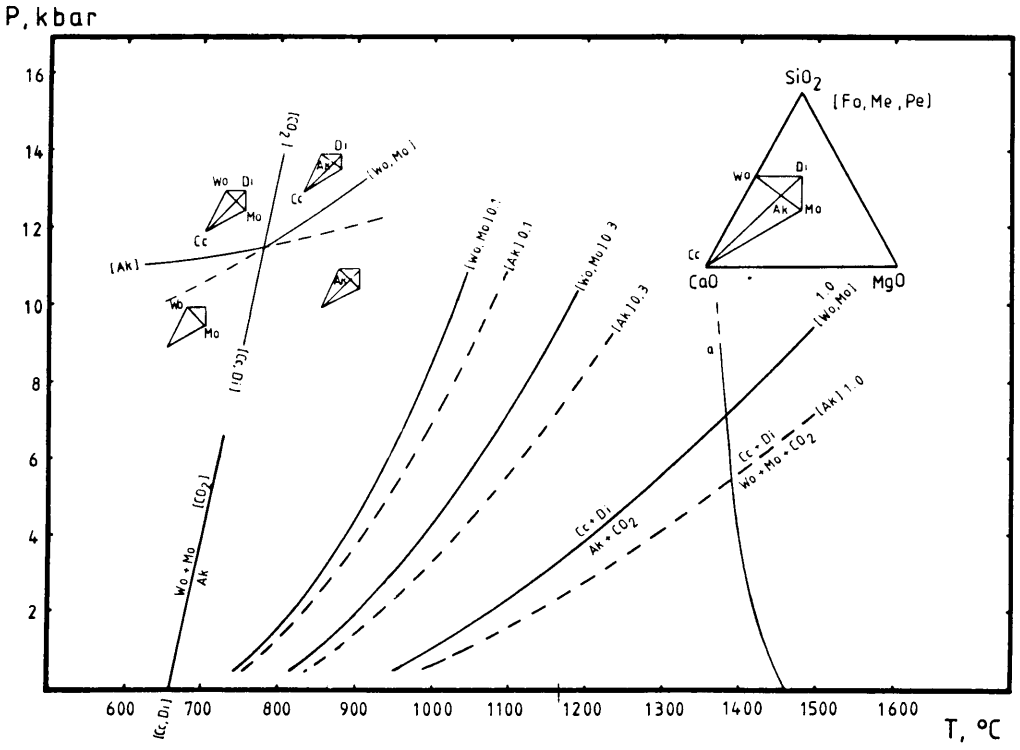

Subsystem 22

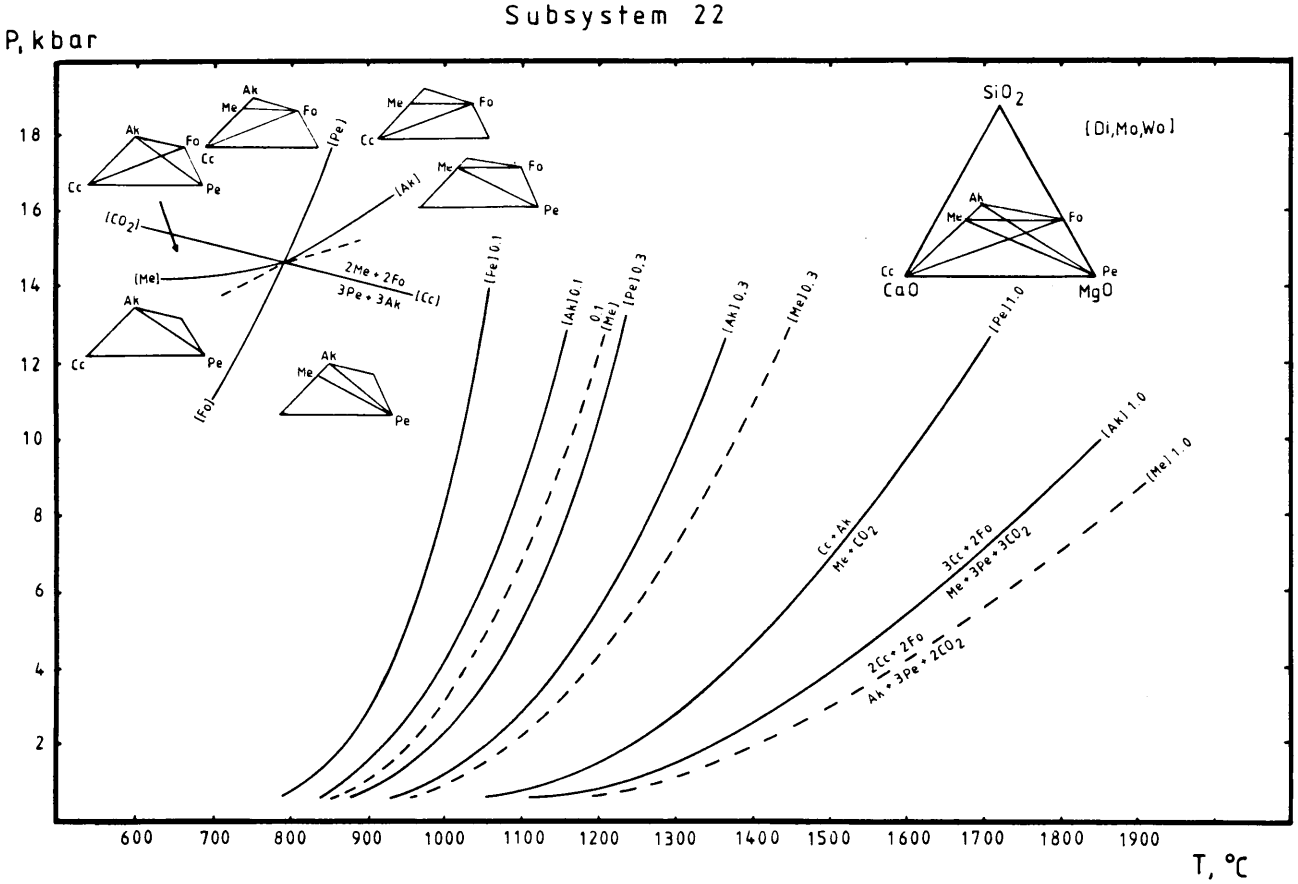

Subsystem 23 (59)

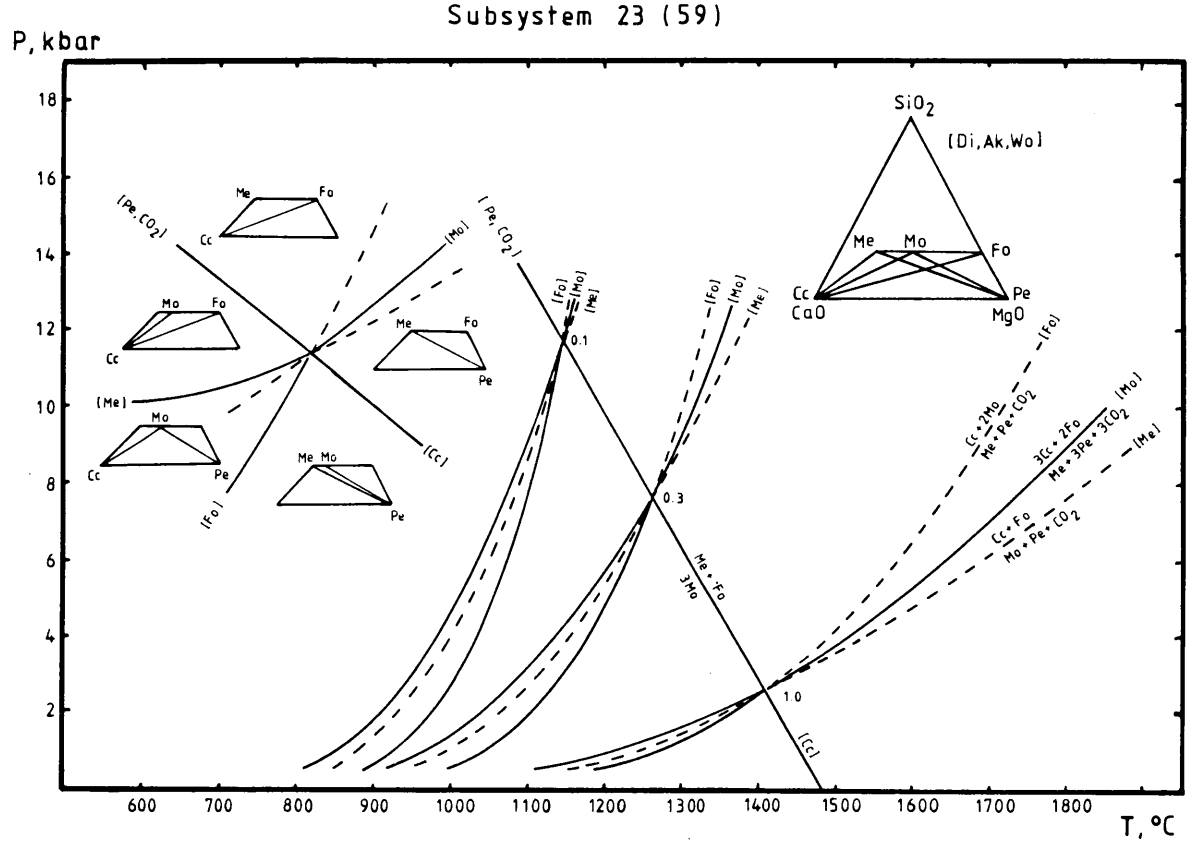

Subsystem 24

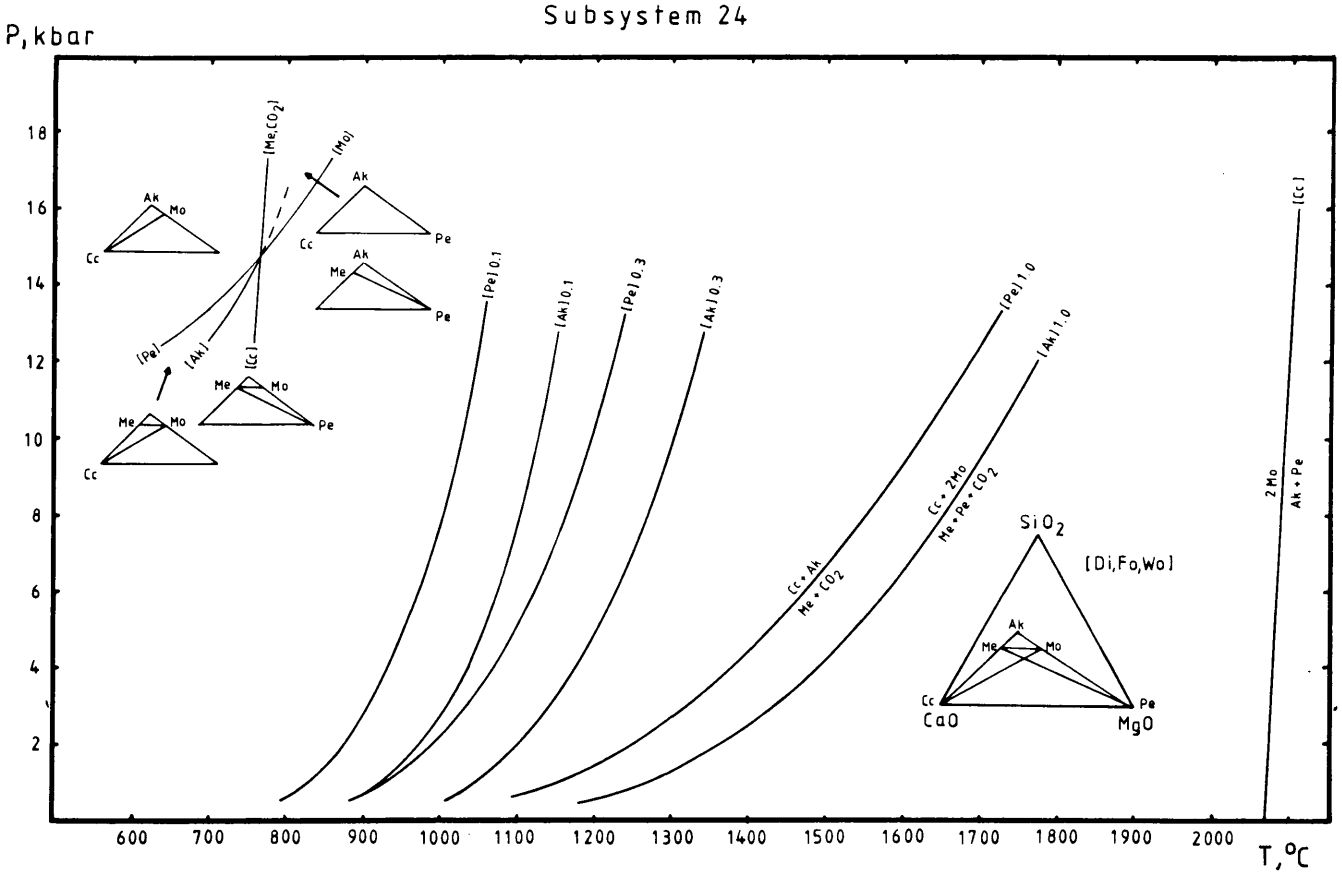

Subsystem 25

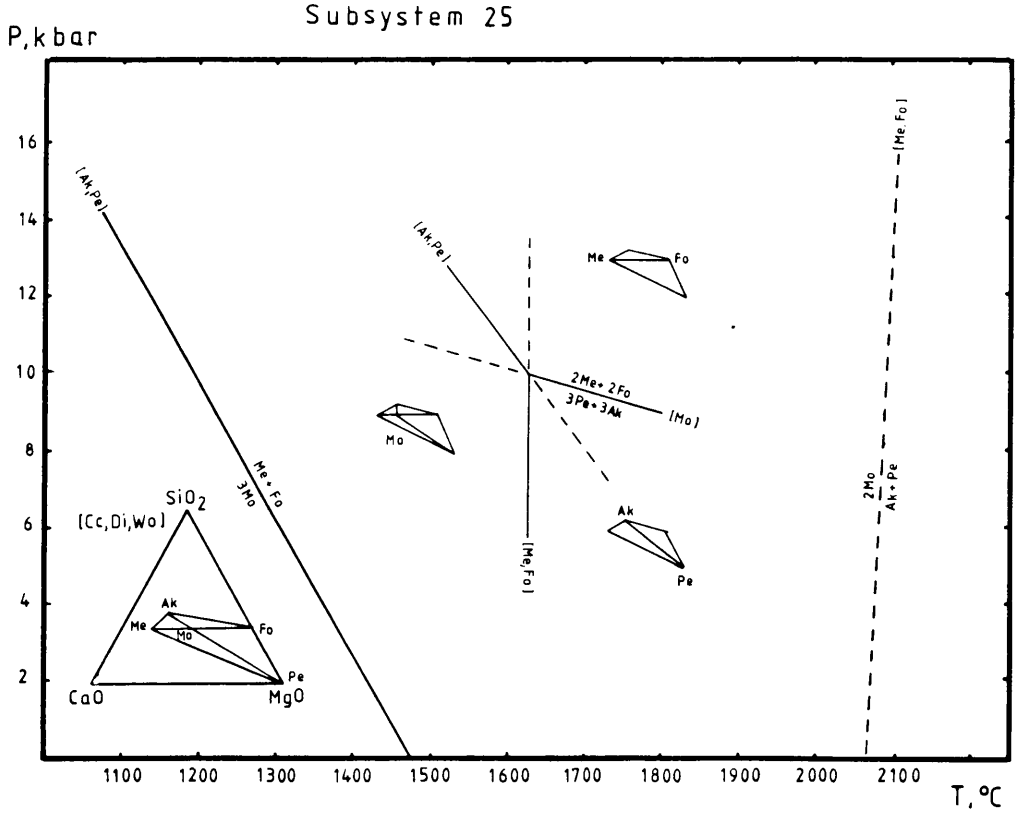

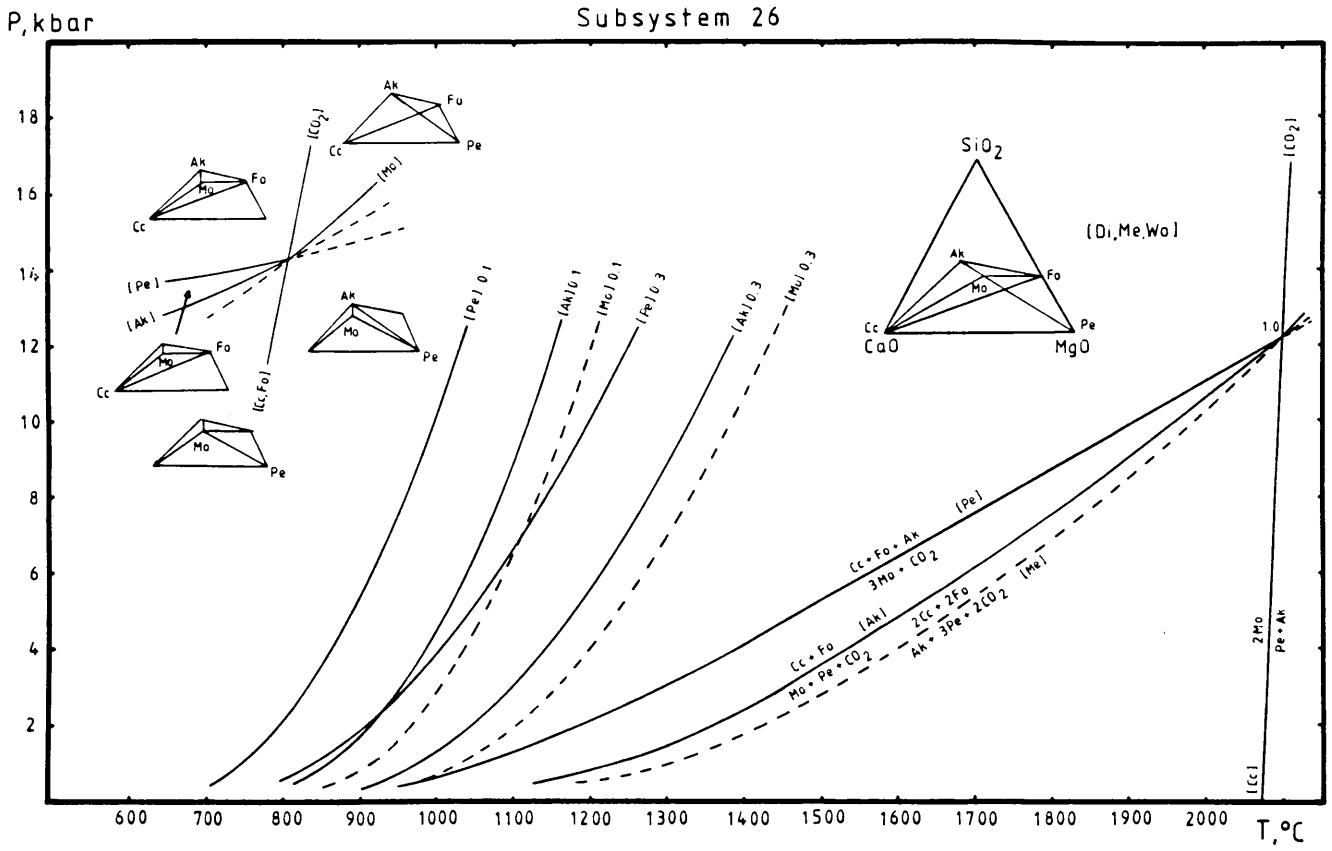

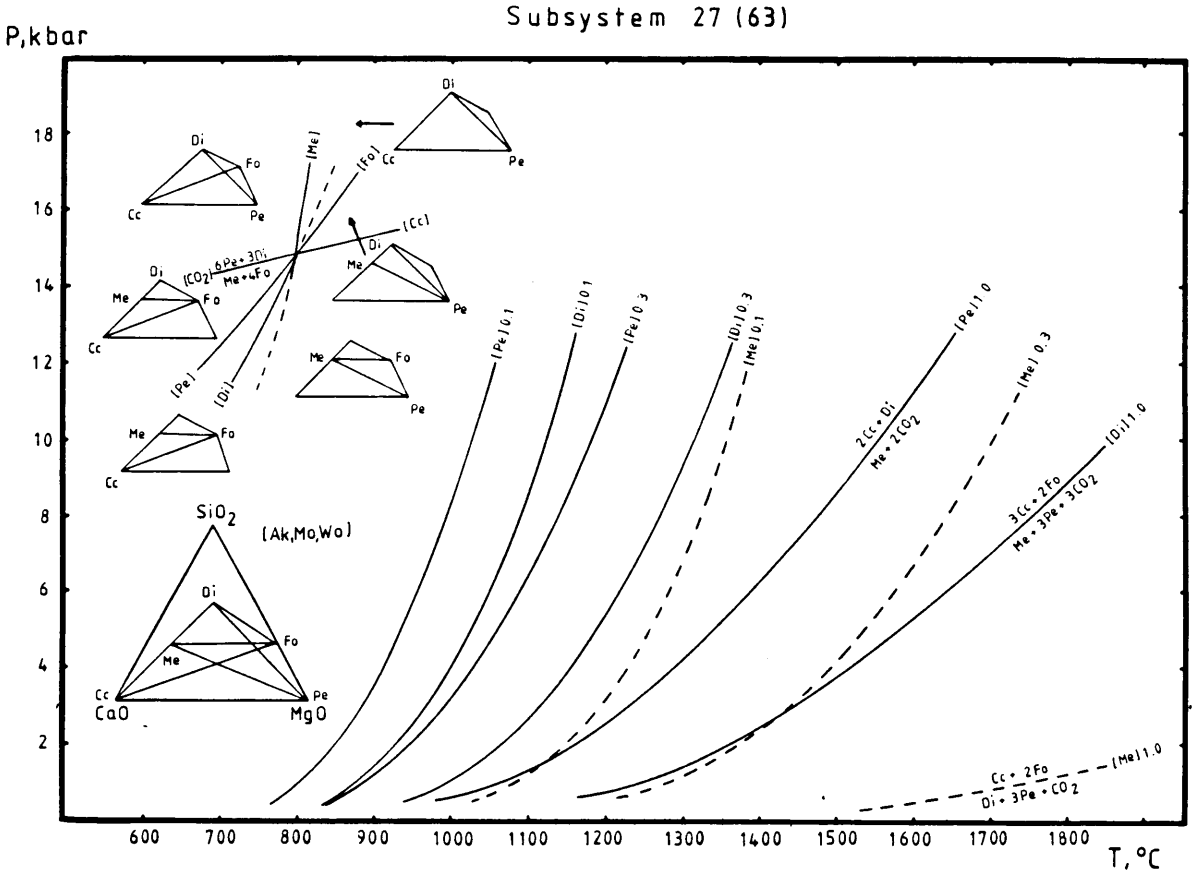

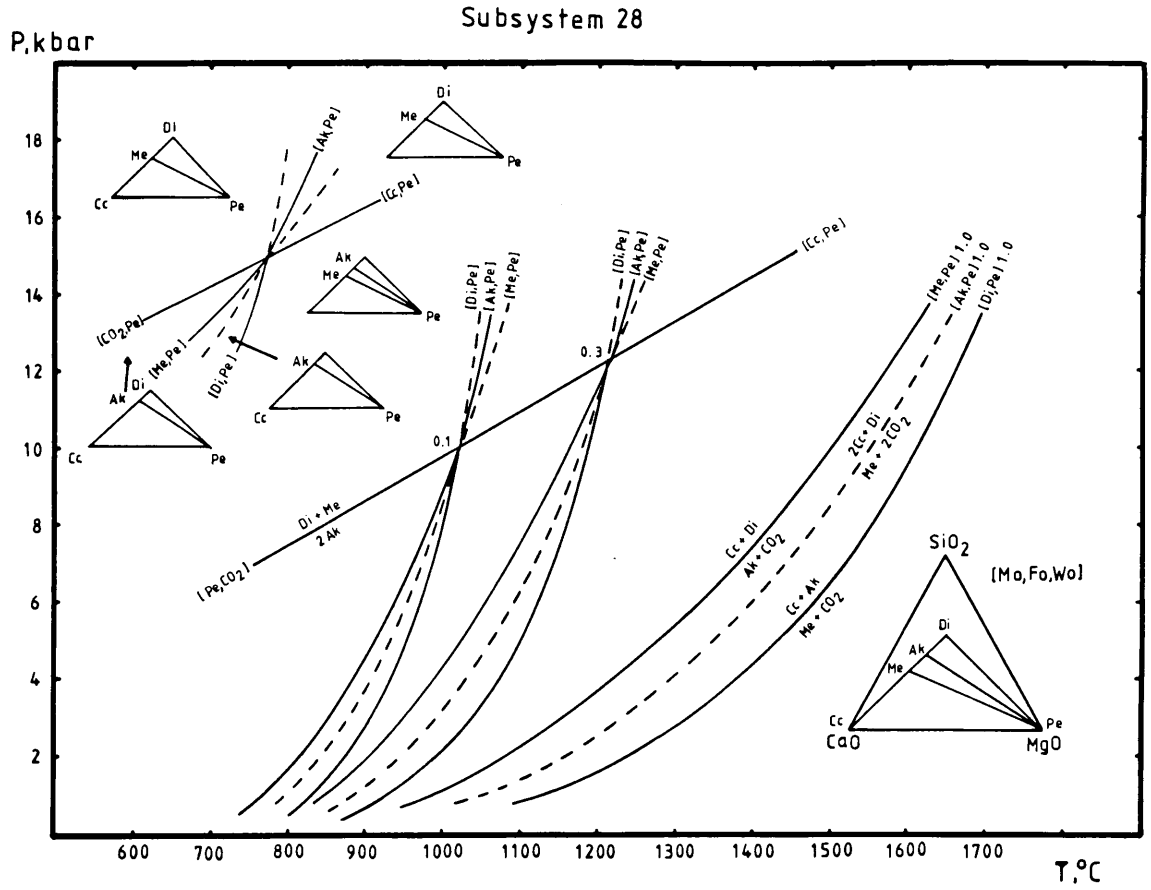

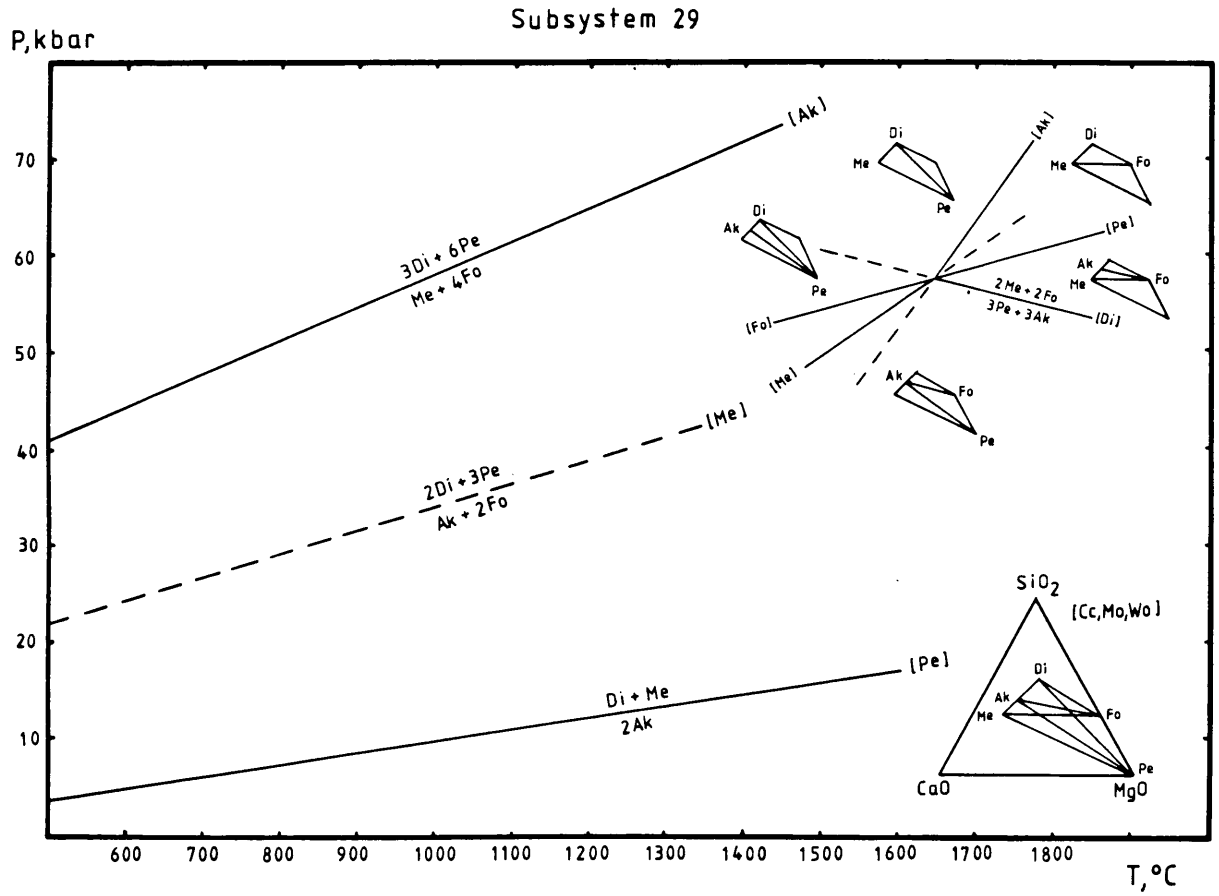

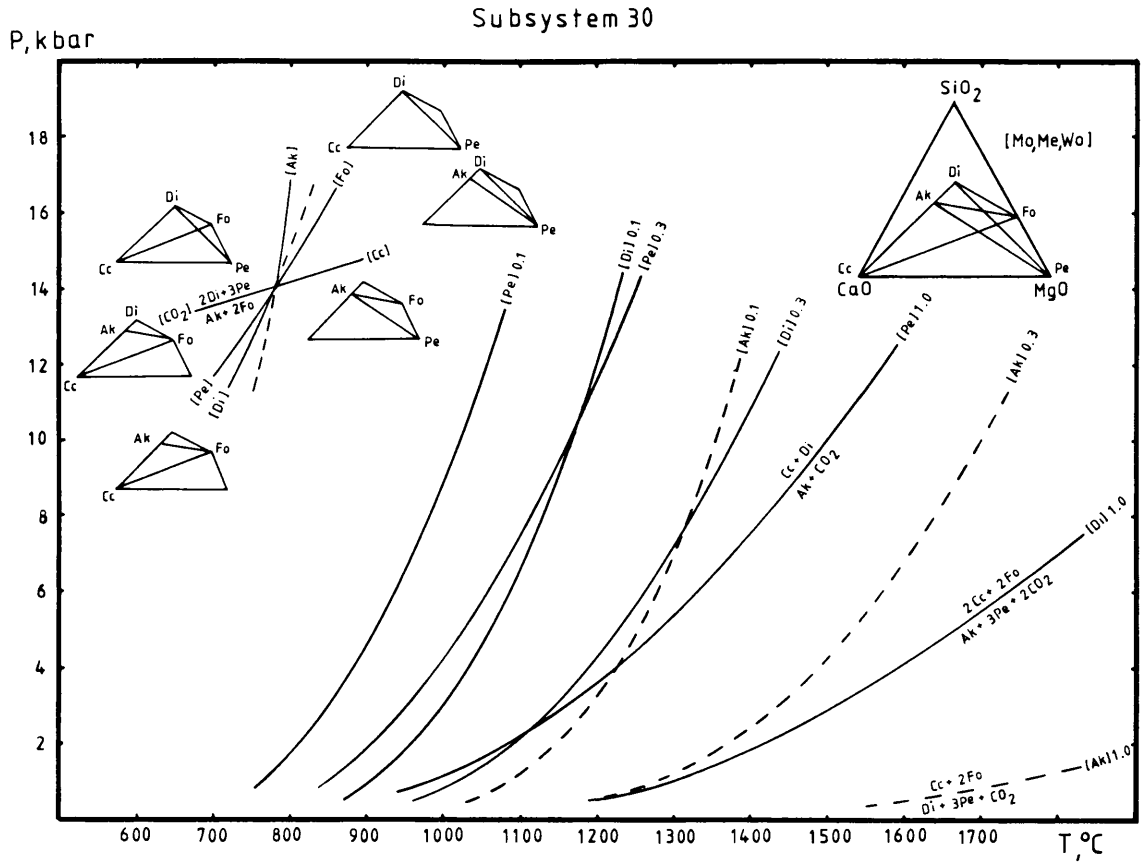

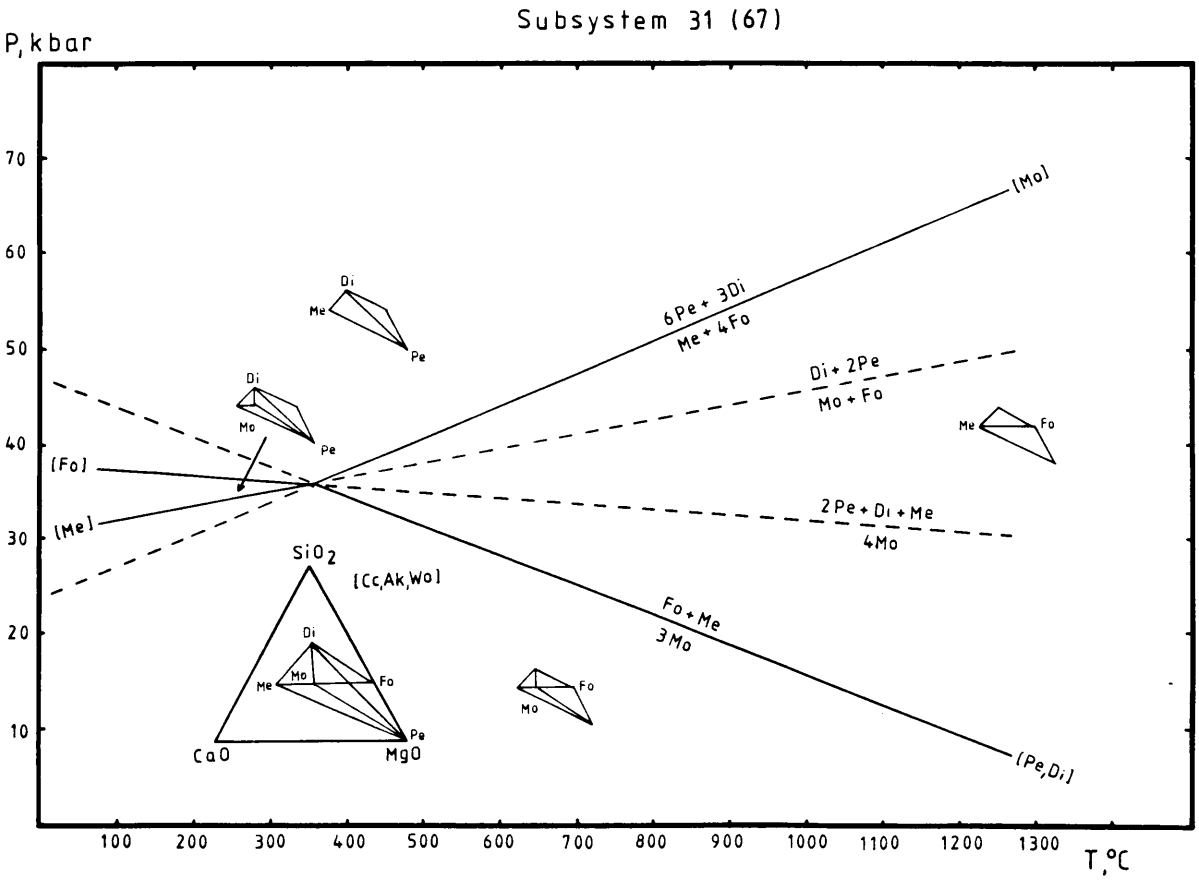

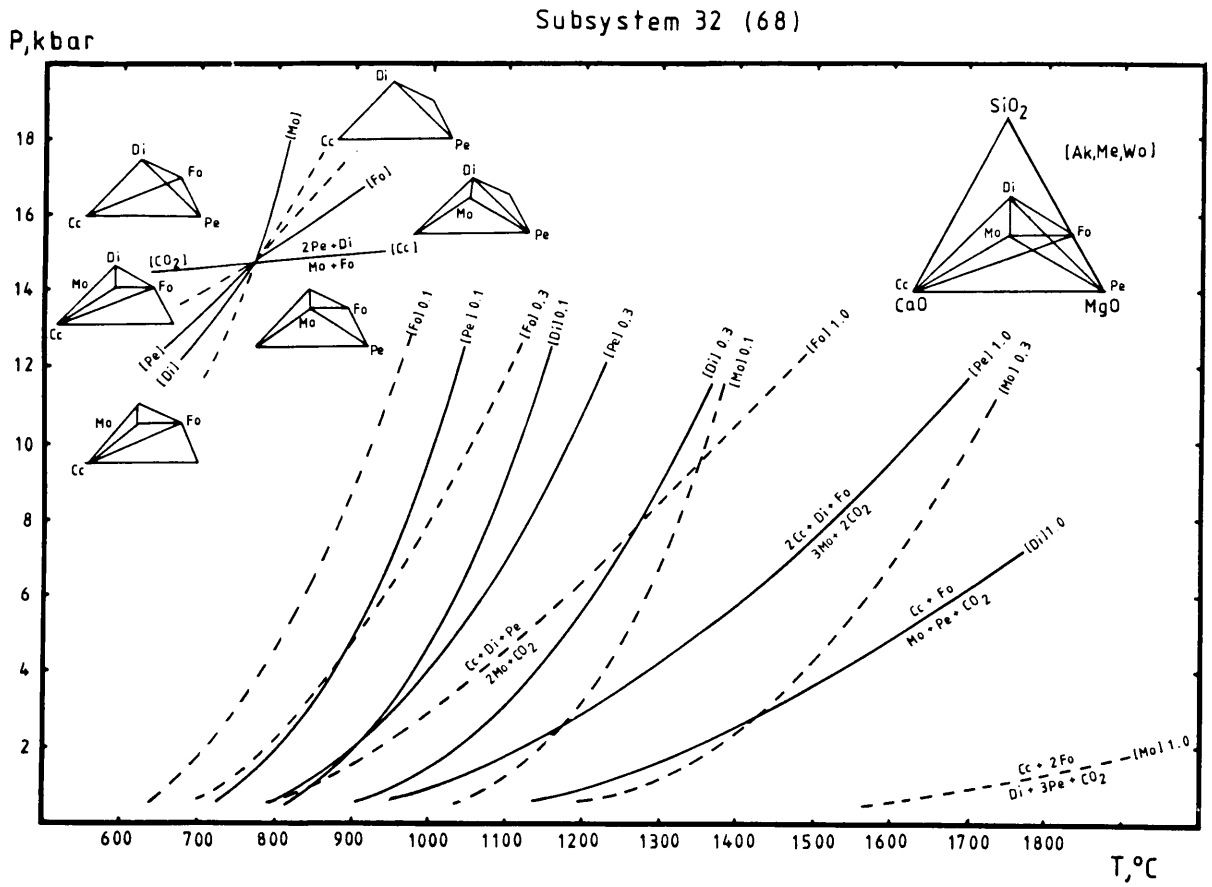

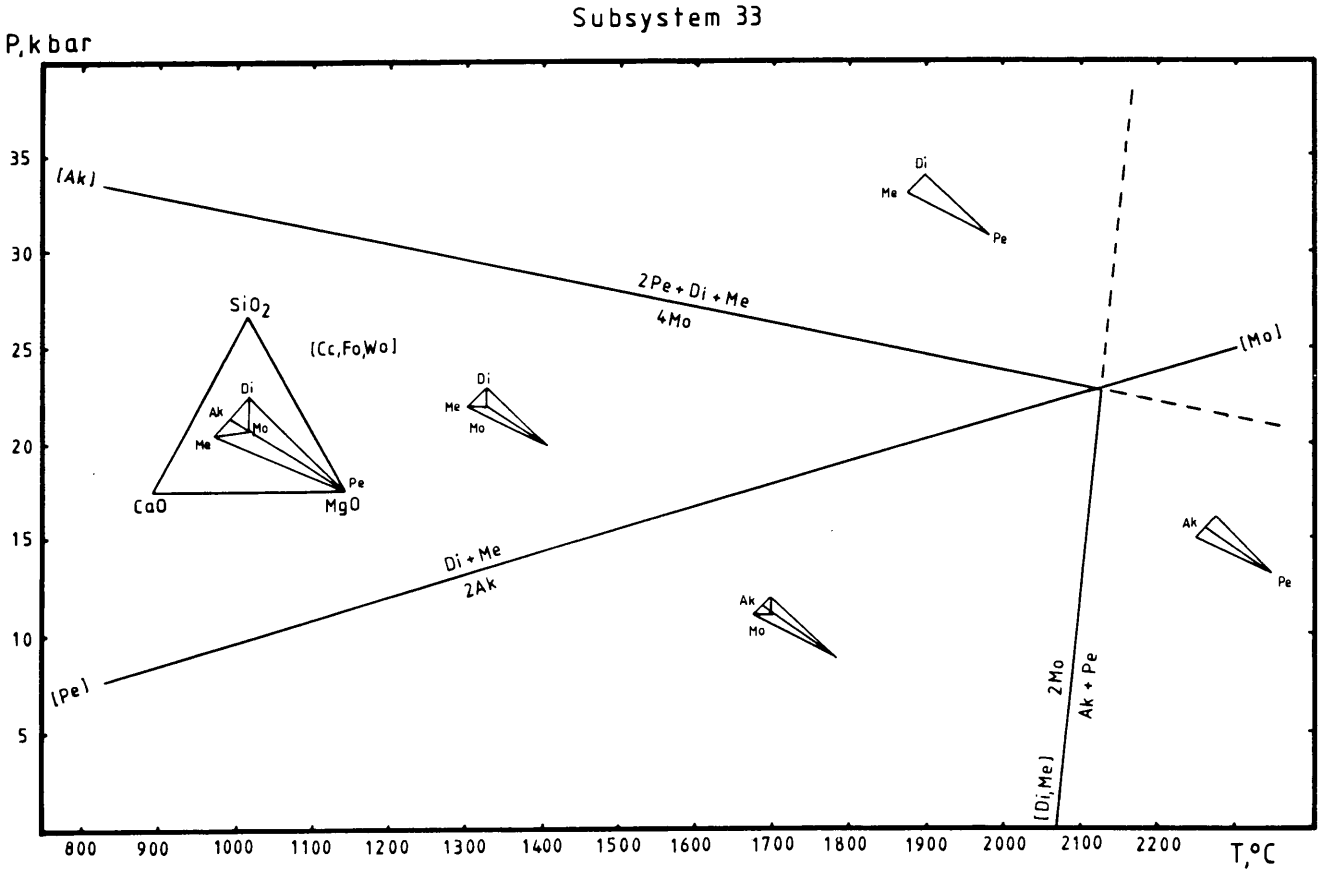

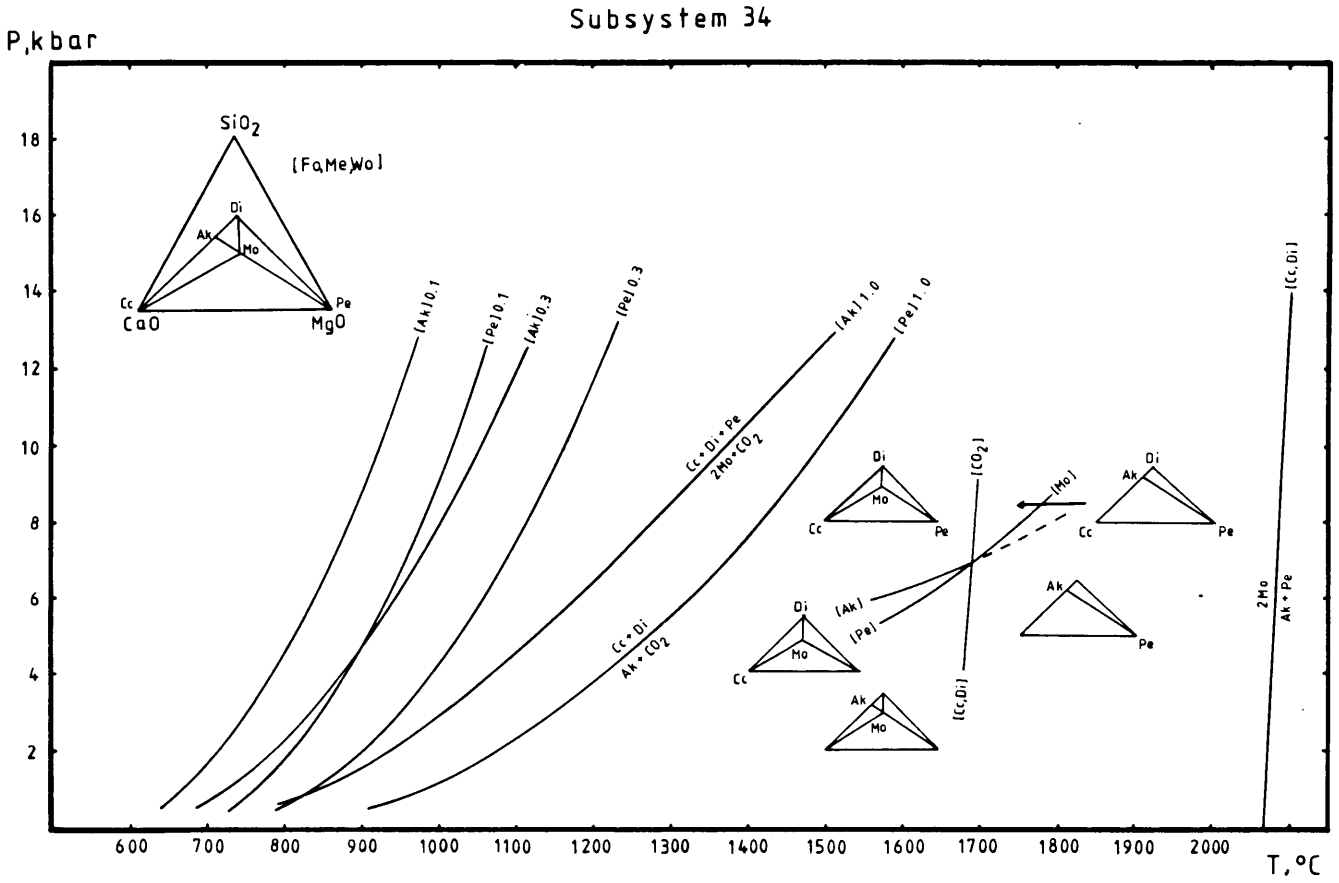

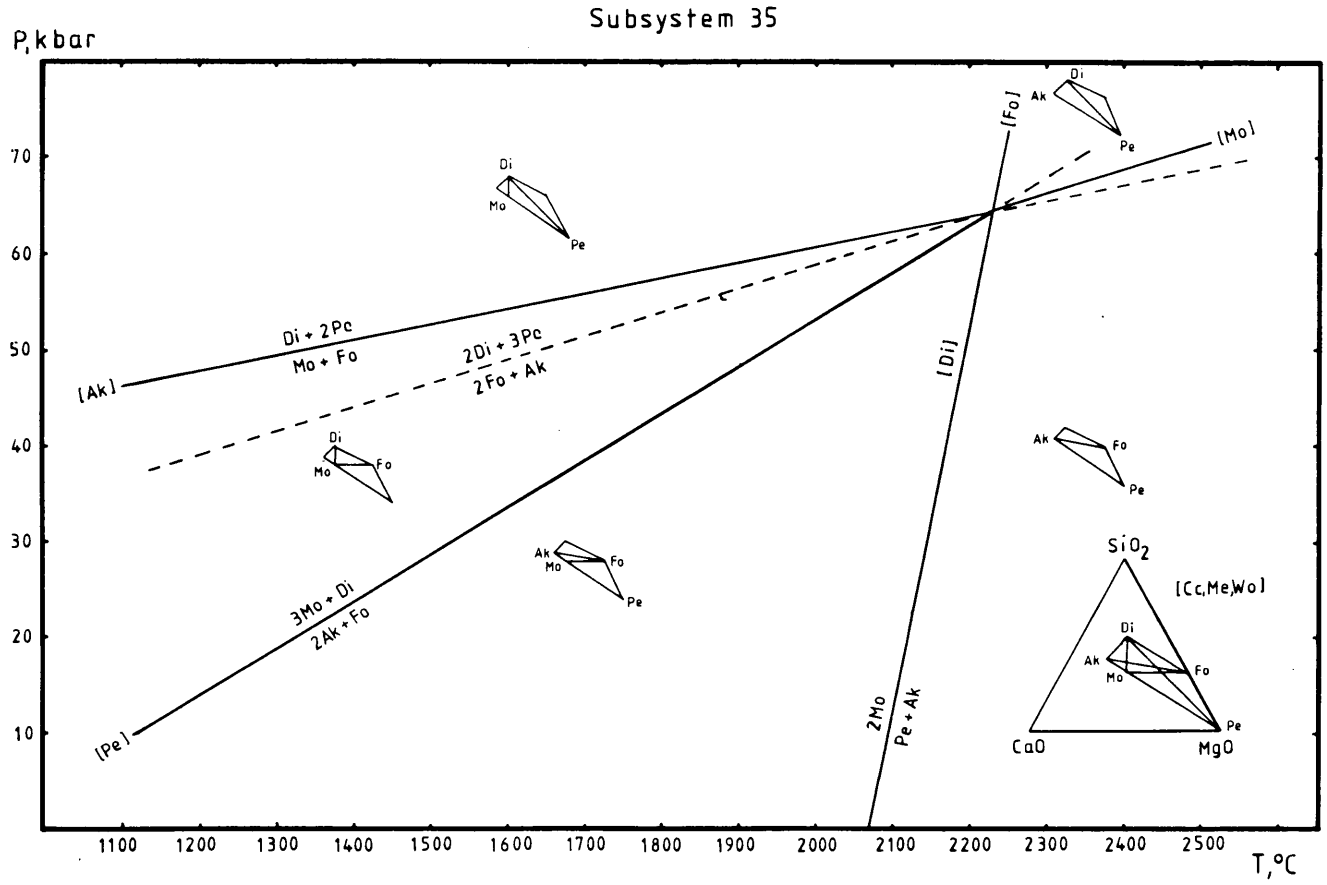

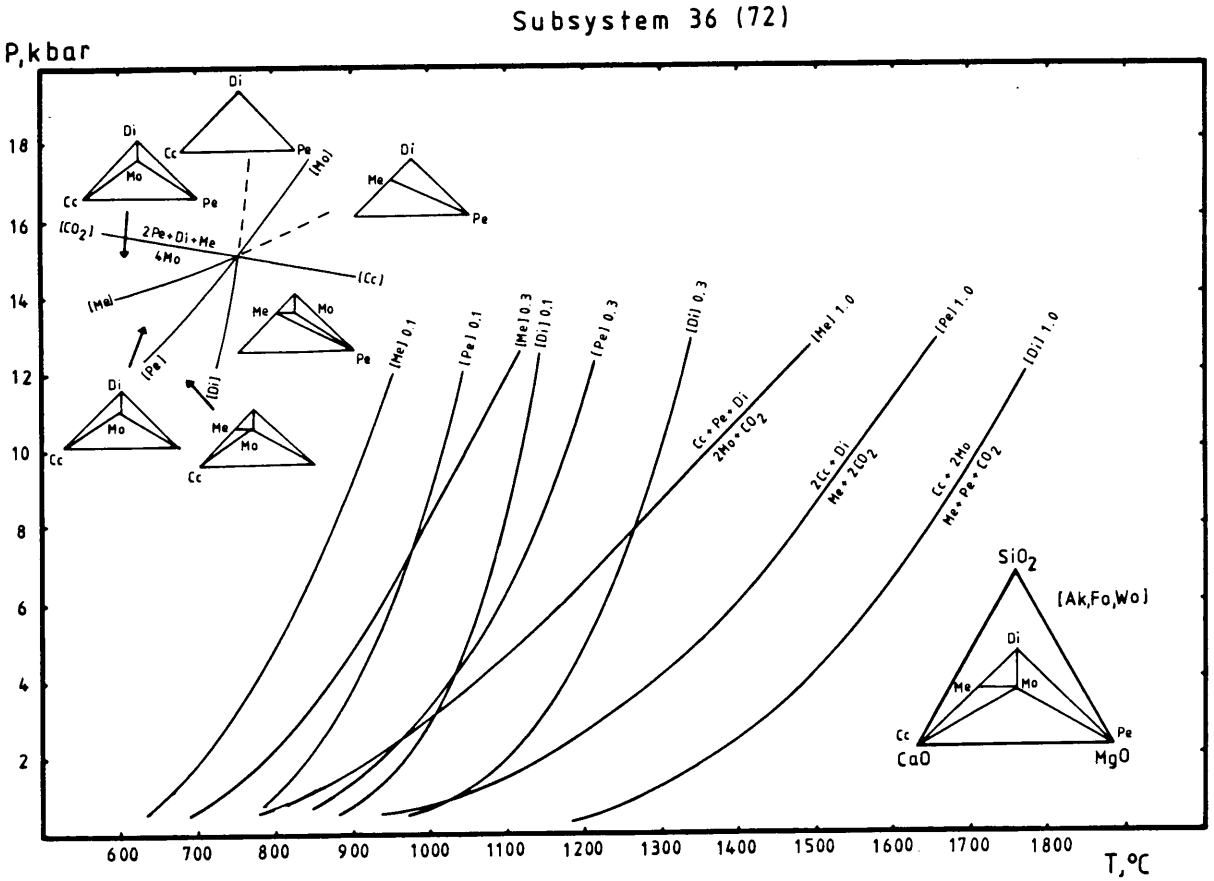

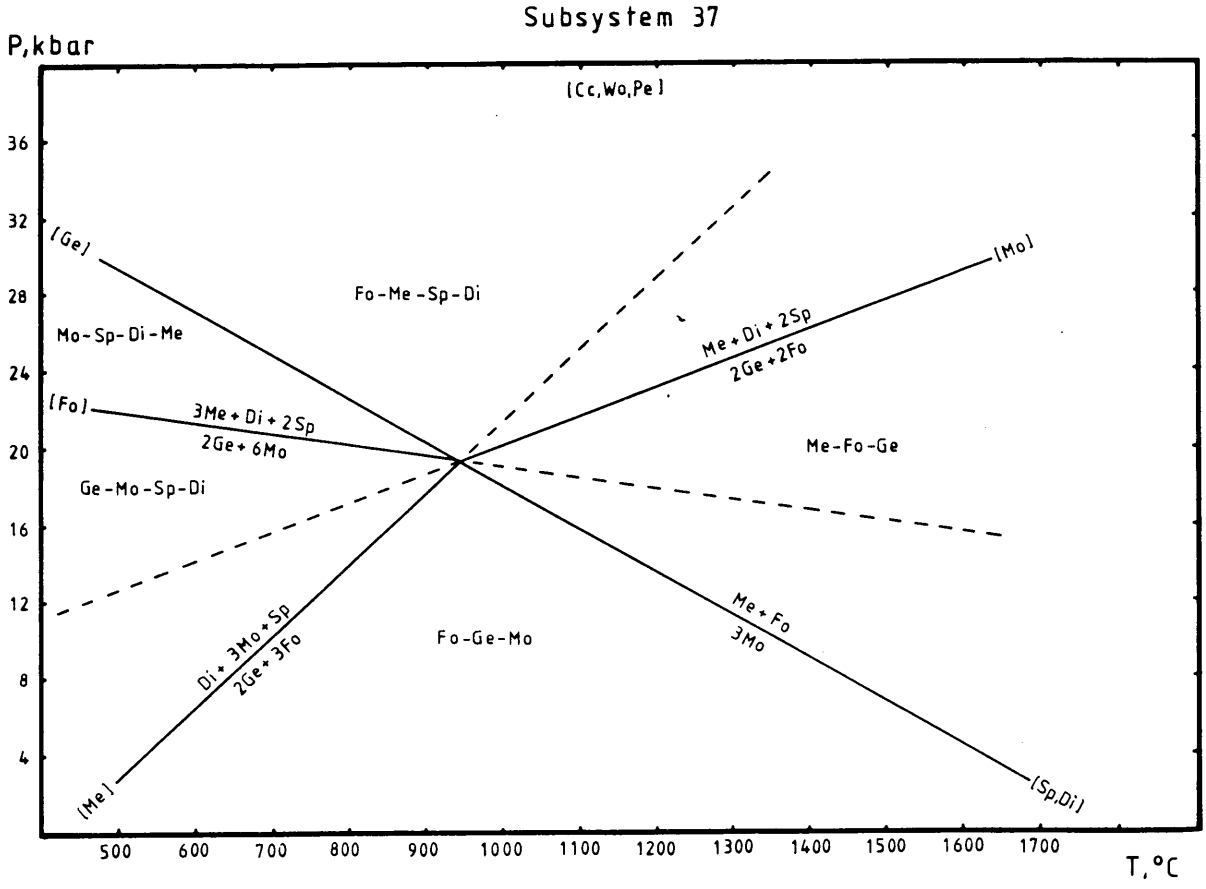

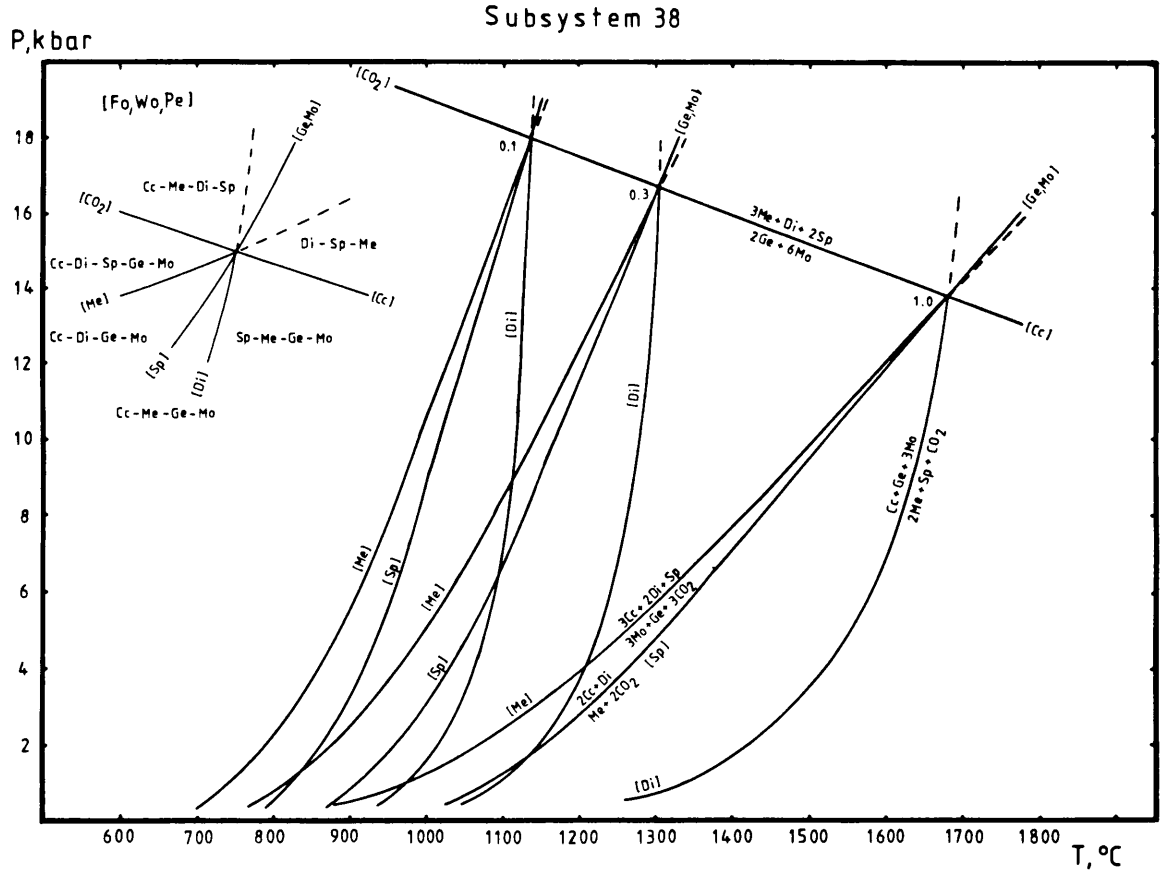

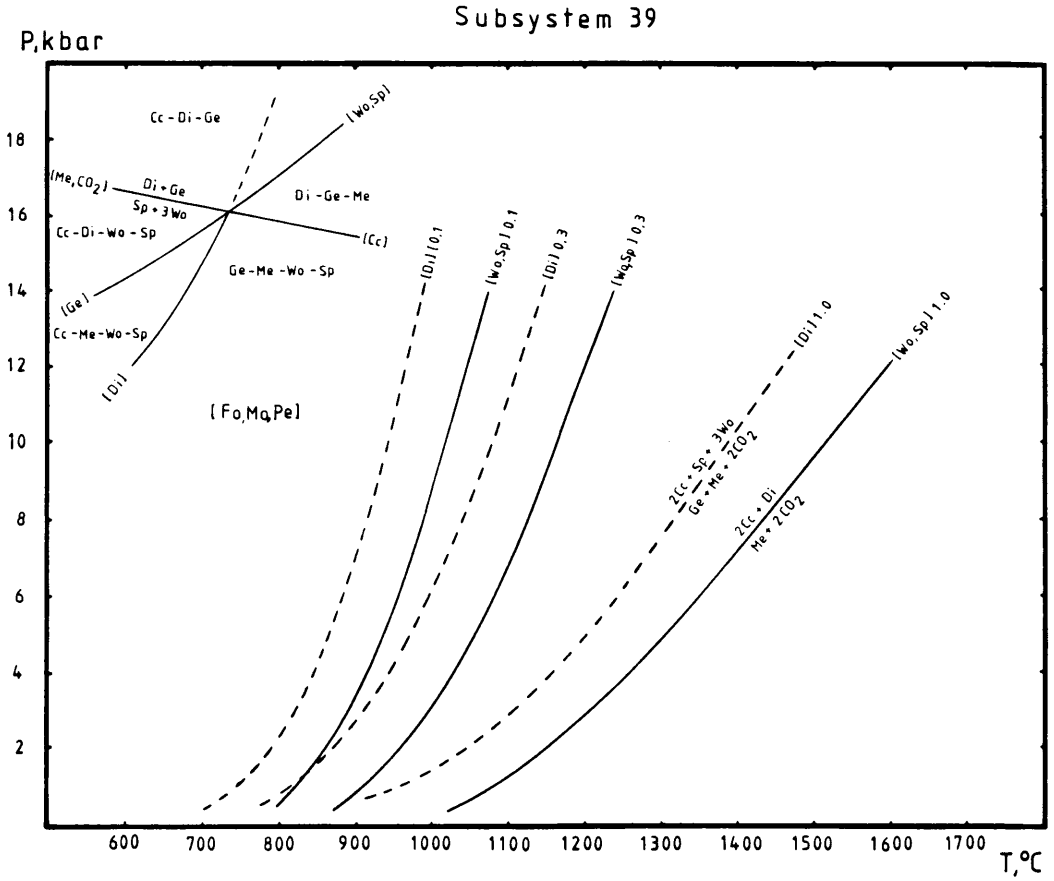

Subsystem 40

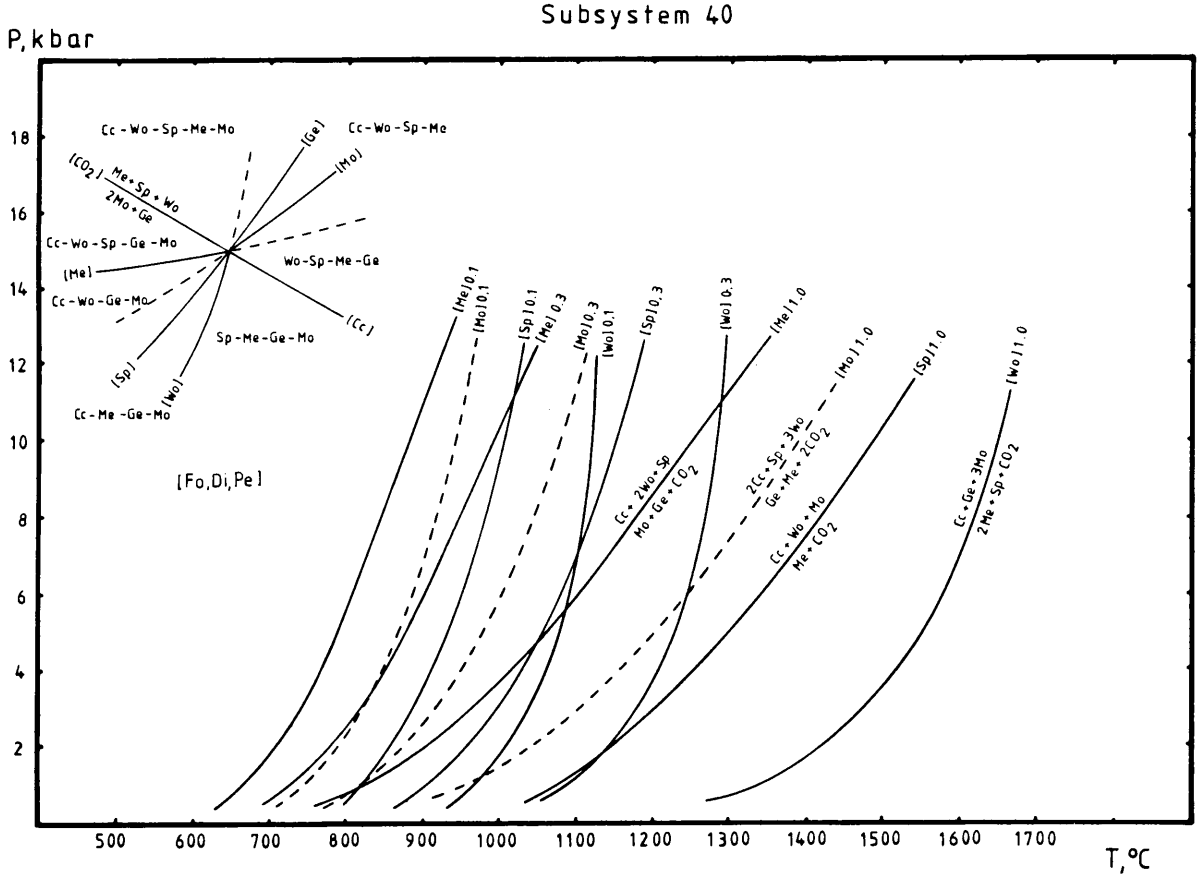

Subsystem 41

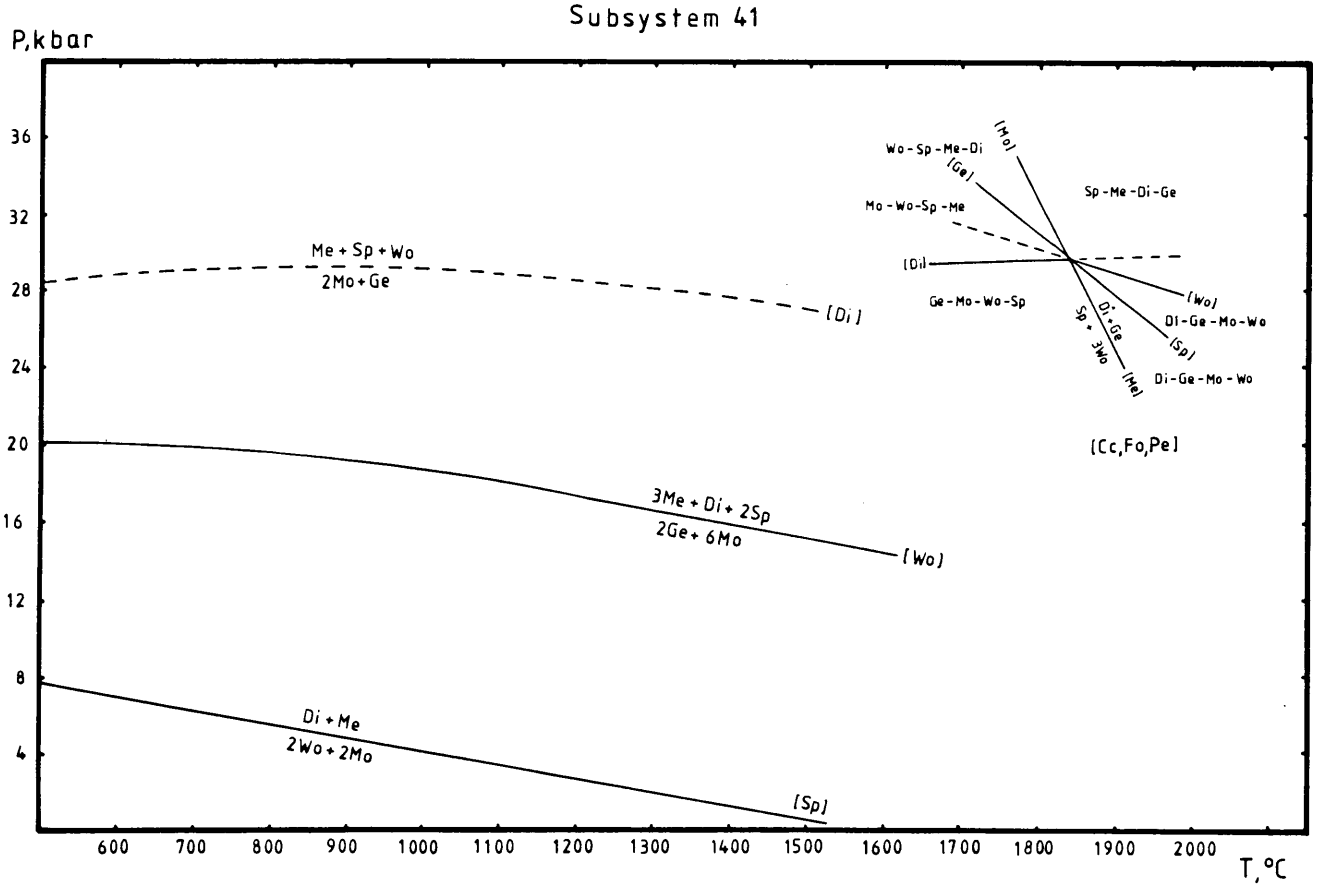

Subsystem 42

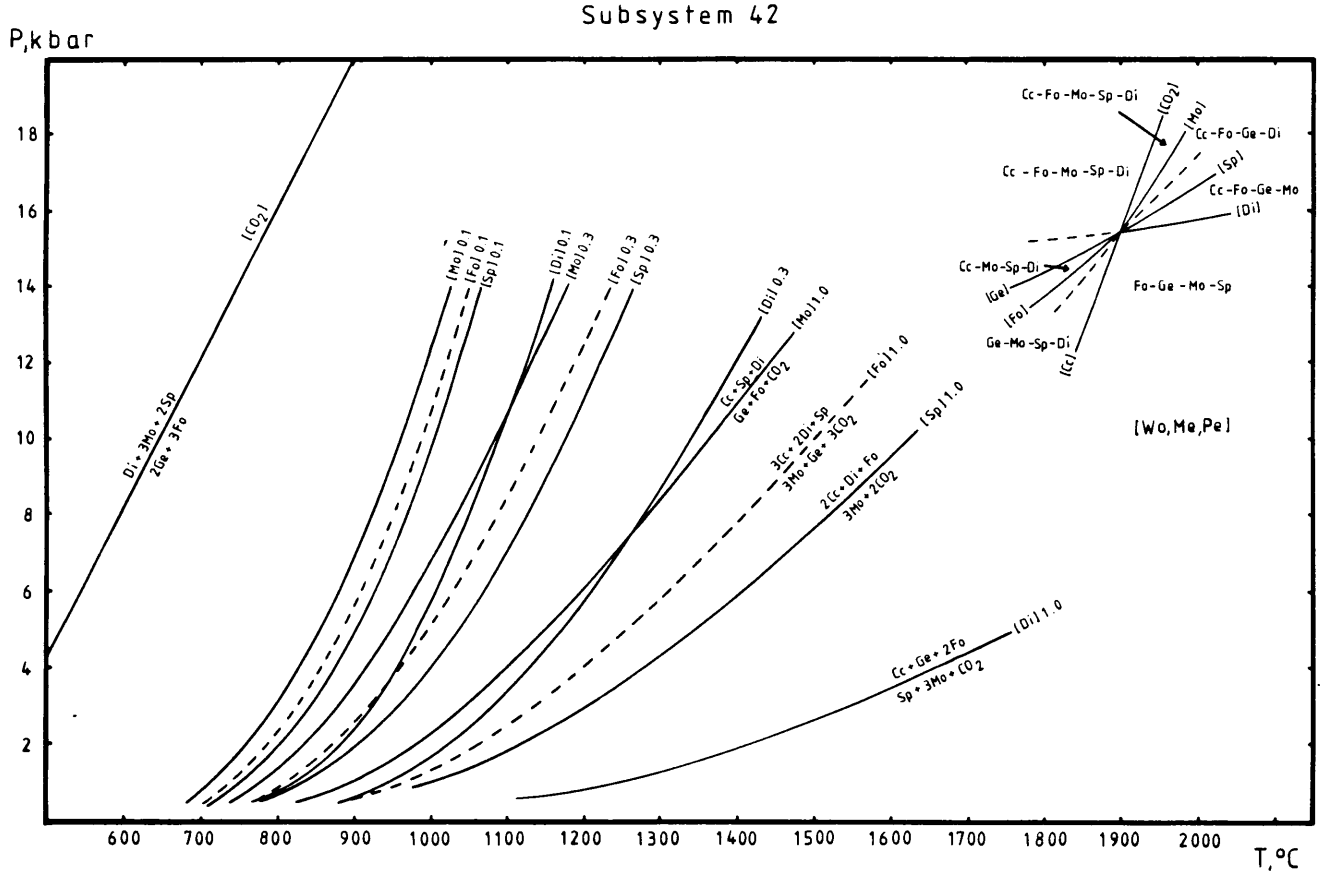

Subsystem 45

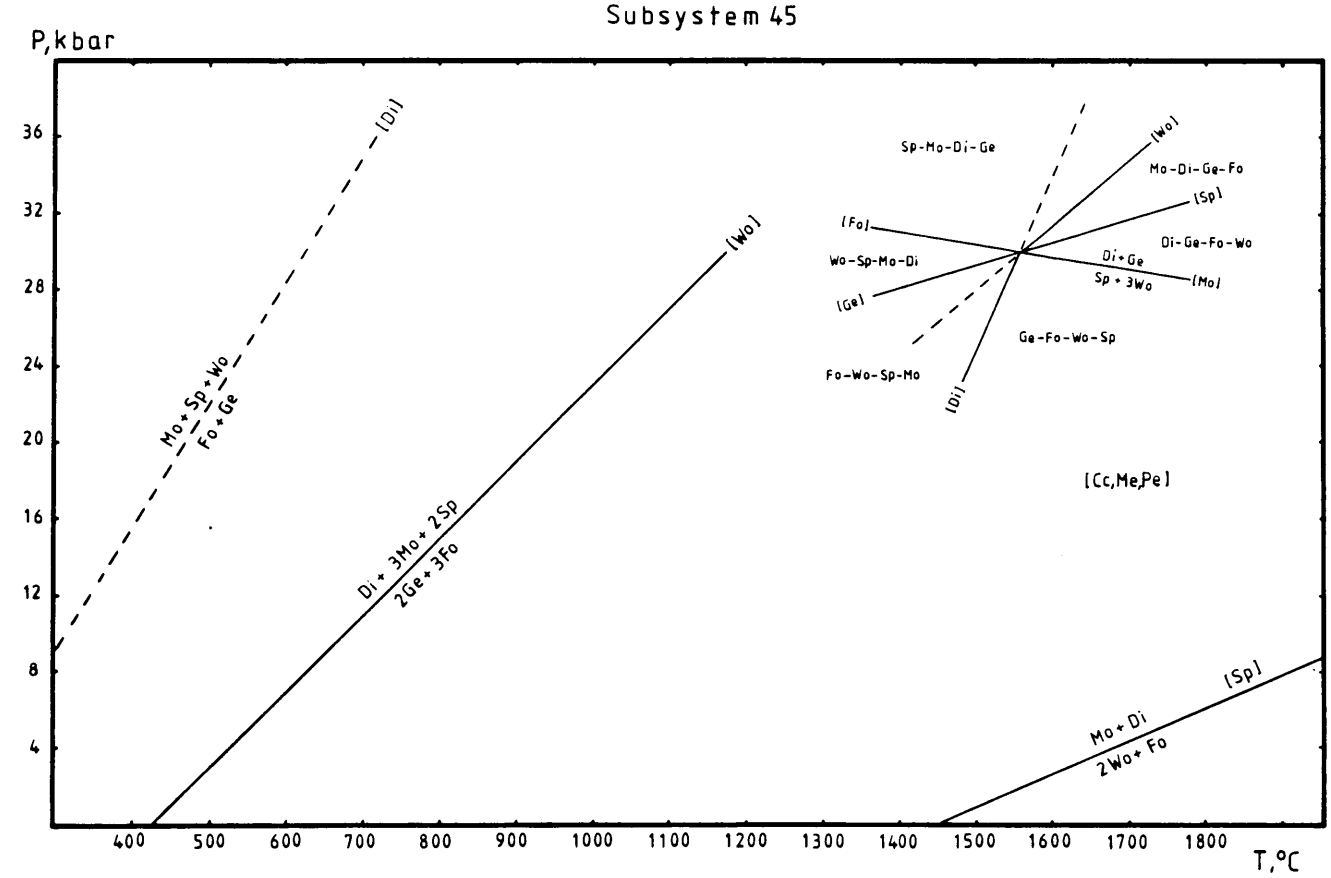

Subsystem 46

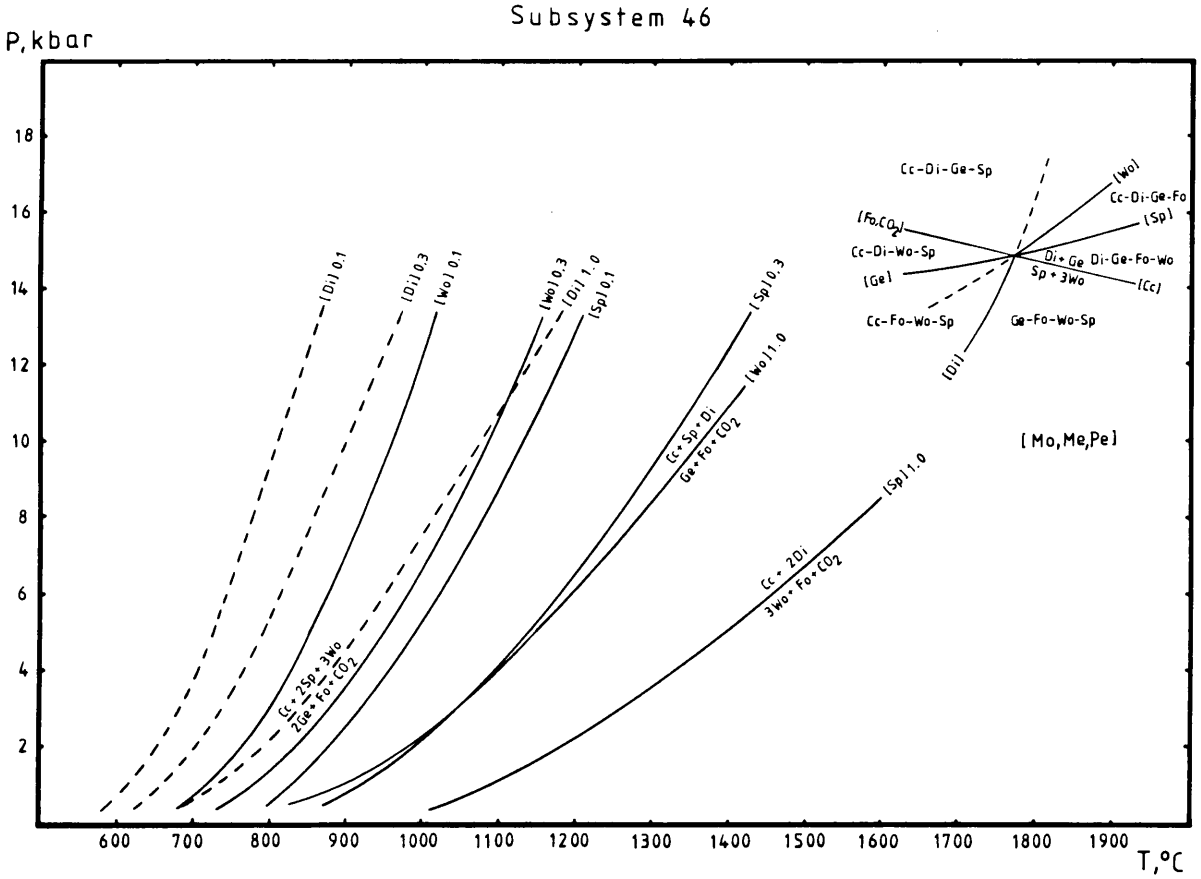

Subsystem 48

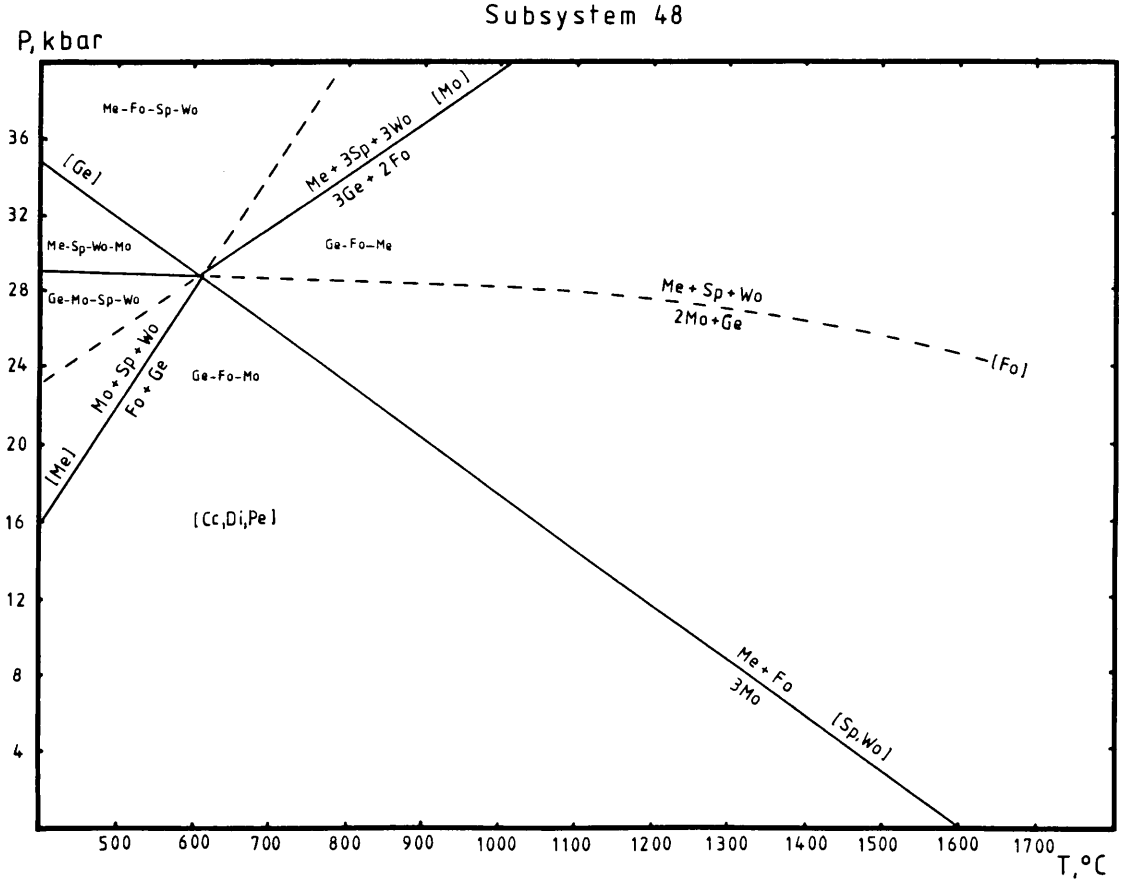

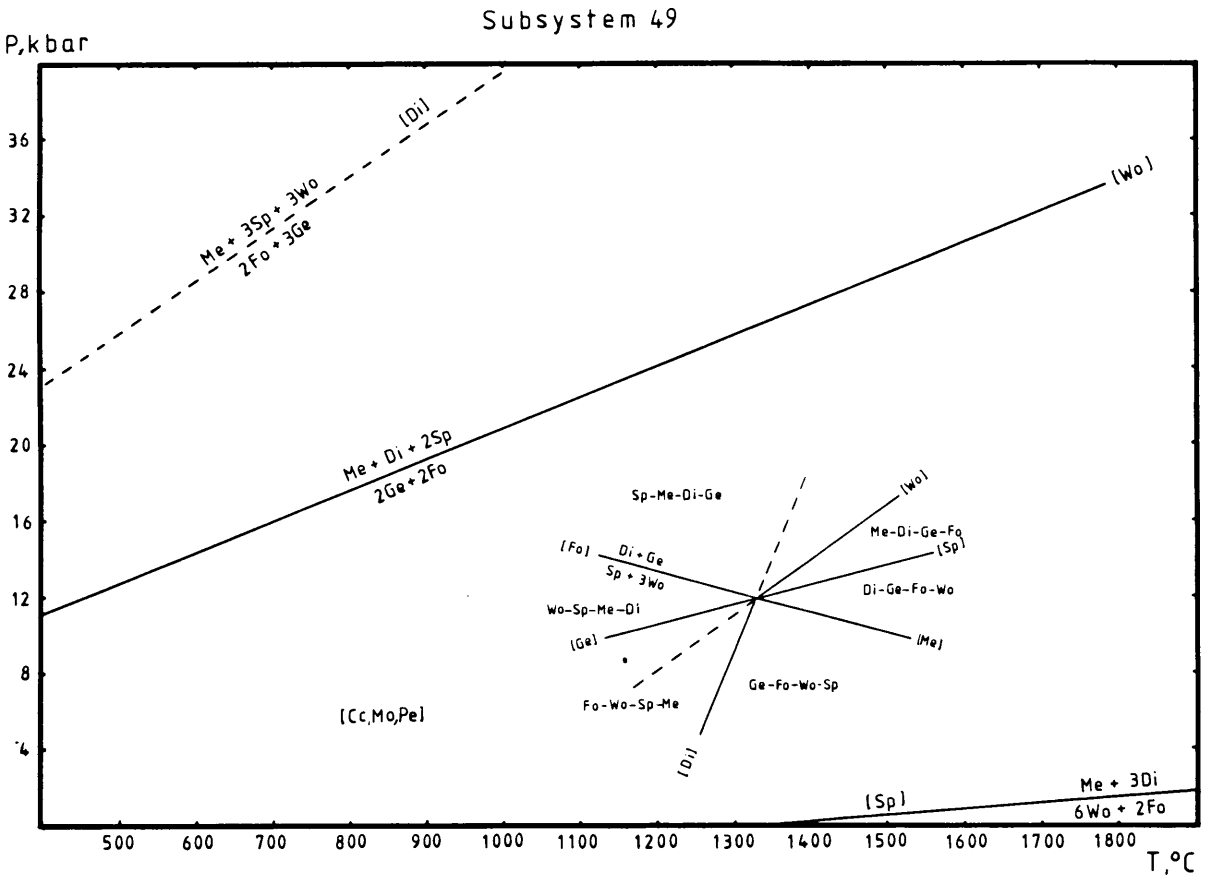

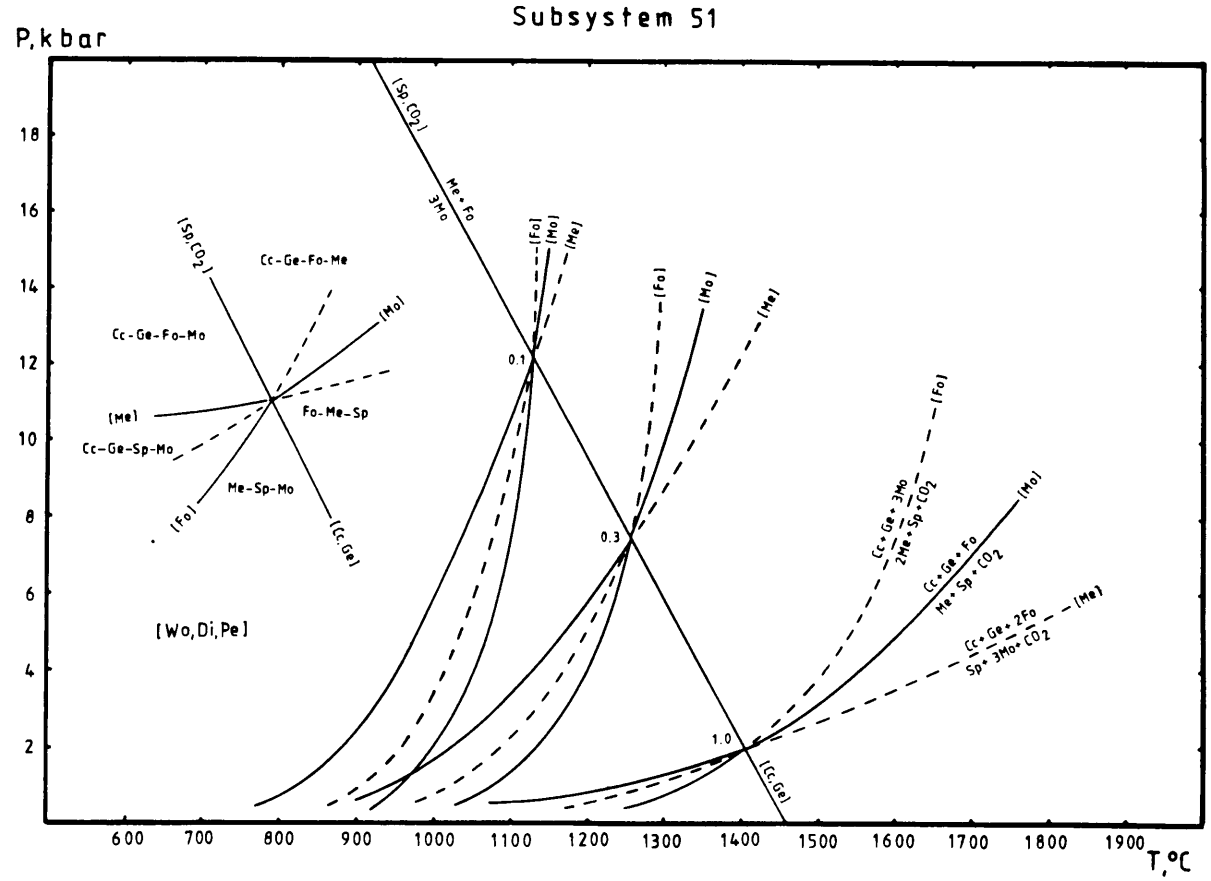

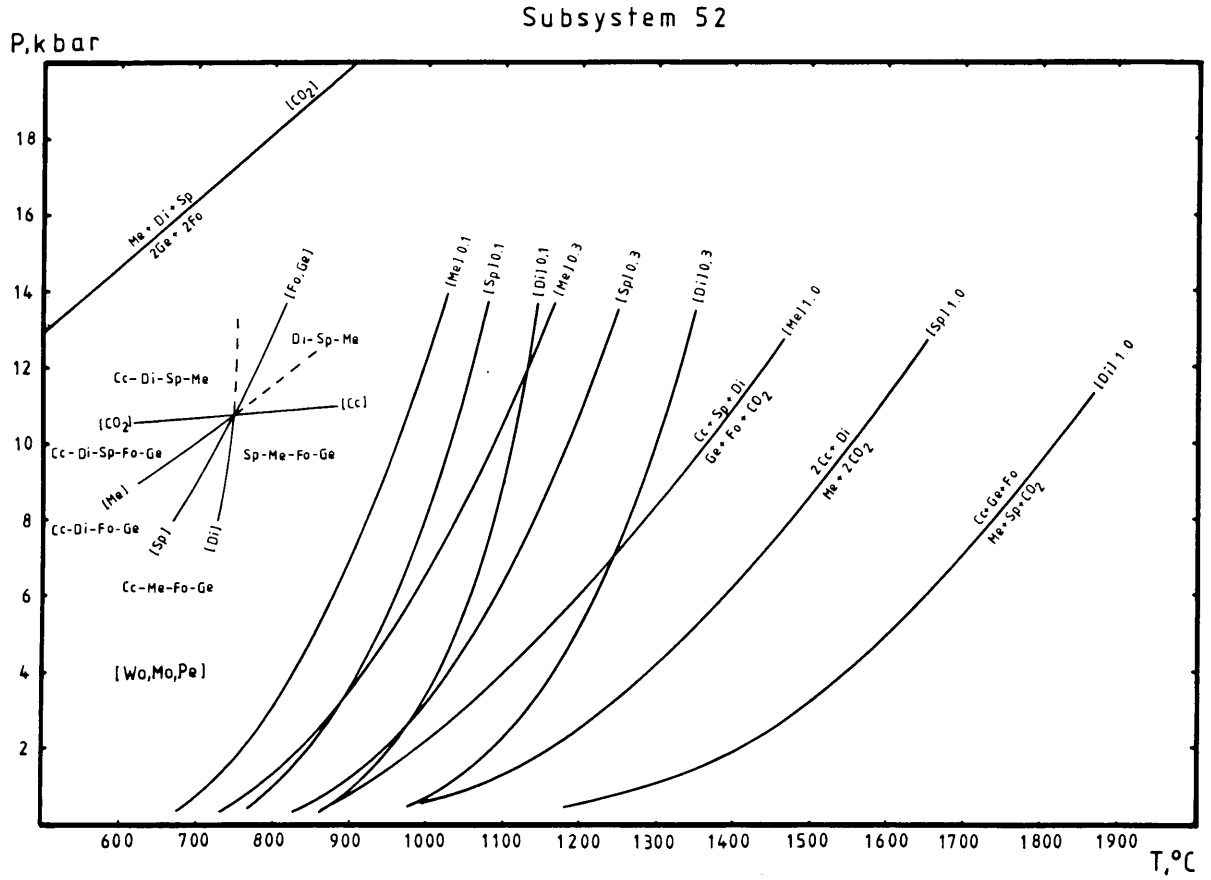

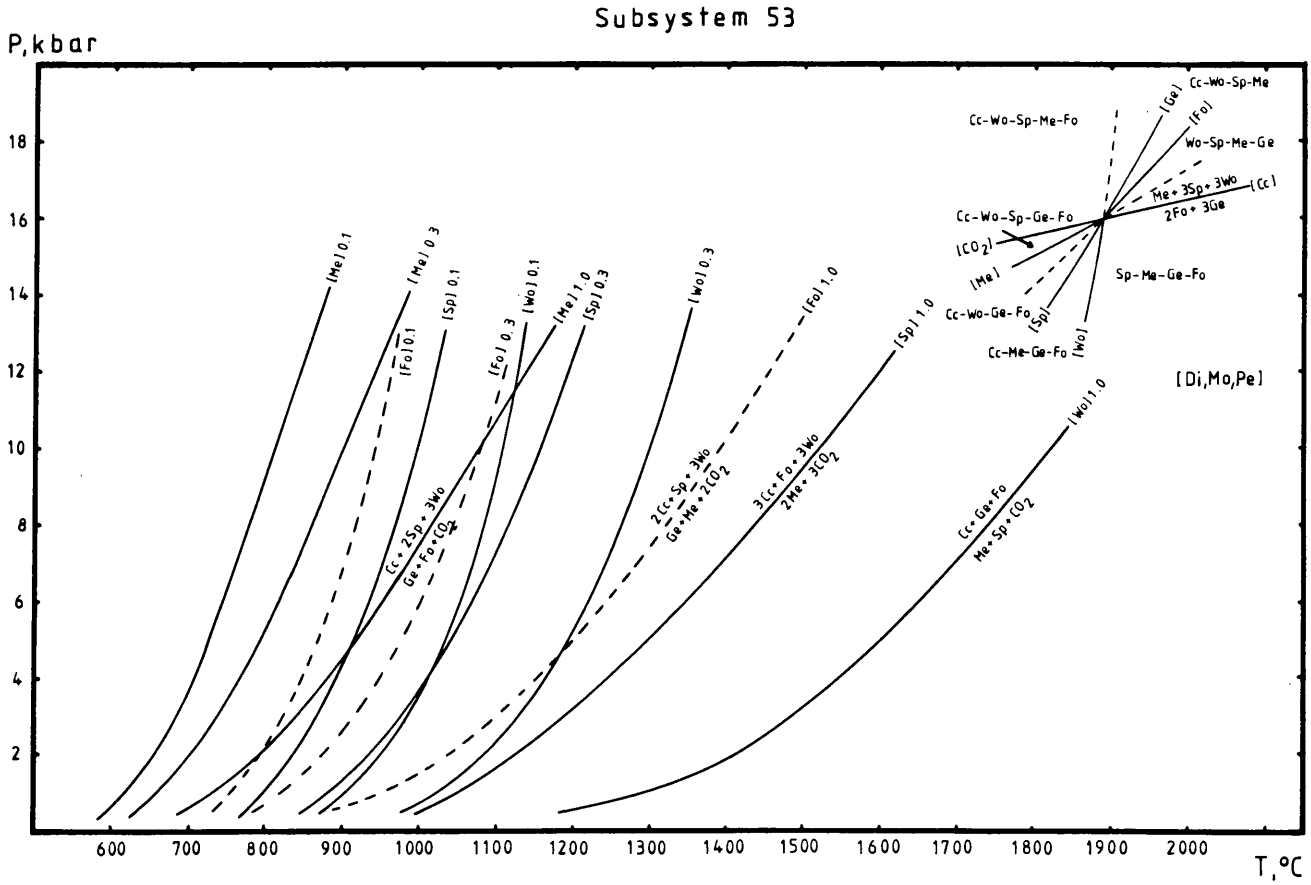

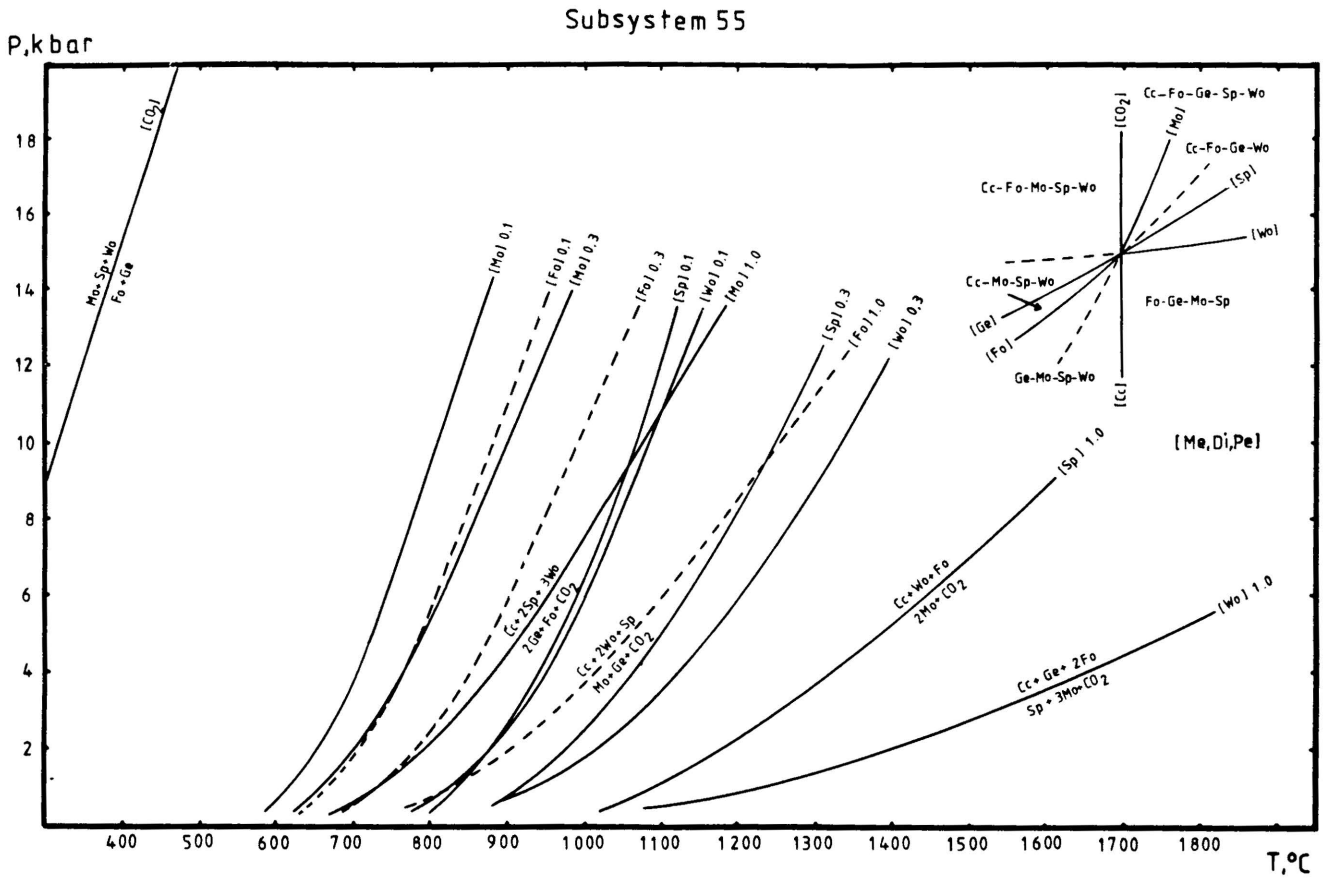

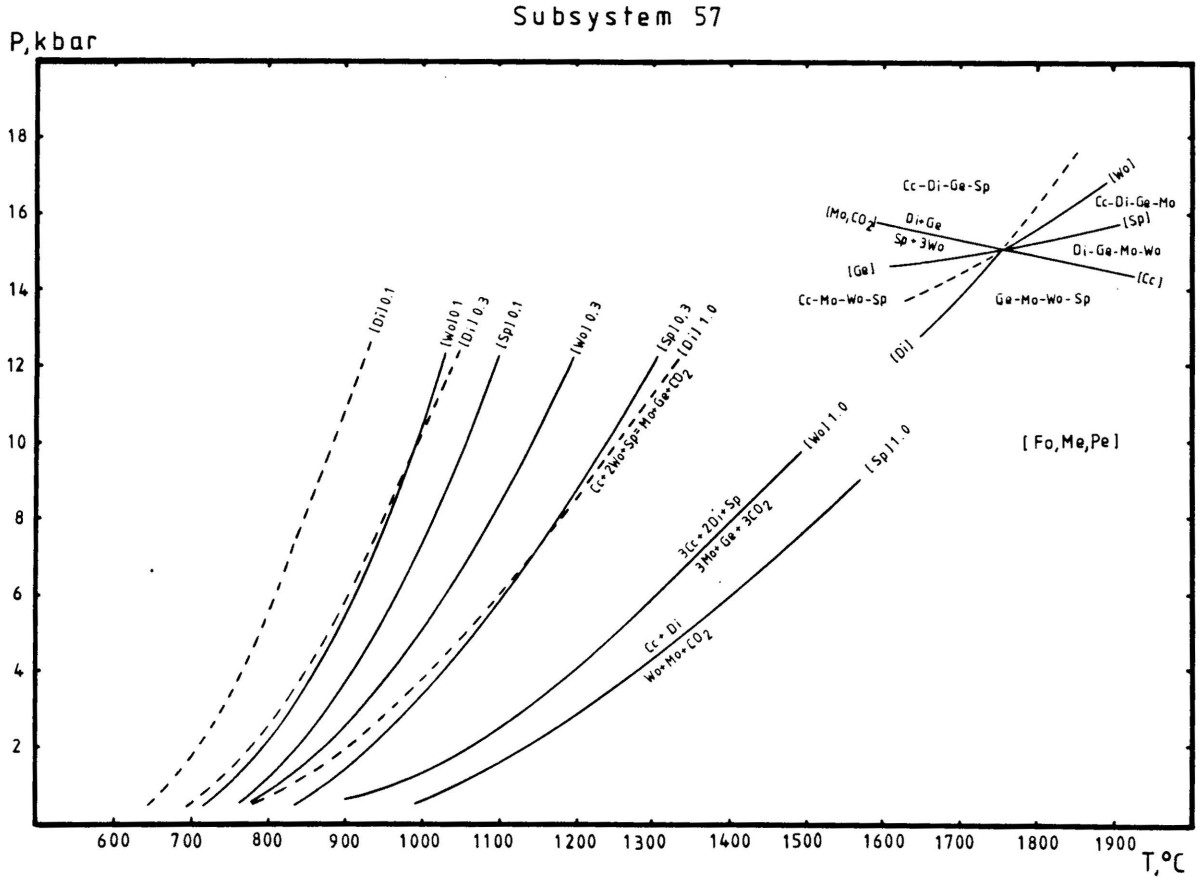

Subsystem 58

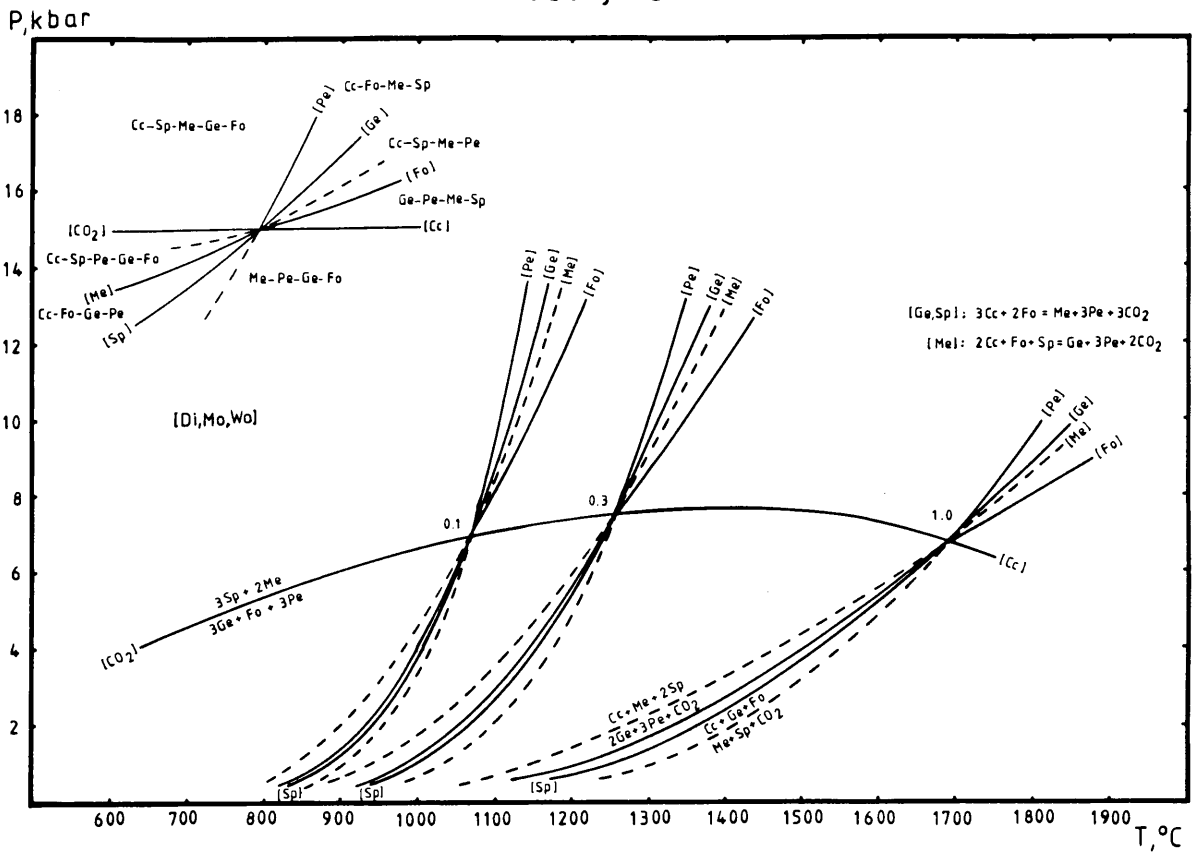

Subsystem 60

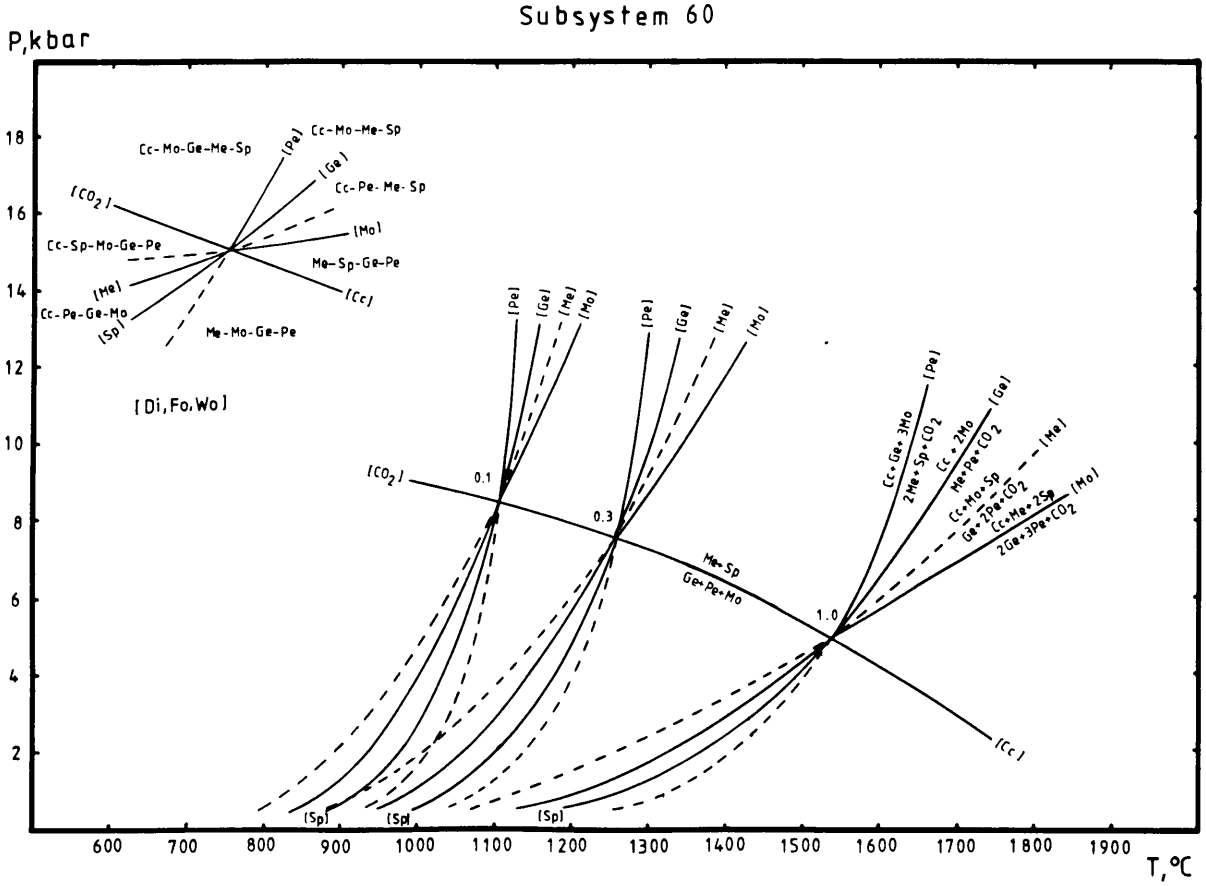

Subsystem 61

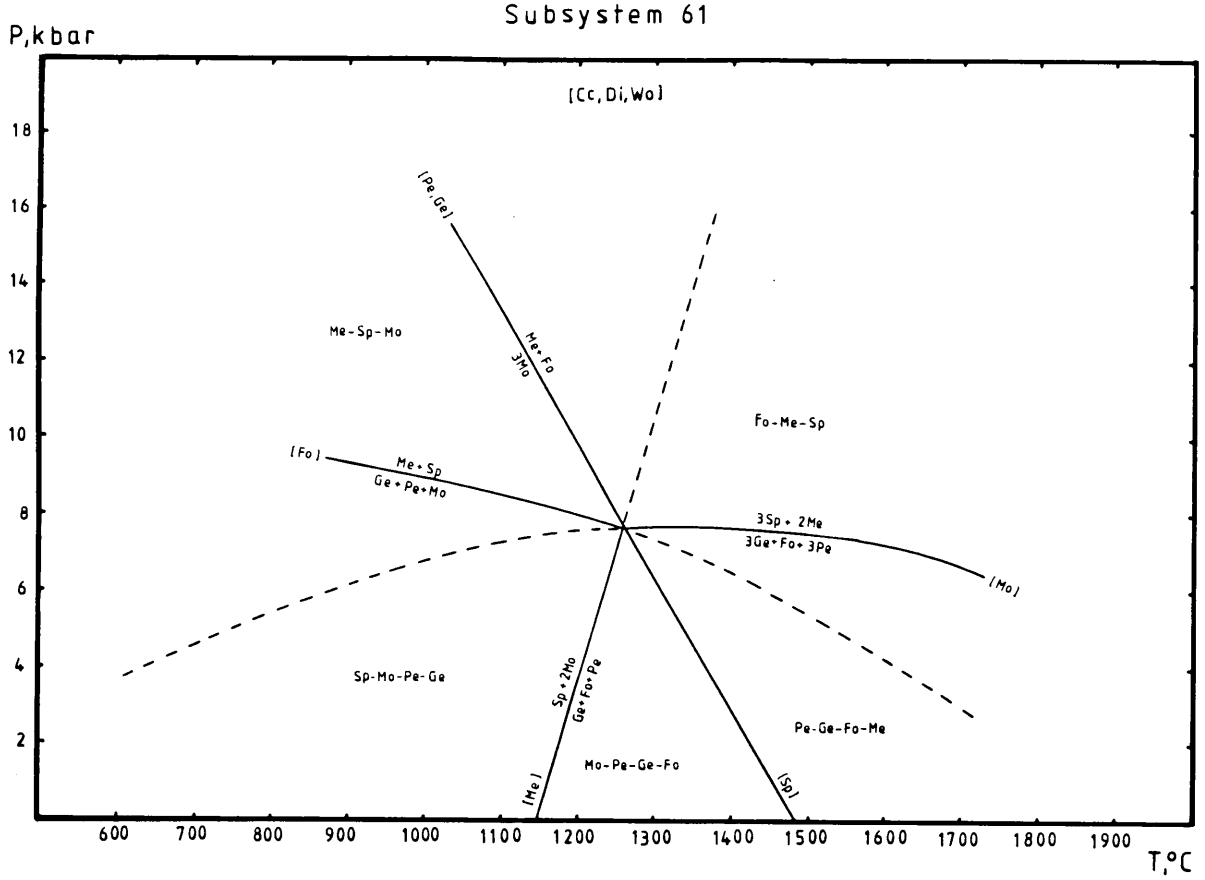

Subsystem 62

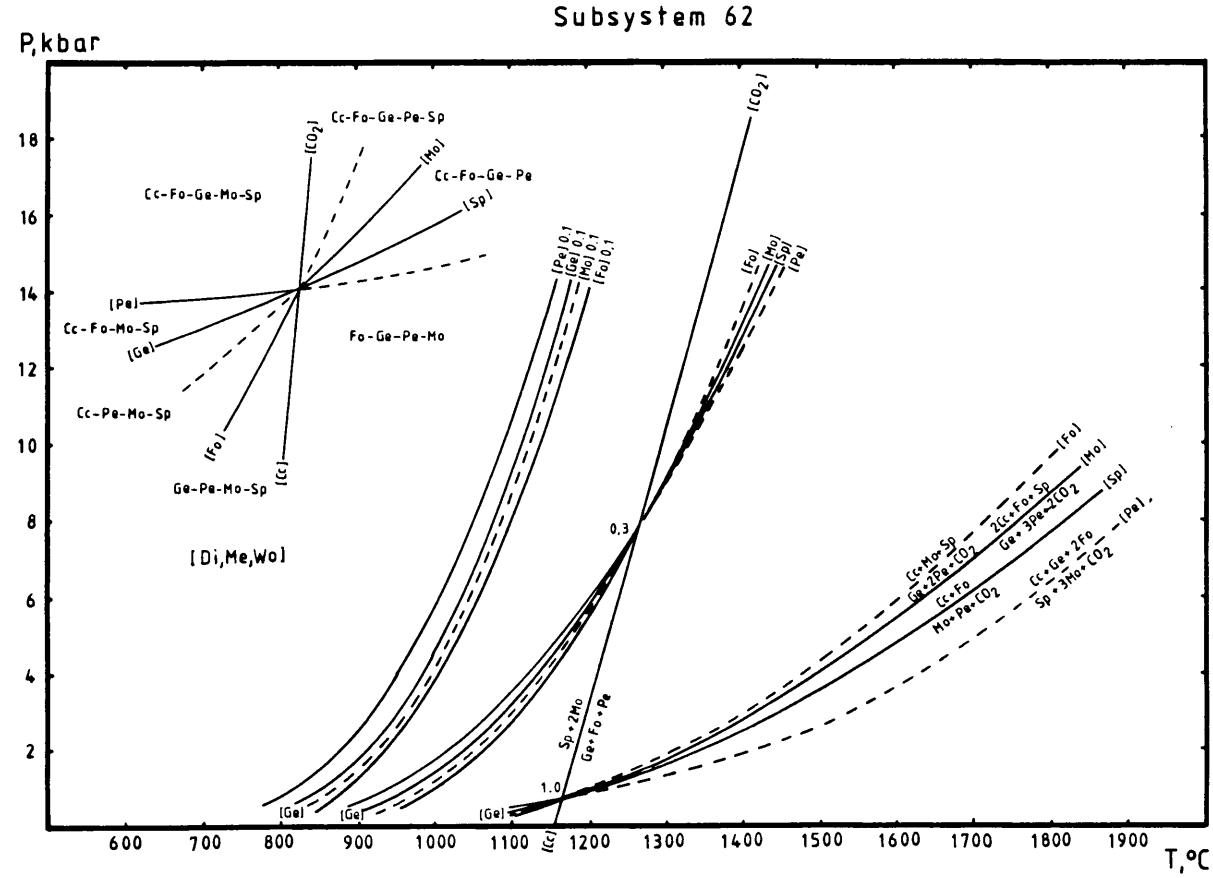

Subsystem 64

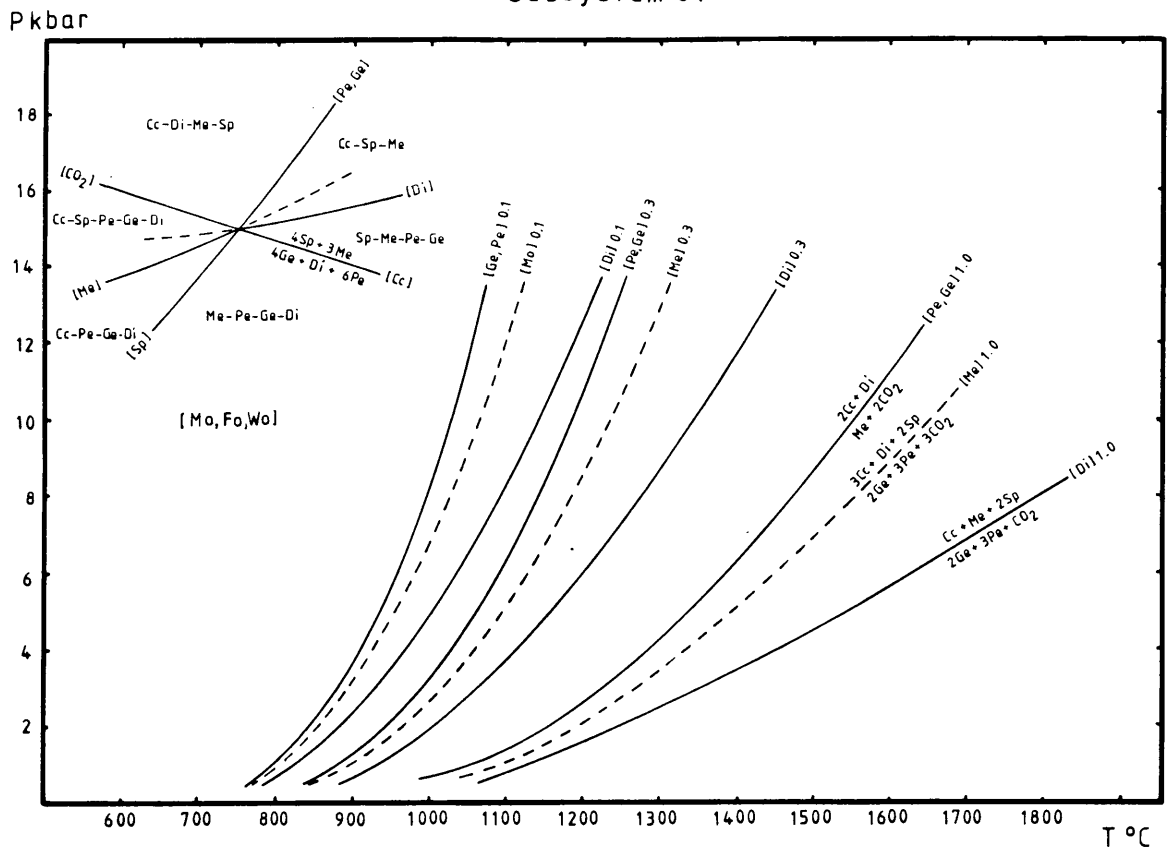

Subsystem 65

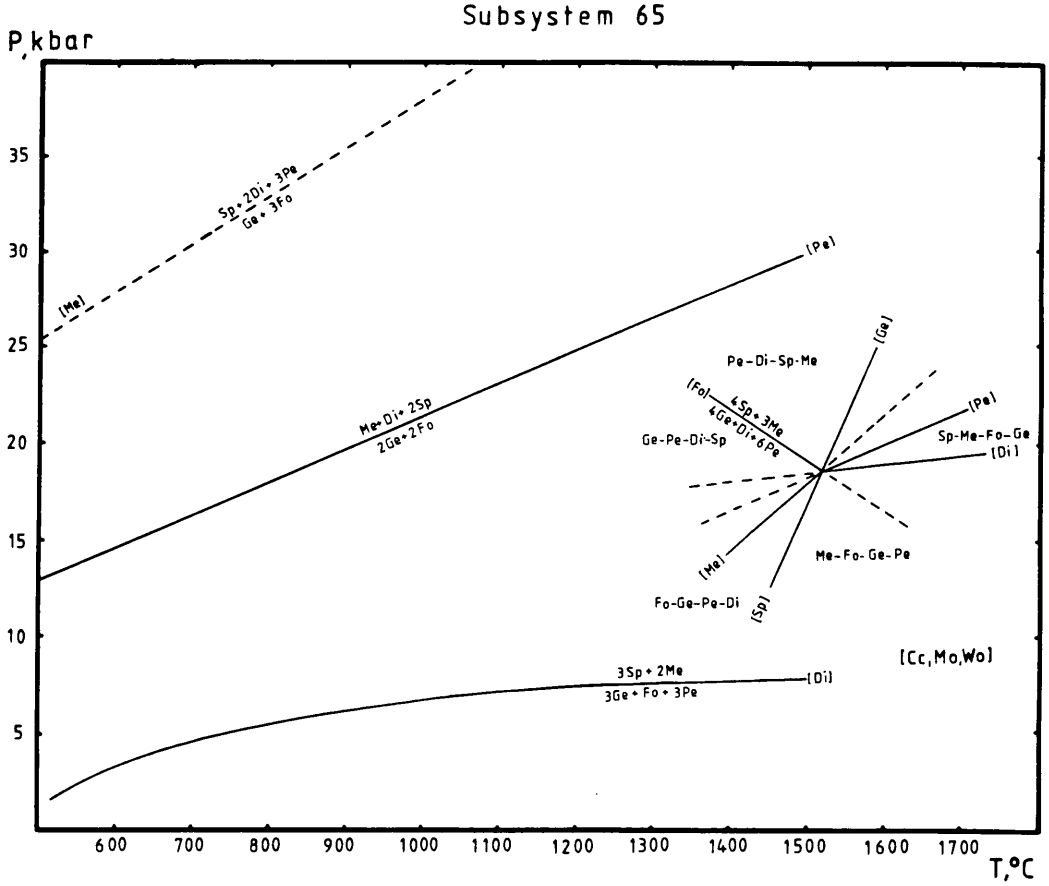

Subsystem 66

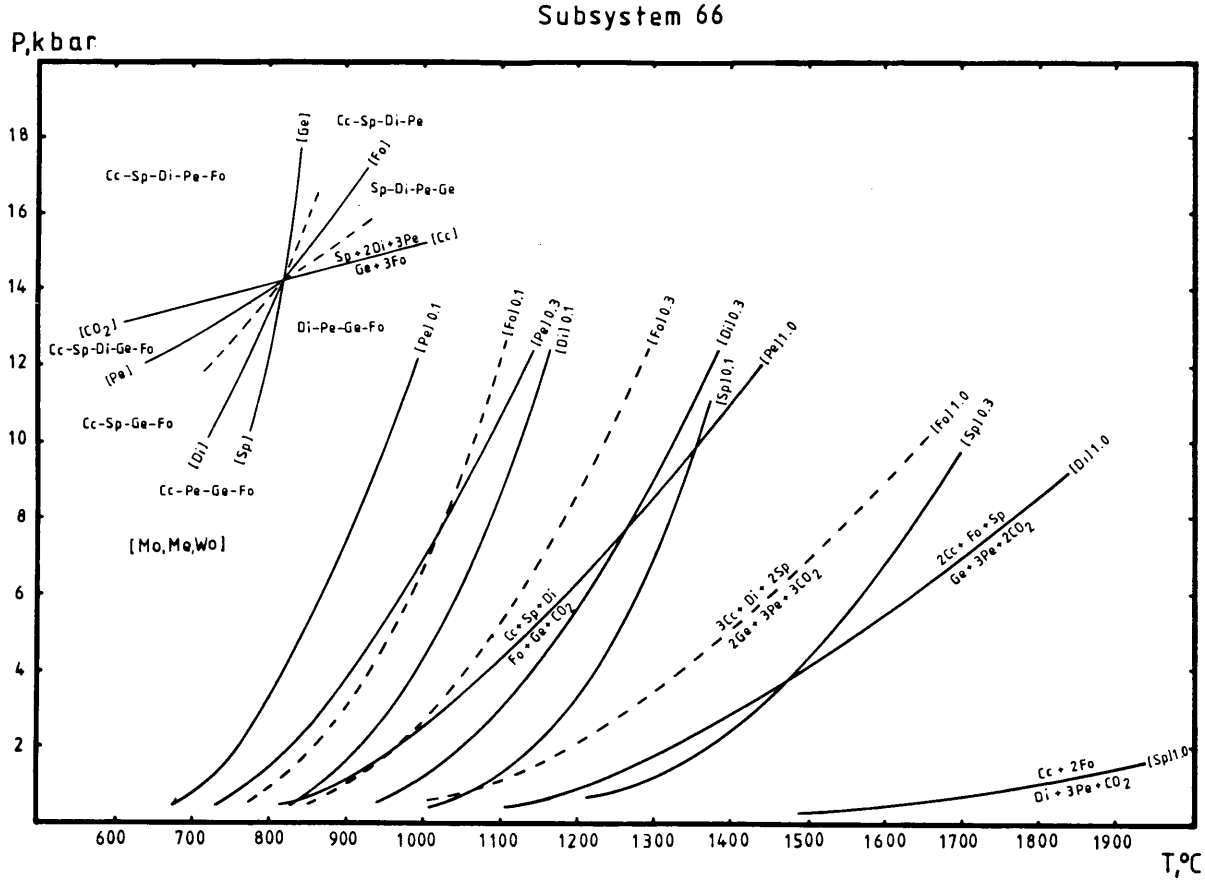

Subsystem 69

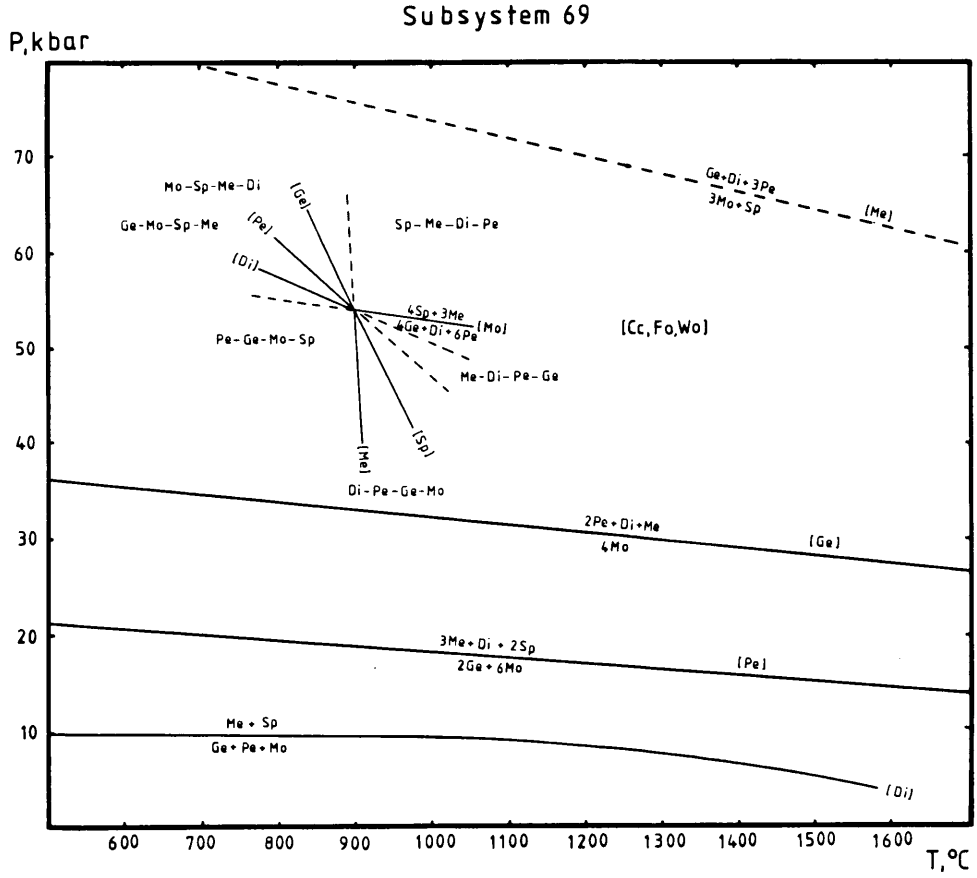

Subsystem 70

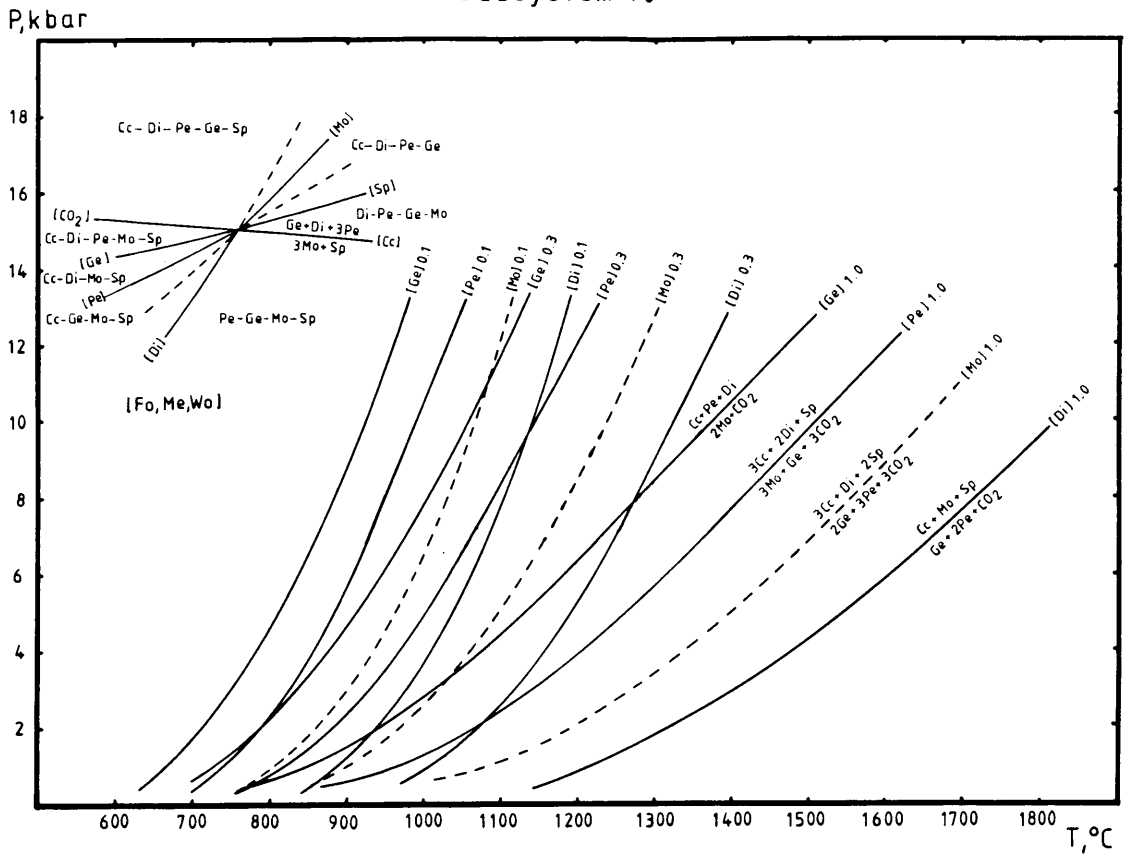

Subsystem 71

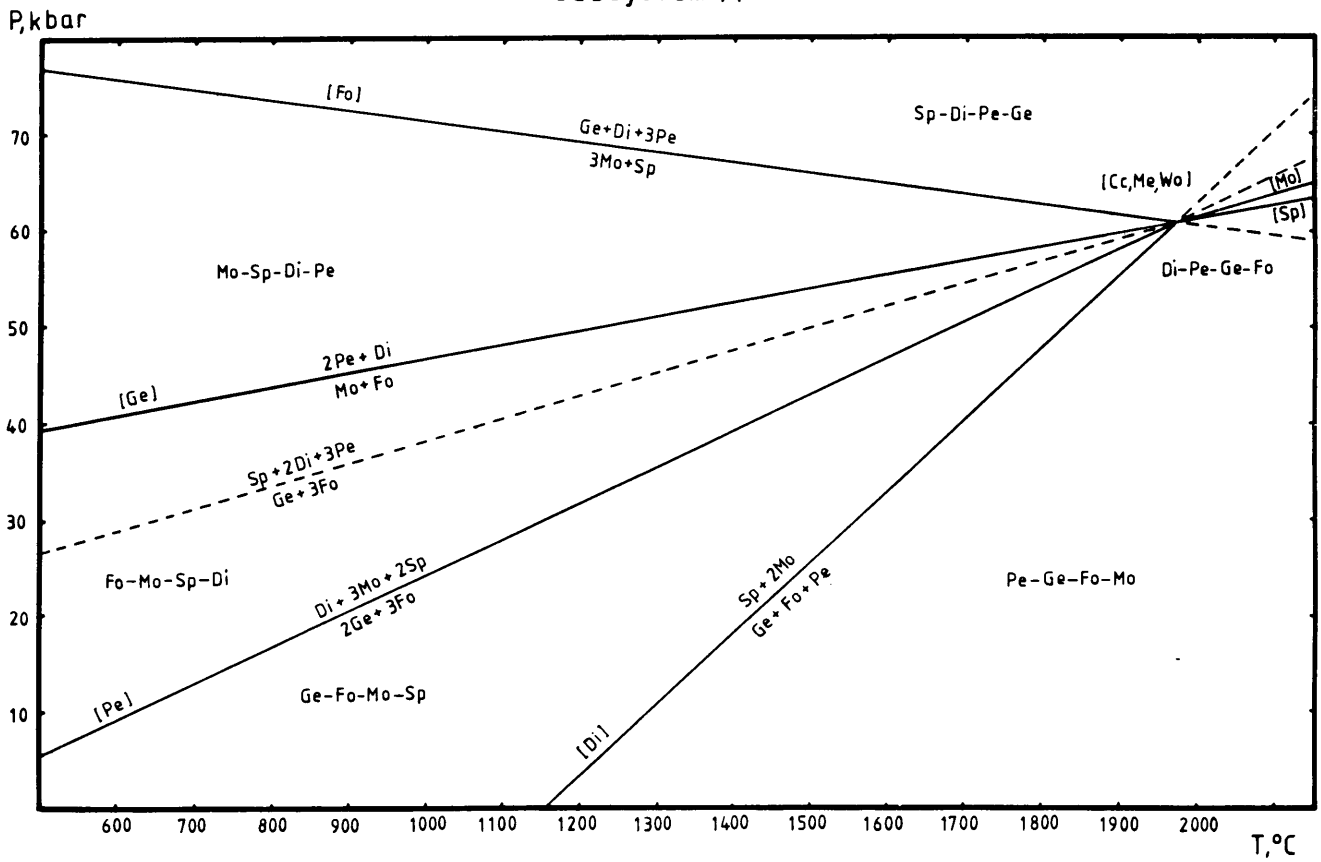

Addendum to Chapter 5

Basic assumptions for the study of multisystem phase equilibria

This addendum is a brief discussion concerning the graphical representation of heterogeneous phase equilibria, by means of phase diagrams and petrogenetic grids comprising n+k (k>2) phases (n=number of components).

Figure 1a can be used to derive the amount of in-, uni-, and divariant assemblages. For reasons discussed in Chapter 5, merwinite is included in the following considerations as an additional phase. This results in a 7 phase multisystem in which n+k=7, k=4 and n=3. The number of invariant points or invariant assemblages (${}^{n+k}C_{n+2}$) can be calculated by means of the combinatorial rule, which is represented by the following formula (Guo, 1984):

$${}^{n+k}C_{n+2}(n+k)!/(n+2)!(k-2)!, \text{ where}$$

$$(n+k)!=7!=1\cdot2\cdot3\cdot4\cdot5\cdot6\cdot7=5040$$

$$(n+2)!=5!=1\cdot2\cdot3\cdot4\cdot5=120$$

$$(k-2)!=2!=1\cdot2=2.$$

From the calculation results that ${}^{n+k}C_{n+2}=21$.

The number of possible (nondegenerate) univariant and divariant assemblages in the same n+k(n>2) multisystem will, respectively, be:

$${}^{n+k}C_{n+1}=(n+k)!/(n+1)!(k-1)!, \text{ and}$$

$${}^{n+k}C_{n}=(n+k)!/(n)!(k)!, \text{ where}$$

$(n+k)!=7!=5040$; $(n+1)!=4!=24$; $(n)!=3!=6$; $(k-1)!=3!=6$; $(k)!=4!=24$. A possible (nondegenerate) 35 univariant assemblages and reaction curves, and 35 divariant assemblages can therefore be inferred.